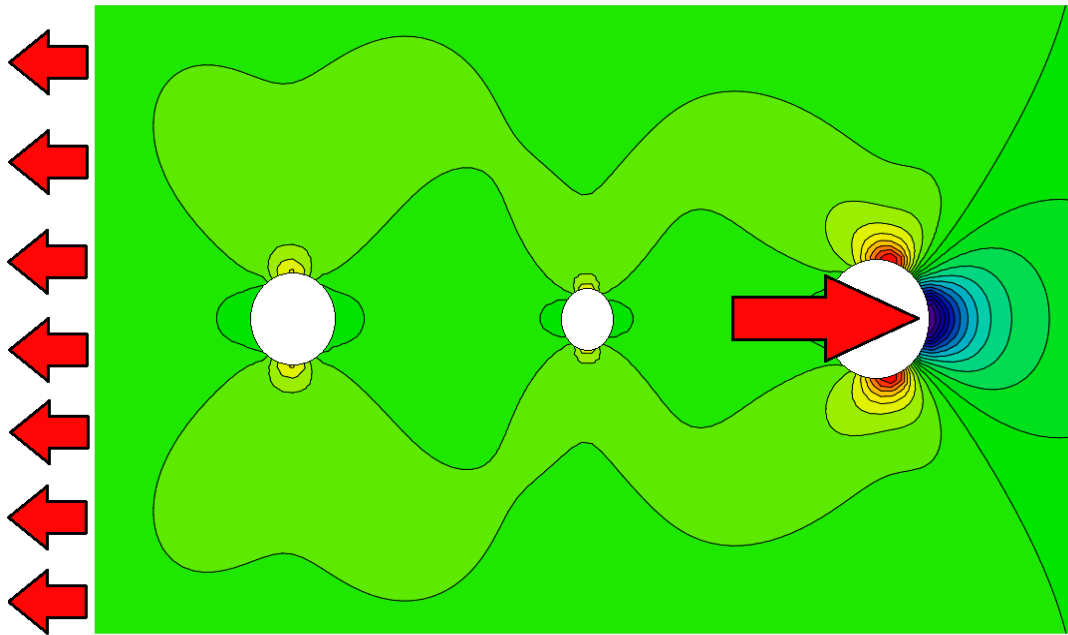


MASTER OF SCIENCE THESIS

Stress Analysis and Failure Prediction for Orthotropic Plates with Holes

An Analytic Tool for Orthotropic Plates with Loaded/Unloaded Holes Subjected to Arbitrary In-Plane Loads

R.D.B. Sevenois



Faculty of Aerospace Engineering · Delft University of Technology

UNCLASSIFIED

Stress Analysis and Failure Prediction for Orthotropic Plates with Holes

**An Analytic Tool for Orthotropic Plates with Loaded/Unloaded
Holes Subjected to Arbitrary In-Plane Loads**

MASTER OF SCIENCE THESIS

For obtaining the degree of Master of Science in Aerospace Engineering
at Delft University of Technology

R.D.B. Sevenois

December 6, 2013

Faculty of Aerospace Engineering · Delft University of Technology

The work in this thesis was supported by Fokker Aerostructures B.V. Their cooperation is gratefully acknowledged.



Copyright © R.D.B. Sevenois
All rights reserved.



DELFT UNIVERSITY OF TECHNOLOGY
FACULTY OF AEROSPACE ENGINEERING
DEPARTMENT OF AEROSPACE STRUCTURES AND MATERIALS
CHAIR STRUCTURAL INTEGRITY & COMPOSITES

GRADUATION COMMITTEE

Dated: December 6, 2013

Chair holder:

Prof.dr.ir. R. Benedictus

Committee members:

Dr.ir. S. Koussios

Ing. H. de Frel

Dr. C. Kassapoglou

Abstract

To allow structural designs with lower mass, it is necessary to have access to accurate failure prediction theories for composite plates with holes subjected to arbitrary loading conditions. For design purposes, however, the most accurate failure theories require a considerable amount of computational resources which is often not available. Additionally, current theories allowing less computational resources are unfortunately only valid for a specific load, material, hole or specimen size and their reliability is still questioned [1].

The purpose of this work is to examine the existing methods to estimate stress and failure in composite plates with holes and subsequently join or modify them to provide an analytic tool for a quick and fairly accurate estimation of the static failure load. The plate is represented as a two-dimensional structure containing arbitrary loaded/unloaded holes and edge force boundary conditions. From a literature study, it is decided that an analytical model based on the method by Xiong and Poon [2] is used for the determination of the stress field. A new general failure criterion on the basis of Kweon [3] is constructed to determine failure. The stress and failure theories are implemented in a software package, verified by hand calculation and validated with finite element analysis and experimental data. The performance of the new failure theory was also compared to the performance of the in-house Point Stress Criterion at the company where the work was performed.

The stress field methodology is able to accurately determine the stress field in two-dimensional plates with holes. The performance of the new failure criterion is better with respect to the in-house criterion and has a maximum discrepancy of +20% which is acceptable for design purposes. Unfortunately, due to issues with the assumption of the stress boundary conditions for loaded holes, the method is restricted to laminates with a directionality lower than 1.13. Once these issues are resolved, the method will be generally applicable.

Preface

I first contacted Dr. Koussios about this project in January 2012. Being optimistic about obtaining the MSc degree in 2 years, I had envisioned to start this project (literature study and thesis) in July 2012 and graduate in June 2013. An unexpected opportunity, however, forced me to temporarily move to Canada and delay the start to January 2013. Luckily no additional delays were encountered and with perseverance, regularity and some luck I managed to deliver this work to you within the intended timeframe. This project involves two reports describing the development, verification and validation of an analytic tool for the determination of stress and failure in finite width orthotropic plates with holes subjected to arbitrary in-plane loads. The first report is an extensive literature study in the field of stress analysis and failure prediction in laminated plates. In the second report, which is this work, the conclusions from the first report are followed to result in the completion of the analytic tool. I have put a considerable amount of time and effort in this work and I hope that reading it will give you the same satisfaction as when I finished it.

It is expected that you have knowledge of Mathematics, Classical Lamination Theory (CLT), Complex Stress Analysis and Failure Prediction with application to laminated plates to understand the theory explained in this work which is outlined in Chapter 3 and Chapter 4. Contentwise, approximately one third of the pages you are about to read are appendices. They contain the detailed results and workout of some theories which serve as ultimate proof for the points made and are required to ensure a correct chain of custody. Unless you are extremely interested, you are not expected to read them.

This work would not be what it is without the help of my friends, colleagues and supervisors. In this paragraph I would like to thank Dr. ir. S. Koussios and Dr. C. Kassapoglou, MSc for their advice during the execution of the project and being my main supervisors. M. Bakker, MSc for his insights in the stress theories and advice during the construction of the computer algorithm. Ing. H.C. de Frel and B. Tijs for their advice and knowledge to make this work compatible with the designer environment at Fokker Aerostructures B.V. The Tools and Methods team at Fokker Aerostructures B.V. and especially ir. Tim Janssen, R. Hoogendoorn, BSc and F. Gerhardt for providing support, advice, insights and a stimulating work environment. And last but not least my friends from Aerospace Structures and Materials and Aerodynamics for the coffee, fun conversations and movie nights.

Summary

The more accurate one can predict the failure load of an aircraft component, the lower safety factor for the design is required. This results in a lower structural mass and translates into a lower fuel consumption which is beneficial for the aircraft operator. Using metals, static failure loads of components can relatively easy be determined by looking at the stress concentrations in the design. For composites, because of their complexity, determining failure is not so straightforward. This complexity and the lack of a reliable model [1] led to an abundance in failure criteria for (un)notched laminated plates. Some quite accurate models exist but they can require a significant amount of computational resources which is often not available. Therefore many design organizations still use the basic, less accurate, criteria. Most of these criteria, however, are only valid for a specific load, material, hole or specimen size. Often, for more complicated scenarios, failure can not confidently be estimated.

The purpose of this work is to present the development of an analytic tool for the prediction of failure in orthotropic plates with holes subjected to arbitrary loading which can be used by Fokker Aerostructure B.V. in the design of aircraft components. First the state of the art is determined with a literature survey on existing theories for stress evaluation and static failure prediction in composite plates with holes. Next, the theories obtained from the survey are evaluated for their applicability, joined and/or modified to form the analytic tool. The tool is then verified by simple hand calculations and validated with finite element analysis and experimental data.

The basic problem, which is shown in Figure 1, consists of a two-dimensional flat rectangular orthotropic plate containing m holes. The edges of the plate and holes can be loaded or unloaded as defined by the user. From the literature survey it is determined that, to estimate the stress field for this type of problem, a complex stress analysis on the basis of Lekhnitskii [4] and Xiong and Poon [2] is best to use. Advantages of this method for the determination of the stress field is that it results in a single expression for the entire stress field and that arbitrary boundary conditions can be used. For failure prediction, it is clear that, for both notched and unnotched plates, there is no consensus on which failure criterion is best to use. To predict unnotched ultimate failure in two-dimensional loading conditions, one needs to construct an algorithm on the basis of a progressive failure model. This model consist of an algorithm which takes the degradation of lamina properties due to matrix cracking

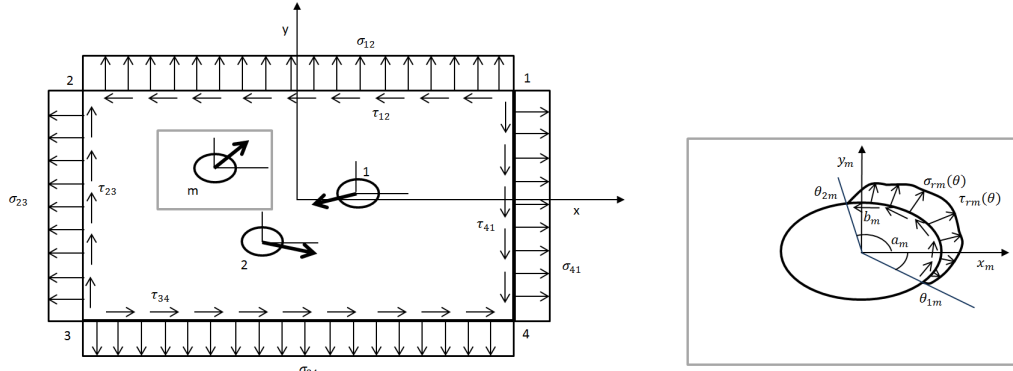


Figure 1: A rectangular plate with multiple holes subjected to arbitrary loading

and the non-linearity of the material into account in conjunction with a failure model to predict onset of failure. To predict failure onset, the phenomenological failure criteria by Puck [5], LaRC03 [6], LaRC04 [7] and the Tsai-Wu [8] are the best criteria with an accuracy of $\pm 10\%$ [1]. An accuracy of $\pm 50\%$ in 85% of the cases has been shown for Puck's final failure progressive model [5] which will be used. From the identified notched failure criteria, the Linear Elastic Fracture Mechanics (LEFM) [9], Average Stress Criterion (ASC) [10] and Point Stress Criterion (PSC) [10] were selected as most promising when taking into account the intended use of the analytic tool. Eventually, because an analytic method to determine the characteristic length is available from Kweon [3], the PSC [10] was selected to form the basis for the notched failure criterion.

Following Lekhnitskii [4] an appropriate solution for the stress functions $\varphi_j(z_j)$, $j = 1, 2$ to determine the stresses, strains and displacement for arbitrary boundary conditions as shown in Figure 1 is:

$$\varphi_j(z_j) = C_{0j} + \sum_{n=1}^N C_{n_j} z_j^n + \sum_{k=1}^m \left\{ C_{(k+kN)_j} \ln(\xi_{mj}) + \sum_{n=1}^N C_{(k+kN+n)_j} \xi_{mj}^{-n} \right\} \quad (1)$$

$j = 1, 2$

In Eq. (1), ξ_j is the mapping function of the m -th hole to the complex plane, C_{n_j} , $j = 1, 2$ are complex coefficients which must be determined through the problem boundary conditions. These coefficients are determined using the principle of minimum potential energy. This principle states that the minimum total potential energy of the structure is reached given the external loading conditions. Thus, the derivative of the total elastic strain energy in the problem should be zero. Integrating for the elastic strain energy over the domain and boundaries of the plate and taking its derivative, it is observed that, due to satisfaction of the equilibrium equations by Eq. (1), the part related to the domain becomes zero and only the boundary terms remain. Working out these boundaries with the stress function (1) and solving for $\partial\Pi = 0$ eventually results in a linear system of equations which can easily be solved.

For an accurate representation of the stress field, one now only has to define valid stress boundary conditions. This is especially important when loaded holes need to be evaluated. Many researchers assume that the pin-load on a hole edge can be represented by a radial cosine shaped compression load on the hole edge [2, 11, 12]. Several studies [13, 14], however, have

ergies which are not only uniaxial tension or uniaxial compression. Therefore, in a similar way as is for the CPSED for tension, the CPSED for transverse tension, transverse compression, tension-tension, tension-compression, compression-tension and compression-compression loading is defined. The algorithm to predict failure of a notched plate is now given by:

1. Calculate the CPSED for compression by analysis of a pin-loaded joint
2. Calculate the CPSED for tension and the other multiaxial loading conditions
3. Calculate the stress field of the problem
4. Set an initial characteristic distance and determine the minimum Reserve Factor and critical loading angle around each hole
5. At the critical angle, calculate the Potential Strain Energy Density (PSED) at failure from the hole edge to the characteristic distance
6. When the CPSED equals the PSED, the ultimate failure load is obtained. Otherwise, a new characteristic distance is chosen based on whether the PSED is higher or lower than the CPSED and the procedure is repeated from step 4.

The algorithm above is implemented in a routine regulated by a Visual Basic Script and calculated with MathCAD13.1©. The functioning of the routing is verified by comparing the stress for several configurations at the hole edge to analytic solutions from Lekhnitskii [4] and simple hand calculations. The convergence behaviour of the algorithm is determined by investigating the influence of the numerical integration parameter TOL (internal MathCad13.1©) and the amount of summations N in the stress function (Eq. (1)). Finally, from this investigation it is concluded that good working ranges for N and TOL , when less than 6 holes are present, are:

$$\begin{aligned} N &\geq 7 \\ 10^{-3} &\geq TOL \geq 10^{-6} \vee 10^{-13} \geq TOL \geq 10^{-16} \end{aligned} \quad (4)$$

where \vee is the OR operator. The performance of the contact angle and stress field methodology are further investigated by comparing the results from these analysis to Finite Element Analysis. More complicated configurations are analyzed and the ability of the tool to take into account the finite size of the plate is determined. From these investigations it is determined that, for an accurate representation of the stress field, the ratio of the hole edge distance and diameter over panel width should be larger than 2.5 and 4 respectively. For design purposes, an $E/D \geq 2.5 + 1.3$ [mm] [16] and $W/D \geq 4.7$ [17] is advised. These boundaries are thus well within limits. Unfortunately, the validation of the contact angle algorithm, revealed that, for the current assumptions for the pin-hole stress boundary condition, the estimation is only conservative for laminates with a directionality lower than 1.13. It is recognized that this restriction greatly affects the laminate design space for this tool. This issue was, during the construction of this work, addressed by Gerhardt [18] but could unfortunately not be implemented due to time constraints.

In preparation to validate the notched failure method with experimental data, the hole diameter to determine the CPSED is determined by making predictions for a selection of the experimental data points for multiple hole diameters. The selection of data contains both

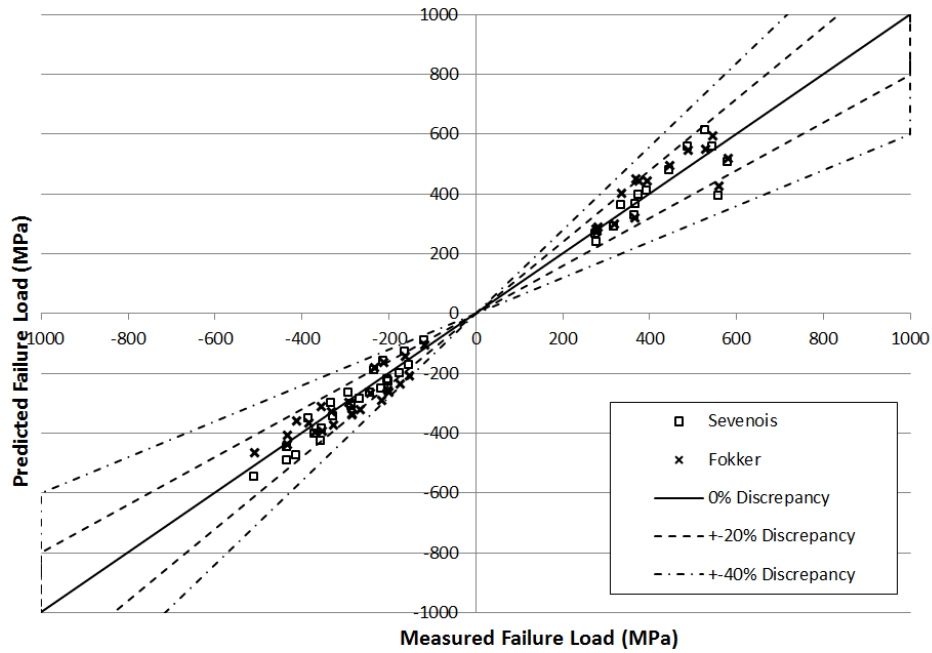


Figure 3: Predicted vs measured failure for unloaded hole configurations, screened

open hole tension and compression as well as pinned hole bearing experiments. Next, the requirement that none of the predicted values should overestimate the measured values by 10% and be as close as possible to the measured values, result in a hole diameter of 5 [mm]. Finally, by screening a dataset of 151 experimental values to the tool boundaries, a total amount of 92 (38 measurement points unloaded and 54 measurement points loaded holes together) are selected and predictions for these data points are made. The results are presented in Figure 3 and Figure 4 from which it can be seen that, for the unloaded experimental points, all but a few data points are within $\pm 20\%$ of the measured experimental value. For the loaded data-points, the scatter is much larger but concentrates between -20% and -60% . The prediction for loaded holes is thus almost always conservative. It is thought that, however no definite proof can be delivered, the source of this conservatism is due the fact that, in literature, the ultimate failure load after occurrence of significant damage is reported and not the onset of failure. For unloaded holes the difference between onset and ultimate failure is often small which is why the same conservatism is not seen in these predictions. For loaded holes, however, as observed by Crews [19], this difference can be significant due to interactions of failure modes and strengthening effects. The algorithm is not able to take these interactions and strengthening effects into account and therefore will always predict a lower failure load. It is worthwhile to investigate whether this PSC failure criterion actually predicts onset of failure as indicated by the definition from Whitney and Nuismer [10].

Apart from the issues with the loaded hole predictions and the assumption for the pin-hole edge stress distribution, it is emphasized that the new methodology is an improvement over the current in-house failure criterion at Fokker Aerostructures B.V. For loaded hole configurations, the majority of the predictions are moderately to highly conservative while the unloaded predictions are situated in the $\pm 20\%$ region. It is recognized that, initially, a maximum discrepancy of $+10\%$ was set for the method, and although the internal parameters

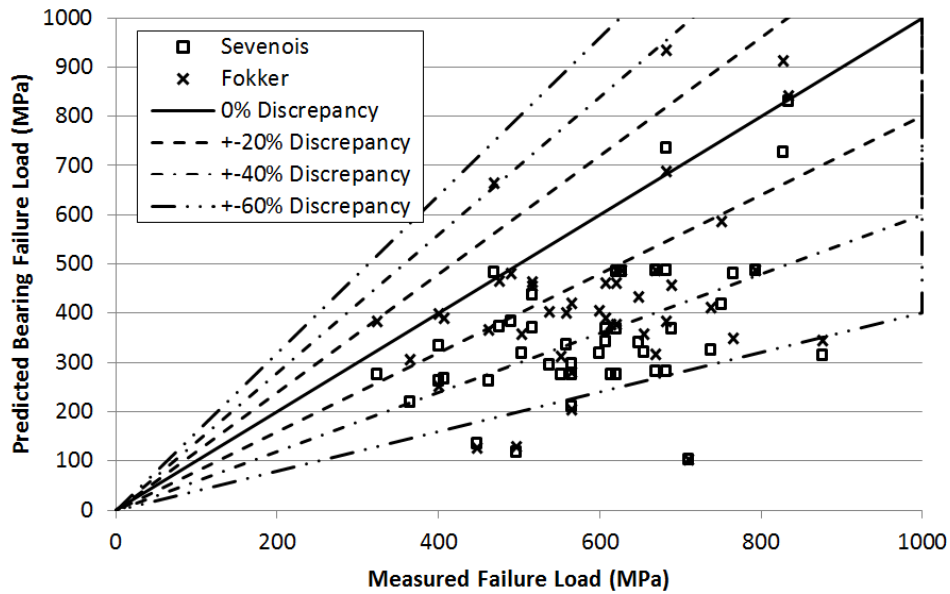


Figure 4: Predicted vs measured failure for loaded holes configurations, screened

were scaled to obtain this result, the finally obtained +20% for the entire dataset is still remarkably close. This overestimation can easily be eliminated by changing the hole size for the determination of the CPSED to a lower value. Additionally, the pin-hole edge stress distribution should be improved to eliminate the directionality boundary of 1.13. When these issues are resolved, the method will be available for design purposes in the entire design envelope.

Frequently Used Symbols and Abbreviations

Symbol	Explanation
α	Displacement angle
α_j	Real part of μ_j
β_j	Imaginary part of μ_j
γ_{xy}	Shear strain in the xy-plane
$\boldsymbol{\varepsilon}$	In-plane strain vector
ε_x	Normal strain in x-direction
ε_y	Normal strain in y-direction
θ_{1m}	Start contact angle for hole m
θ_{2m}	End contact angle for hole m
θ_B	Contact angle
λ	Absolute difference between pin size and hole size
μ_j	Material eigenvalue
ν_{ij}	Poissons ratio in ij -plane
ξ_{mj}	Mapping function of the m -th hole to the complex plane
Π	Total potential strain energy
$\Pi_{cr,c}$	Critical potential strain energy density compression
$\Pi_{cr,-c}$	Critical potential strain energy density transverse compression
$\Pi_{cr,cc}$	Critical potential strain energy density biaxial compression-compression
$\Pi_{cr,ct}$	Critical potential strain energy density biaxial compression-tension
$\Pi_{cr,t}$	Critical potential strain energy density tension
$\Pi_{cr,-t}$	Critical potential strain energy density transverse tension
$\Pi_{cr,tc}$	Critical potential strain energy density biaxial tension-compression
$\Pi_{cr,tt}$	Critical potential strain energy density biaxial tension-tension
$\boldsymbol{\sigma}$	In-plane stress vector
σ_θ	Tangential stress on the hole edge
σ_{12}	Normal stress on plate edge 1-2

σ_{23}	Normal stress on plate edge 2-3
σ_{34}	Normal stress on plate edge 3-4
σ_{41}	Normal stress on plate edge 4-1
σ_{rm}	Radial stress on the edge of hole m
$\sigma_{un,t/c}$	Unnotched failure stress tension/compression
σ_b	Bearing stress
σ_r	Radial stress on the edge of a hole
σ_x	Normal stress in x-direction
σ_y	Normal stress in y-direction
τ	Shear stress
τ_{12}	Shear stress at plate edge 1-2
τ_{23}	Shear stress at plate edge 2-3
τ_{34}	Shear stress at plate edge 3-4
τ_{41}	Shear stress at plate edge 4-1
τ_{rm}	Shear stress on the edge of hole m
τ_{xy}	Shear stress in the x-y plane
φ_j	Complex stress function
a_{ij}	Entry i, j in the laminate compliance matrix
A_{ij}	Entry i, j in the laminate stiffness matrix
a_0	Characteristic length for average stress criterion
a_m	Semi major axis of hole m
aa	Material angularity
b_m	Semi minor axis of hole m
\mathbf{C}	Elastic stiffness matrix
C_{-j}	Complex coefficient of the stress function
D	Hole diameter
d_{0c}	Compressive characteristic distance
d_0	Characteristic distance for point stress criterion
E	Hole center edge distance
E_i	Engineering Young's modulus in i direction
f_E	Stress exposure
G_{Ic}	Mode I fracture toughness
G_{IIc}	Mode II fracture toughness
G_{ij}	Engineering shear modulus in ij -plane
K_T	Stress concentration factor
K_T^{inf}	Stress concentration factor at infinity
L	Specimen length
N	Amount of summations in the stress function
p_{21}^c	Slope of the fracture curve to the left of $\sigma_2 = 0$
p_{21}^t	Slope of the fracture curve to the right of $\sigma_2 = 0$
P_b	Total bearing force
R_{22}^A	Fracture resistance of the action plane parallel to the fibre direction
R_{mj}	Coefficient for the m -th hole

r_h	Hole radius
r_p	Pin radius
rr	Material directionality
S	Elastic compliance
S_{12}	In-plane shear strength
S_{12}	Ply shear strength
t	Laminate thickness
t_{mj}	Coefficient for the m -th hole
t_{ply}	Lamina ply thickness
u	Displacement in x-direction
u_α	Displacement in x-direction at angle α on the hole edge
u_0	Displacement in x-direction at 0° on the hole edge
v	Displacement in y-direction
W	Specimen width
X^c	Longitudinal compressive strength
X^t	Longitudinal tensile strength
x_m	Center of hole m with respect to the x-coordinate
X_n	External force component parallel to x
Y^c	Transverse compressive strength
Y^t	Transverse tensile strength
y_m	Center of hole m with respect to the y-coordinate
Y_n	External force component parallel to y
z_j	Complex coordinate

Abbreviation	Explanation
ASC	Average Stress Criterion
CFRP	Carbon Fibre Reinforced Plastics
CID	Coordinate IDentified
CPSED	Critical Potential Strain Energy Density
CPU	Central Processing Unit
DZM	Damage Zone Model
ESDU	Engineering Sciences Data Unit
FEA	Finite Element Analysis
FEM	Finite Element Method
FF	Fibre Failure
FPF	First Ply Failure
FRP	Fibre Reinforced Plastics
GFRP	Glass Fibre Reinforced Plastics
IFF	Inter Fibre Failure
LaRC	Langley Research Center
LEFM	Linear Elastic Fracture Model
MCFE	Most Conservative Fracture Envelope
PSC	Point Stress Criterion
PSED	Potential Strain Energy Density
QI	Quasi-Isotropic
RF	Reserve Factor
SCF	Stress Concentration Factor
UD	Uni-Directional
UF	Ultimate Failure
VBScript	Visual Basic Script
VDI	Verein Deutscher Ingenieure
WWFE	World Wide Failure Exercsice
XFEM	eXtended Finite Element Method

Table of Contents

List of Figures	xxvii
List of Tables	xxix
Acknowledgments	xxix
1 Introduction	1
2 Literature Survey	3
2.1 Stress Analysis	3
2.1.1 Analytic Stress Analysis	3
2.1.2 Finite Element Analysis	8
2.2 Strength Prediction	11
2.2.1 Unnotched Strength	11
2.2.2 Notched Strength	14
3 Determination of the Stress Field	19
3.1 Expansion of Xiong's Method	19
3.2 Pin Contact Angle	28
4 Failure Prediction	33
4.1 Unnotched Failure Prediction	34
4.2 Notched Failure	38
4.3 General Program Layout	40
5 Tool Verification	45

6	Validation, Comparison to FEA and Experimental Data	51
6.1	Stress Analysis	52
6.1.1	Influence of accuracy parameters TOL and N	52
6.1.2	Influence of contact angle estimation	57
6.1.3	Comparison to FEA	62
6.2	Failure Prediction - Comparison to Test Results	70
6.2.1	Unnotched Failure Criterion	70
6.2.2	Notched Failure Criterion - Clearance and Hole Size for CPSED	74
6.2.3	Notched Failure Criterion - Comparison to Experimental Data	76
7	Discussion, Conclusions and Recommendations	87
	References	91
A	Derivation of the Sign Selection Algorithm	105
B	Discussion on Kweon's Tensile Characteristic Length	115
C	Flow Charts of Individual Code Segments	117
D	Results from Verification	125
E	Contact Angle Comparisons FEA	145
F	Results from Stress Validation	157

List of Figures

1	A rectangular plate with multiple holes subjected to arbitrary loading	xii
2	Definition of the compressive characteristic distance by Kweon [3] and the CPSED	xiii
3	Predicted vs measured failure for unloaded hole configurations, screened	xv
4	Predicted vs measured failure for loaded holes configurations, screened	xvi
2.1	Evolution of FEA, references can be obtained from [20]	9
2.2	Discretizations of a grain boundary problem for (a) an XFEM/GFEM model with a structured (Cartesian) mesh and (b) a FEM model [21]	10
3.1	A rectangular plate with multiple holes subjected to arbitrary loading	20
3.2	Two-dimensional anisotropic body with two contours	21
3.3	Computation algorithm for stress field determination. The subscript j is dropped for convenience	28
3.4	A hole loaded by a distributed cosine distributed radial load	29
3.5	Exaggerated view of deformed hole by rigid pin	29
3.6	Iterative procedure for the determination of the contact angle θ_B	31
3.7	Schematic of pin locally deforming the hole shape	31
4.1	IFF failure modes [15]	34
4.2	IFF σ_2, τ_{21} fracture plane [15]	35
4.3	Unnotched failure algorithm, continued in Figure 4.4	36
4.4	Unnotched failure algorithm, first part in Figure 4.3	37
4.5	Keon definition compressive characteristic distance	38
4.6	Main program assembly algorithm	41
4.7	Notched failure algorithm, continued in Figure 4.8	42
4.8	Notched failure algorithm, first part in Figure 4.7	43

5.1	Stress concentration factor at hole edge and difference between tool and Lekhnitskii. 100% UD uniform pressure at hole edge, $a = 5$ [mm], $b = 2$ [mm]	47
5.2	Stress concentration factor at hole edge and difference between tool and Lekhnitskii. 100% $\pm 45^\circ$ uniform pressure at hole edge, $a = 5$ [mm], $b = 2$ [mm]	47
5.3	Stress concentration factor at hole edge and difference between tool and Lekhnitskii. 50% 0° , 50% $\pm 90^\circ$ uniform pressure at hole edge, $a = 5$ [mm], $b = 2$ [mm]	47
5.4	Stress concentration factor at hole edge and difference between tool and Lekhnitskii. 100% UD, uniaxial tension at 0° , $a = 5$ [mm], $b = 2$ [mm]	48
5.5	Stress concentration factor at hole edge and difference between tool and Lekhnitskii. 100% $\pm 45^\circ$, uniaxial tension at 0° , $a = 5$ [mm], $b = 2$ [mm]	48
5.7	Change of load reserve factor, r and critical energy ratio throughout iterations	49
5.8	Configuration 1,2 and 3 (left to right) used for assembly verification.	50
6.1	Influence of N for a centered single hole subjected to uniaxial tension (left) and multiaxial tension-tension (right) in a 4D size square plate	53
6.2	Influence of N for a centered single hole subjected to uniaxial tension in a 2D size square plate	54
6.3	Influence of N for a serie of 5 (left) and a rectangular pattern of 4 (right) circular holes in a finite width sheet subjected to uniaxial tension.	54
6.4	Influence of TOL for a centered single hole subjected to uniaxial tension(left) and multiaxial tension-tension (right) in a 4D size square plate	55
6.5	Influence of TOL for a centered single hole subjected to uniaxial tension in a 2D size square plate	55
6.6	Influence of TOL for a serie of 5 (left) and a rectangular pattern of 4 (right) circular holes in a finite width sheet subjected to uniaxial tension	56
6.7	Influence of TOL for a single elliptical (right) and circular hole in a quasi-infinite sheet	56
6.8	Influence of N for a centered single hole subjected multiaxial tension-tension (right) in a 4D size square plate when $TOL = 10^{-6}$	57
6.9	Schematic representation for the calculation of the CPSED whith a higher or lower contact angle	58
6.10	Change in contact angle with increasing bearing stress for Tomlinson, FEA and Sevenois	59
6.11	Effect of directionality on contact angle prediction (FEA) [18]	60
6.12	Effect of clearance on contact angle prediction (FEA) - QI layup [18]	61
6.13	Effect of α on contact angle prediction (Sevenois's model) and comparison to FEA. Clearance 2% - QI layup in coöperation with [18]	61
6.14	Example of the FEM mesh around a hole	62
6.15	Boundary condition	64
6.16	Config. 1, SCF of σ_θ at the hole edge (left) and SCF of σ_y at $y = 0$ (right) when $E/D = 2.5$	65
6.17	Config. 1, SCF of σ_θ at the hole edge (left) and SCF of σ_y at $y = 0$ (right) when $E/D = 1$	65
6.18	Config. 2, SCF of σ_θ at the hole edge (left) and SCF of σ_x at $x = 0$ (right) when $W/D = 4$	66

6.19	Config. 2, SCF of σ_θ at the hole edge (left) and SCF of σ_x at $x = 0$ (right) when $W/D = 2$	66
6.20	Config. 3, SCF of σ_θ at the hole edge (left) and SCF of σ_x at $x = x_{hole}$ (right) when $E/D = 2.5$	67
6.21	Config. 3, SCF of σ_θ at the hole edge (left) and SCF of σ_x at $x = x_{hole}$ (right) when $E/D = 1.5$	67
6.22	Difference in SCF between FEM and Tool for a hole in a plate with varying E/D and W/D	69
6.23	Tangential SCF from config. 4 for an unloaded (left) and loaded (right) hole	69
6.24	Biaxial failure envelope for QI AS4-3501 [22]	70
6.25	Biaxial failure envelope for QI IM7-8551 [23, 24]	71
6.26	Biaxial failure envelope for $[\pm 15]_s$ IM7-8551 [23, 24]	71
6.27	Biaxial failure envelope for $[\pm 30]_s$ IM7-8551 [23, 24]	72
6.28	Biaxial failure envelope for $[\pm 45]_s$ IM7-8551 [23, 24]	72
6.29	Biaxial failure envelope for $[0]_8$ IM7-9772 [25]	72
6.30	Uniaxial-Shear failure envelope for $[0]_{32}$ IM7-8552 [26]	73
6.31	Uniaxial compressive and tensile test and predictions for material TH5.698/6 for QI, soft and hard laminate	73
6.32	Discrepancy with experiments from [27] (right) and [28] (left) when the hole size for the determination of the CPSED is varied. OHT = Open Hole Tension, OHC = Open Hole Compression, PHT = Pinned Hole Tension, S = Soft, H = Hard, QI = Quasi-Isotropic, N = Narrow W/D, W = Wide W/D, L = Large hole	75
6.33	Uniaxial tensile (left) and compressive (right) failure for AS4/3501-6 [29], QI CFRP layup, fixed specimen size	76
6.34	Uniaxial tensile and compressive failure for TH5.698/601 [27], Hard, Soft and QI layup, hole diameter: normal = 6.35 [mm], Large = 9.52 [mm]	77
6.35	Uniaxial compressive failure for IM7/8552-1 [30] when changing hole size, fixed specimen size	77
6.36	Uniaxial compressive failure for T800/924C [31] when changing hole size, fixed specimen size, part 1	78
6.37	Uniaxial compressive failure for T800/924C [31] when changing hole size, fixed specimen size, part 2	78
6.38	Biaxial failure strength and prediction [32, 33] for SP-286T300	79
6.39	Biaxial failure envelope for QI laminate of IM7/8552 with 10 [mm] hole [34] and prediction	79
6.40	Failure strength of single hole specimens wrt predictions [35]	81
6.41	Failure strength of holes in series specimens wrt predictions [35]	82
6.42	Failure strength of holes in parallel specimens wrt predictions [35]	83
6.43	Bearing-bypass envelope for QI graphite epoxy laminate [19]	83
6.44	Prediction vs measurement for unloaded hole experiments, unlimited	84
6.45	Prediction vs measurement for loaded hole experiments, unlimited	84
6.46	Prediction vs measurement for unloaded configurations, limited	85
6.47	Prediction vs measurement for loaded configurations, limited	85

List of Tables

4.1	Recommended values for slope parameters p_{21}^c and p_{21}^t [36]	35
5.1	System test results unnotched failure criterion	49
5.2	Verification result of assembly tests	50
6.1	Analysis parameters for optimal α determination	59
6.2	Test cases for comparison between FEA and analytic tool	63
6.3	Least square error for hole sizes below 6 [mm] based on Figure 6.32	75

Acknowledgments

I hereby acknowledge the support of Fokker Aerostructures B.V. and the Department of Aerospace Structures and Materials, Faculty of Aerospace Engineering, Delft University of Technology for their support during the writing of this thesis.

Delft, University of Technology
December 6, 2013

R.D.B. Sevenois

“ Theoretically, a model always matches reality. ”

“ Assumptions are at the basis of all problems in this world. ”

Chapter 1

Introduction

When introducing composite structures as a replacement for (metal) components engineers are confronted with many issues. One of these issues is that the standard, isotropic, stress and failure prediction methods for basic structural elements are unusable. To allow composite structural design, each of these structural elements must therefore be reevaluated. One of these structural elements is a rectangular plate with (un)loaded holes subjected to external loads. Over the years, the complexity of these materials resulted in an abundance of failure prediction methods for this type of structures which often have a limited applicability and questionable reliability [1]. In addition, the more accurate failure prediction models can require significant computational resources which is often unavailable and renders them less suitable for fast prediction of multiple scenarios. There is thus the need for a fast, straightforward, validated method to predict stress and failure in rectangular composite plates with (un)loaded holes.

In this work the development of an analytic tool and its supporting theories for the determination of the stress and prediction of failure in a rectangular orthotropic plate with multiple elliptical holes subjected to arbitrary in-plane loading conditions is described. The tool is intended to be used by engineers at Fokker Aerostuctures B.V. for the design of aerospace structural parts. Hence it is imperative that the analytic tool is easy to use, fool proof and well documented. First, to establish the state-of-the art in stress analysis and failure prediction for composite materials, a literature survey is performed. Next, flowing from the survey, the most suitable methods for the purpose of the tool are selected to serve as a basis for the development of the theory. Finally, the tool is implemented in a software package, verified by hand calculations and validated with experimental data.

The structure of this report is as follows. In Chapter 2 the results of the literature are presented. Next, the theory used to determine the stress field is given in Chapter 3. In Chapter 4 a discussion is provided on the theory for failure prediction followed by verification and validation of the model in Chapter 5 and 6 respectively. A discussion on the usability and validity of the tool is provided in Chapter 7 as well as the conclusions and recommendations.

Chapter 2

Literature Survey

An argued choice for a suitable stress analysis and failure prediction methodology can only be made if the state-of-the-art about these theories, their expansions, advantages and disadvantages is known. For this purpose the scientific literature was investigated by the author in a previous study [37]. The discussion below is a brief summary of this study.

2.1 Stress Analysis

The mathematical determination of stresses in any structure can be performed using two methods: analytic analysis or Finite Element Analysis (FEA). In analytic stress analysis the problem to be solved is reduced to solving a set of equations which represent the stress state with respect to the boundary conditions. However, due to the complexity of some problems, this process often involves assumptions and simplifications. Fueled by the need for solutions of problems for which no analytic solution exist, FEA [20, 38] is currently one of the most popular methods for the analysis of stress fields. While fairly easy to use, however, it can also be dangerous in the hands of an unexperienced engineer/scientist. In the following sections both methods are briefly discussed.

2.1.1 Analytic Stress Analysis

In literature three methods for analytic determination of the stress field exist: “Lekhnitskii Formalism” [4, 39], “Stroh Formalism” [40, 41] and approximate analytical methods [42, 43].

During the sixties and seventies Lekhnitskii [4] and Savin [39] provided the basis for what is now called “Lekhnitskii Formalism”. This method essentially generalizes Muskhelishvili’s approach for solving two-dimensional deformations of isotropic materials [44] with complex stress analysis. Lekhnitskii [4] and Savin [39] obtained solutions for circular, elliptical, triangular and square holes in, mainly, infinite orthotropic plates. Lekhnitskii’s approximate solution for stresses around rectangular and square openings in orthotropic plates was further

improved by De Jong [45] who used a Cauchy type integral instead of a series to approximate the boundary conditions. Sufficient accuracy was obtained by using only the first three terms of the series after which numerical values were obtained for six laminates under various loading conditions. In a similar fashion Rajaiah [46] also obtained the solution for quasi-rectangular holes in an infinite orthotropic plate by using the superposition principle but focused his work on finding the configurations leading to minimum stress concentrations. In the meantime, the “Lekhnitskii Formalism” became well known in the engineering community which led to the release of ESDU85001 [47] in 1985 by the Engineering Sciences Data Unit (ESDU). This document contains explicit equations for the stresses around circular holes in infinite orthotropic plates. By 1995 a Fortran computer program (ESDUpac A8501) which performs the calculation automatically was added. Expanding the Formalism continued when Tung [48] provided an approximate solution for the case when the material is close to isotropy or displays specially orthotropic behaviour. This case was initially ignored by Lekhnitskii because his solution produced a singularity. Tung found that, by letting the roots of the material eigenvalues (complex constants which characterize the anisotropy of a material) differ a small amount, a solution can be obtained while the discrepancy between the results and actual values is within one hundredth of a percent. In 1988, the concept of finite size composite laminates was introduced in the Formalism by Lin and Ko [49]. They obtained solutions for a single elliptical hole in a rectangular finite width plate by using a Laurent series in conjunction with the least squares boundary collocation method. The hole is mapped using a complex series and the square boundary is approached using a Taylor series. The stresses in the doubly connected region are obtained by truncating the series to a finite series after which suitable points on the inner and external boundary are chosen. The stresses are imposed at these points to satisfy the boundary conditions by the “least-squares boundary collocation method”.

Some time later Xu [50] recognized that the work provided by Lin and Ko [49] and Gerhardt [51] is good but suffers from computational drawbacks as long CPU time and low accuracy. In order to reduce these drawbacks, Xu used a Faber series for the stress function instead of a Taylor series. Additionally, his solution allows for the introduction of any plate boundary shape in contrast to the rectangular shape by Lin and Ko. Again the unknown coefficients are determined using the “boundary collocation method” as also used by Lin and Ko [49]. In the current solution the inner boundary can be satisfied accurately (error less than 10^{-5}) while the outer boundary can be well satisfied to ensure a relative error within 1%. In the same year Xu [52] published an expansion of this work to account for multiple (unloaded) elliptical holes in finite width plates. Xu claimed that the accuracy of this method is equal to this from his previous research and that considerably less computation time is required. No comparison to FEA was presented and therefore it is not proven that his results are accurate. By further developing his work, Xu [12] expanded the formulation of the stress function to incorporate multiple loaded holes. The stress function is extended with a logarithmic part and the same method of solving is used. After the findings by Xu, developments with respect to a finite size plate solution have only been presented by Hufenbach [53, 54] who incorporated the effects of hygrothermal loading and a layer by layer analysis for the determination of first ply failure. This is obtained from the average strain by assuming that the strain in every layer is equal, as is often done in classical lamination theory. His work has been validated with results from FEA.

On the subject of infinite plates Daoust and Hoa [55] investigated the analytical solution

for triangular holes. By introducing a single parameter any shape of triangular hole can be analysed. On this basis Ukadgaonker [56] investigated the stresses in laminated plates subjected to uniaxial, biaxial and shear stresses. Already it was recognized that a similar method can be applied for different hole shapes. In addition, similar to Daoust and Hoa, by introducing a parameter which links tension/compression stress in x and y direction, Gao [57] solved the problem for an infinite plate subjected to biaxial loads with an elliptical hole without having to use the superposition principle. An explicit expression was obtained by using an elliptic-hyperbolic coordinate system in contrast to the often used cartesian or cylindrical system. Whitworth [58] used the solution from Lekhnitskii for anisotropic infinite plates with holes to investigate the effect on the stress field when the fibre orientation is changed. Early 2000, Ukadgaonker [59] adapted the “Lekhnitskii Formalism” with the aid of the Schwarz-Christoffel formulation to obtain the stresses around arbitrarily shaped holes in an infinite plate subjected to any combination of in-plane loads. Ukadgaonker proposed a mapping function which, if provided with the right coefficients, can map any hole shape to a unit circle. Subsequently, a very methodical approach to determine the stress function was introduced which returns in all of his later work. Due to the superposition principle it is possible to split the solutions of the stress functions into the sum of the solution for a pristine plate subjected to in-plane loads and the solution of the hole shape when a negative of the load is applied to its boundary. Ukadgaonker obtained the solutions for several hole shapes and loading cases. In the same year Ukadgaonker [60] modified this work to accommodate in-plane moments at infinity. In 2005 the results of the analyses were compared to FEA [61] from which it was concluded that there is an excellent agreement between both. Since Ukadgaonker, few developments for the “Lekhnitskii Formalism” and solving the stress-state problem itself were presented. Most recent works focus more on the effect of changing fibre orientations and looking for configurations which produce minimum stress concentrations in the plates. Nageswara [62] does this for square and rectangular cut-outs while Sharma [63] investigates circular, elliptical and triangular shapes.

Up to now this discussion mainly concerned problems with finite and infinite symmetrical or orthotropic plates with one or multiple unloaded holes. Progress has also been made with other configurations. The case of unsymmetric laminates has been investigated by Becker, Chen and Ukadgaonker [64–66]. In these works several hole shapes in an infinite plate are investigated with incorporation of the bending-extension coupling effect. Configurations which involve loaded holes have also been investigated. Already mentioned was the work by Xu [12] who derived expressions for finite width orthotropic plates with multiple loaded holes. Xiong [2, 67, 68] derived expressions for multiple pin-loaded holes with biaxial loading conditions. Using the minimum potential energy principle, Xiong avoids the issues originating from the “least square boundary collocation” method which resulted in a versatile method for stress analysis. Gruber [69] analytically performed a layer by layer analysis in conjunction with a parameter study to determine the optimal laminate layout for fasteners. Solutions for plates with holes containing a rigid/semi-rigid inclusion have also been obtained. Examples are Berbinau and Soutis [70], Zheng [71] and Lin [72].

Next to the “Lekhnitskii Formalism” there also exists another method for the analysis of two-dimensional deformation of an anisotropic linear elastic solid. This method is called “Stroh Formalism”. The “Stroh Formalism” can be traced back to the work of Eshelby [73] and Stroh [74, 75]. Similar to the “Lekhnitskii Formalism”, an Airy stress function is used to obtain the stresses in the plate. By assuming a suitable function which satisfies the boundary

conditions, the stresses and strains of the problem can be obtained. The major contributors to this method are Ting and Hwu [40, 41] who both devoted a lot of studies and a book to the subject. Ting started out by investigating the effect of change of reference coordinates on the stress analyses of anisotropic elastic materials [76]; this to facilitate his further research for the analysis of stress singularities in anisotropic wedges [77, 78]. In later work Ting investigated the role of the Barnett-Lothe tensors and the issues when the matrix \mathbf{N} in the eigenrelation $\mathbf{N}\boldsymbol{\xi} = \mathbf{p}\boldsymbol{\xi}$ is non-semisimple [79, 80]. In 1992 Ting proposed a generalized Stroh formalism for generalized boundary conditions [81] which will eventually form the basis for his book “Anisotropic Elasticity, Theory and Applications” [40] in 1996. In this book, next to the explanation of basic theory, Ting bundled all his and the existing work from other authors to provide a thorough investigation into Stroh Formalism and its defining parameters (Barnett-Lothe tensors, material eigenvalues, etc...). In the book, Ting also presents some applications of the Formalism for stress analysis. These are mainly applications in infinite space, half-space, bimetals, wedges and cracks in plates as well as applications to elliptic holes, inclusions and surface waves. Additionally, an attempt is made to generalize the Stroh Formalism for three-dimensional deformations. After publishing his book Ting continued to investigate the formalism and provided more insight into the physical meaning of Barnett-Lothe tensors [82]. In 1999 Ting presented a modification to the “Lekhnitskii Formalism” which simplifies the classification of materials [83]. In 2000 Ting provided a summary of developments since 1996 [84]. It appears that the “Stroh Formalism” is especially popular in the analysis of wedges, cracks, inclusions and the characterization of surface waves and piezoelectric materials. Some developments were made in the analysis of stresses around holes but so far only elliptical holes were investigated. After 2000 the most of Tings works were on the subject of surface waves [85–87].

Hwu started as a researcher in 1989 by presenting an analysis of the problem of an elliptic inclusion in an anisotropic plate based on the “Stroh Formalism” [88]. In the following years Hwu expanded his work to include any type of opening in an infinite plate [89], solve thermal problems [90] and any type of inclusion [91, 92]. In 1994 Hwu developed a special boundary element for the numerical analysis of multi-hole regions [93]. Later on, besides other publications, Hwu mainly focuses on the coupled stretching-bending problem [94–97]. His most important publication is, obviously, his book: “Anisotropic Elastic Plates” [41]. This book can be seen as an extension to Tings book [40] with a focus on problem solving and more recent developments. Next to the basic theories subjects as wedges, interfaces, cracks, holes, inclusions, contact problems, piezoelectric materials, thermal stresses and boundary element analysis are also discussed. Apart from Ting and Hwu also others have used the “Stroh Formalism” in their research. Gao [98] studied the use of conformal mapping for almost-circular holes. The topic of (acoustic) surface waves has been especially popular in recent years [99–102]. Also, behavioural prediction of piezoelectric materials with or without holes/inclusions has been reported [103–105]. Although the “Stroh Formalism” has been applied to many subjects, no solutions have been presented for the analysis of finite width anisotropic plates with multiple (un)loaded holes.

Next to the “Lekhnitskii Formalism” and “Stroh Formalism”, several authors have attempted to find approximate, engineering wise easier, methods for the determination of stresses around holes in (finite) width plates. Mostly, these methods are a derivation from the exact analytical solutions and are often limited to the determination of stresses in specific problems. In 1975 Konish and Whitney [106] recognized that the methods used for isotropic materials to

determine stress concentrations cannot simply be transferred to composites because the stress in the laminate is very dependent on the chosen lay-up which shifts the location of the highest stresses. Additionally, at that time, current techniques to determine the stress field around holes in anisotropic plates were cumbersome to be used for engineering purposes. Therefore Konish and Whitney identified two other approximate methods to determine the critical stresses. A solution for the stress field can either be obtained by scaling the isotropic solution with a measure for the anisotropy or extending the isotropic solution to account for anisotropic materials. After comparing both methods to the exact solution it was concluded that scaling the isotropic solution leads to unsatisfactory results while extending the isotropic solution produced good agreement with results in cross-ply dominated laminates. The results are poor when unidirectional material is used. The approximate solution of Konish and Whitney is restricted to problems where uniaxial tensile loading in the x direction is applied in an infinite plate with a central circular hole. Also, only the stresses in a radial direction perpendicular to the loading can be obtained. For other hole shapes, apart from the exact solution, one is left with the isotropic solution. For isotropic plates the way to (easily) determine stress concentrations around holes is documented in Peterson's Stress Concentration Factors [107]. This book contains fast methods to determine stress concentrations for a whole number of cases. These cases range from isotropic plates with holes, notches, cracks, grooves, fillets, etc..., each of which can be loaded or reinforced. Since the third edition a small section is also dedicated to elliptical holes in infinite orthotropic plates in which the solutions from Tan [108] are presented. Tan performed research to determine correction factors to incorporate the effect of a finite width in anisotropic plates. In 1988 [42] this research was started to present a closed-form solution for anisotropic plates with a central elliptic opening. Two finite width correction factors are proposed for an ellipse size ratio $a/b \geq 1$ and $a/b \leq 4$. These correction factors are only valid for the problem of uniaxial loading and a centered elliptical hole (the origin of the hole is the origin of the coordinate system). They were compared to experimental data in [109] from which it is concluded that a good comparison with reality is present. Later, these findings have also been published in Tan's book on stress concentrations [108].

Zhang [110] derived an approximate solution for stresses around pin-loaded holes in symmetric composite laminates using the "Reissner variational principle". In order to be able to use this principle one first has to compute the stress and displacements on the hole edge from the "Lekhnitskii Formalism". Next, a power and exponential function is employed to estimate the distribution around the hole. After comparing the results to experimental data it was concluded that there is a good agreement between both. In the same year Soutis [111] devised an improvement for the solution of Konish and Whitney by incorporating biaxial loading. His solution has its limitations because it is only valid for infinite plates and only stresses along the two principle axes can be obtained. Although in good agreement with the analytical solution, the degree of accuracy of the approximate method is strongly influenced by the laminate lay-up and the biaxiality ratio. For laminates with mainly 45°plies the agreement is excellent while the analysis of unidirectional laminates can become inaccurate up to 32%. In 2007, Russo [112] published a hybrid theoretical-numerical method for determining stresses in finite width laminates containing a circular hole subjected to uniaxial tensile loading. The model is based on a correction function for the stress distribution in a infinite width plate which is determined by comparing the infinite analytical results to finite size results from FEA. A comparison between numerical and experimental data resulted in an accuracy within 2-3% of the experimental values. Additionally, in contrast to the model from Konish and Whitney [106],

the model is not restricted to certain laminates and is therefore an improvement.

Although approximate methods greatly simplify the determination of the stress field around holes, they are restricted to very specific problems. Because of this none of the existing approximate solutions can efficiently account for the case of a finite width plate with multiple elliptical holes at random locations. The use of approximate methods for the problem at hand is therefore excluded. Compared to the “Lekhnitskii Formalism”, “Stroh Formalism” has remained in the background as a method of choice for many researchers which developed solutions for problems with anisotropic plates. By inspecting both methods the following can be concluded: solutions exist for the problem at hand which uses the “Lekhnitskii Formalism” [2, 50] while, although it is possible, no solution has yet been presented by the “Stroh Formalism”. The “Stroh Formalism” is mathematically more elegant because of the use of tensors and matrix notation which simplifies changing coordinate systems. For both methods, however, a mapping to the complex plane is required to be able to solve the problem. Since this is regarded as the most difficult part of the solution algorithm, one can conclude that the difference between the “Lekhnitskii Formalism” and “Stroh Formalism” is minimal. Therefore, and because a solution based on the “Lekhnitskii Formalism” already exists, the “Lekhnitskii Formalism” will be used in the eventual analytic tool.

Within the “Lekhnitskii Formalism” Lin [49] and Xu [50] presented a solution for the case of a finite width plate with multiple (loaded) holes using the “least squares boundary collocation method”. Xiong [2, 67, 68] presented a method for multi-fastener finite width plates using the minimum potential energy principle. It is either one of these methods which will be used in the analytic tool. The decision is argued in Chapter 3.

2.1.2 Finite Element Analysis

Since the first use of FEA in 1960 [20] much progress has been made and a standard methodology for FEA has been formed. First the continuum to be analysed is divided in a finite number of parts (elements). The behaviour of each element is defined by a number of parameters. Next the solution of the complete system is obtained by solving the mathematical rules set for each element for the applied boundary conditions. The evolution of FEA and the implementation of several methods for analysis is shown in Figure 2.1.

Due to the discretization approximation of the continuum, problems may arise during analysis. First, it is not always easy to ensure that the chosen displacement functions will satisfy the requirement of displacement continuity between adjacent elements. Second, by concentrating the equivalent forces at nodes, equilibrium conditions are satisfied in the overall sense only. Local violation of equilibrium conditions within each element and on its boundaries will thus usually arise. Convergence problems may arise because the assumed element shape functions limit the infinite degrees of freedom which may result in never reaching the true minimum energy state of the continuum. In general, accuracy and singularity problems improve as the amount of elements is increased. Other errors may occur due to the computation capabilities of the used computer. As the computer uses finite (rounded-off) numbers for computation the accuracy of the calculation is reduced every time an operation is performed. This reduction of accuracy is mostly quite small as modern computers can carry a large number of significant digits. Many of these possible errors can be avoided by appropriately modeling the problem in the computer environment. To do this, the choice of element shape and mesh size is crucial.

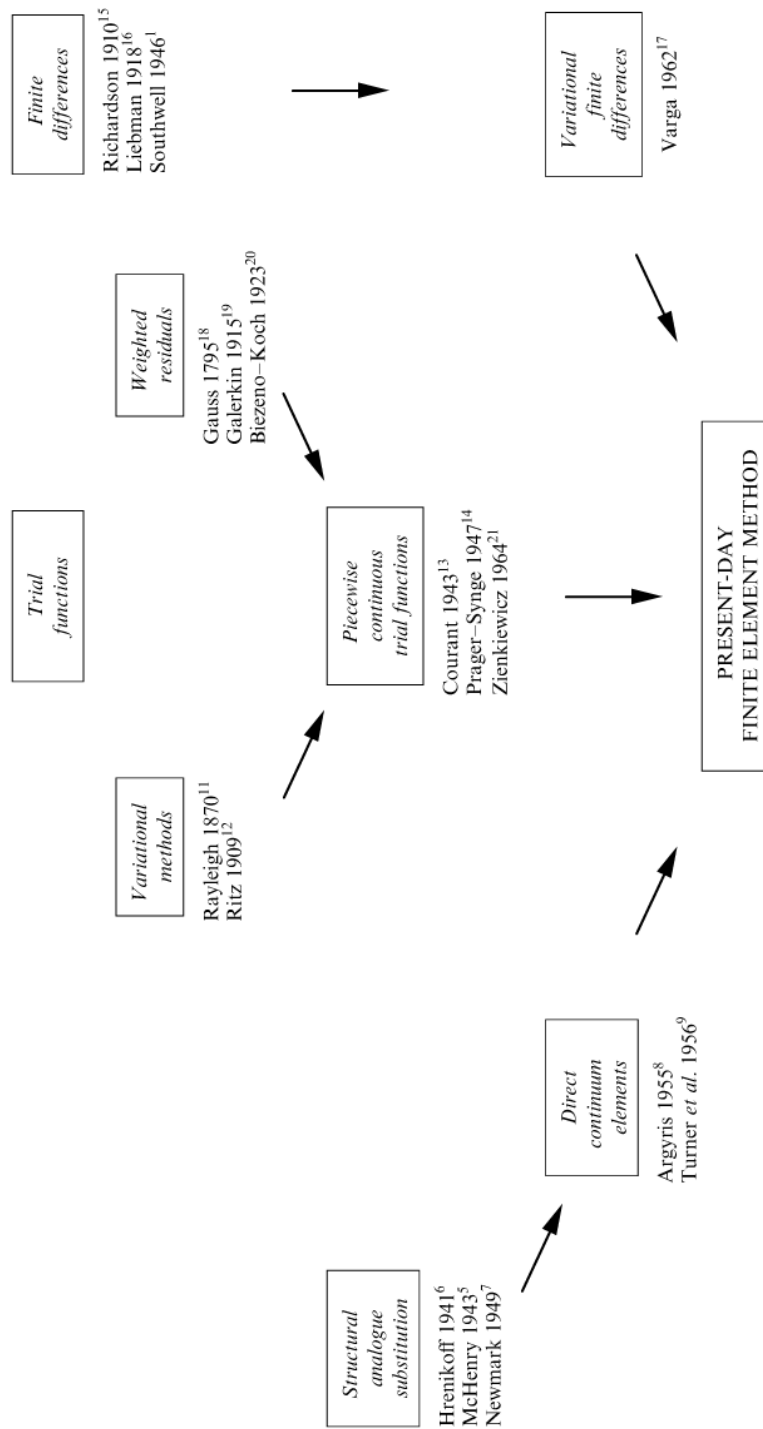


Figure 2.1: Evolution of FEA, references can be obtained from [20]

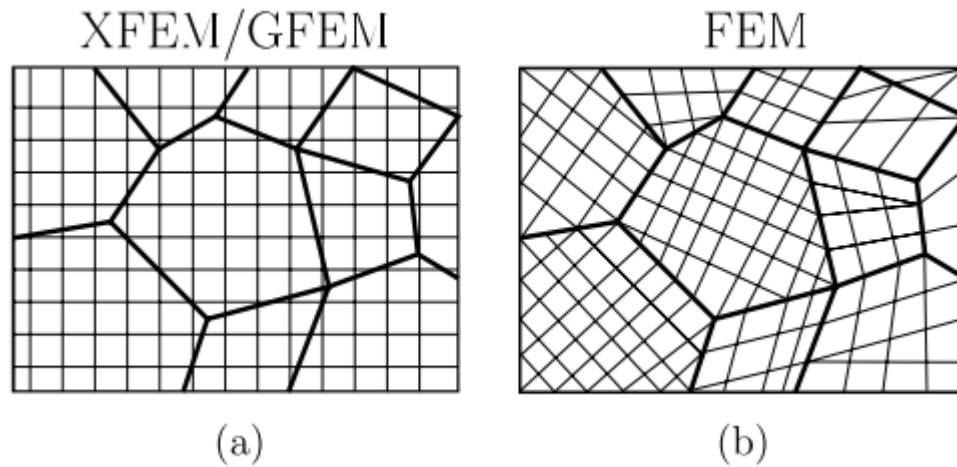


Figure 2.2: Discretizations of a grain boundary problem for (a) an XFEM/GFEM model with a structured (Cartesian) mesh and (b) a FEM model [21]

There exists, however, a multitude of elements and infinite possibilities of meshing. Therefore: “Although the finite element method can make a good engineer better, it can make a poor engineer more dangerous” [38]. It takes skill and knowledge to obtain good results.

Examples of researchers who investigated the stress field around holes in composite laminates are Gerhardt [51], who proposed a hybrid-finite element approach for stress analysis of notched anisotropic plates, Shiau [113], who investigated the effect of variable fiber spacing on the stress concentrations by defining a new triangular plane stress element and Ozbay [114] who used FEA to analyse elastic and elasto-plastic stresses on the cross section of a composite material with a circular hole subjected to in-plane loads. FEA has also successfully been used to investigate (progressive) failure in notched composite laminates. For this the reader is referred to Section 2.2.2.

One of the problems with FEA is that it is required for the elements to follow the physical boundaries of the problem. This leads, amongst other effects, to the requirement of remeshing the structure when evolution of damage is investigated. Additionally, at the crack tip, due to this requirement, a singularity exists at the tip of, e.g. a crack. To avoid this, Belytschko developed the eXtended Finite Element Method (X-FEM) [21,115,116]. X-FEM is a numerical method to model internal (or external) boundaries such as holes, inclusions, or cracks, without requiring the mesh to conform to these boundaries. This allows for faster and more reliable analysis of dynamic stress fields including progressive analysis of damage because it is not necessary to re-mesh the structure between loading steps which is illustrated in Figure 2.2. To simulate the boundaries a method is derived to ‘enrich’ the elements based on the Partition-of-Unity Method (PUM). An advantage of X-FEM is that more accurate numerical results can be obtained than with FEA. The rate of convergence, however, is not optimal with respect to the mesh parameter “ h ”. The X-FEM method has mainly been used in the (progressive) analysis of cracks but also in the modeling of solidification problems, fluid mechanics, biofilms, piezoelectric materials and complex industrial structures.

For the purpose of this project, FEA will be used as a validation for the analytic tool. The

choice for FEA has multiple reasons. Firstly, the analysis of a linear elastic stress field around holes is well established in the engineering community using FEA methods. Secondly, X-FEM was mainly developed to provide a better method for the prediction of damage growth. It is recognized that one could propose not only to validate the stress field, but also validate the ultimate failure prediction using finite elements. This would put X-FEM in the advantage but it would also require to build a significantly complex progressive damage model. This would require additional research and time which is out of the scope of this project. Hence the ultimate failure prediction has to be validated with test data. At Fokker Aerostructures B.V. the software in use for stress analysis is MSC Patran/Nastran®. The MSC.Laminate Modeler [117] is a readily usable tool to design and analyse composite plates. The solver includes the use of QUAD4/8 and TRI3/6 laminate shell elements to account for bending and extension deformation as well as HEX8/20 and WEDGE6/15 elements to model the flexibility of the laminate in all directions.

2.2 Strength Prediction

Next to the determination of the stress field, one has to be able to evaluate the field for the estimation of failure. Several researchers have developed methods to do this such as the Point Stress (PSC) and Average Stress Criteria (ASC) from Whitney and Nuismer [10] or the Linear Elastic Fracture Model (LEFM) by Waddoups [9]. More advanced methods try to predict the growth and development of damage which lead to failure in an area called progressive damage modeling (e.g. [118, 119]). Many, not to mention all, models determine the notched strength of laminates by using the unnotched mechanical properties of a lamina or laminate which are determined from micromechanics and strength fracture criteria. Therefore first an overview of the existing strength criteria for an unnotched laminate in Section 2.2.1 is given followed by a discussion on the determination of notched failure strength in Section 2.2.2.

2.2.1 Unnotched Strength

The existing failure criteria for unnotched laminated composites can be categorized in multiple ways. Interactive criteria [120, 121] take into account the stresses and strengths from multiple directions while non-interactive criteria are composed of multiple requirements for each loading direction. Some criteria have to be evaluated on the ply level while others are only valid for the entire laminate. In addition, criteria on a phenomenological [5, 122] basis exist. In the following the author is more interested in the performance and application of the existing theories rather than their categorization. This has the consequence that the theories presented are discussed in a more intuitive way.

The most widely used failure theories are included in composite textbooks as Daniel [123] or Kassapoglou [16]. These are the “Maximum Stress or Strain”, “Tsai-Wu”, “Tsai-Hill” and “Hashin-Rotem” criteria. According to the “Maximum Stress” criterion, failure occurs when at least one stress component along the principal material axis of a lamina inside a laminate exceeds the strength in that direction. The “Tsai-Hill” failure criterion is an energy based interactive criterion similar to the Von-Mises criterion for isotropic materials. The “Tsai-Wu” criterion, proposed by Tsai and Wu [120], was one of the first attempts to develop a general theory for failure in anisotropic materials. An advantage of the “Tsai-Wu” criterion is that it

is operationally simple for implementation in a computer environment and is expressed in a single criterion in which all strengths are incorporated. The “Hashin-Rotem” criterion [122] is a collection of phenomenological criteria, e.g. for each failure mode of the laminate a different criterion is used which are evaluated simultaneously. The criterion consists of two separate failure modes, one for fibre failure and one for interfibre failure. Next to the aforementioned, an enormous amount of other criteria or expansions of existing ones were developed by other researchers. Examples are Yamada and Sun [121] who proposed a failure criterion based on the assumption that, upon ultimate failure, all transverse plies have already failed due to microcracking which leaves only the plies in the loading direction. Whitworth [124], who proposed a failure theorem based on the strain energy and Hart-Smith [125, 126], who proposed several adaptations of the maximum stress theory. By 1991, partly due to this uncontrolled growth of failure criteria, it became clear that doubts existed about whether “failure criteria in the current (1991) use were genuinely capable of accurate and meaningful prediction of failure in composite components” [127]. In an effort to resolve this issue, it was decided to attempt to establish the state-of-the-art of failure prediction in composite laminates by launching a project which is now known as the “First World Wide Failure Exercise” (WWFE-I) [1, 128, 129]. In this project, managed by Hinton, Kaddour and Soden, leading researchers in the field were asked to predict failure in a predefined set of test cases [130] of several composite laminates under various in-plane loading conditions. This using their favourite failure theory. The exercise was divided in two parts: part A [128] in which the theoretical results of the contributing theories were compared and part B [129] in which theoretical results were compared to experimental results. Ultimately, the exercise was expanded with a part C which included additional failure criteria which were developed during the course of the exercise [131] and a recommendation to designers [1] of composite structures. In the end a total of 19 different failure theories were evaluated from which it was concluded that 5 theories had the most utility for designers. These are the theories provided by Zinoviev [132, 133], Tsai [134, 135], Bogetti [136, 137], Puck [5, 138] and Cuntze [139, 140]. No straightforward conclusion was given on which theory was best to use. In predicting the final strength of multidirectional laminates none of the failure theories were able to predict within $\pm 10\%$ of the measured strengths in more than 40% of the cases. Puck and Cuntze performed best being able to predict within $\pm 50\%$ in 85% of the test cases. For final failure it is recommended to use Puck or Cuntze’s theory.

In an effort to improve the predictions from WWFE-I. Davila [6] proposed a set of six phenomenological failure criteria denoted LaRC03. A mix of methods ranging from fracture mechanics to adaptations of the Mohr-Coulomb interaction criterion. Three criteria are proposed for matrix cracking and three criteria are proposed for fibre failure. Using these criteria and the definitions of the non-trivial parameters (e.g. σ_2^m , τ_{eff}^m , etc...), which are described in [6], the following ply properties E_1 , E_2 , G_{12} , ν_{12} , X^T , X^C , Y^T , Y^C , S^L , $G_{Ic}(L)$ and $G_{IIc}(L)$ are required to determine failure. The properties α_0 and η^L (angle of the fracture plane and longitudinal coefficient of influence) can be assumed or experimentally obtained (additional accuracy). A comparison of the use of these failure criteria with results from WWFE-I led to the conclusion that LaRC03 is a significant improvement over the commonly used Hashin criteria. This statement should however be approached with caution. Only two test cases from WWFE-I are compared and the description of how the results for the laminate final failure results are obtained is missing (progressive failure model or first-ply-failure? (FPF)). Nevertheless, LaRC03 must however be quite useful as in later years, Pinho, in cooperation

with Davila, expanded LaRC03 for shear non-linearity and general three-dimensional stress to LaRC04 [7]. Additionally, improvements for some criteria from LaRC03 are presented. A similar comparison to test data is provided as in LaRC03. This again adds to the uncertainty in the correctness of LaRC04 but, as with LaRC03, it can be noted that they were used for the assessment of the damage tolerance of postbuckled hat-stiffened panels by Bisagni [141] and to develop a continuum damage model by Maimi [142]. Also Vyas [143] (in cooperation with Pinho) constructed from LaRC04 a constitutive damage model for multidirectional composites incorporating the effects of hydrostatic pressure and softening due to matrix cracking by using a finite element formulation. The use of LaRC04 in progressive models indicates that the criteria are only capable of predicting the onset of damage. Las [144] attempted to investigate the differences in the use of the LaRC04 and Puck criteria for progressive failure analysis up to final rupture. In his progressive analysis, upon detection of failure, the ply stiffnesses associated with a failure mode (matrix or fibre) are immediately reduced to zero. Obviously, since this approach does not take into account the gradual stiffness degradation, the results did not satisfactory match the experiments and no conclusion could be made. Regardless of other theories, most recently, Satheesh [145] decided to return to the simpler failure criteria (maximum stress, Tsai-Wu and Micromechanism failure) to construct a Most Conservative Failure Envelope (MCFE). This most conservative envelope is subsequently used in a genetic algorithm to construct minimum weight laminates.

After the conclusion of WWFE-I in 2004 it was clear that a lot of improvements in failure prediction of composite laminates still had to be made. Additionally, the desire was expressed to perform a similar exercise for laminates under general 3-dimensional loading (e.g. thick laminates, etc...) and laminates with stress concentrations (e.g. notches, cracks, etc...). These desires were eventually converted in the Second World Wide Failure exercise (WWFE-II) [146] and the Third World Wide Failure exercise (WWFE-III) [147]. Originally it was envisioned to have WWFE-II completed by the end of 2011 [148]. However, as often happens, delays resulted in the recent release of Part B (March 2013) [149] in which the contributing theories are compared to experiments. In WWFE-II a total of 12 models participated, some of which also participated in WWFE-I (e.g. Bogetti [150], Chamis [151], Puck [152], etc...). The models presented are increasingly complex with three of the twelve participants resolving to FEA-codes for the analysis of the stresses [153]. Furthermore it is concluded that the better theories are the ones from Pinho [154], Carrere [155] and Puck [156] producing estimations within $\pm 10\%$ of the experimental values in approximately 30% of the cases and estimations between $\pm 10\%$ and $\pm 50\%$ in a further 50% of the cases.

From the discussion above it can be concluded that, for two-dimensional loading, the phenomenological failure criteria by Puck [5], LaRC03 [6], LaRC04 [7] and the Tsai-Wu [8] are the best criteria to determine the onset of failure (FPF) with an accuracy of $\pm 10\%$. To determine ultimate failure using semi-analytical means one needs to construct an algorithm on the basis of a progressive failure model in which one takes the degradation of lamina properties due to matrix cracking and the non-linearity of the material into account. An accuracy of $\pm 50\%$ in 85% of the cases has been shown for Puck's progressive model [5]. For this progressive analysis, however, it should be noted that more test data needs to be available than the linear lamina stiffnesses, strengths and fracture energies. Additionally, it is advised to include the effect of thermal stresses and moisture absorption due to manufacturing into account. The progressive analysis, although more accurate, will also lead to increased computing time.

The attentive reader may have noticed that the discussed failure criteria are only applicable

to laminates constructed from unidirectional (UD) laminae. This has multiple reasons. First, the available knowledge on failure in unidirectional laminae is much greater than for woven laminae. Secondly, woven laminae are even more complicated than UD laminae because of their three-dimensional internal structure making it difficult for researchers to define a relatively simple description of their behaviour. Thirdly, in the aerospace industry, for plates, shells and pressure vessels, it is preferred to use UD laminae because of their anisotropic characteristics. This, however, does not imply that woven laminae are not useful. They are especially suitable for the absorption of impact damage, crack stopping and improving the residual strength after occurrence of damage. Examples of some failure models can be found in [157–159]. For this thesis, it is not of interest to further investigate this topic since the aerospace industry uses mostly UD laminae. Therefore, use of a failure model which includes UD and fabric material will result in unnecessary complexity of the tool.

2.2.2 Notched Strength

In metals, one can reliably use the maximum stress in the structure to predict failure. In laminates, this cannot freely be done (it is possible but one has to be careful) because a laminate is a non-homogeneous material. Over the years several researchers have developed and expanded several methods to predict failure of a composite laminate with stress concentrations (e.g. notches). Some rely on the Point Stress Criterion (PSC) or Average Stress Criterion (ASC) from Whitney and Nuismer [10]. Others follow a Linear Elastic Fracture Mechanics (LEFM) approach [9] or apply a fictitious crack model [160] in conjunction with a progressive damage approach. Many of these methods rely on the ability to accurately predict the stress field around a (growing) damage and use FEA or a simplified analytical solution. Some also require the unnotched strength σ_{un} or the critical energy release rate G as input.

One of the earliest methods to predict failure was proposed by Waddoups et al [9]. Waddoups model, which is currently known as the “inherent flaw model”, assumes that a characteristic crack length a exists away from a notch. When the energy in the region of the “crack” is higher than the critical energy, the plate is considered failed. The length a and critical energy K_{Ic} are obtained from experimental data. Soutis et al [161] used LEFM as a starting point to predict (progressive) failure in compression loaded open hole specimens. The notch is modeled as a hole with two cracks with an applied stress on the surface. Then, using the in-plane fracture toughness and remote stress, a model for the stable crack growth is derived. Comparison to experimental data [31] resulted in the conclusion that for UD laminates, the Soutis model is able to accurately predict the compressive strength, damage zone size at failure and compressive strength for UD composites. In later work [111] the model is expanded to account for biaxial compression tension load.

As an alternative to the LEFM method, Whitney and Nuismer developed the PSC and ASC [10, 162]. In the PSC it is assumed that a characteristic distance d_0 away from the hole edge exists. When the stress at this distance reaches the unnotched material strength, the notched plate is considered failed. In the ASC, if the average stress over some characteristic distance a_0 from the edge of the hole reaches the unnotched strength, the notched plate failed. This leads to two two-parameter criteria (σ_{un} and a_0 or d_0) for which the parameters need to be determined experimentally. The basic models were proposed in 1974. The ASC was further elaborated upon by the authors for the uniaxial tension [163], compression and hole bearing

strength [162] cases. Already it was found that the characteristic distances for compression and tension were no material constants (which was initially proposed). Pipes [164], discovered that the characteristic distance is dependent on the size of the hole and developed a three-parameter strength model based on the stress concentration factor, an exponential parameter and notch sensitivity factor which have to be determined experimentally. Using the increased amounts of curve fitting parameters, it should come to no surprise that this model gave good results with experimental data. In 1982 Garbo [165] recognized the power of the PSC as a simple, effective, readily usable method and generalized it for general far field and bearing loading. Garbo's proposal is to evaluate the stress field in the laminate and evaluate ply-by-ply failure at a characteristic distance R_c from the hole boundary at all angles using an unnotched failure criterion of choice. After FPF one can assume the panel to be broken or perform a post-FPF analysis. Next to investigation of UD materials, Naik and Shembekar [166, 167] used the PSC and ASC to predict the notched strength of fabric laminates. From their investigation, it was concluded that the characteristic dimensions are no material parameters (as was already suspected by earlier authors) and very much dependent on the hole size and stacking sequence. In an attempt to solve this issue, Potti [168] proposed a polynomial formulation for the characteristic length. Although Potti is able to work with changing characteristic lengths, experimental data is still required for its execution. For the analytic tool in this work, however, it is intended to use only the mechanical properties of a single ply as input.

A possible solution for this problem has been proposed by Kweon [3] for the PSC. By assuming new definitions for the characteristic lengths, Kweon was able to determine the distances for the compression and tension case based on the stress field around the hole. There is therefore no need for additional experimental data. Kweon's definition for the compressive characteristic length is: "The distance from the front hole-edge to a point where the local compressive stress by the arbitrarily applied load is the same as the mean bearing stress when a bearing load is applied to the hole edge". Kweon's definition for the tensile characteristic length is: "The distance from the side edge of the fastener hole to a point where the tensile stress by the failure load of the notched laminate is the same as the tensile strength of the notched laminate". In his work, Kweon shows that the new definition for the compressive characteristic length is justified. The definition for the tensile characteristic length, however, is doubtful since it implies that the mean stress in the cross-section should equal the unnotched strength. A discussion on this topic is given in Appendix B. Apart from the issues with obtaining experimental data and non-constant characteristics lengths, several authors have successfully used the PSC and ASC for the prediction of ultimate failure. Xiong [2] used the PSC to (analytically) predict failure in composite joints with multiple fasteners. For tension and compression two separate distances were used which were taken from other research. Xu [169], building on his earlier work in stress analysis [12, 50], obtained strength predictions for finite width laminates with multiple elliptical holes using the PSC, the Yamada-Sun criterion [121] and the characteristic distance from Garbo [165]. His results were within 10% accuracy for a range of QI laminates. More recently, Green [170] re-evaluated the ASC against experimental data and concluded that the ASC is quite accurate except for configurations which exhibit extensive delamination prior to failure. Interest in Whitney and Nuismer's model is also expressed to be used in braided composite plates. Hwan [171] investigated this possibility and determined new characteristic lengths for fabric composites with holes. Additionally, a modification for the variation in strength due to the size of the hole is adapted from [172], which is similar to

Pipes [164] formulation. A good correlation between experiments and results was shown.

Next to the LEFM, PSC and ASC some researchers have proposed other methods to predict ultimate failure. Backlund [160] developed the damage zone model (DZM), which is also called the fictitious crack model. In this model it is assumed that, in the intense energy region next to the notch, a fictitious crack forms when the uniaxial tensile strength is exceeded. When the crack forms, cohesive forces try to keep the crack closed until the crack has a certain length and the crack becomes a real crack. Using the assumptions of a linear decrease in stress from the notch edge and a crack opening for stable and unstable crack growth and a finite element analysis, Backlund was able to predict crack growth and notched strength. In later work with Carlsson [173], the results from the DZM were validated for graphite-epoxy and graphite-PEEK composite laminates. Furthermore, Aronsson extended the model to account for countersunk holes [174] and Hollman [175] used it to predict failure in bolted composite joints. Advantages of the DZM over the aforementioned model are the fact that only the unnotched strength and fracture energy are required. Therefore there is no need for additional experiments. Also, the damage growth can be monitored. Downside is that this is a type of progressive failure model which requires FEA to monitor damage growth and ultimate failure. In an attempt to join the advantages of the PSC (simple to apply) and the DZM (higher accuracy), Eriksson [176] proposed the damage zone criterion (DZC). By assuming a critical length of the damage zone d_I^* and using the critical energy release rate G_c Eriksson was able to obtain a simple relation depending on the plate dimensions and d_I^* . His method is effective and has higher accuracy than PSC but one needs to perform additional experiments to determine the characteristic length d_I^* . A different model is proposed by Liu [177] to more easily predict ultimate failure. Using the stress concentration at the edge the “damaged” stress concentration is calculated by using a geometrical factor, stacking sequence factor and a stress concentration factor from FEA.

Over the years, with the increase of cheap computing power, more methods have emerged to predict progressive failure in notched composite laminates. One of the earliest were Lo et al. [118] who constructed an analytical model on the basis of the PSC and complex stress analysis to predict sequential failure in laminate with stress raisers. Chang [178] performs a similar analysis but uses FEA to analyze the stress field. More recently, Shah [179] created a full size ABAQUS constitutive model which uses the “Tsai-Wu” criterion as a damage initiation criterion to predict failure envelopes for open hole tension and open hole compression specimens. The gradual degradation of the material properties is accounted for by using the ply-discounting approach developed by Knight [180]. Satyanarayana [181] constructed a progressive failure model where the failure criterion is Hashin-Rotem and the degradation model is instantaneous complete stress reduction. Flatscher [182] constructed a constitutive model which incorporates material non-linearity (hardening and softening) and the accumulation of plastic strains. The model is implemented in FEA code and, in subsequent work, compared to experimental data [183] for open hole tension specimens. An excellent agreement with the experimental results is shown.

In the last few years, a type of damage models called “damage mesomodels” have been given more attention. The damage mesomodel is “a continuum mechanics approach which aims to maintain a complete predictive description of the physics of a composite’s degradation during the simulation of structural tests” [184]. On the assumptions that the behaviour of any laminated structure can be reconstructed from the properties of its main constituents, a micromechanical model is constructed which is able to describe the evolution of damage

in a laminated composite. As such, it is able to predict all laminate failure modes and subsequent growth. The model is incorporated in a finite element formulation. These models (e.g. Abisset [184], Farrokhabadi [185], etc...) generally have an excellent agreement with experimental results.

As so much different models exist it would have been strange if no researchers attempted to compare the prediction of existing models. Curtis [186] evaluated three stress criteria, LEFM, ASC and PSC for Quasi-Isotropic (QI) carbon fibre laminates and concluded that the ASC, closely followed however by the PSC and LEFM, performs best in predicting ultimate strength under various loading conditions. The main deficiency of all methods is that they cannot account for progressive failure and delaminations because they lack a micromechanics approach. Toll [187] provided a similar comparison applied to injection moulded composites and also concluded that the ASC gives most accurate predictions with a maximum error of 9%. For PSC the maximum error was 22%. Rao [188] compared and adapted the inherent flaw model and PSC and ASC for the case of reinforced polyester composites. It was concluded that all three criteria, when applied to the specific cases they were designed for (uniaxially loaded laminates), correlate well with test results. Kannan [189] performed a similar evaluation but also included weft-knitted and pultruded composites. In Kannan's work a maximum relative error of 3% and 8% is obtained for UD and QI carbon laminates built from UD plies respectively. The maximum relative error for weft-knitted glass fibre laminates is 10% and for pultruded glass fibre it is 17%. In further work Kannan [190] attempted to use the stress concentration factor from FEA and the unnotched strength for failure prediction which turned out to be highly conservative. Subsequently, modifications were made in the PSC to incorporate the effect of hole size which resulted in a maximum relative error of 10% for knitted glass fiber composite plates. Su [191] applied the PSC, ASC and DZC to graphite aluminium composite plates with holes. Up to a certain hole size a good agreement with experimental results was obtained. This is partly due to the fact that no hole size correction for the characteristic lengths was used. Wang [192] compared predictions obtained from the inherent flaw model and a continuum damage model. The continuum damage model provided the best correlation and is most promising for more accurate predictions.

From the discussion above it is clear that numerous methods to predict ultimate (and progressive) failure in notched composite laminates exist and each one has its own advantages and disadvantages. Keeping the goal of this project (development of an analytic tool for the prediction of failure in anisotropic plates with holes) in mind it can, however, be immediately determined that the methods which rely on some sort of Finite Element code have to be discarded. Therefore the continuum damage models and progressive models are eliminated. This leaves the choice between LEFM, ASC and PSC. A decision on these models is elaborated upon in Chapter 4.

Determination of the Stress Field

In Chapter 2 it is concluded that two methods are suitable to analytically determine the stress field in a finite size plate with holes subjected to in-plane loading conditions. Both methods use the complex stress analysis principle known as the “Lekhnitskii Formalism”. Their application of the boundary conditions, however, is different. The first method, developed by Xiong [2, 67, 68], uses the principle of minimum potential energy while the second, Xu and others ([49, 52, 193]), use the “least squares boundary collocation method”. Both methods are able to accurately predict the stress field. The “least squares boundary collocation method”, however, involves choosing a number of collocation points on the boundaries of the hole(s) and plate-edge. These points have to be chosen wisely or the solution may become erroneous. Therefore, if this method would be used in the analytic tool, it is required for the user to have knowledge about choosing collocation points. Consequently, the tool would not be fool proof which is one of the initial requirements, Chapter 1. Luckily, the method developed by Xiong does not require any user input other than the problem definition and required accuracy of the solution. Hence it is evident that Xiong’s method is the best choice for the analytic tool.

In Section 3.1 the theory by Kweon is expanded to account for multiple holes in a rectangular plate with arbitrary boundary conditions. Arbitrary boundary conditions, however, imply that also load boundary conditions can be placed on the edges of the hole. This can be used to simulate a pin load. For this, it is required to have a good estimate of the stress a pin exerts on the hole edge. This is elaborated upon in Section 3.2.

3.1 Expansion of Xiong’s Method

The basic problem is shown in Figure 3.1. A rectangular plate with m elliptical holes is subjected to distributed loads on the plate as well as the hole edges. These loads can be shear and or normal stresses. The loads on the edges are constant distributed loads while the loads on the holes is a function applied between angle θ_{1m} and θ_{2m} . Consider a two-dimensional anisotropic medium in a Cartesian coordinate system. Then the three-dimensional equilibrium

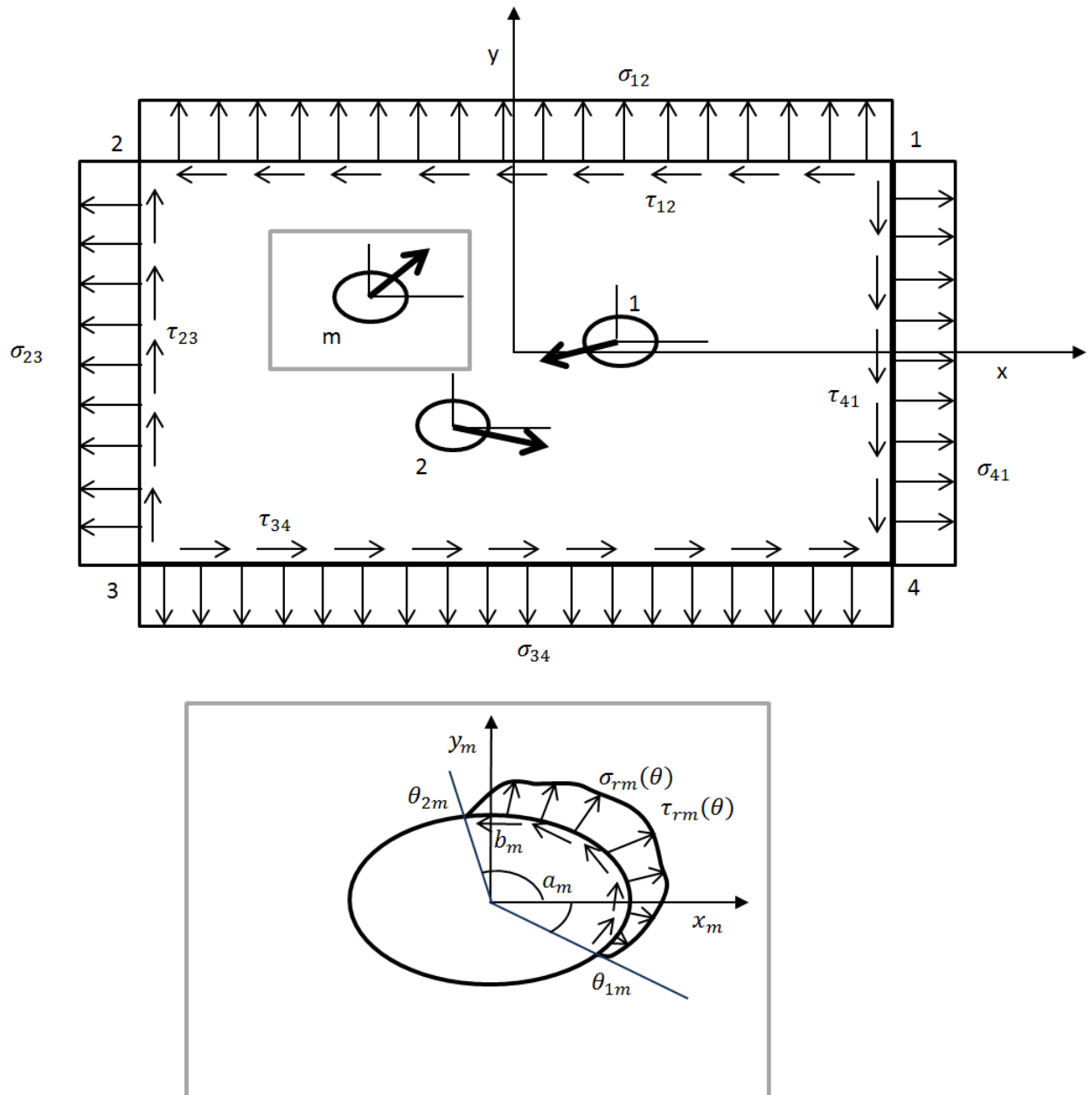


Figure 3.1: A rectangular plate with multiple holes subjected to arbitrary loading

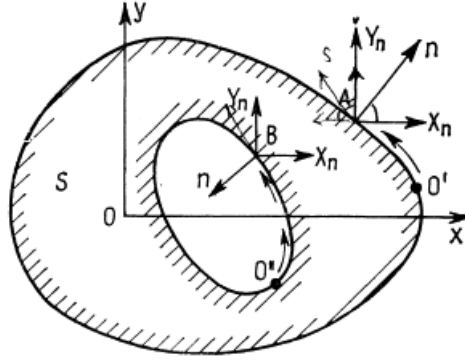


Figure 3.2: Two-dimensional anisotropic body with two contours

equations can be reduced to:

$$\left. \begin{aligned} \frac{d\sigma_x}{dx} + \frac{d\tau_{xy}}{dy} + X &= 0 \\ \frac{d\sigma_y}{dy} + \frac{d\tau_{xy}}{dx} + Y &= 0 \end{aligned} \right\} \quad (3.1)$$

where σ_x , σ_y and τ_{xy} are the normal and shear stress in the body and X and Y are the external force components parallel to the x and y axis. When the body consists of n contours on which forces act as shown in Figure 3.2, the forces on each contour can be expressed as:

$$\left. \begin{aligned} X_n &= \sigma_x \cos(n, x) + \tau_{xy} \cos(n, y) \\ Y_n &= \sigma_y \cos(n, y) + \tau_{xy} \cos(n, x) \end{aligned} \right\} \quad (3.2)$$

To be able to solve the equilibrium equation, Eq. (3.1), the strain compatibility equation is used:

$$\frac{d^2\varepsilon_x}{dy^2} + \frac{d^2\varepsilon_y}{dx^2} - \frac{d^2\gamma_{xy}}{dxdy} = 0 \quad (3.3)$$

where ε_x , ε_y and γ_{xy} are the normal and shear strains in the body. The relation between the stresses and strains is given by Hooke's law:

$$\boldsymbol{\sigma} = \mathbf{C}\boldsymbol{\varepsilon} \quad (3.4)$$

in which \mathbf{C} is the material stiffness matrix, $\boldsymbol{\sigma}$ is the stress and $\boldsymbol{\varepsilon}$ the strain vector. Lekhnitskii [4] derived, on the basis of a complex variational approach, that the solution of the equilibrium and compatibility equation, Eq. (3.1) and Eq. (3.3), in any problem involving anisotropic plates can be reduced to the sum of two stress functions $\varphi_j(z_j)$, $j = 1, 2$. z_j is a complex coordinate variable given by:

$$z_j = x + \mu_j y \quad j = 1, 2 \quad (3.5)$$

With these stress functions the stresses and displacements in the plate can be determined using Eq. (3.6) and Eq. (3.7).

$$\sigma_x = 2\Re \left[\mu_1^2 \frac{d\varphi_1(z_1)}{dz_1} + \mu_2^2 \frac{d\varphi_2(z_2)}{dz_2} \right] \quad (3.6a)$$

$$\sigma_y = 2\Re \left[\frac{d\varphi_1(z_1)}{dz_1} + \frac{d\varphi_2(z_2)}{dz_2} \right] \quad (3.6b)$$

$$\tau_{xy} = -2\Re \left[\mu_1 \frac{d\varphi_1(z_1)}{dz_1} + \mu_2 \frac{d\varphi_2(z_2)}{dz_2} \right] \quad (3.6c)$$

$$u = 2\Re [p_1\varphi_1(z_1) + p_2\varphi_2(z_2)] \quad (3.7a)$$

$$v = 2\Re [q_1\varphi_1(z_1) + q_2\varphi_2(z_2)] \quad (3.7b)$$

In Eq. (3.5) and Eq. (3.6) $\mu_j, j = 1, 2$ are complex coefficients called the material eigenvalues. For orthotropic materials, they are defined by:

$$\mu_1 = \sqrt{\frac{aa - rr}{2}} + i\sqrt{\frac{aa + rr}{2}} \quad (3.8a)$$

$$\mu_2 = -\sqrt{\frac{aa - rr}{2}} + i\sqrt{\frac{aa + rr}{2}} \quad (3.8b)$$

where:

$$rr = \sqrt{\frac{a_{22}}{a_{11}}} \quad (3.9a)$$

$$aa = \left(a_{12} + \frac{a_{33}}{2} \right) \frac{1}{a_{11}} \quad (3.9b)$$

and a_{ij} are the entries in the compliance matrix of the material. For an orthotropic material, the use of μ_j in the ‘‘Lekhnitskii Formalism’’ provides no problems. However, when an isotropic material is used $\mu_1 = \mu_2 = i$, the solution cannot be solved due to a singularity. This can be solved by, upon detection of a isotropic material, letting the roots differ a small amount, see Chapter 2. In this work it is chosen to change to the roots when the layup contains $\pm 44^\circ$ plies instead of $\pm 45^\circ$ degree plies. This results in the following values for μ_1 and μ_2 :

$$\mu_1 = 1.04i \quad \mu_2 = 0.98i \quad (3.10)$$

The complex coefficients $p_j, q_j, j = 1, 2$ in Eq. (3.7) are defined as:

$$p_j = a_{11}\mu_j^2 + a_{12} - a_{16}\mu_j \quad (3.11a)$$

$$q_j = a_{12}\mu_j + \frac{a_{22}}{\mu_j} - a_{26} \quad (3.11b)$$

From Hooke’s law, Eq. (3.4), the relation between the in-plane stress and displacement components can be written as:

$$\sigma_x = A_{11} \frac{\partial u}{\partial x} + A_{12} \frac{\partial v}{\partial y} + A_{16} \left(\frac{\partial u}{\partial y} + \frac{\partial v}{\partial x} \right) \quad (3.12a)$$

$$\sigma_y = A_{12} \frac{\partial u}{\partial x} + A_{22} \frac{\partial v}{\partial y} + A_{26} \left(\frac{\partial u}{\partial y} + \frac{\partial v}{\partial x} \right) \quad (3.12b)$$

$$\tau_{xy} = A_{16} \frac{\partial u}{\partial x} + A_{26} \frac{\partial v}{\partial y} + A_{66} \left(\frac{\partial u}{\partial y} + \frac{\partial v}{\partial x} \right) \quad (3.12c)$$

in which A_{ij} are the in-plane stiffness coefficients of the material. Following Lekhnitskii [4], an appropriate solution for the stress functions $\varphi_j(z_j), j = 1, 2$ for arbitrary boundary conditions is:

$$\varphi_j(z_j) = C_{0j} + \sum_{n=1}^N C_{n_j} z_j^n + \sum_{k=1}^m \left\{ C_{(k+kN)_j} \ln(\xi_{mj}) + \sum_{n=1}^N C_{(k+kN+n)_j} \xi_{mj}^{-n} \right\} \quad (3.13)$$

$j = 1, 2$

where C_{n_j} , $j = 1, 2$ are complex coefficients to be determined through the boundary conditions. ξ_{mj} is the mapping function of the m -th hole to the complex plane given by:

$$\xi(x, y)_{mj} = \frac{-(z_{mj} - z_j(x, y)) + s(x, y, j, m)\sqrt{(z_{mj} - z_j(x, y))^2 - 4R_{mj}^2 t_{mj}}}{2R_{mj}} \quad (3.14)$$

where z_{mj} is the location of the centre of the m -th hole in the complex plane according to Eq. (3.5). R_{mj} and t_{mj} are given below:

$$R_{mj} = \frac{a_m - i\mu_j b_m}{2} \quad (3.15a)$$

$$t_{mj} = \frac{a_m + i\mu_j b_m}{a_m - i\mu_j b_m} \quad (3.15b)$$

in which a_m and b_m are the semi-major and minor axis of the m -th hole. The function $s(x, y, j, m)$ in Eq. (3.14) has either the value $+1$ or -1 depending on the x, y location in the plate and the material eigenvalue μ_j to assure that the hole is mapped correctly to the complex plane. This value is determined by a sign selection algorithm rather than a simple equation. In this work the algorithm developed by Koussios [194] is used as a basis. Adaptations were made to ensure its validity for unusual layups, such as $[\pm 45]_4$, and for the case where holes have their centre unequal to the origin of the global coordinate system. The resulting algorithm is presented below. For convenience, the derivation and adaptations made are given in Appendix A. First some definitions are set. Since μ_j is a complex number, it can be decomposed as:

$$\mu_j = \alpha_j + i\beta_j \quad (3.16)$$

Next, the imaginary and real part of the expression inside the square root in Eq. (3.14) are defined as ImR and ReR respectively. Additionally, the function $S(x, y, m, j)$ is defined by :

$$S(x, y, m, j) = y - y_m + \frac{x - x_m}{\alpha_j} \quad (3.17)$$

Then, the sign selection algorithm is given by the following (\vee and \wedge stand for OR and AND respectively) :

IF $\alpha_j = 0$

$s(x, y, j, m) = \text{sign}(y - y_m)$ IF $x = 0$

OTHERWISE $s(x, y, j, m) = \text{sign}(x - x_m)$

IF $\beta_j > |\alpha_j|$

IF $\alpha_j > 0$

IF $\{(y - y_m \leq 0 \wedge \text{ReR} < 0 \wedge \text{ImR} < 0 \wedge x - x_m \geq 0) \vee$

$(S(x, y, m, j) > 0 \wedge \text{ReR} > 0 \wedge x - x_m \geq 0) \vee$

$(S(x, y, m, j) > 0 \wedge \text{ImR} \geq 0) \vee$

$(S(x, y, m, j) > 0 \wedge \text{ReR} < 0 \wedge x - x_m \geq 0) \vee$

$(S(x, y, m, j) < 0 \wedge \text{ReR} > 0 \wedge x - x_m \geq 0)\}$

$$\begin{aligned}
& s(x, y, j, m) = +1 \\
& \text{OTHERWISE } s(x, y, j, m) = -1 \\
& \text{IF } \alpha_j < 0 \\
& \quad \text{IF } \{(y - y_m \leq 0 \wedge \text{ReR} < 0 \wedge \text{ImR} \geq 0 \wedge x - x_m \leq 0) \vee \\
& \quad (S(x, y, m, j) > 0 \wedge \text{ReR} > 0 \wedge x - x_m \leq 0) \vee \\
& \quad (S(x, y, m, j) > 0 \wedge \text{ImR} < 0) \vee (S(x, y, m, j) > 0 \wedge \text{ReR} < 0 \wedge x - x_m \leq 0) \vee \\
& \quad (S(x, y, m, j) < 0 \wedge \text{ReR} > 0 \wedge x - x_m \leq 0)\} \\
& \quad s(x, y, j, m) = -1 \\
& \quad \text{OTHERWISE } s(x, y, j, n) = +1 \\
& \text{OTHERWISE} \\
& \quad \text{IF } \alpha_j > 0 \\
& \quad \quad \text{IF } \{(y - y_m \leq 0 \wedge \text{ReR} < 0 \wedge \text{ImR} < 0 \wedge x - x_m \geq 0) \vee \\
& \quad \quad (S(x, y, m, j) > 0 \wedge \text{ReR} > 0 \wedge x - x_m \geq 0) \vee \\
& \quad \quad (S(x, y, m, j) > 0 \wedge \text{ImR} \geq 0) \vee \\
& \quad \quad (S(x, y, m, j) > 0 \wedge \text{ReR} < 0 \wedge x - x_m \geq 0)\} \\
& \quad \quad s(x, y, j, m) = +1 \\
& \quad \quad \text{OTHERWISE } s(x, y, j, m) = -1 \\
& \quad \text{IF } \alpha_j < 0 \\
& \quad \quad \text{IF } \{(y - y_m \leq 0 \wedge \text{ReR} < 0 \wedge \text{ImR} \geq 0 \wedge x - x_m \leq 0) \vee \\
& \quad \quad (S(x, y, m, j) > 0 \wedge \text{ReR} > 0 \wedge x - x_m \leq 0) \vee (S(x, y, m, j) > 0 \wedge \text{ImR} < 0) \vee \\
& \quad \quad (S(x, y, m, j) > 0 \wedge \text{ReR} < 0 \wedge x - x_m \leq 0)\} \\
& \quad \quad s(x, y, j, m) = -1 \\
& \quad \quad \text{OTHERWISE } s(x, y, j, n) = +1
\end{aligned}$$

With Eq. (3.6) through Eq. (3.17) one can find the stress function φ_j , $j = 1, 2$ and subsequently the stress and strain distribution by determining the complex coefficients $C_{n,j}$, $j = 1, 2$. First, as the coefficients $C_{(k+kN)_j}$ are multiplied by a “ln” term, the following additional constraints are used to ensure single-valued displacements (“ln (e^i)” has infinitely many solutions). In the case when hole k is unloaded:

$$C_{(k+kN)_j} = 0 \quad (3.18)$$

In the case when hole k is loaded:

$$\Im(p_1 C_{(k+kN)_1} + p_2 C_{(k+kN)_2}) = 0 \quad (3.19a)$$

$$\Im(q_1 C_{(k+kN)_1} + q_2 C_{(k+kN)_2}) = 0 \quad (3.19b)$$

The remaining coefficients are determined by applying the principle of minimum potential energy. This fundamental concept asserts that a body will deform in a way such that the

minimum total potential energy of the structure is reached given the external loading conditions. The total potential energy in the plate is given by:

$$\begin{aligned} \Pi = & \frac{1}{2} \int_{\Omega} \left\{ A_{11} \left(\frac{\partial u}{\partial x} \right)^2 + 2A_{12} \left(\frac{\partial u}{\partial x} \frac{\partial v}{\partial y} \right) + A_{22} \left(\frac{\partial v}{\partial y} \right)^2 \right. \\ & + 2 \left(A_{16} \frac{\partial u}{\partial x} + A_{26} \frac{\partial u}{\partial y} \right) \left(\frac{\partial u}{\partial y} + \frac{\partial v}{\partial x} \right) + A_{66} \left(\frac{\partial u}{\partial y} + \frac{\partial v}{\partial x} \right)^2 \Big\} dxdy \\ & + \text{Boundary terms} \end{aligned} \quad (3.20)$$

where Ω is the domain of the plate. Using integration by parts, the first order variation of the energy with respect to u and v can be written as:

$$\begin{aligned} \partial \Pi = & \int_{\Omega} \left\{ - \left(\frac{\partial \sigma_x}{\partial x} + \frac{\partial \tau_{xy}}{\partial y} \right) \partial u - \left(\frac{\partial \tau_{xy}}{\partial x} + \frac{\partial \sigma_y}{\partial y} \right) \partial v \right\} dxdy \\ & + \text{Boundary terms} \end{aligned} \quad (3.21)$$

Eq. (3.21) consists of one area integration and boundary terms. The stress functions φ_j , $j = 1, 2$ already comply to the equilibrium equations, Eq. (3.1), and therefore the area integration in Eq. (3.21) is zero. Thus only the boundary terms remain which are, in expanded form:

$$\begin{aligned} \partial \Pi = & - \int_{\frac{L}{2}}^{-\frac{L}{2}} \left\{ \left[\sigma_y \left(x, \frac{W}{2} \right) - \bar{\sigma}_{12} \right] \partial v + \left[\tau_{xy} \left(x, \frac{W}{2} \right) - \bar{\tau}_{12} \right] \partial u \right\} dx \\ & + \int_{\frac{W}{2}}^{-\frac{W}{2}} \left\{ \left[\sigma_x \left(-\frac{L}{2}, y \right) - \bar{\sigma}_{23} \right] \partial u + \left[\tau_{xy} \left(-\frac{L}{2}, y \right) - \bar{\tau}_{23} \right] \partial v \right\} dy \\ & - \int_{-\frac{L}{2}}^{\frac{L}{2}} \left\{ \left[\sigma_y \left(x, -\frac{W}{2} \right) - \bar{\sigma}_{34} \right] \partial v + \left[\tau_{xy} \left(x, -\frac{W}{2} \right) - \bar{\tau}_{34} \right] \partial u \right\} dx \\ & + \int_{-\frac{W}{2}}^{\frac{W}{2}} \left\{ \left[\sigma_x \left(\frac{L}{2}, y \right) - \bar{\sigma}_{41} \right] \partial u + \left[\tau_{xy} \left(\frac{L}{2}, y \right) - \bar{\tau}_{41} \right] \partial v \right\} dy \\ & - \sum_{k=1}^m \left\{ \int_0^{2\pi} \left\{ \sigma_r^k(a_k, \theta) \partial u_r^k + \tau_{r\theta}^k(a_k, b_k, \theta) \partial u_{\theta}^k \right\} \sqrt{a_k^2 \sin^2(\theta) + b_k^2 \cos^2(\theta)} d\theta \right. \\ & \quad \left. + \int_{\theta_1^k}^{\theta_2^k} \left\{ \left[\sigma_r^k(a_k, \theta) - \overline{\sigma_{rk}}(\theta) \right] \partial u_r^k \right. \right. \\ & \quad \left. \left. + \left[\tau_{r\theta}^k(a_k, b_k, \theta) - \overline{\tau_{r\theta k}}(\theta) \right] \partial u_{\theta}^k \right\} \sqrt{a_k^2 \sin^2(\theta) + b_k^2 \cos^2(\theta)} d\theta \right\} \end{aligned} \quad (3.22)$$

In Eq. (3.22) it is observed that the boundary conditions, which are the loads at the edges, are incorporated in the equation. Hence, satisfaction of the minimal potential energy theorem can be seen as satisfaction of the boundary conditions of the problem. The minimal potential energy theorem requires that:

$$\partial \Pi = 0 \quad (3.23)$$

Next, since the stress and displacement resultants σ_x , σ_y , τ_{xy} , u and v are a linear combination of the stress functions φ_j , $j = 1, 2$ (Eq. (3.6)) and the stress functions are a linear combination

of the complex coefficients C_{n_j} (Eq. (3.13)) the variational energy formulation can be rewritten as:

$$\begin{aligned}
0 = & \left[- \int_{-\frac{L}{2}}^{-\frac{L}{2}} \left\{ \left[\sigma_y \left(x, \frac{W}{2} \right) \right] \frac{\partial v}{\partial C_{n_j}} + \left[\tau_{xy} \left(x, \frac{W}{2} \right) \right] \frac{\partial u}{\partial C_{n_j}} \right\} dx \right. \\
& + \int_{\frac{W}{2}}^{-\frac{W}{2}} \left\{ \left[\sigma_x \left(-\frac{L}{2}, y \right) \right] \frac{\partial u}{\partial C_{n_j}} + \left[\tau_{xy} \left(-\frac{L}{2}, y \right) \right] \frac{\partial v}{\partial C_{n_j}} \right\} dy \\
& - \int_{-\frac{L}{2}}^{\frac{L}{2}} \left\{ \left[\sigma_y \left(x, -\frac{W}{2} \right) \right] \frac{\partial v}{\partial C_{n_j}} + \left[\tau_{xy} \left(x, -\frac{W}{2} \right) \right] \frac{\partial u}{\partial C_{n_j}} \right\} dx \\
& \left. + \int_{-\frac{W}{2}}^{\frac{W}{2}} \left\{ \left[\sigma_x \left(\frac{L}{2}, y \right) \right] \frac{\partial u}{\partial C_{n_j}} + \left[\tau_{xy} \left(\frac{L}{2}, y \right) \right] \frac{\partial v}{\partial C_{n_j}} \right\} dy \right. \\
& - \sum_{k=1}^m \left\{ \int_0^{2\pi} \left\{ \left[\sigma_r^k(a_k, \theta) \frac{\partial u_r^k}{\partial C_{n_j}} + \tau_{r\theta}^k(a_k, b_k, \theta) \frac{\partial u_\theta^k}{\partial C_{n_j}} \right] \sqrt{a_k^2 \sin^2(\theta) + b_k^2 \cos^2(\theta)} \right\} d\theta \right\} \\
& - \int_{-\frac{L}{2}}^{-\frac{L}{2}} \left\{ [-\bar{\sigma}_{12}] \frac{\partial v}{\partial C_{n_j}} + [-\bar{\tau}_{12}] \frac{\partial u}{\partial C_{n_j}} \right\} dx + \int_{\frac{W}{2}}^{-\frac{W}{2}} \left\{ [-\bar{\sigma}_{23}] \frac{\partial u}{\partial C_{n_j}} + [-\bar{\tau}_{23}] \frac{\partial v}{\partial C_{n_j}} \right\} dy \\
& - \int_{-\frac{L}{2}}^{\frac{L}{2}} \left\{ [-\bar{\sigma}_{34}] \frac{\partial v}{\partial C_{n_j}} + [-\bar{\tau}_{34}] \frac{\partial u}{\partial C_{n_j}} \right\} dx + \int_{-\frac{W}{2}}^{\frac{W}{2}} \left\{ [-\bar{\sigma}_{41}] \frac{\partial u}{\partial C_{n_j}} + [-\bar{\tau}_{41}] \frac{\partial v}{\partial C_{n_j}} \right\} dy \\
& - \sum_{k=1}^m \left\{ \int_{\theta_1^k}^{\theta_2^k} \left\{ \left[[-\bar{\sigma}_0^k(\theta)] \frac{\partial u_r^k}{\partial C_{n_j}} + [-\bar{\tau}_0^k(\theta)] \frac{\partial u_\theta^k}{\partial C_{n_j}} \right] \sqrt{a_k^2 \sin^2(\theta) + b_k^2 \cos^2(\theta)} \right\} d\theta \right\} \Big] \partial C_{n_j} \\
& k = 1, 2, \dots, m \quad n = 1, 2, \dots, (m+1)(N+1) \quad j = 1, 2
\end{aligned} \tag{3.24}$$

Since Eq. (3.24) should equate to 0, the multiplication by ∂C_{n_j} can be omitted. Additionally, using the following definitions:

$$\begin{aligned}
a_{n_j} = & - \int_{-\frac{L}{2}}^{-\frac{L}{2}} \left\{ \left[\sigma_y \left(x, \frac{W}{2} \right) \right] \frac{\partial v}{\partial C_{n_j}} + \left[\tau_{xy} \left(x, \frac{W}{2} \right) \right] \frac{\partial u}{\partial C_{n_j}} \right\} dx \\
& + \int_{\frac{W}{2}}^{-\frac{W}{2}} \left\{ \left[\sigma_x \left(-\frac{L}{2}, y \right) \right] \frac{\partial u}{\partial C_{n_j}} + \left[\tau_{xy} \left(-\frac{L}{2}, y \right) \right] \frac{\partial v}{\partial C_{n_j}} \right\} dy \\
& - \int_{-\frac{L}{2}}^{\frac{L}{2}} \left\{ \left[\sigma_y \left(x, -\frac{W}{2} \right) \right] \frac{\partial v}{\partial C_{n_j}} + \left[\tau_{xy} \left(x, -\frac{W}{2} \right) \right] \frac{\partial u}{\partial C_{n_j}} \right\} dx \quad (3.25a) \\
& + \int_{-\frac{W}{2}}^{\frac{W}{2}} \left\{ \left[\sigma_x \left(\frac{L}{2}, y \right) \right] \frac{\partial u}{\partial C_{n_j}} + \left[\tau_{xy} \left(\frac{L}{2}, y \right) \right] \frac{\partial v}{\partial C_{n_j}} \right\} dy \\
& - \sum_{k=1}^m \left\{ \int_0^{2\pi} \left\{ \left[\sigma_r^k(a_k, \theta) \frac{\partial u_r^k}{\partial C_{n_j}} + \tau_{r\theta}^k(a_k, b_k, \theta) \frac{\partial u_\theta^k}{\partial C_{n_j}} \right] \sqrt{a_k^2 \sin^2(\theta) + b_k^2 \cos^2(\theta)} \right\} d\theta \right\}
\end{aligned}$$

$$\begin{aligned}
b_{n_j} = & - \int_{-\frac{L}{2}}^{\frac{L}{2}} \left\{ [-\bar{\sigma}_{12}] \frac{\partial v}{\partial C_{n_j}} + [-\bar{\tau}_{12}] \frac{\partial u}{\partial C_{n_j}} \right\} dx + \int_{-\frac{W}{2}}^{\frac{W}{2}} \left\{ [-\bar{\sigma}_{23}] \frac{\partial u}{\partial C_{n_j}} + [-\bar{\tau}_{23}] \frac{\partial v}{\partial C_{n_j}} \right\} dy \\
& - \int_{-\frac{L}{2}}^{\frac{L}{2}} \left\{ [-\bar{\sigma}_{34}] \frac{\partial v}{\partial C_{n_j}} + [-\bar{\tau}_{34}] \frac{\partial u}{\partial C_{n_j}} \right\} dx + \int_{-\frac{W}{2}}^{\frac{W}{2}} \left\{ [-\bar{\sigma}_{41}] \frac{\partial u}{\partial C_{n_j}} + [-\bar{\tau}_{41}] \frac{\partial v}{\partial C_{n_j}} \right\} dy \\
& - \sum_{k=1}^m \left\{ \int_{\theta_1^k}^{\theta_2^k} \left\{ \left[[-\bar{\sigma}_0^k(\theta)] \frac{\partial u_r^k}{\partial C_{n_j}} + [-\bar{\tau}_0^k(\theta)] \right] \frac{\partial u_\theta^k}{\partial C_{n_j}} \sqrt{a_k^2 \sin^2(\theta) + b_k^2 \cos^2(\theta)} \right\} d\theta \right\}
\end{aligned} \tag{3.25b}$$

The variational energy formulation can be rewritten as:

$$\begin{aligned}
0 &= a_{n_j} + b_{n_j} \\
n &= 1, 2, \dots, (m+1)(N+1) \quad j = 1, 2
\end{aligned} \tag{3.26}$$

Note that b_{n_j} is a function of the boundary stresses only and will therefore result in a complex number for each n . a_{n_j} is a linear function of the complex coefficients C_{n_j} . Since the following property exists between the sum of the product of a constant with a function:

$$\sum_{i=1}^{\infty} a_i f_i = \sum_{i=1}^{\infty} \frac{\partial a_i f_i}{\partial a_i} a_i \tag{3.27}$$

a_{n_j} can be decomposed into the product of two vectors:

$$a_{n_j} = \mathbf{a}_{n_j} \mathbf{C} \tag{3.28}$$

where:

$$\mathbf{C} = \begin{bmatrix} C_{0_1} & C_{0_2} & C_{1_1} & C_{1_2} & \dots & C_{(N+1)(m+1)_2} \end{bmatrix}^T \tag{3.29a}$$

$$\mathbf{a}_{n_j} = \begin{bmatrix} \frac{\partial a_{n_j}}{\partial C_{0_1}} & \frac{\partial a_{n_j}}{\partial C_{0_2}} & \frac{\partial a_{n_j}}{\partial C_{1_1}} & \frac{\partial a_{n_j}}{\partial C_{1_2}} & \dots & \frac{\partial a_{n_j}}{\partial C_{(N+1)(m+1)_2}} \end{bmatrix} \tag{3.29b}$$

Recall that this operation needs to be performed for every coefficient C_{n_j} . Hence one will obtain $2(m+1)(N+1)$ equations which form a linear system of equations given by:

$$\mathbf{A} \mathbf{C} + \mathbf{B} = 0 \tag{3.30}$$

where:

$$\mathbf{A} = \begin{bmatrix} \mathbf{a}_{0_1} & \mathbf{a}_{0_2} & \mathbf{a}_{1_1} & \mathbf{a}_{1_2} & \dots & \mathbf{a}_{(n+1)(m+1)_2} \end{bmatrix}^T \tag{3.31a}$$

$$\mathbf{B} = \begin{bmatrix} b_{0_1} & b_{0_2} & b_{1_1} & b_{1_2} \dots & b_{(n+1)(m+1)_2} \end{bmatrix}^T \tag{3.31b}$$

Solving for Eq. (3.30) now results in a solution vector containing all the constants C_{n_j} $j = 1, 2$. Once these constants are determined, the stress and displacement field are obtained using Eq. (3.6) and Eq. (3.7).

The above theory is transformed into an algorithm for MathCAD13.1 ©. The structure of the algorithm is as shown in Figure 3.3. The algorithm starts with the definition of the necessary input parameters. Most of these input parameters shown in Figure 3.3 do not require explanation except for “Summation” and “Tolerance”. “Summation” is the amount of the summation terms N that are taken in the stress function φ_j , Eq. (3.13). The higher N , the higher the accuracy of the solution but the higher computation time. “Tolerance”, TOL , represents the accuracy of the numerical integrator provided by MathCAD13.1©. Normally this value is between 10^{-4} and 10^{-9} . The optimal values for these two parameters are determined in Section 6.1.

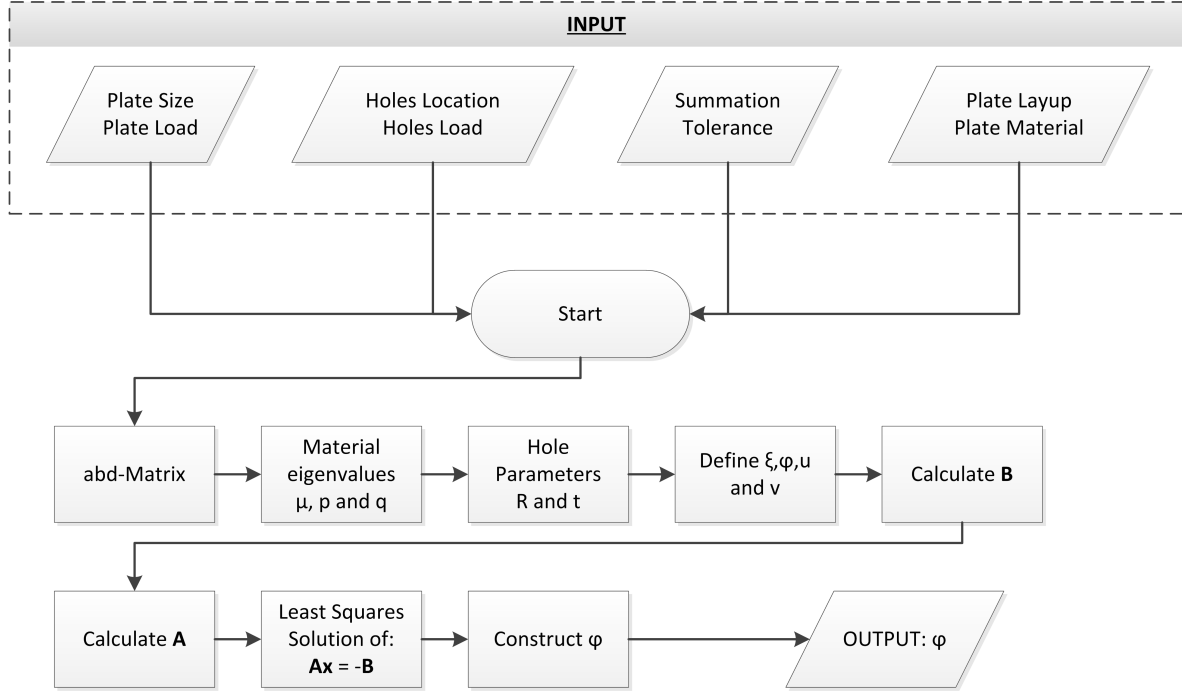


Figure 3.3: Computation algorithm for stress field determination. The subscript j is dropped for convenience

3.2 Pin Contact Angle

With the theory provided in the previous section it is possible to determine the stress field in plates with loaded holes provided that the load boundary condition due to the pin is known. Often it is assumed that the pin-load can be represented by a radial cosine shaped compression load on the hole edge [2, 11, 12] represented by Eq. (3.32) and shown in Figure 3.4.

$$\left. \begin{aligned} \sigma_r &= \frac{4P}{Dt} \cos(\theta) & -\frac{\pi}{2} \leq \theta \leq \frac{\pi}{2} \\ \sigma_r &= 0 & \frac{\pi}{2} \leq \theta \leq -\frac{\pi}{2} \end{aligned} \right\} \quad (3.32)$$

Several studies [13, 14], however, have shown that this assumption is essentially wrong because it neglects the effects of pin-hole clearance, flexibility, friction, material orthotropy and applied load. Tomlinson [13] attempted to incorporate the effect of clearance by assuming that the hole deforms in an elliptical fashion under the influence of the pin. With this assumption and the assumption that the pin is rigid, the pin-hole contact angle can be computed using goniometry as shown in Figure 3.5 and Eq. (3.33).

$$\begin{aligned} 0 &= \left\{ (\lambda + u_0) \cos(\theta_B) + \sqrt{r_p^2 - (\lambda + u_0)^2 (1 - \cos^2(\theta_B))} \right\}^2 \\ &\quad * \left\{ r_h^2 \cos^2(\theta_B) + (1 - \cos^2(\theta_B)) (\lambda + u_0 + r_p)^2 \right\} - r_h^2 (\lambda + u_0 + r_p)^2 \end{aligned} \quad (3.33)$$

where $\lambda = r_h - r_p$ is the hole clearance, u_0 the horizontal displacement of the hole edge at 0° , r_p is the pin radius, r_h is the hole radius and θ_B is the pin contact angle. The function for the applied stress on the hole edge is modified to a cosine distribution between θ_{1m} and

θ_{2m} , Figure 3.1, and an elliptical hole shape.

$$\sigma_{rm}(\theta) = P \left[\frac{1}{\pi \sqrt{a_m^2 \cos^2(\theta) + b_m^2 \sin^2(\theta)}} \cos \left(\frac{\theta - \theta_{1m}}{\theta_{2m} - \theta_{1m}} \pi + \frac{\pi}{2} \right) \right] \frac{1}{S_m} \quad (3.34)$$

where P is the total load in the direction $\frac{\theta_{2m} + \theta_{1m}}{2}$ and S_m is defined by:

$$S_m = \int_{\theta_{1m}}^{\theta_{2m}} \left[\frac{1}{\pi \sqrt{a_m^2 \cos^2(\theta) + b_m^2 \sin^2(\theta)}} \cos \left(\frac{\theta - \theta_{1m}}{\theta_{2m} - \theta_{1m}} \pi + \frac{\pi}{2} \right) * \sqrt{a_m^2 \cos^2(\theta) + b_m^2 \sin^2(\theta)} \cos \left(\theta - \frac{\theta_{1m} + \theta_{2m}}{2} \right) \right] d\theta \quad (3.35)$$

The displacement u_0 in Eq. (3.34) is not only dependent on the magnitude of the load but also on the contact angles θ_{1m} and θ_{2m} . Therefore, the contact angles for a certain load can only be determined with an iterative procedure. This procedure is shown schematically in Figure 3.6. Normally, convergence is obtained within approximately 5 iterations. Sometimes, however, it occurs that using the new contact angle results in the contact angle of the previous iteration which leads to a never converging state. Fortunately, when this happens, both the old and new contact angle are close (in the order of 0.1 [deg]) and using the one or the other does not significantly change the final solution. To avoid this state, in the procedure, a counter X is embedded which breaks the loop as soon as more than 20 iterations have been executed without reaching convergence.

At first, having confidence in Tomlinson's model, his model was used to estimate the contact angle of pin-loaded holes. However, during validation, Section 6.1.2, it was discovered that this model does not perform well when compared to FEA simulations. Eventually, in the search for a better model to estimate pin-hole contact angle it was found that, instead of assuming that the hole deforms in an elliptical fashion, it is better to assume that the pin locally deforms the hole as shown in Figure 3.7. In the Figure, angle θ_B is the contact angle of the pin and the hole while u_α is the horizontal displacement of the hole at an angle α with respect to the x-axis. Using the horizontal displacement at an angle instead of 0° is more advantageous than using the horizontal displacement at 0° since it allows, by varying this angle, "tuning" of the results. Again assuming a rigid pin, the hole and pin can be represented by Eq. (3.36) and Eq. (3.37).

$$x^2 + y^2 = r_h^2 \quad (3.36)$$

$$(x - (\lambda + u_\alpha))^2 + y^2 = r_p^2 \quad (3.37)$$

Solving for the intersection of both functions results in the following for the x-coordinate:

$$x_\alpha = \frac{r_h^2 - r_p^2 + (\lambda + u_\alpha)}{2(\lambda + u_\alpha)} \quad (3.38)$$

From which θ_B is determined using Eq. (3.39).

$$\theta_B = \arccos \left(\frac{x_\alpha}{r_h} \right) \quad (3.39)$$

One now only has to determine the horizontal displacement angle α to be able to solve for θ_B . The optimal value for this angle is determined in Section 6.1.2.

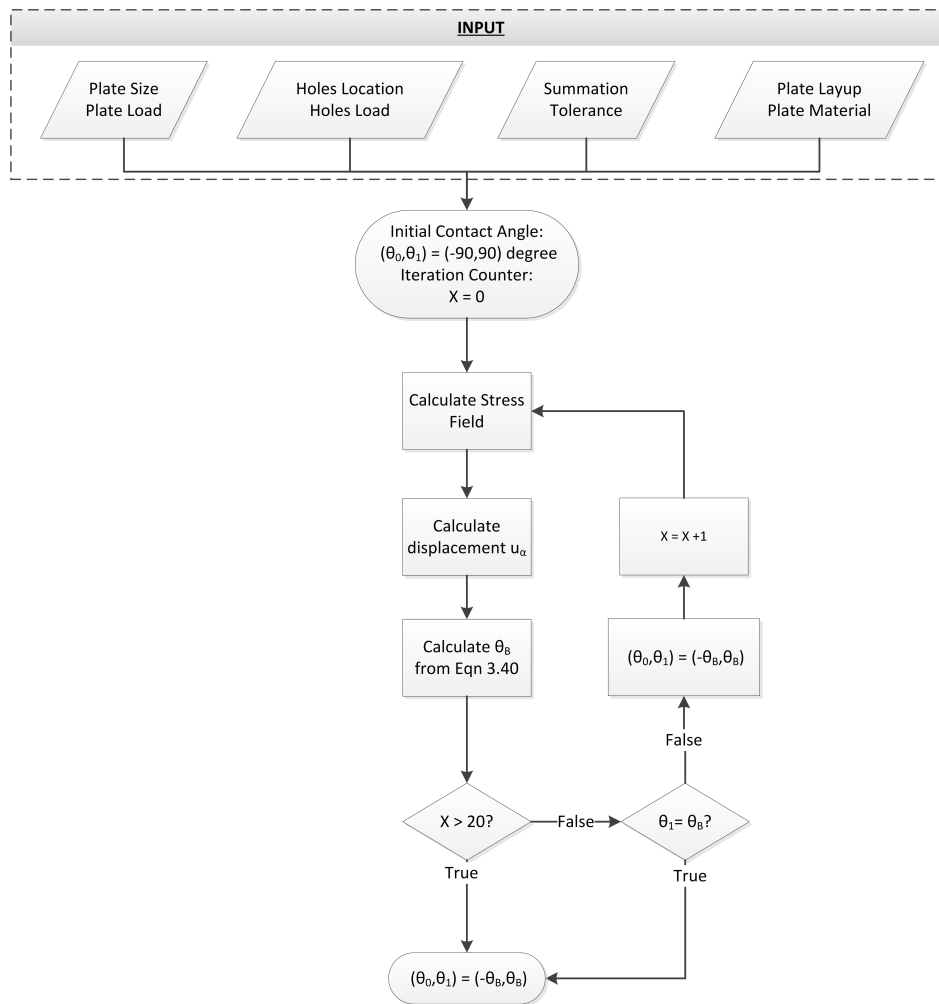


Figure 3.6: Iterative procedure for the determination of the contact angle θ_B

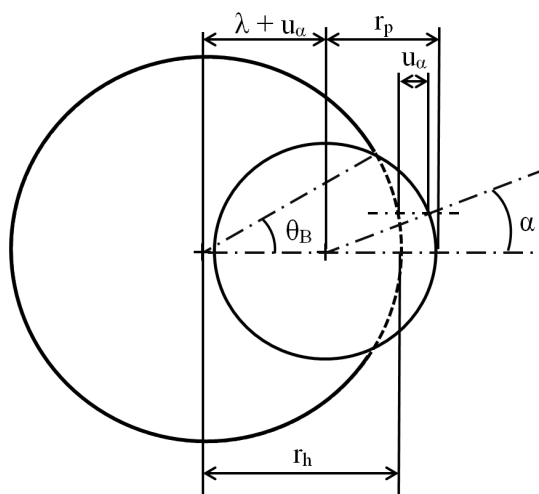


Figure 3.7: Schematic of pin locally deforming the hole shape

Together, the estimation of the contact angle, pin-hole edge stress distribution and stress determination method allow the determination of the stress field in a rectangular orthotropic plate with multiple (un)loaded holes subjected to arbitrary in-plane loads. The method described here is verified in Chapter 5 and its performance assessed in Section 6.1. To be able to predict failure, a failure criterion on the basis of this stress method is required which is discussed in the next Chapter.

Chapter 4

Failure Prediction

From Chapter 2, it is evident that currently, there is no consensus on which failure criterion is best to use for the determination of unnotched/notched laminate failure. None of the existing, engineering wise feasible, criteria perform well in all quadrants of the failure envelope and therefore it is as choosing between the lesser of evils. Nevertheless, an attempt is made for an argued choice.

In Section 2.2.2 the choice is left between LEFM, ASC and PSC for the prediction of notched strength of a laminated plate. A major disadvantage of all three techniques is that one has to experimentally determine a characteristic distance for accurate predictions. For the analytic tool, however, as a more general approach is required, this experimental information is not available. Therefore this characteristic distance will either have to be assumed or, in some way, analytically determined. Because of the diversity of composites, however, a consequence of assuming a characteristic distance is that the use of the tool would be limited to a particular type of composite laminate configuration (e.g. graphite-epoxy, glass fibre-epoxy, etc..) and loading conditions (uniaxial, biaxial, etc..) . This is, however, not desired and therefore it is required to analytically estimate the characteristic distance. An analytic expression for the characteristic distance has been identified for only one method, the PSC, by Kweon [3]. Thus, use of the PSC in conjunction with an analytic expression for the characteristic lengths is preferred. Caution is expressed since Kweons formulation for the characteristic lengths is proven to be flawed for the tensile case (Appendix B). In Section 4.2 this issue is further addressed.

For the PSC, an unnotched strength criterion is also required. In Section 2.2.1 the progressive phenomenological failure criterion as Puck [5] is one of the favourites. At Fokker Aerostructures B.V., a Puck-like failure criterion is currently in use. The desire exists, however, to replace this criterion with a more recent version of Puck described in VDI2014 [15]. VDI2014 is a guideline for engineering purposes of fibre-reinforced plastics (FRP) by the German Association of Engineers (Verein Deutscher Ingenieure) which is essentially a contraption of the phenomenological theories by Puck, Flemming, Schürmann and Knops [195–198]. The criterion is meant for FRP's with thermoset matrices and UD laminae but can restrictedly be extended to thermoplastic matrix and woven reinforcements. In this work, it is chosen to use

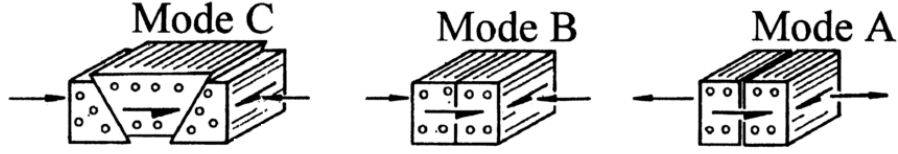


Figure 4.1: IFF failure modes [15]

the VDI2014 [15] to predict unnotched failure as it is expected to give better predictions than the current Fokker criterion. Whether this expectations are true is shown in Section 6.2. The criterion is explained in Section 4.1.

4.1 Unnotched Failure Prediction

When one desires to follow VDI2014 [15] to the letter, it is necessary to perform a non-linear analysis which requires detailed knowledge about the stress-strain behaviour of the used material (complete stress-strain curves in all quadrants of the in-plane loading). Other parameters, like the slopes of the (σ_2, τ_{21}) fracture curve at several locations, also need to be known. At Fokker Aerostructures B.V., however, for basic analysis, no other material parameters than the standard strengths and stiffnesses of the lamina are known rendering these advanced analysis methods virtually unusable. Thus, the method in VDI2014 needs to be adapted for efficient use at the company. Therefore it is chosen to neglect non-linear material behaviour, 3D effects such as interlaminar stresses, residual stress in the laminate due to manufacturing process and the effect of high σ_1 on IFF criteria. Not neglected are the material properties when a ply is loaded in tension or compression.

The determination of failure is based on a layer by layer analysis of the laminate. From the laminate loads, the strains and stresses for every ply are determined and passed through several failure criteria to assess failure. VDI2014 distinguishes between two types of failure: Fibre Failure (FF) and Inter Fibre Failure (IFF). FF occurs in a ply when:

$$\frac{\sigma_1}{X^t} = 1 \text{ if } \sigma_1 > 0 \quad (4.1a)$$

$$\frac{\sigma_1}{-X^c} = 1 \text{ if } \sigma_1 < 0 \quad (4.1b)$$

in Eq. (4.1), X^t and X^c (values have to be positive) are the tensile and compressive lamina strength in the direction parallel to the fibres. IFF can occur in three ways due to the possible fracture planes on the load as shown in Figure 4.1. They are defined as Mode A, B and C. For each mode there is a separate criterion based on the so-called action-plane related fracture criteria. For Mode A ($\sigma_2 \geq 0$) the stress exposure f_E is calculated using:

$$f_E|_{\theta_{fp}=0 \text{ deg}} = \frac{1}{S_{12}} \left[\sqrt{\left(\frac{S_{12}}{Y^t} - p_{21}^t \right)^2 \sigma_2^2 + \tau_{21}^2 + p_{21}^t \sigma_2} \right] \quad (4.2)$$

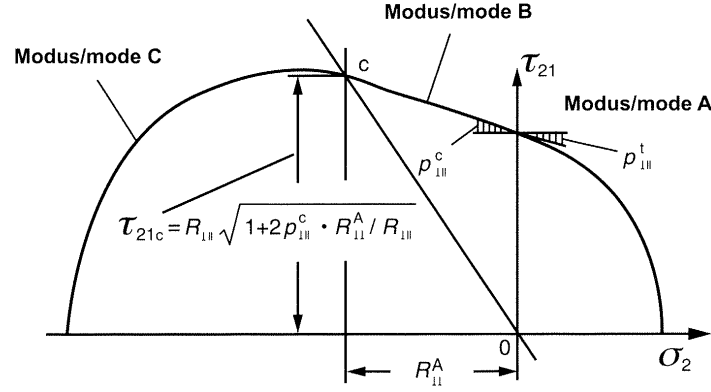


Figure 4.2: IFF σ_2, τ_{21} fracture plane [15]

Whether failure Mode B or Mode C ($\sigma_2 < 0$) occurs is dependent on the ratio (τ_{21}, σ_2) denoted by point C in Figure 4.2. For Mode B the stress exposure f_E is:

$$f_E|_{\theta_{fp}=0 \text{ deg}} = \frac{1}{S_{12}} \left(\sqrt{\tau_{21}^2 + (p_{21}^c \sigma_2)^2} + p_{21}^c \sigma_2 \right) \quad (4.3)$$

and for Mode C:

$$f_E|_{\theta_{fp}=\text{crit.}} = \frac{\tau_{21}^2}{4 (S_{12} + p_{21}^c R_{22}^A)^2} \frac{-Y^c}{\sigma_2} + \frac{\sigma_2}{-Y^c} \quad (4.4)$$

In Equation (4.2) through Eq. (4.4) S_{12} , Y^t and Y^c are the lamina shear, transverse tensile and transverse compressive strength respectively. R_{22}^A is the fracture resistance of an action plane parallel to the fibre direction against fracture due to τ_{22} . This is calculated using:

$$R_{22}^A = \frac{S_{12}}{2p_{21}^c} \left(\sqrt{1 + 2p_{21}^c \frac{Y^c}{S_{12}}} - 1 \right) \quad (4.5)$$

p_{21}^t and p_{21}^c are the slopes of the (σ_2, τ_{21}) fracture curve (Figure 4.2) at the location $\sigma_2 = 0$. Ideally, these values must be obtained from material tests. If no experimentally determined value is available, the values shown in Table 4.1 can be used for Glass Fibre Reinforce Plastics (GFRP) and Carbon Fibre Reinforced Plastics (CFRP).

Table 4.1: Recommended values for slope parameters p_{21}^c and p_{21}^t [36]

	p_{21}^c	p_{21}^t
GFRP	0.25	0.30
CFRP	0.30	0.35

Since VDI2014 is a progressive criterion, there is a roadmap for the determination of final failure. First, when given an initial load vector, the minimum Reserve Factor (RF) for all plies of the laminate for FF and IFF is calculated. When the minimum RF is coincident with IFF, that ply is considered as IFF failed but the laminate is still able to carry load. When Mode A occurs the secant modulus of that ply, the shear modulus and the Poisson's ratio are reduced to 1/10th of their original value. When mode B or C occur no reduction in

modulus is applied because matrix failure due to compression is expected to have no effect on the compressive properties of the ply. After marking a ply as IFF and/or performing the necessary reduction in properties, the minimum RF is again determined until it is coincident with FF or, in the case of UD or angle plied laminates, when all plies have IFF. Then the laminate is considered failed. The aforementioned procedure translates into the algorithm shown in Figure 4.3 and Figure 4.4.

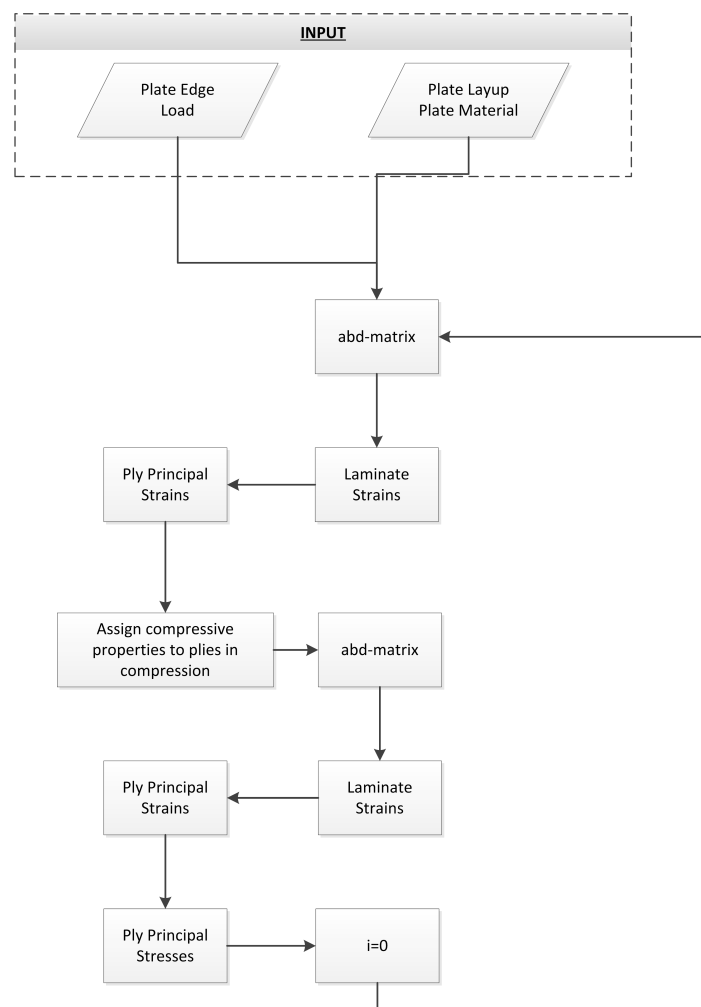


Figure 4.3: Unnotched failure algorithm, continued in Figure 4.4

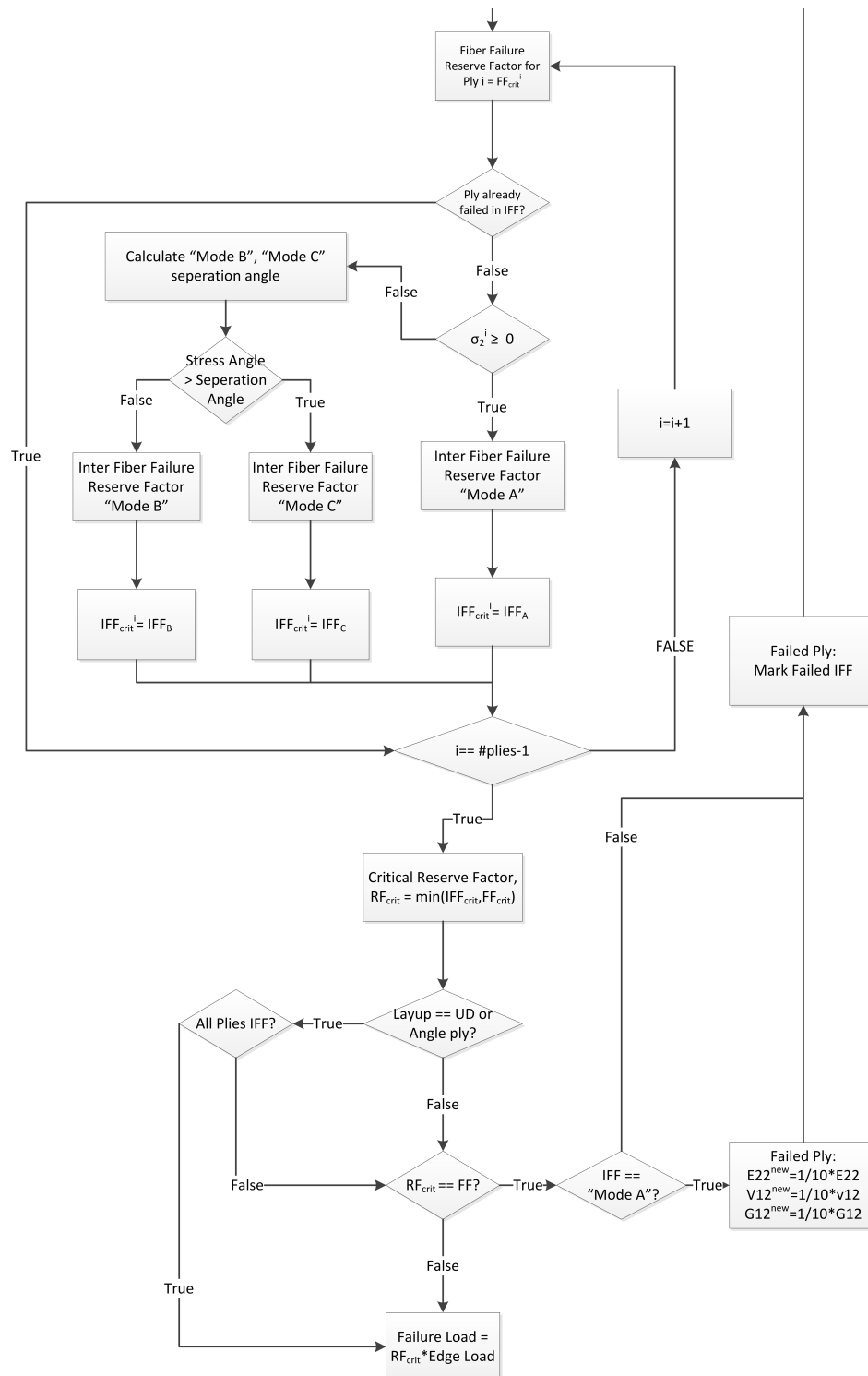


Figure 4.4: Unnotched failure algorithm, first part in Figure 4.3

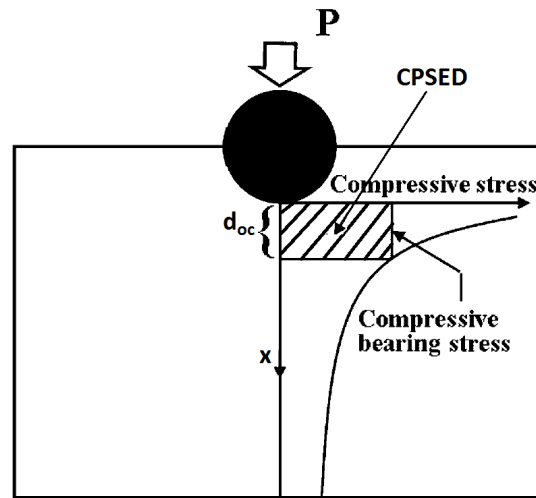


Figure 4.5: Keon definition compressive characteristic distance

4.2 Notched Failure

As determined in the introduction of this chapter, it is chosen to use the PSC as a basis to predict notched failure. The PSC, originally formulated by Whitney and Nuismer, assumes that failure occurs when the stress over some distance away from the hole is equal to or greater than the strength of the unnotched material. This distance, d_0 , represents “the distance over which the material around the hole must be critically stressed in order to find a sufficient flaw size to initiate failure” [10]. Initially it was assumed that d_0 would be a material constant but this was quickly proven wrong [164]. Nonetheless, with sufficient reliable test data, the PSC is still in use as a good method to quickly estimate failure in notched plates. Ideally, d_0 is determined with experimental data which is expensive and results in characteristic lengths only valid for uniaxially loaded specimens. Therefore, in this work, a new definition of the characteristic length is proposed which allows for an analytic estimate. It is recognized that the new formulation for characteristic distances has not been tried in other research. The only alternative however is to assume a constant characteristic distance, which was already proven wrong [164, 165], or use one of the empirically calibrated expansions by other researchers [164, 165, 168]. Hence, attempting to analytically formulate a characteristic distance in an effort to get rid of empirical calibration is not a waste of resources. To evaluate the new formulation, its performance will be compared to the constant characteristic distance approach, which is currently in use at Fokker Aerostructures B.V., and experimental data in Section 6.2.3.

A possible solution to analytically determining d_0 is provided by Kweon [3] who proposed two analytic definitions for the tensile and compressive characteristic length in pinned lugs. Kweon’s definition for the compressive characteristic length is: “The distance from the front hole edge to a point where the local compressive stress by the arbitrarily applied load is the same as the mean bearing stress”, Figure 4.5. The definition for the tensile characteristic length is: “The distance from the side edge of the fastener hole to a point where the tensile stress by the failure load of the notched laminate is the same as the tensile strength of the

notched laminate”. Upon inspection of Kweon’s method for the compressive characteristic distance, it was noticed that the presented results are reproducible. The definition of the tensile characteristic distance, however, results in different values than for the standard characteristic distance approach. Taking a closer look, it is discovered that it actually implies that the mean stress in the cross section can be used as the failure stress, Appendix B. This is, obviously, nonsense and the tensile definition should be discarded.

The establishment of an analytical method to determine the compressive characteristic length for pin-loaded lugs grew a curiosity. Would it be possible to use this analytical definition to determine characteristic lengths for general loading conditions? Consider the aforementioned definition of Whitney and Nuismer [10] for d_0 : “The distance over which the material around the hole must be critically stressed in order to find a sufficient flaw size to initiate failure”. Assuming a linear material behaviour, one can compute the potential strain energy density in this region. Since the material in this region is critically stressed, one can call this strain energy the Critical Potential Strain Energy Density ($\Pi_{cr,c}$) (CPSED) for the failure of the material due to the compressive bearing load of the pin. The definition of the CPSED for compression is given by Eq. (4.6) and shown in Figure 4.5.

$$\Pi_{cr,c} = \int_0^{d_{0c}} \sigma \epsilon dx \quad (4.6)$$

This critical energy density can now be used to establish a new definition for the characteristic distance d_0 . This distance is then defined as: “The distance from the hole edge where the strain energy density over this distance equals the CPSED”. Furthermore, considering that the characteristic distances for tension and compression are unequal, it is fair to consider that the CPSED for the tension and compression case are unequal. A CPSED for compression is already obtained but what is the CPSED for tension? As no analytic solution for the tensile characteristic distance exists, it is chosen to estimate the CPSED for tension by scaling the CPSED for compression with the ratio of the strain energy density of an unnotched plate subjected to uniaxial tension and compression at failure load respectively. This is given by Eq. (4.7).

$$\Pi_{cr,t} = \frac{\Pi(\sigma_{un,t})}{\Pi(\sigma_{un,c})} \Pi_{cr,c} \quad (4.7)$$

In a multiaxial loading condition, however, it can be required to have definitions for critical energies which are not only uniaxial tension or uniaxial compression. Therefore, in a similar way as for the CPSED for tension, the CPSED for transverse tension, transverse compression, tension-tension, tension-compression, compression-tension and compression-compression loading are defined as:

$$\Pi_{cr,-t} = \frac{\Pi(\sigma_{un,t})}{\Pi(\sigma_{un,c})} \Pi_{cr,c} \quad (4.8a)$$

$$\Pi_{cr,-c} = \frac{\Pi(\sigma_{un,c})}{\Pi(\sigma_{un,c})} \Pi_{cr,c} \quad (4.8b)$$

$$\Pi_{cr,tt} = \frac{\Pi(\sigma_{un,tt})}{\Pi(\sigma_{un,c})} \Pi_{cr,c} \quad (4.8c)$$

$$\Pi_{cr,tc} = \frac{\Pi(\sigma_{un,tc})}{\Pi(\sigma_{un,c})} \Pi_{cr,c} \quad (4.8d)$$

$$\Pi_{cr,cc} = \frac{\Pi(\sigma_{un,cc})}{\Pi(\sigma_{un,c})} \Pi_{cr,c} \quad (4.8e)$$

$$\Pi_{cr,ct} = \frac{\Pi(\sigma_{un,ct})}{\Pi(\sigma_{un,c})} \Pi_{cr,c} \quad (4.8f)$$

Note that a CPSED for shear is not defined. This is not necessary as no shear load will be present on the hole edge since the pin is assumed to be frictionless.

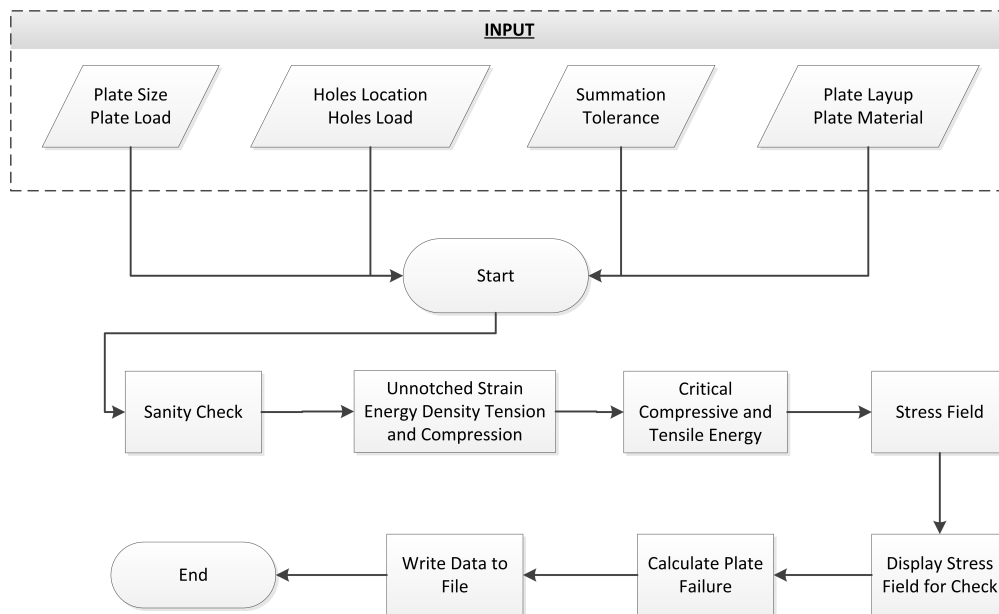
Having established the new definitions for the tensile and compressive characteristic distances, the following method is used to determine failure of a laminate with stress concentrations. First, the stress field in a uniaxial joint is used to determine the CPSED for uniaxial compression. Next, using the unnotched failure criterion, Eq. (4.7) and Eq. (4.8), the CPSED's for tensile, transverse tensile, transverse compression and biaxial tension-tension, tension-compression, compression-tension and compression-compression loading are obtained. Third, an initial characteristic distance is chosen and for every location around the shape of the holes in the stress field of the actual problem (this stress field is obtained earlier) a minimum RF and critical angle are obtained. At that critical angle, the Potential Strain Energy Density (PSED) from the hole edge to the characteristic distance is calculated and compared to the CPSED at that angle. When the CPSED equals the PSED, the ultimate failure load is found. Otherwise, a new characteristic distance is chosen based on whether the PSED is higher or lower than the CPSED and the procedure is repeated. The procedure is schematically shown in Figure 4.7 and Figure 4.8. Note that, in this procedure, as with the contact angle algorithm, an iteration counter X is present to protect against infinite loops (although this has never been encountered during validation).

4.3 General Program Layout

Having determined a methodology for stress analysis and failure prediction of notched plates with general stress boundary conditions, the layout of the complete analytic tool is constructed. Eventually, the code consists of one VBScript and 7 MathCAD13.1©calculation sheets. Each calculation sheet calculates a specific part of the complete solution. Their tasks are:

- Sanity Check: symmetric and balanced laminate, input loads are static equilibrium
- Calculate CPSED's
- Calculate unnotched failure RF
- Calculate pin contact angle
- Calculate the plate stress field coefficients
- Show the plate stress field for approval by user
- Calculate plate ultimate failure

The VBScript interprets a problem input file, handles input and output from each calculation sheet and writes the results file. By only requiring an input file and providing a results file, the analytic tool can be used by Fokker Engineers to estimate failure of a notched plate with arbitrary stress boundary conditions. The assembly is shown in Figure 4.6.

**Figure 4.6:** Main program assembly algorithm

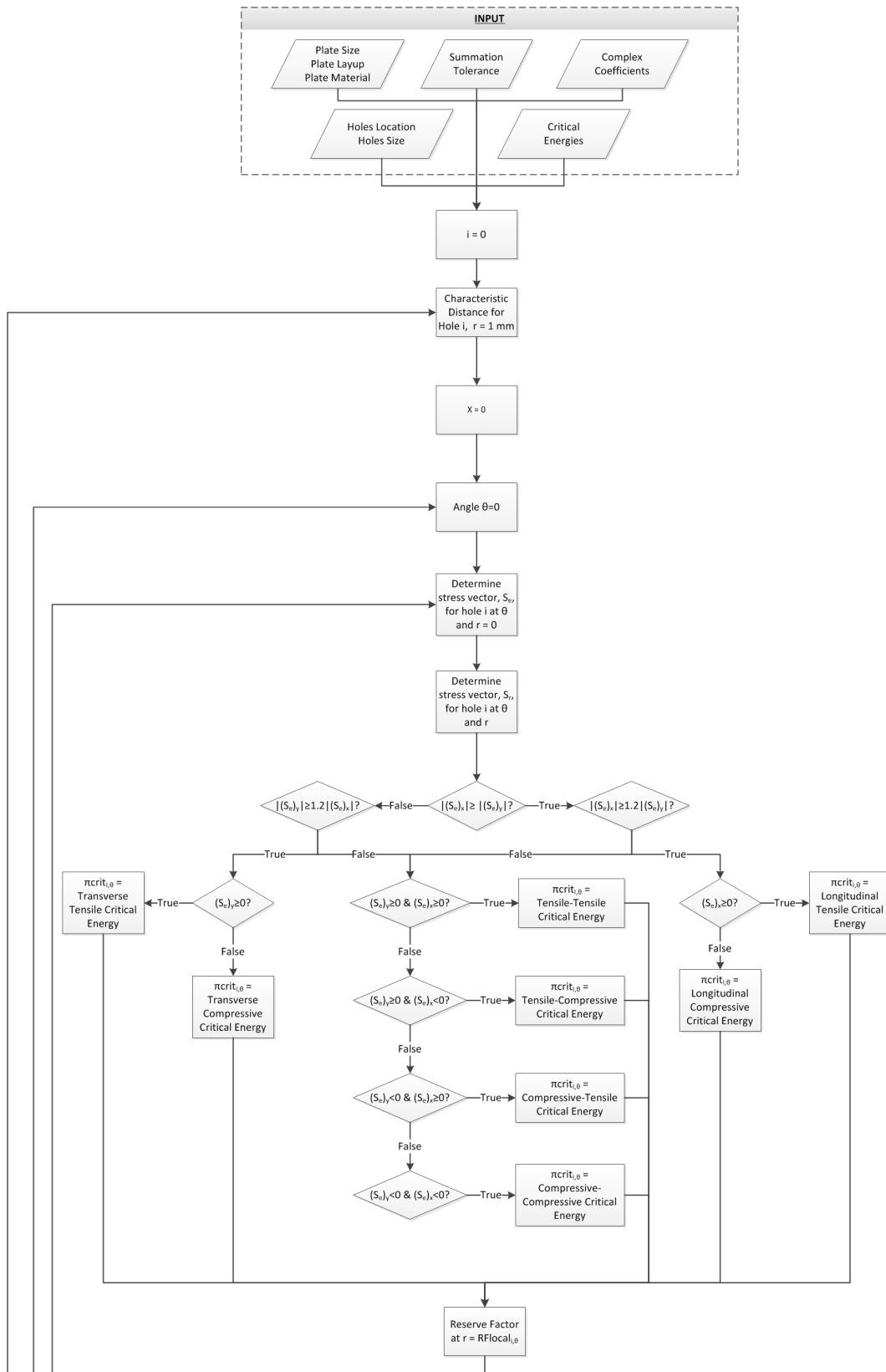


Figure 4.7: Notched failure algorithm, continued in Figure 4.8

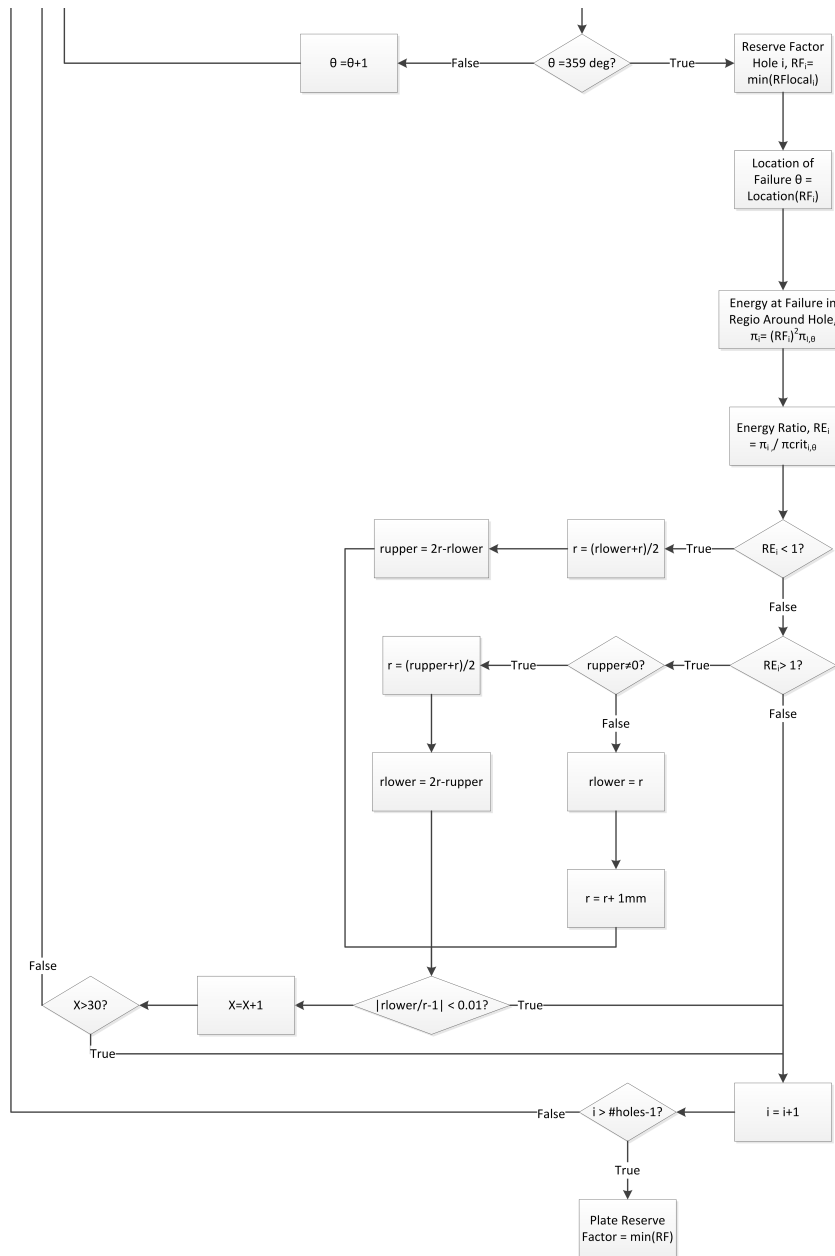


Figure 4.8: Notched failure algorithm, first part in Figure 4.7

Chapter 5

Tool Verification

Although verifying whether the analytic tool functions as intended does not contribute to the scientific value of this report, it is required for use in a design environment. For verification, every code block in the analytic tool was tested individually by providing a suitable input, calculating the expected output by hand and comparing this to the value from the tool. The tested code blocks are listed below. For convenience, the numerical results are not shown here but located in [Appendix D](#).

Stress Algorithm:

- Sanity check
- Laminate compliance-matrix
- Material eigenvalues
- Complex parameters p_j, q_j, R_j, t_j
- z_j^k, ξ_j^k and their derivatives
- Sign selection
- Matrices **B** and **A**
- Contact angle

Failure Algorithm:

- Ply property selection compression/tension
- Laminate strains
- Ply stresses
- FF and IFF exposures
- Change of material properties upon IFF
- Calculation and selection of CPSED

From the unit tests it is concluded that there is a maximum difference in the order of 0.1% between the hand calculation and analytic tool. This difference is attributed to round-off errors. Next to unit tests, system tests were performed to assure overall functionality of the analytic tool. The system tests are divided into tests for stress determination, failure prediction and a general tool test. For stress determination, the results from the tool are compared to the analytical, infinite plate, solution obtained by Lekhnitskii [4]. The following configurations are used:

- Infinite plate with elliptical hole and uniform pressure at the opening contour
- Infinite plate with elliptical hole and uniaxial tension at the plate edge

When a uniform pressure q is applied at the edge of an elliptical hole, the closed form solution for the tangential stress around the hole is [4]:

$$\sigma_\theta = \frac{q}{l^2} \Re \left\{ \frac{ie^{-i\theta}}{(a \sin \theta - \mu_1 b \cos \theta)(a \sin \theta - \mu_2 b \cos \theta)} \right. \\ \times \left[(\mu_1 \mu_2 a - i \mu_1 b - i \mu_2 b) a^3 \sin^3 \theta + i (\mu_1 \mu_2 - 2) a^2 b^2 \sin^2 \theta \cos \theta \right. \\ \left. \left. + (2 \mu_1 \mu_2 - 1) a^2 b^2 \sin \theta \cos^2 \theta + (\mu_1 a + \mu_2 a - ib) b^3 \cos^3 \theta \right] \right\} \quad (5.1)$$

where a is the semi major axis and b is the semi minor axis of the hole. l is defined as:

$$l^2 = a^2 \sin^2 \theta + b^2 \cos^2 \theta \quad (5.2)$$

In the case where a uniaxial load p is present at the plate edges and the hole is unloaded the closed form solution for the tangential stress around the hole is given by [4]:

$$\sigma_\theta = p \frac{a^2}{l^2} \sin^2(\theta) + \frac{pb}{l^2} \Re \left\{ \frac{e^{-i\theta}}{(a \sin \theta - \mu_1 b \cos \theta)(a \sin \theta - \mu_2 b \cos \theta)} \right. \\ \left[(\mu_1 + \mu_2) a^3 \sin^3 \theta \right. \\ \left. \left. + (2 - \mu_1 \mu_2) a^2 b \sin^2 \theta \cos \theta + b^3 \cos^3 \theta \right] \right\} \quad (5.3)$$

The closed form solutions for infinite plates cannot simply be reproduced by the analytic tool. This because the analytic tool has, as input, finite size plate edges and holes. As such, to simulate infinite boundary conditions, a large plate (1m by 1m) with small hole ($a = 5$ [mm], $b = 2$ [mm]) is modeled. The material for the plate is a layup of UD carbon-epoxy laminates with a symmetric layup and varying amounts of 0° , 45° and 90° plies. The presence of each of these three angles is varied between 0% and 100% which resulted in a total of 10 configurations. For precision parameters; $N = 6$ and $TOL = 10^{-12}$ are used. To illustrate the results from both comparisons, the tangential stress concentration factor when a UD, $\pm 45^\circ$ and $[0/90]_s$ layup is used are shown in Figure 5.1 to Figure 5.3 for the case of uniform pressure at the hole edge and Figure 5.4 and Figure 5.6 for the case of uniform tension. The complete results of the comparisons between the tangential stress concentration factor around the hole with different materials is given in Appendix D. From the comparisons it is concluded that a maximum discrepancy of $\pm 0.5\%$ exists between the analytic tool and theoretical solution which is attributed to round-off errors in the computation and errors due to numerical integration. The discrepancy is small enough to conclude that the algorithm for stress determination is verified.

For failure prediction, the system tests are divided into one for unnotched failure and one for notched failure. The system test for the unnotched failure criterion is done by supplying uniaxial loading conditions in compression, tension and shear to some laminates. By hand, the failure load is estimated by considering only the fibres in the direction of the load and their respective strengths. The result from the tool should be in the same order of magnitude.

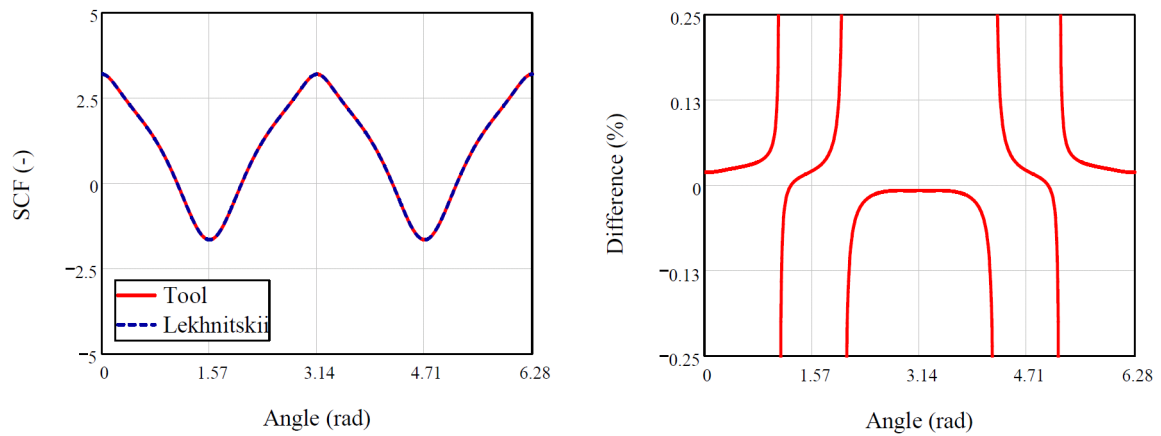


Figure 5.1: Stress concentration factor at hole edge and difference between tool and Lekhnitskii. 100% UD uniform pressure at hole edge, $a = 5$ [mm], $b = 2$ [mm]

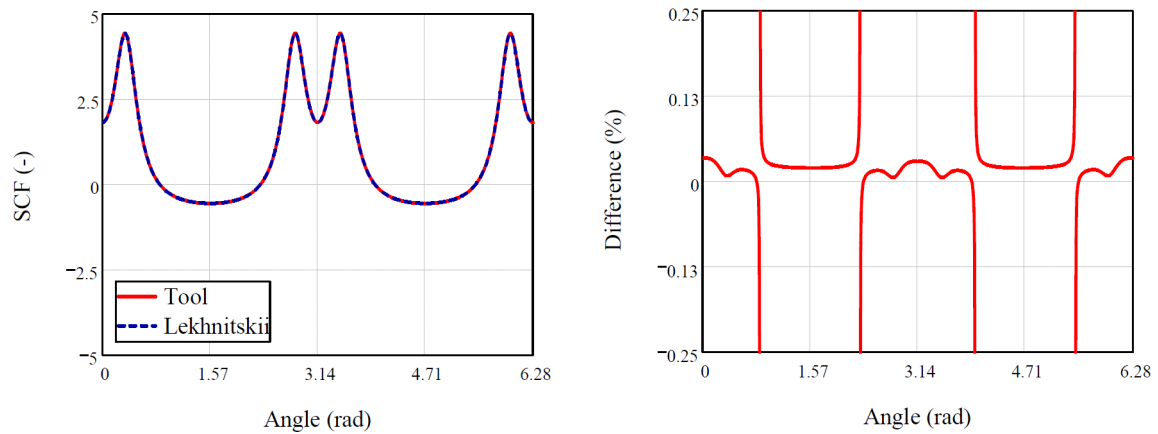


Figure 5.2: Stress concentration factor at hole edge and difference between tool and Lekhnitskii. 100% $\pm 45^\circ$ uniform pressure at hole edge, $a = 5$ [mm], $b = 2$ [mm]

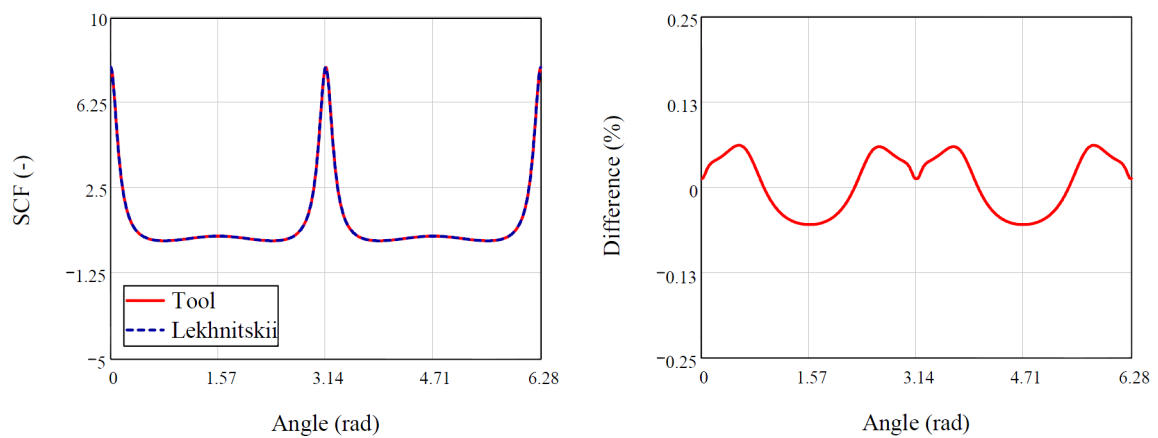


Figure 5.3: Stress concentration factor at hole edge and difference between tool and Lekhnitskii. 50% 0° , 50% $\pm 90^\circ$ uniform pressure at hole edge, $a = 5$ [mm], $b = 2$ [mm]

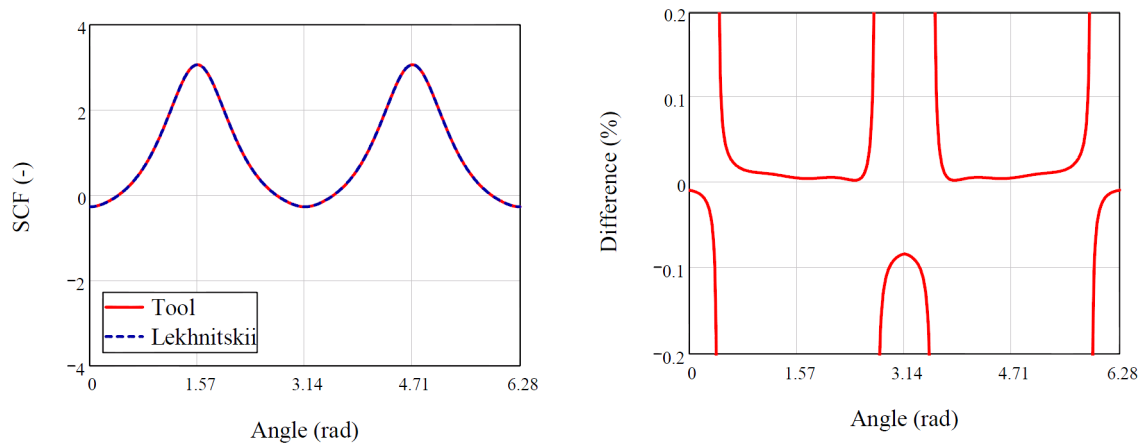


Figure 5.4: Stress concentration factor at hole edge and difference between tool and Lekhnitskii. 100% UD, uniaxial tension at 0° , $a = 5$ [mm], $b = 2$ [mm]

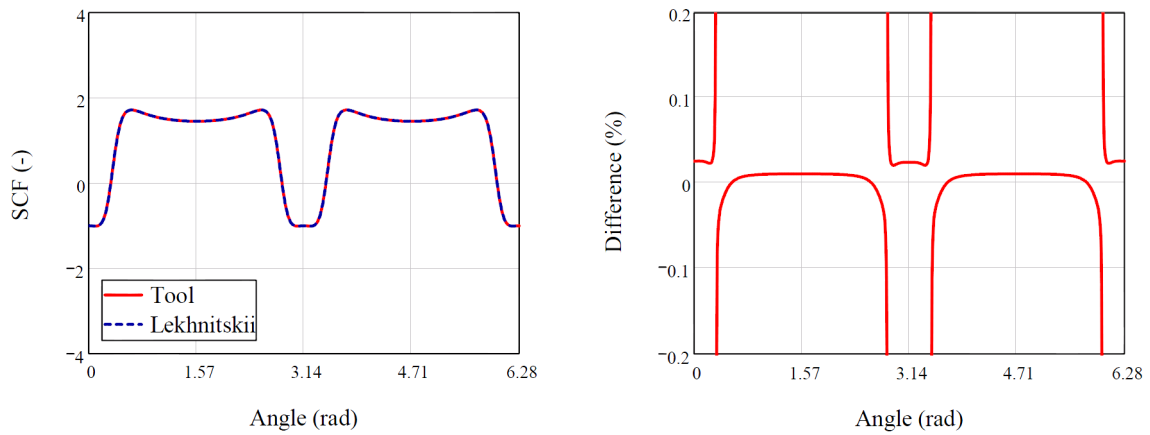


Figure 5.5: Stress concentration factor at hole edge and difference between tool and Lekhnitskii. 100% $\pm 45^\circ$, uniaxial tension at 0° , $a = 5$ [mm], $b = 2$ [mm]

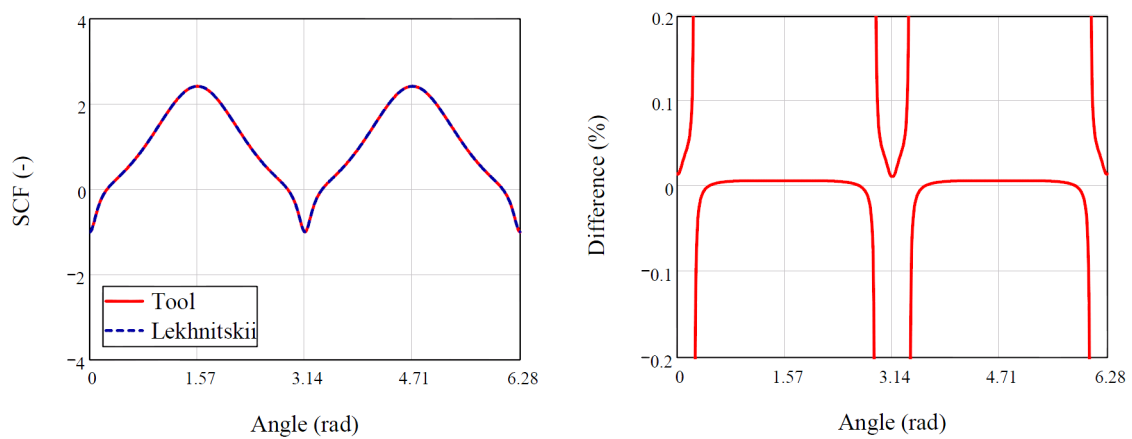


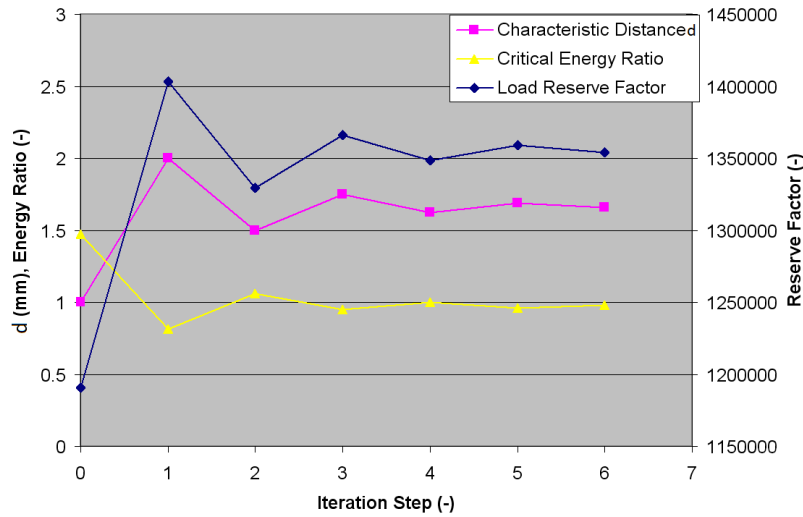
Figure 5.6: Stress concentration factor at hole edge and difference between tool and Lekhnitskii. 50% 0° , 50% 90° uniaxial tension at 0° , $a = 5$ [mm], $b = 2$ [mm]

Table 5.1: System test results unnotched failure criterion

Layup	Load Vector	Tool (MPa)	Hand (MPa)
42% 0°, 42% $\pm 45^\circ$, 16% 90°	(1,0,0)	816	826
42% 0°, 42% $\pm 45^\circ$, 16% 90°	(-1,0,0)	-629	-629
100% 0°	(1,0,0)	1575	1575
100% 0°	(0,1,0)	60	60
100% 0°	(0,0,1)	113	113
50% 0°, 50% 90°	(1,0,0)	792	787.5
50% 0°, 50% 90°	(0,1,0)	792	787.5

They are shown in Table 5.1 where it can be seen that they are as expected. The algorithm for unnotched failure prediction is considered verified.

For notched failure prediction, the algorithm is verified by looking at the change in characteristic distance d , Reserve factor and CPSED ratio with every new iteration. This is illustrated in Figure 5.7 where it can be seen that, after a few iterations, all values converge to a steady value which is as expected. The notched failure algorithm is considered verified.

**Figure 5.7:** Change of load reserve factor, r and critical energy ratio throughout iterations

Verification of the stress analysis and failure prediction assembly is done using three configurations. In configuration one, a uniaxial load in the longitudinal direction is applied to a rectangular plate with an open circular hole in a quasi-isotropic sheet. The expected angle of failure is $\pm 90^\circ$. The failure load must, at least, be higher than one third of, and lower than, the unnotched failure strength since a stress concentration factor of three is present at the hole edge. In the second configuration, a uniaxial load in transverse direction is applied to the same setup. Since the layup is quasi-isotropic, the expected failure load is equal to the failure load of configuration 1 while the failure angle should either be 0° or 180° . In the third configuration, the hole is loaded with a cosine distributed radial load between $\pm 90^\circ$. The load is balanced by a distributed edge load on the opposite edge. In this case it is expected to have (bearing) failure at 0° at a load which is lower than the compressive strength of the

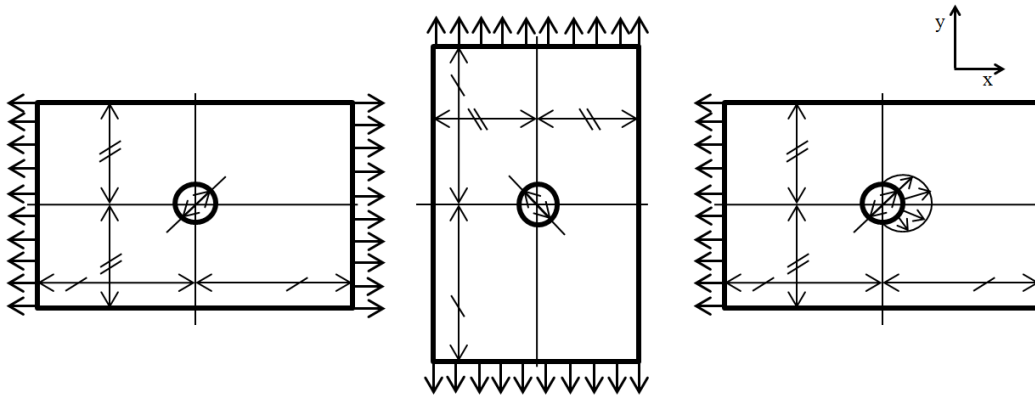


Figure 5.8: Configuration 1,2 and 3 (left to right) used for assembly verification.

Table 5.2: Verification result of assembly tests

Case	Angle of failure (deg)		Failure Load (MPa)	
	Tool	Hand	Tool	Hand
1	270	$90^\circ \vee 270^\circ$	610	$372 \leq X \leq 1115$
2	0	$0^\circ \vee 180^\circ$	611	$372 \leq X \leq 1115$
3	358	0°	834	$0 \leq X \leq 905$

laminate. The configurations are shown in Figure 5.8. The results from the analysis are given in Table 5.2 where it can be seen that all three test cases produce results which are within expected bounds. Note, however, that the failure load for case one and two differs slightly while it is expected to be equal since, virtually, the same case is investigated twice (only rotated by 90°). This discrepancy is attributed to round-off errors in the calculation. Additionally, it is observed that a failure angle of 358° was predicted for case three while it is expected to have a failure angle of 0° . This does not raise any concern as it is sufficiently close to 0° . It only indicates that failure occurs at a different angle than expected because of the complex two-dimensional stress state in front of the pin.

By passing the units, systems and assembly verification tests it is confirmed that the analytic tool produces results as intended. The tool can now be used to compare against experimental data for validation which is done in Chapter 6.

Validation, Comparison to FEA and Experimental Data

Before the tool is ready to be used in a design environment, its performance and operational boundaries must be assessed. First, however, optimal values for the remaining “free” parameters need to be determined. These “free” parameters are required for the algorithm but not directly related to the problem configuration. Since they are not directly related to the problem, the future user of the tool will have no physical connection to these parameters and will, if inexperienced, not be able to choose suitable values. Hence it is necessary to provide a guideline for these parameters. For stress analysis, the “free” parameters are:

- MathCAD13.1@integration tolerance TOL
- The summation parameter N
- The horizontal displacement angle α

For failure prediction these parameters are:

- The pin-hole clearance λ
- The hole size for determination of the CPSED

In this chapter, the optimal values for these parameters are determined by investigating their influence on the results. Next, the results from the stress field analysis and failure prediction are compared to, respectively, FEA and experimental data to validate the analytic tool and determine the operational boundaries and performance of the new criterion.

6.1 Stress Analysis

Since FEA is also a model instead of reality itself, it can be argued that it should not be used for validation. Over the years, however, FEA, when well constructed, has been generally accepted to provide an accurate representation of reality. Additionally, data from experiments where the entire stress field is measured are very hard to get by and limited to specific cases only. For this reason and the fact that FEA can provide an accurate representation of the stress field, FEA is used as validation for the stress field method. Before a comparison to FEA can be made, the “free” parameters: MathCAD13.1@integration tolerance TOL , the summation parameter N and the the pin-hole contact angle α ; need to be determined. This is done in Section 6.1.1 and Section 6.1.2. Next, in Section 6.1.3 the comparison to FEA is provided.

6.1.1 Influence of accuracy parameters TOL and N

It is difficult to determine the exact influence of TOL and N because they interact with the specific configuration of a problem. For example, the impact of these parameters will be different for problems with one hole or multiple holes. Also the type and amount of loading as well as the size and material of the plate has an influence. For this work it is not intended, nor required to perform a complete parametric study on the influence of TOL and N . Therefore, five configurations, representative for the intended use of the tool are chosen for this evaluation. The configurations are:

1. Circular hole, diameter D , in square sheet size $4D$ subjected to uniaxial tension
2. Circular hole, diameter D , in a square sheet size $4D$ subjected to multiaxial tension-tension
3. Circular hole, diameter D , in a square sheet $2D$ subjected to uniaxial tension
4. Serie of 5 circular holes, diameter D , in a quasi-infinite length sheet with width $4D$ subjected to uniaxial tension
5. 4 circular holes, diameter D , in a rectangular pattern subjected to uniaxial tension

In the configurations, circular holes are chosen because these are the most common in aircraft structures. Configuration 1 is used as baseline. To provide an indication on whether an increase in boundary conditions influences the behaviour of the algorithm, an additional tension load is added which results in configuration 2. Next, to test whether the size of the plate has an influence, the plate size is halved (increasing edge effects) which results in configuration 3. The effect of multiple holes and their location is investigated by adding more holes and changing patterns which results in configuration 4 and 5. The material used is representative for a carbon fibre reinforced lamina (material 2, Table D.1) with layup $[-45/45/-45/45/90/0/0/0]_s$. From practical experience with the tool it is noticed that N has the largest influence on the results. Therefore this parameter is investigated first.

N represents the amount of summations, thus the accuracy, of the solution given by Eq. (3.13). By increasing N , it is expected that the solution will converge to a steady value.

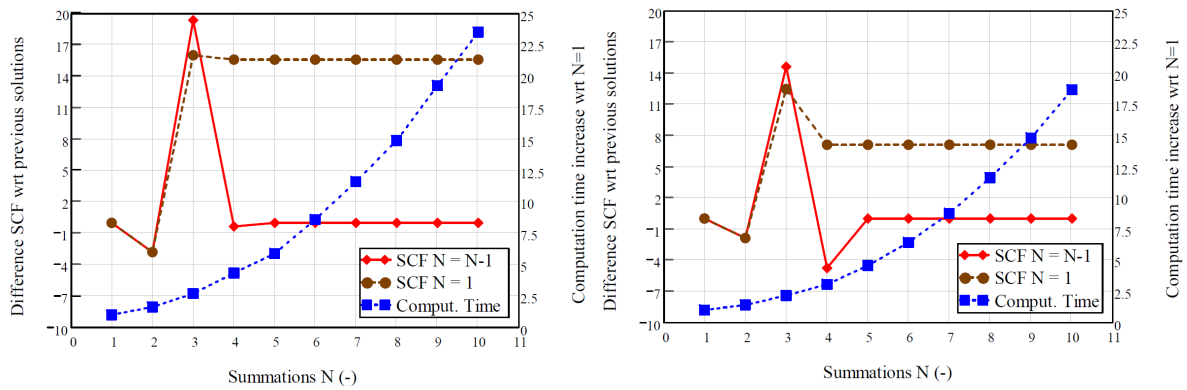


Figure 6.1: Influence of N for a centered single hole subjected to uniaxial tension (left) and multiaxial tension-tension (right) in a 4D size square plate

If the solution converges to a steady value, increasing N might return the same stress field because convergence is reached. Increasing N , however, will always result in an increase in computation time because the size of the solution vector increases. To minimize computational time, it thus needs to be determined which minimum value of N results in a converged solution.

For the five aforementioned configurations, the difference between the maximum stress concentration factor with the current solution (N) and the first solution ($N = 1$), the difference between the maximum stress concentration factor with the current solution (N) and the previous solution ($N = N - 1$) and the increase in computation time is plotted while varying N from 1 to 10. The value of TOL is set to 10^{-12} . The results are shown in Figure 6.1 to Figure 6.3. Note that in the figures only relative calculation time is given because it will differ depending on the performance capabilities of the computer used. For convenience, computation time for a single hole in a rectangular sheet 4D, $N = 1$ and $TOL = 10^{-12}$ is approximately 7 seconds.

The configurations with a single hole in a rectangular sheet subjected to uniaxial tension and the same configuration with multiaxial tension-tension are shown in Figure 6.1. From the Figure it is observed that, as expected, computation time increases exponentially when increasing the accuracy of the solution. Additionally, one can see that, for both cases, the solution does not change significantly when the amount of summations is larger than or equal than 5. Increasing the amount of boundary conditions thus does not have a significant effect on the convergence behaviour of the algorithm. To investigate whether the size of the plate influences this behaviour, the same uniaxial problem is taken but the size of the plate is reduced to 2D which induces significant edge effects. The results are shown in Figure 6.2. Comparing both figures one can see an increase in required summations ($N \geq 6$) before a stable solution is obtained.

The results from a serie of 5 circular holes in a quasi-infinite length sheet with width 4D and 4 holes in a rectangular pattern subjected to uniaxial tension is shown in Figure 6.3. Comparing Figure 6.3 with Figure 6.1 it is observed that, because more holes are present, the amount of summations required for a convergent solution is higher ($N \geq 7$). Again, the computational time increases exponentially with each increase in summations. It is concluded that, providing that the amount of holes is lower than 6, it is sufficient to use $N = 7$ for a convergent solution of the stress field.

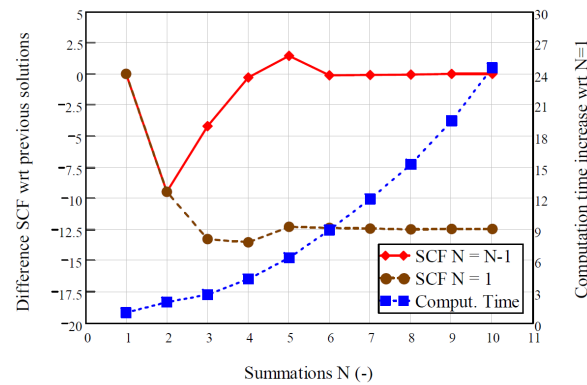


Figure 6.2: Influence of N for a centered single hole subjected to uniaxial tension in a 2D size square plate

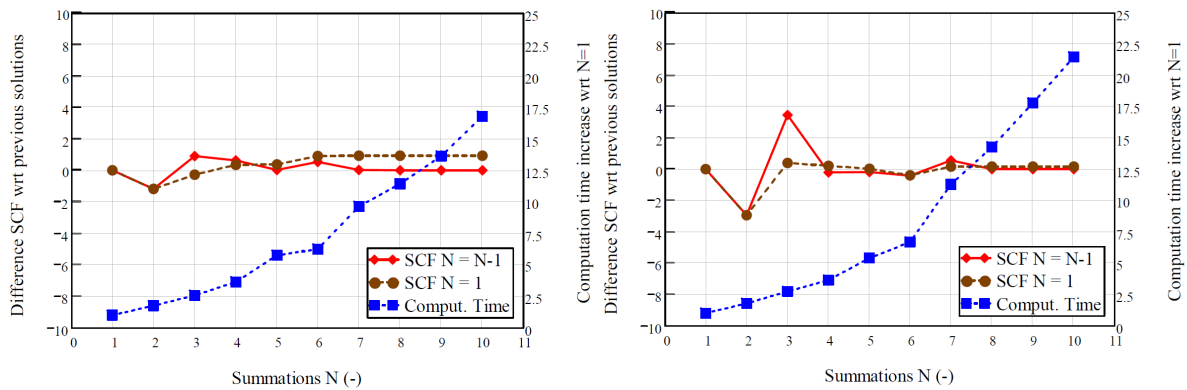


Figure 6.3: Influence of N for a series of 5 (left) and a rectangular pattern of 4 (right) circular holes in a finite width sheet subjected to uniaxial tension.

TOL regulates the convergence of the numerical integration in MathCAD13.1©. Generally, the lower TOL , the more accurate the solution should be. The lower this tolerance, however, the longer computation time and the higher the chance that the solution may not converge. This can happen when the function to be integrated is discontinuous, very sharp or has singular endpoints. Then it is possible that the differences between discretization steps does not decrease, resulting in a non-convergent solution. Using $N = 7$, and varying TOL between 10^{-3} and 10^{-15} (ultimate boundaries by MathCAD13.1©) for the same configurations, the results shown in Figure 6.4 through 6.6 are obtained. In general, one would expect that, as the integration tolerance decreases, the solution becomes more accurate, hence converge to a steady value. This is however not the case which can be seen in the fluctuations when $10^{-6} > TOL > 10^{-13}$. Outside this range the solution does, except for a single hole in a 2D rectangular plate (Figure 6.5), not significantly change. In search for an explanation of this behaviour, MathCAD13.1©key users were contacted from which it was concluded that the behaviour is a product of the MathCAD©numerical integration algorithm (based on Gaussian-Quadrature integration) and cannot be avoided easily. A possible solution is to construct a Monte-Carlo integration, which was attempted, but discarded due to a significant penalty in computational time when requiring the same accuracy. Despite this drawback, it

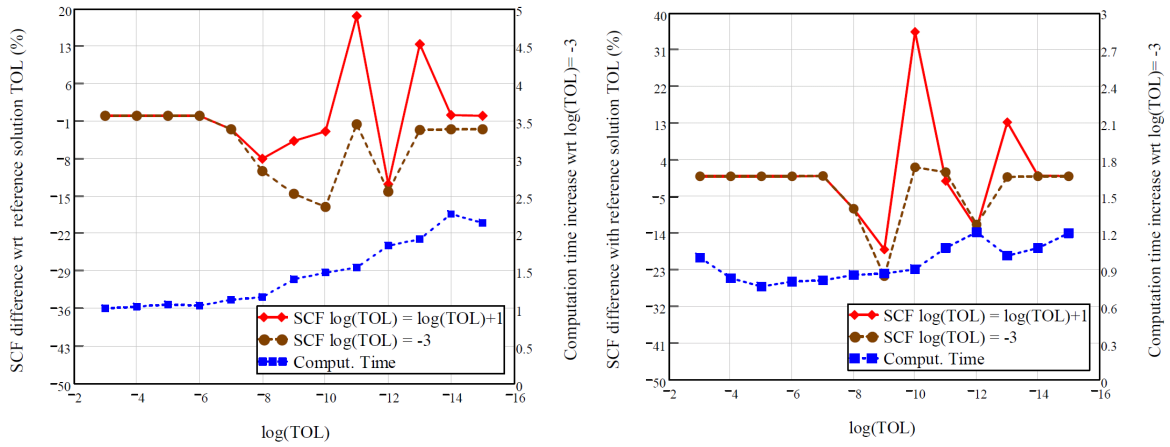


Figure 6.4: Influence of TOL for a centered single hole subjected to uniaxial tension(left) and multiaxial tension-tension (right) in a 4D size square plate

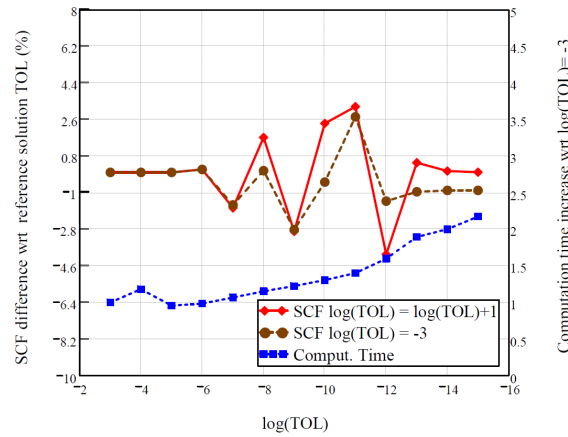


Figure 6.5: Influence of TOL for a centered single hole subjected to uniaxial tension in a 2D size square plate

is concluded that a safe working range for the analysis of a general problem is $10^{-3} \geq TOL \geq 10^{-6} \vee 10^{-13} \geq TOL \geq 10^{-16}$.

The attentive reader might have noticed that, due to this conclusion, the investigations performed for stress verification, Chapter 5, and to determine a good value for N are invalid because a value $TOL = 10^{-12}$ was used for the analysis. Contradictory, despite that this “unreliable” value was used for stress verification, the difference between Lekhnitskii’s solutions were negligible which points towards a correct solution. Both statements can only be true if, for the case of a quasi-infinite plate, the influence of TOL on the results is negligible. This is shown in Figure 6.7 where additional results are presented for a single elliptical and circular hole in a quasi-infinite sheet with $N = 7$. One can see that in these cases the solution, when varying TOL , does not differ significantly. Also, these experiments differ only from the previous experiments in the size of the plate. Hence the plate size plays a role in the convergence of the solution. Consequently, one might conclude that the results obtained to determine N have to be recalculated using a proper value of TOL because, in the used configurations, there

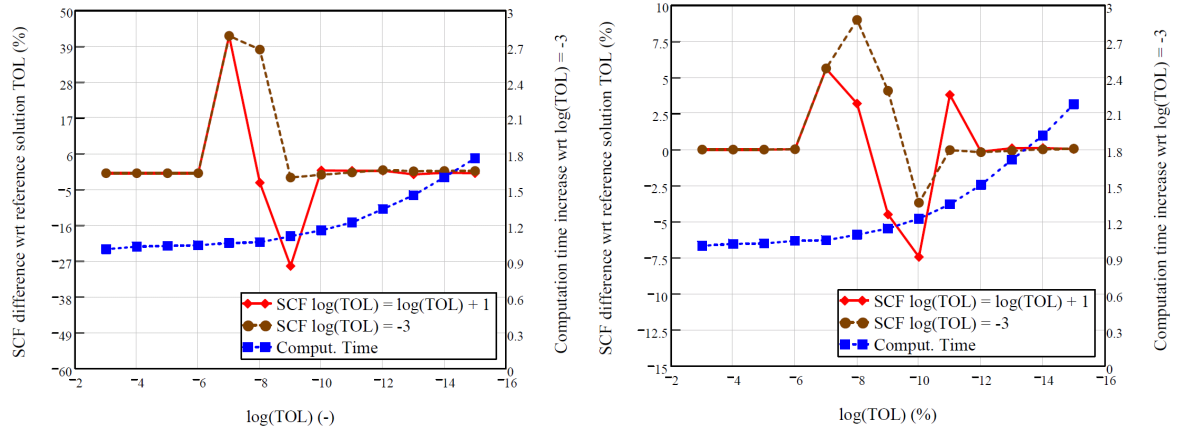


Figure 6.6: Influence of TOL for a series of 5 (left) and a rectangular pattern of 4 (right) circular holes in a finite width sheet subjected to uniaxial tension

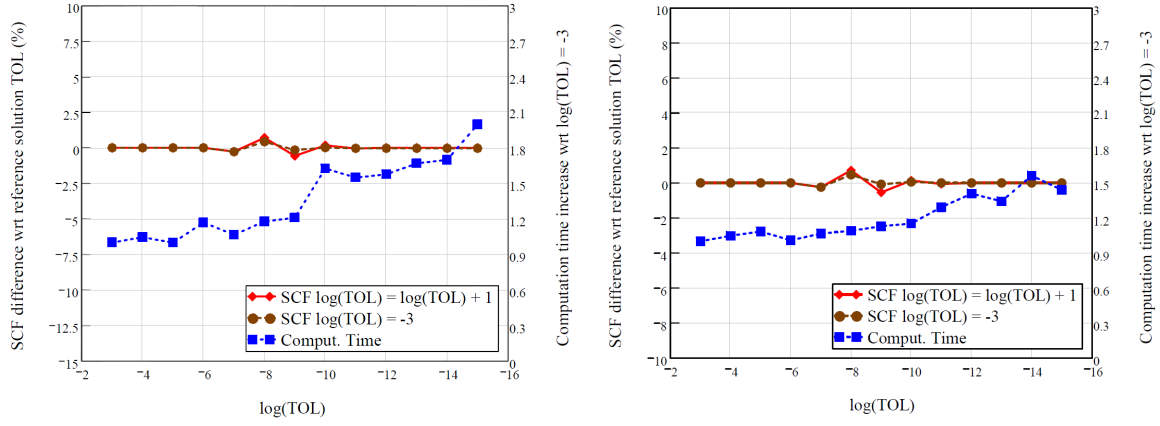


Figure 6.7: Influence of TOL for a single elliptical (right) and circular hole in a quasi-infinite sheet

is a significant edge effect. This, however, does not necessarily need to be true if it can be shown that the same behaviour for changing N exists when using another value for TOL . The reason being that, if one does a calculation with an initial error (e.g. using “unreliable” value for TOL), and compares the outcome to an outcome where the same error is incorporated, the errors will cancel each other out. This is illustrated by Figure 6.8 where the configuration with a single hole subjected to multi-axial tension-tension is recalculated for $TOL = 10^{-6}$. Comparing the outcome to the earlier results in Figure 6.1 ($TOL = 10^{-12}$) shows that the behaviour of both graphs is the same. Thus, the earlier obtained results are valid.

Finally, from this investigation on the effect of the accuracy parameters TOL and N on the obtained solution, it is concluded that good working ranges for N and TOL , when maximum 6 holes are present, are:

$$10^{-3} \geq TOL \geq 10^{-6} \vee 10^{-13} \geq TOL \geq 10^{-16} \quad (6.1)$$

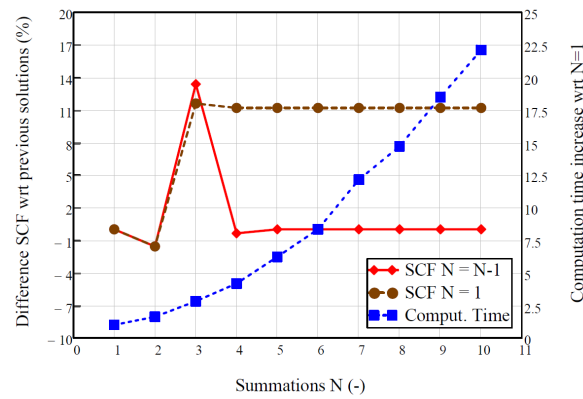


Figure 6.8: Influence of N for a centered single hole subjected multiaxial tension-tension (right) in a 4D size square plate when $TOL = 10^{-6}$

6.1.2 Influence of contact angle estimation

A satisfactory estimation of the contact angle for a pin-loaded hole is essential for a reliable estimation of the stress field. In Section 3.2 two models based on an iterative process were explained. A model developed by Tomlinson [13] and a model developed by the author. In this section the performance of both models is compared to results from FEA after which the most suitable model is chosen. FEA for this subsection were performed by Gerhardt [18] and comprise of a two-dimensional simulation of a rigid pin in a circular hole. Friction of the pin and hole edge is neglected. The results from the FEA analysis were validated with results obtained from an earlier study on bearing bypass loads in pin loaded composite joints by Crews [14].

Before proceeding to the discussion of the configurations and results, an explanation on results being (not) conservative is required. The graphs produced in this subsection are constructed by applying a bearing load $\sigma_b = P_b/(Dt)$ on a pinned hole and letting the algorithm determine the accompanying contact angle. Therefore, if for a given load σ_b , the contact angle is smaller than in the real (FEA) case, the stress concentration factor at the hole edge will be larger than in reality. Since the opposite is true when the contact angle is larger than the real case, one might say that the smaller contact angle estimation is more conservative as it will result in a lower ultimate failure load. This is true when one is focussing on the stress concentration factor on the hole edge. However, the model described in this work does not use the highest stress concentration factor at the hole edge but uses the CPSED to determine a characteristic distance away from the hole at which failure is evaluated, Section 4.1. The CPSED is calculated using a pinned hole configuration and Kweon's definition of compressive characteristic distance. Recall the aforementioned definition: "The distance from the front hole-edge to a point where the local compressive stress by the arbitrarily applied load is the same as the mean bearing stress when a bearing load is applied to the hole edge". When a small contact angle is used, the location where the local compressive stress is the same as the mean bearing stress will be further away from the hole edge compared to a larger contact angle due to the higher stresses, Figure 6.9. The CPSED is calculated as the sum of the strain energy density along d . Hence for the smaller contact angle a higher CPSED will be obtained than for the larger contact angle. In turn, the CPSED is a measure for the ability

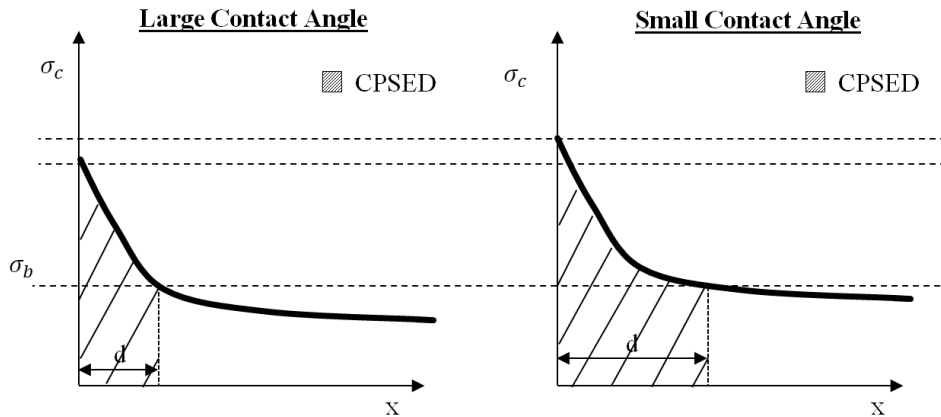


Figure 6.9: Schematic representation for the calculation of the CPSED with a higher or lower contact angle

of the material to absorb energy. Therefore, if the material is able to absorb more energy, the estimated failure load of the plate will be higher with respect to a lower CPSED. Since the lower CPSED is associated with a higher contact angle, in this work, a higher contact angle is considered conservative as it results in a lower predicted failure load.

An initial comparison between the model by Tomlinson and Sevenois model (author) is shown in Figure 6.10. In the Figure the contact angle associated with a fixed bearing load σ_b is shown. The configuration used is a rectangular plate size 125 [mm] x 25 [mm] containing one circular hole with a diameter of 5 [mm] and a QI layup. Clearance between the pin and the hole is 1.5% and α , Figure 3.7, equals half of the contact angle. In the Figure it is observed that the contact angle from Tomlinson's model remains 0° at low bearing stress levels. At higher stress levels the model converges rapidly towards FEA data but stays in the non-conservative region (smaller contact angle than expected). The contact angle being zero at low bearing stress levels has to do with the assumption of an elliptical deformation of the hole. At a lower load level, thus lower horizontal displacement, the elliptical curve, Eq. (3.33), only intersects the pin shape at 0° . Therefore the result is also 0° . Compared to Tomlinson's model, Sevenois' model approaches the curve from FEA much better and the contact angle is, in all cases, conservative. Furthermore no unexpected behaviour is observed. From this first investigation it is clear that the performance of Sevenois's model is better, therefore it is chosen to be used in the analytic tool.

To produce the results in Figure 6.10, a value for the displacement angle α was chosen to be half of the contact angle. Noting that there is a discrepancy with respect to FEA, it is further investigated if changing α would be beneficial for the prediction. Additionally, different laminate directionalities ($= \sqrt{E_{xx}/E_{yy}}$) and pin hole clearances might also have an influence on the predictions and this should also be investigated. For this purpose a parametric study is set up where a total of 10 different layups with 6 different clearances for a typical CFRP laminate are investigated resulting in 24 analysis. Graphs of bearing load vs contact angle are produced from FEA and Sevenois' model. For Sevenois' model a value for α equal to the contact angle, half the contact angle and 0° is investigated. The ply properties, layups and clearances are shown in Table 6.1.

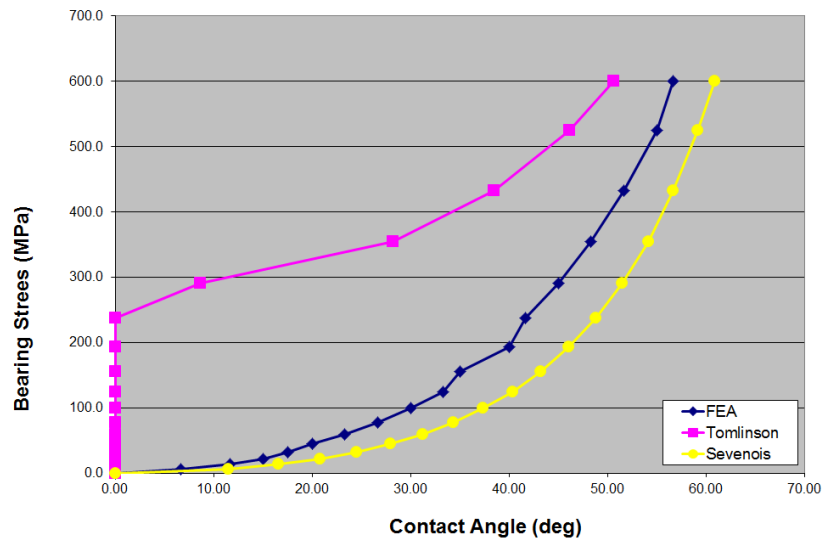


Figure 6.10: Change in contact angle with increasing bearing stress for Tomlinson, FEA and Sevenois

Table 6.1: Analysis parameters for optimal α determination

Layups - in % 0/ \pm 45/90 degrees	
20/70/10	25/50/25
50/40/10	30/40/30
20/20/60	60/20/20
20/60/20	40/30/30
0/0/100	100/0/0
Clearances (%)	
2.0,1.5,1.0,0.5,0.1,0.01	
Material Properties	Dimensions
E11(GPa): 133.5	Laminate thickness: 1 [mm]
E22(GPa): 8.3	Plate length: 125 [mm]
G12(GPa): 40.5	Plate width: 25 [mm]
ν 12(GPa): 0.3	Hole diameter: 5 [mm]

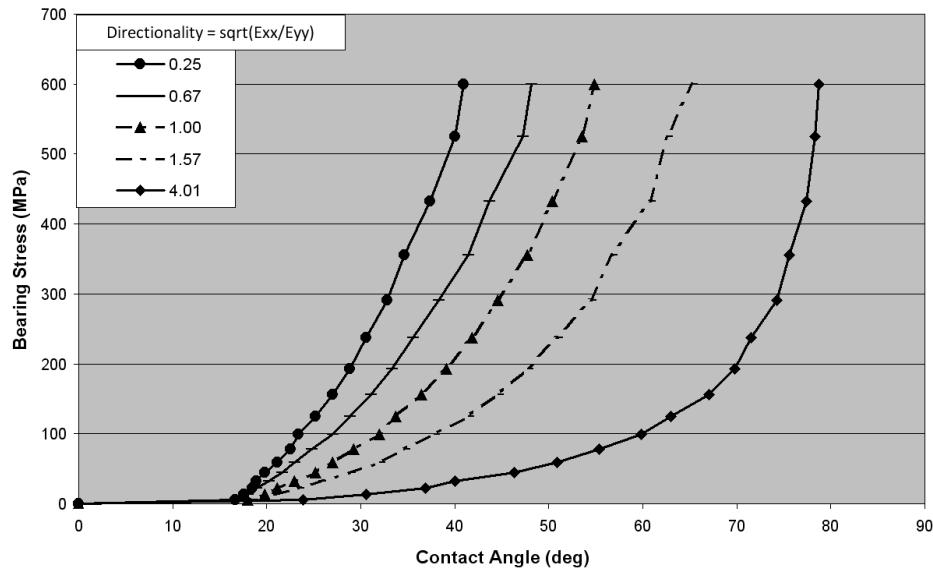


Figure 6.11: Effect of directionality on contact angle prediction (FEA) [18]

The directionality of each laminate was computed and associated with the results. For convenience, in this subsection only the most important result of the analyses are shown. All results are given in Appendix E. First the effects of laminate directionality and pin-hole clearance are investigated. As is illustrated in Figure 6.11 the higher the directionality, the higher the contact angle given a certain bearing load. Furthermore, from Figure 6.12 it is concluded that a lower pin-hole clearance results in a higher contact angle. This is as expected since a smaller clearance implies a bigger pin for the same hole size. Thus the contact angle will automatically increase. A comparison between FEA and Sevenois's model for different values of α (equal to the contact angle, half the contact angle and 0° denoted by 1.0, 0.5 and 0.0 respectively) is shown in Figure 6.13. In the figure results for a QI layup and a clearance of 2.0% are presented. From the figure it is observed that increasing α results in a lower contact angle when given a certain load. This results in non-conservative predictions when α is equal to the contact angle. Therefore this value for α is excluded for analysis. Furthermore it can be seen that when α is equal to half the contact angle, the prediction is conservative but less conservative than when α is taken equal to 0° . This conclusion is valid for the tested layups where the directionality is smaller than 1.11. For directionalities between 1.11 and 1.13, the prediction is within 5% of the value from FEA. For higher directionalities the contact angle prediction is conservative for $\alpha = 0^\circ$ up to a directionality of 1.13.

It is recognized that a better approximation of the pin-hole contact problem might be achieved when using displacement boundary conditions. Time constraints however did not allow for adaptation of the model and therefore the validity of the tool has to be restricted to laminates with a directionality lower than 1.13. As to which value of α should be used, it is recommended to use α equal to half the contact angle because it results in the least discrepancy with respect to FEA.

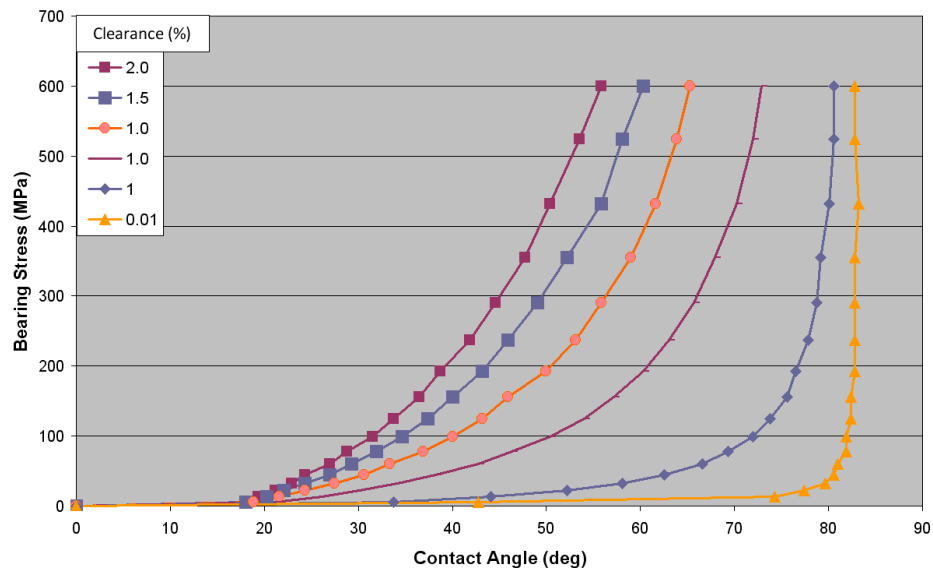


Figure 6.12: Effect of clearance on contact angle prediction (FEA) - QI layup [18]

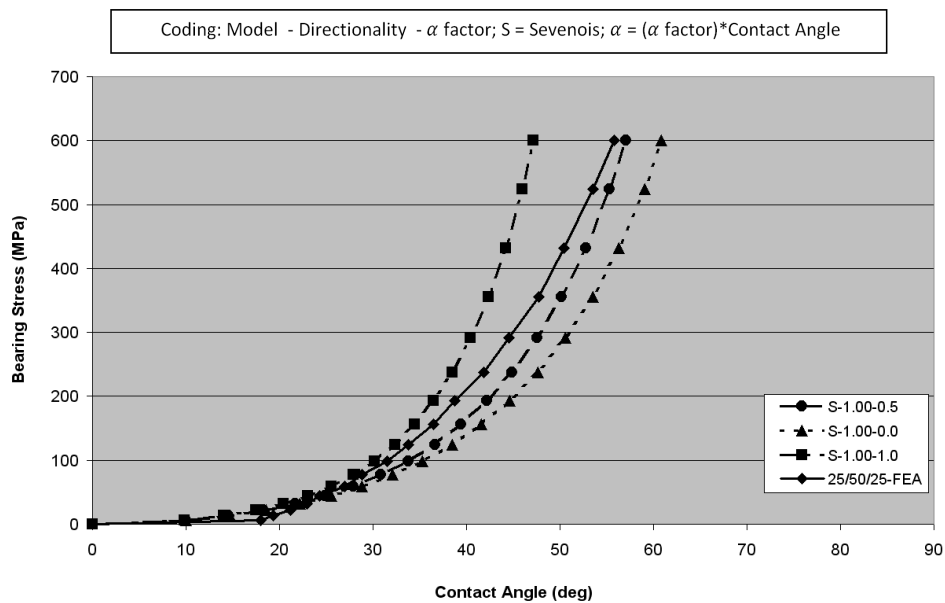


Figure 6.13: Effect of α on contact angle prediction (Sevenois's model) and comparison to FEA. Clearance 2% - QI layup in cooperation with [18]

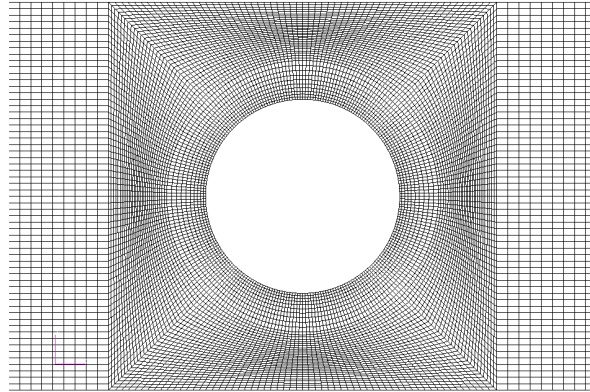


Figure 6.14: Example of the FEM mesh around a hole

6.1.3 Comparison to FEA

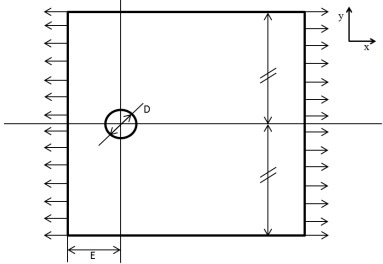
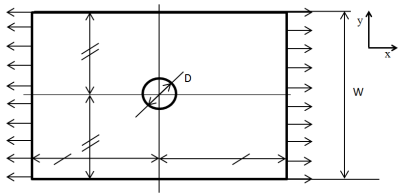
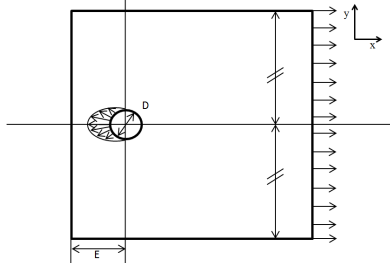
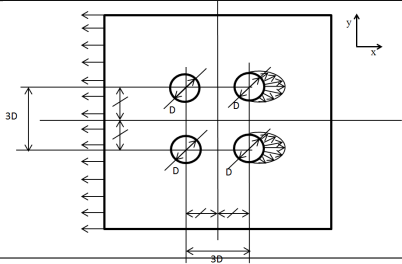
In Section 6.1.1 and Section 6.1.2 optimal parameters for TOL , N and α are established. In Chapter 5 it was demonstrated that the model can accurately produce stress distributions for infinite plates and a single hole. Now, it remains to determine how well the tool is capable of incorporating the effect of edges and multiple holes. For this purpose one needs to know the accuracy of the stress field when:

- a hole is close to a plate edge
- a hole is loaded in the presence of edges
- multiple (loaded/unloaded) holes are present

From these goals suitable test cases are derived which are shown in Table 6.2. In the table it can be seen that, to determine the accuracy of the tool when the hole is close to a plate edge, the configuration of a single hole in a plate subjected to uniaxial tension is used. In configuration 1 the distance to the loaded edge (E/D) and in configuration 2 the diameter to width ratio (W/D) is varied. To determine the accuracy when a hole is loaded, a hole with a radial cos-distributed load, Eq. (3.32), at its edge is modeled in a finite size plate as shown in configuration 3. Lastly, with configuration 4, the ability of the tool to account for a combination of loaded and unloaded holes close to each other is investigated. Four holes with diameter D are placed $3D$ apart in a square pattern. The holes to the right(2) are loaded with a radial cos-distributed load, Eq. (3.32). The remaining holes are unloaded. The loads are balanced with an edge load to one side of the plate.

The configurations in Table 6.2 are modeled in a FEA environment using MSC PATRAN/-NASTRAN®. Since the tool is only capable of calculating the stress field for a 2D-plate use of CQUAD4 shell elements is justified. A mesh refinement is applied around the holes to capture stress concentrations which resulted in 240 elements around each hole. Additionally, in accordance with the Fokker FEM manual [199], it is made certain that the aspect ratio of the elements is lower than 4, the skew is higher than 60 degrees and taper lower than 0.5 in the vicinity of the hole. An example of the mesh is shown in Figure 6.14. A 2D orthotropic

Table 6.2: Test cases for comparison between FEA and analytic tool

1.		Layup: $[0/+45/-45/+45/-45]_s$ Cases: $E/D = 1.0, 1.5, 2.0, 2.5$ Hole diameter: 10 [mm] Plate length: 90 [mm] Plate width: 100 [mm]
2.		Layup: $[0/+45/-45/+45/-45]_s$ Cases: $W/D = 2.0, 2.5, 3.0, 4.0$ Hole diameter: 10 [mm] Plate length: 100 [mm]
3.		Layup: $[0/+45/-45/+45/-45]_s$ Cases: $E/D = 1.5, 2.5$ Hole loaded with edge pressure load radially distributed Hole diameter: 10 [mm] Plate length: 100 [mm] Plate width: 100 [mm]
4.		Layup: $[0/+45/-45/+45/-45]_s$ Cases: two holes unloaded, two holes loaded Hole diameter: 10 [mm] Plate length: 200 [mm] Plate width: 200 [mm]

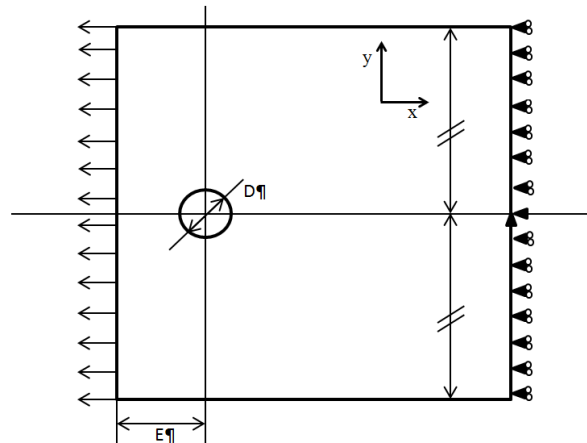


Figure 6.15: Boundary condition

homogeneous material type is used. The engineering properties of the layup are calculated beforehand and inserted as scalars.

Load and boundary conditions are handled in different ways depending on the configuration. For configuration 1 and 2, the load on the plate edge furthest away from the hole is replaced by a displacement restriction in the direction of the load. Additionally, to avoid unnecessary pivot ratios (out-of-plane movements), the central node on that edge is restricted to move or rotate. This is illustrated in Figure 6.15. For configuration 3 and 4 the hole edge load is represented by a CID distributed radial edge load while the edge is replaced by the same displacement boundary condition as described for configuration 1 and 2. Modelling the configurations in the analytic tool is much simpler. The software tool takes edge loads, material properties, plate and hole(s) dimensions as direct input. Therefore it is completely parametric and provides worry-free (no need to check the validity of the mesh) batch processing which is one of the major strengths of this tool. One however does need to check whether the solution is stable with respect to the amount of summations (N) used for the solution. However, as has been shown in Section 6.1.1, using $N = 7$ suffices for problems up to 5 holes where no excessive edge or hole to hole effects are present. Therefore, for all problem cases $N = 7$ and $TOL = 10^{-6}$ is used as accuracy parameters.

The comparison between FEA and the tool is performed by qualitatively and quantitatively assessing the SCF of the tangential stress around each hole. Furthermore, the change of maximum SCF along the length or width of the plate is assessed qualitatively. For convenience, only the most important results from the analyses are shown in this section. All results are presented in Appendix F. The analyses of configuration 1 when $E/D = 2.5$ and $E/D = 1$ are shown in Figure 6.16 and Figure 6.17 respectively. In both figures it is observed that the general behaviour of the SCF when revolving around the hole is the same for FEA and the analytic tool. Four stress peaks in a symmetric fashion are present of which two are higher than the other. For $E/D = 2.5$ there is no apparent difference between both solutions. For $E/D = 1.0$, however, a discrepancy is present between the higher stress peaks. Looking at the change of σ_y/σ_0 along x while $y = 0$ reveals that in the vicinity of the hole the SCF follows the same trend. At the plate edges a discrepancy is also present. The tool predicts a stress value of approximately zero while FEA, especially when $E/D = 1$, expects much higher stress

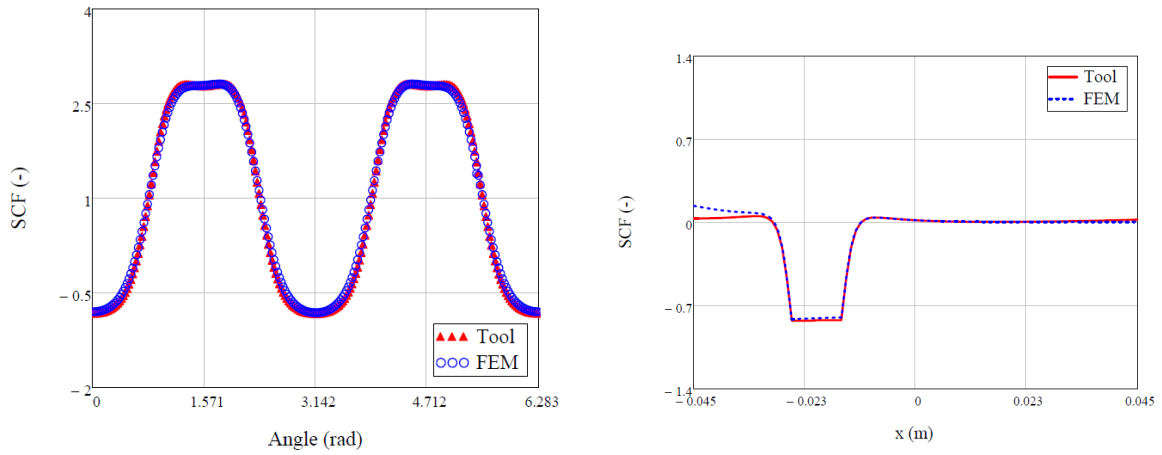


Figure 6.16: Config. 1, SCF of σ_θ at the hole edge (left) and SCF of σ_y at $y = 0$ (right) when $E/D = 2.5$

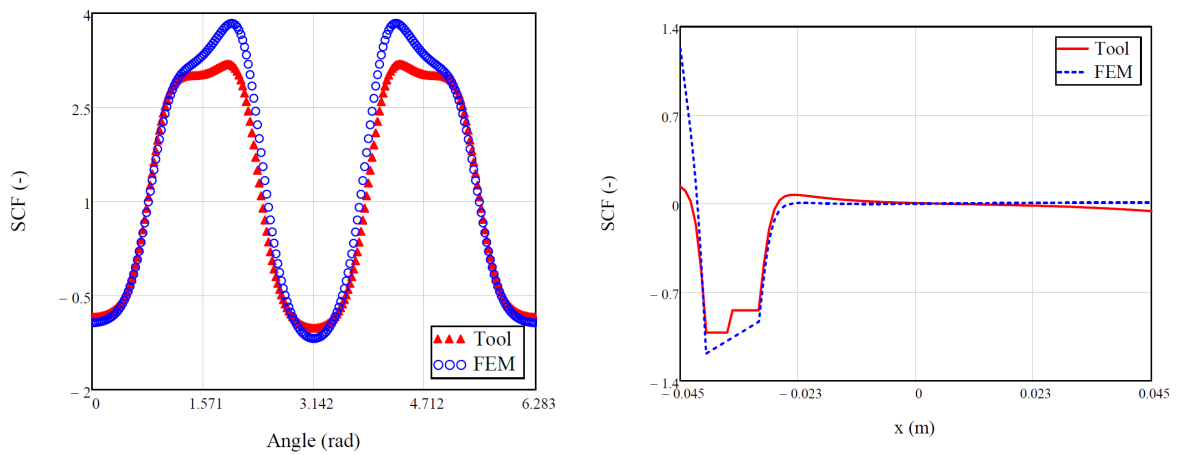


Figure 6.17: Config. 1, SCF of σ_θ at the hole edge (left) and SCF of σ_y at $y = 0$ (right) when $E/D = 1$

in σ_y .

The analyses of configuration 2 for $W/D = 4$ and $W/D = 2$ are shown in Figure 6.18 and Figure 6.19 respectively. Comparing both figures to the figures from configuration 1 it is observed that a similar conclusion can be drawn. For the case where $W/D = 4$, there is a negligible discrepancy between FEA and results from the analytic tool. For $W/D = 2$ there is a larger, but with respect to configuration 1 smaller, discrepancy between both. The analyses for configuration 3, a loaded hole with $E/D = 2.5$ and $E/D = 1.5$ are shown in Figure 6.20 and Figure 6.21 respectively. Just as with configuration 1 and 2 it is seen here that, for the configuration with the hole furthest from the edge, the difference between both methods is smaller compared to the configuration where the hole is closer to the edge.

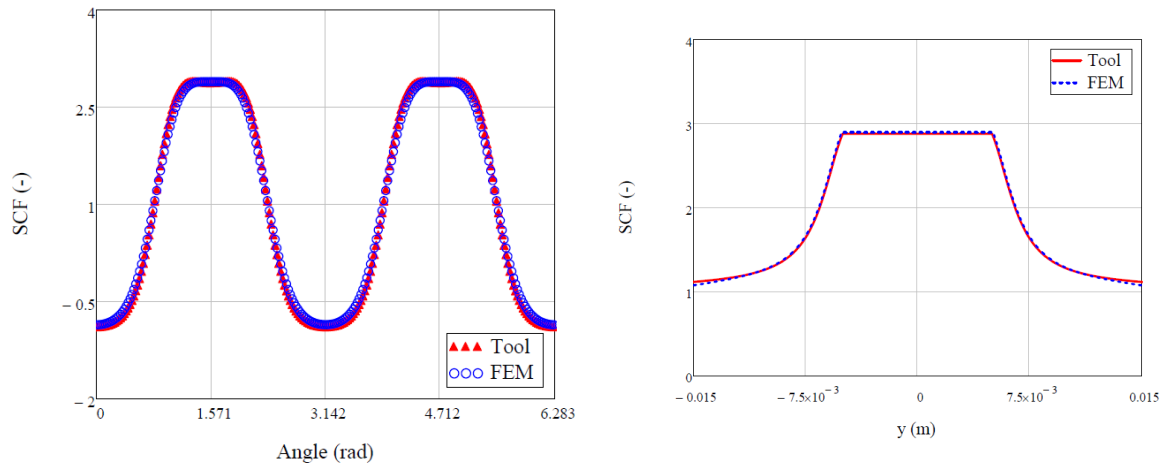


Figure 6.18: Config. 2, SCF of σ_θ at the hole edge (left) and SCF of σ_x at $x = 0$ (right) when $W/D = 4$

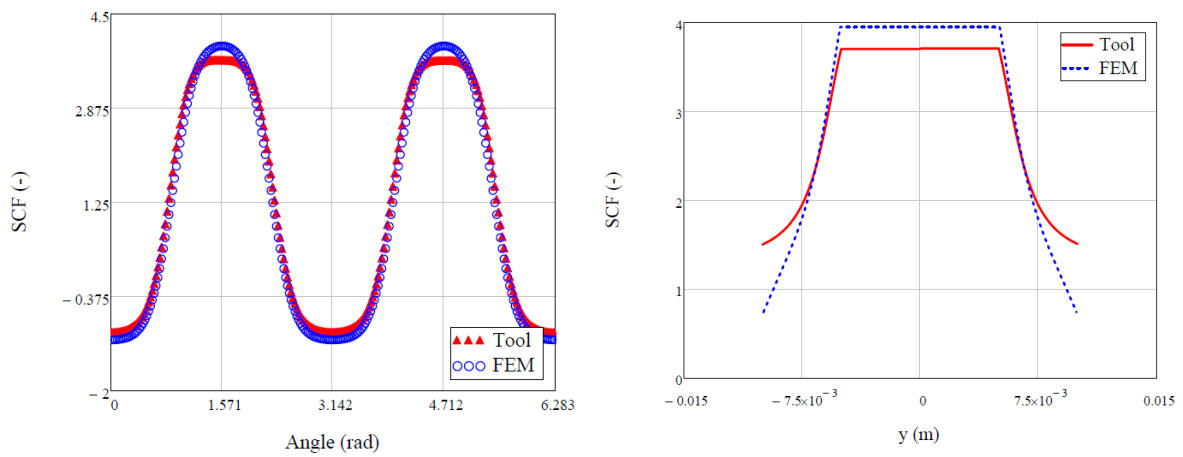


Figure 6.19: Config. 2, SCF of σ_θ at the hole edge (left) and SCF of σ_x at $x = 0$ (right) when $W/D = 2$

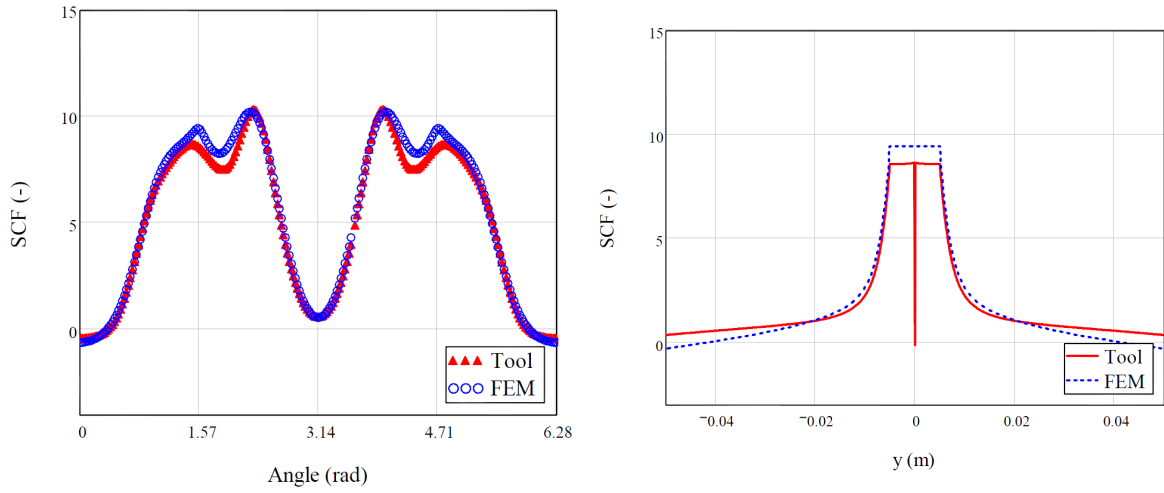


Figure 6.20: Config. 3, SCF of σ_θ at the hole edge (left) and SCF of σ_x at $x = x_{hole}$ (right) when $E/D = 2.5$

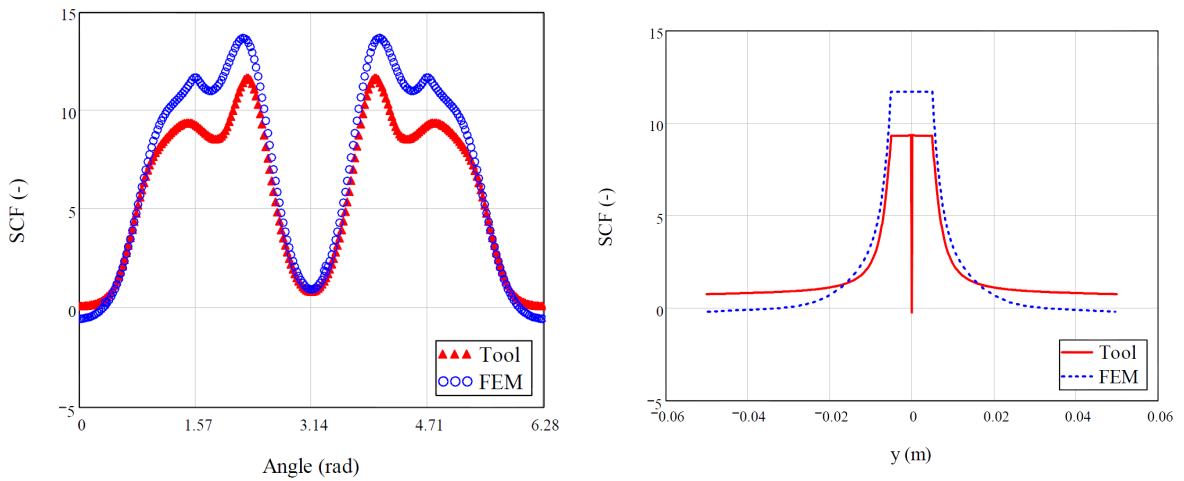


Figure 6.21: Config. 3, SCF of σ_θ at the hole edge (left) and SCF of σ_x at $x = x_{hole}$ (right) when $E/D = 1.5$

As from all three configurations a similar conclusion is drawn, it can be investigated how a different E/D or W/D affects the magnitude of the discrepancy between FEA and the analytic tool. From all three configurations the discrepancy in maximum tangential stress concentration factor was calculated and plotted in Figure 6.22. In the figure the general trend, a closer hole distance means a higher discrepancy, can quite clearly be observed. In the search of why these discrepancies exist the following are noted. Investigating the FEA models themselves did not result in convergence errors. All elements were small enough to lead to stable results. Investigating the parameters used for the analytic analysis itself revealed the following. For all analyses a summation parameter $N = 7$ and integration tolerance parameter $TOL = 10^{-6}$ are used. Since N controls the accuracy of the solution, it is expected that increasing this parameter would result in a better approximation of the problem. However, upon increasing this parameter it was found that the analytic solutions were already converged. This brought the attention to the integration tolerance parameter TOL . Since this parameter controls the accuracy of the numerical integration it is suspected that, for settings with close edges, the convergence criterium for the numerical integration is too high and thus it was attempted whether decreasing this parameter improved the results. Ultimately, this also prove unsuccessful since here also convergence was found. Further testing whether the numerical integration routine could be at the basis of the discrepancies at close hole edges configuration 3 for $E/D = 1.5$ was analyzed with a Mathematica©algorithm developed by Bakker [200]. This algorithm is founded on the same theory but constructed as application for single lap joints. It was expected that the results from the Mathematica©algorithm are closer to FEA because of the better numerical integration procedures in Mathematica©. The opposite turned out to be true for which the cause was found in the initial assumption that:

$$\sigma_x = 2\Re \left[\mu_1^2 \frac{d\varphi_1(z_1)}{dz_1} - \mu_2^2 \frac{d\varphi_2(z_2)}{dz_2} \right] \quad (6.2a)$$

$$\sigma_y = 2\Re \left[\frac{d\varphi_1(z_1)}{dz_1} - \frac{d\varphi_2(z_2)}{dz_2} \right] \quad (6.2b)$$

$$\tau_{xy} = -2\Re \left[\mu_1 \frac{d\varphi_1(z_1)}{dz_1} - \mu_2 \frac{d\varphi_2(z_2)}{dz_2} \right] \quad (6.2c)$$

where it can be seen that the initial summation between the stress functions is replaced by subtraction. One cause for the discrepancies between FEA and the tool remain. The initial assumed shape function, Eq. (3.13), is less suitable of accurately representing the stress field when holes are very close to the edge leading to a less accurate minimum energy solution. Solving this requires trying the assumption of a different shape function which was not attempted due to time constraints.

Nevertheless this drawback, the discrepancy between FEA and the analytic tool vanishes when $E/D \geq 2.5$ and $W/D \geq 4$. Since, for design purposes, an $E/D \geq 2.5 + 1.3$ [mm] [16] and $W/D \geq 4.7$ [17] is advised, the analytic tool can confidently be used for common engineering practice. Finally, the ability of the tool to account for multiple holes which are loaded or unloaded is tested using configuration 4. A rectangular plate size $20D$ is modeled with 4 holes, each $3D$ apart. Two holes are loaded while the other two are unloaded. The total load is balanced with an equivalent edge load. For comparison, the tangential stress concentration factor with respect to the hole angle for the FEA model and the analytic tool is plotted in Figure 6.23. It is observed that there is an excellent agreement between both.

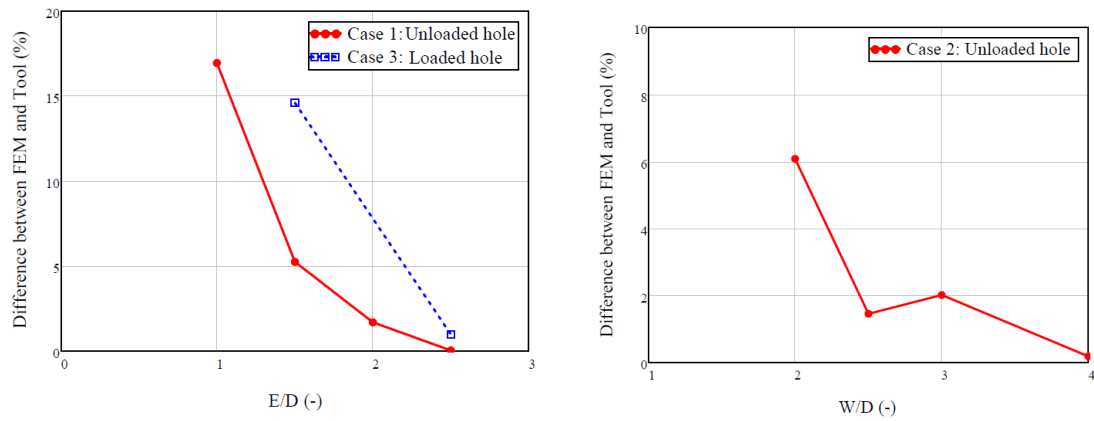


Figure 6.22: Difference in SCF between FEM and Tool for a hole in a plate with varying E/D and W/D

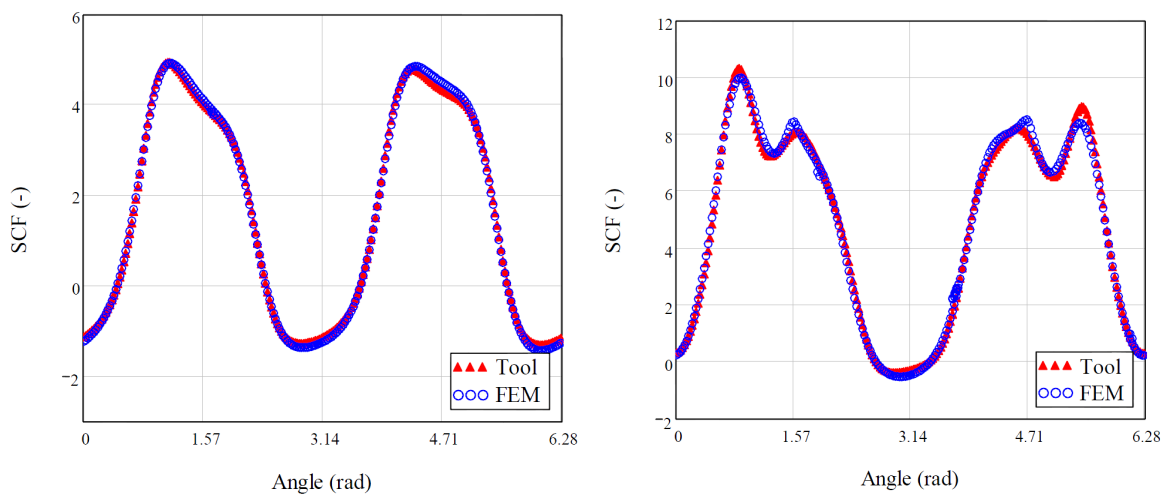


Figure 6.23: Tangential SCF from config. 4 for an unloaded (left) and loaded (right) hole

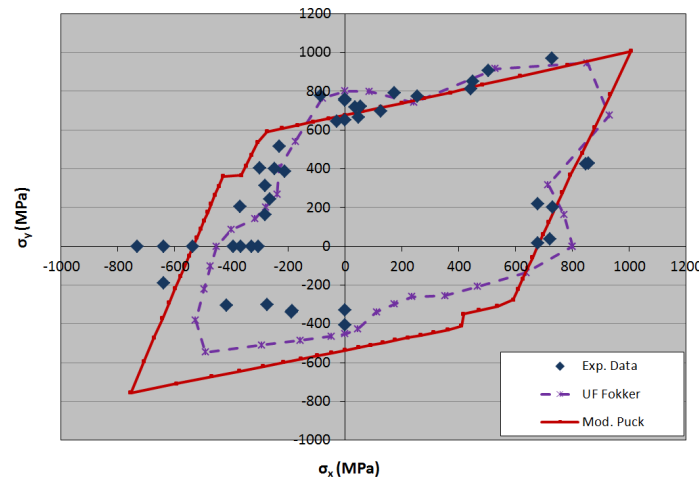


Figure 6.24: Biaxial failure envelope for QI AS4-3501 [22]

6.2 Failure Prediction - Comparison to Test Results

Having determined the validity of the stress field method, the performance of the failure prediction method can be assessed. This is done by comparing the unnotched and notched failure prediction to experimental data from literature. Comparison of the unnotched failure prediction can be done without any adaptations to the algorithm. For notched failure prediction, however, as mentioned in the beginning of this Chapter, the optimal values for the “free” parameters; the pin-hole clearance λ and hole size for determination of the CPSED need to be determined first.

6.2.1 Unnotched Failure Criterion

Using the unnotched failure criterion described in Section 4.1, uniaxial, biaxial and uniaxial-shear failure envelopes are produced to compare to experimental data from various researchers [22–26] and Fokker Aerostructures B.V. [201].

Biaxial failure experimental data and predicted failure envelopes for CFRP material AS4-3501 [22], IM7-8551 [23, 24] and IM7-9772 [25] are shown in Figure 6.24 to Figure 6.29. In Figure 6.24 and Figure 6.25 it can be seen that, for QI layups, the Fokker criterion has a better correlation with experimental data than the modified Puck criterion. This is especially true in the second and third quadrant of the failure envelope where the modified Puck criterion significantly overestimates the strength of the laminate. The Fokker criterion also overestimates the laminate strength in the compression-compression quadrant. In the first quadrant both criteria have a good agreement with experimental data. The fourth quadrant is not investigated since an orthotropic laminate results in a symmetric failure envelope around the axis $\sigma_x = \sigma_y$. Biaxial failure envelopes for compression-compression loaded angle plied $[\pm\alpha]_s$ laminates are shown in Figure 6.26 to Figure 6.28. Observe that the performance of the Fokker criterion in the compression-compression quadrant is better than the Modified Puck criterion but nonetheless significantly overestimates the laminate strength. In the remaining quadrants, no experimental data was obtained but note the apparent infinite strengths predicted by the current Fokker criterion in Figure 6.27 and Figure 6.28. Because the modified

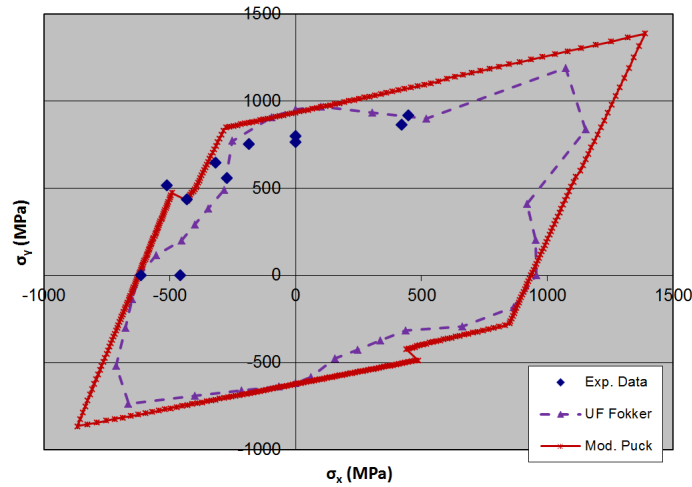


Figure 6.25: Biaxial failure envelope for QI IM7-8551 [23, 24]

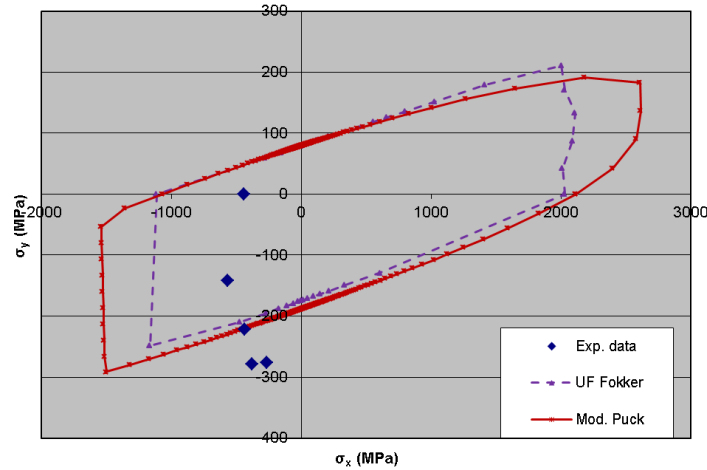


Figure 6.26: Biaxial failure envelope for $[\pm 15]_s$ IM7-8551 [23, 24]

Puck criterion does not contain this region, it is concluded that its performance is better than the Fokker criterion. A biaxial failure envelope for a $[0]_8$ IM7-977-2 laminate is shown in Figure 6.29. Comparing the performance of both failure criteria it is observed that the modified Puck criterion provides a better fit to the test data than the Fokker criterion. This especially in the first quadrant where the experimental data in the upper right corner matches exceptionally well. Furthermore the Fokker criterion is more conservative. Different from the biaxial failure envelopes, a uniaxial-shear failure envelope for a $[0]_{32}$ IM7-8552 laminate is shown in Figure 6.30. Here the Modified Puck criterion has a better fit than the Fokker criterion.

Both criteria were also used to provide a comparison to experimental data from Fokker Aerostructures B.V. [201] Predictions for the uniaxial compressive and tensile strength of a soft, hard and QI laminate made from material TH5.698/6 are shown in Figure 6.31. In the Figure it can be seen that there is virtually no difference between both criteria. A very good correlation with the experimental data is obtained.

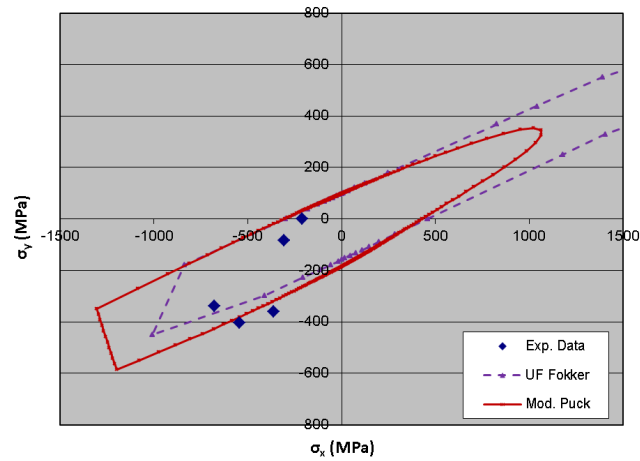


Figure 6.27: Biaxial failure envelope for $[\pm 30]_s$ IM7-8551 [23, 24]

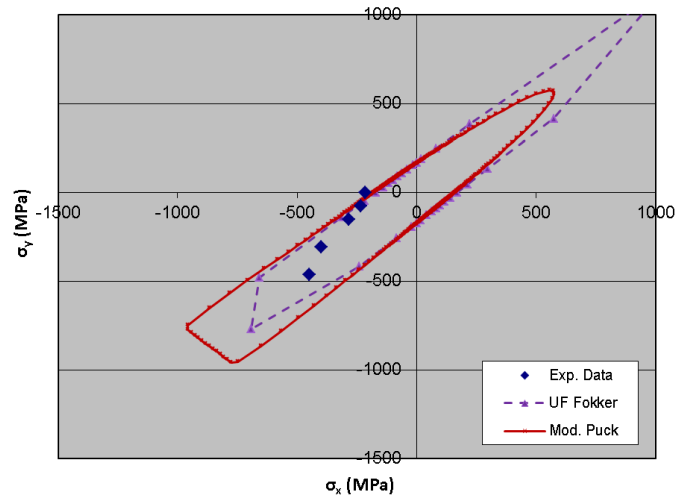


Figure 6.28: Biaxial failure envelope for $[\pm 45]_s$ IM7-8551 [23, 24]

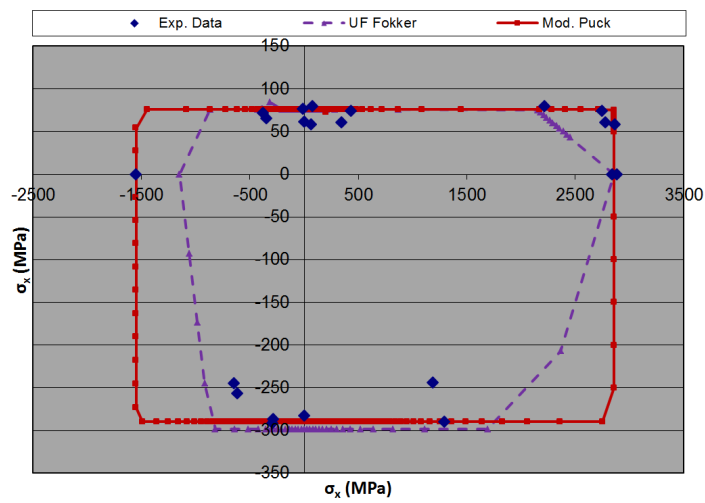


Figure 6.29: Biaxial failure envelope for $[0]_8$ IM7-9772 [25]

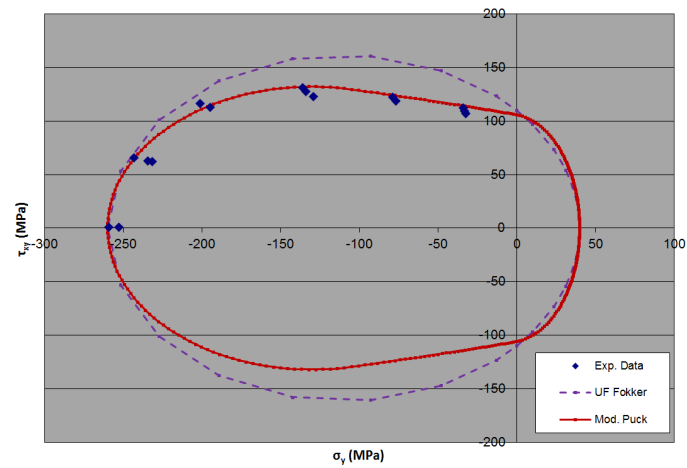


Figure 6.30: Uniaxial-Shear failure envelope for $[0]_{32}$ IM7-8552 [26]

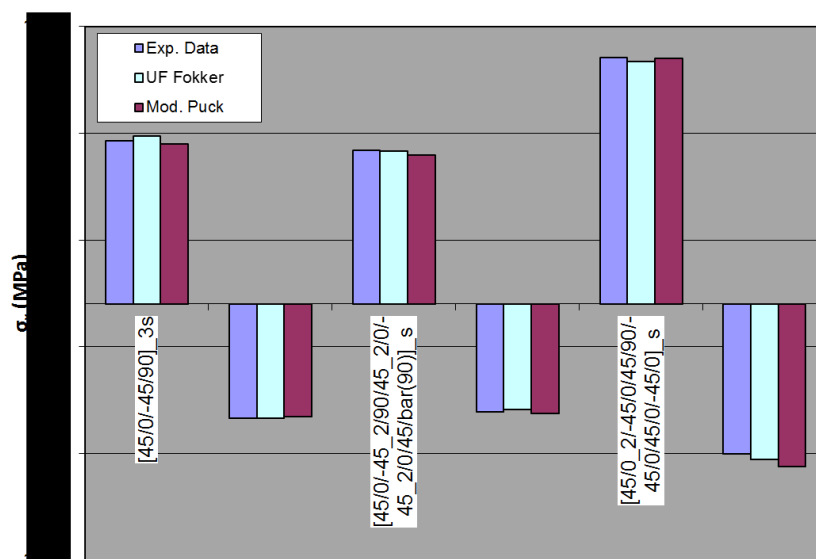


Figure 6.31: Uniaxial compressive and tensile test and predictions for material TH5.698/6 for QI, soft and hard laminate

From the comparisons between the experimental data and both criteria it is difficult to point out which criterion performs best. The Fokker criterion performs better (although not drastic) for QI laminates subjected to biaxial loads while the modified puck criterion is superior in the case of a UD laminate. For angle plied laminates performance of both criteria is questionable because of the apparent lack of test data. Sometimes the Fokker criterion predicts apparent infinite strengths in the first quadrant. It is clear that in this investigation the conclusion from the literature survey, Section 2.2, is encountered again. The current (unnotched) failure models for composite laminates are all but perfect and still require much development. As such the question which criterion in this investigation performs better seems redundant. Both criteria have their advantages and disadvantages and therefore they perform equally good (or bad for the pessimists). In the remainder of this thesis it is decided to use the Modified Puck criterion as a basis for the unnotched laminate strength because the Fokker criterion contains curve fitting elements while in this work a universally applicable failure criterion is sought. Thus, the less curve fitting elements present, the better.

6.2.2 Notched Failure Criterion - Clearance and Hole Size for CPSED

Before the performance of the notched failure criterion can be determined, optimal values for the remaining “free” parameters need to be determined. As aforementioned, these parameters are the pin-hole clearance λ and hole size for determination of the CPSED. The pin-hole clearance is the percentage difference between the size of the pin and the size of the hole with respect to the hole. Usually, there is a measurable clearance between the pin and a hole, however, this is only so for loaded hole experiments where, in the documentation, the pin-hole clearance is reported. Therefore, to be able to estimate hole strengths when pin-hole clearance is unknown, it is necessary to have a recommended value for the pin-hole clearance. By inspection of datasheets with clearance fit allowables [202] it is noted that a hole clearance can be as small as 0.5% for a hole diameter of 10 [mm] (the largest most occurring hole diameter in the experimental dataset) while it can be as large as 11.3% for a hole diameter of 3 [mm]. It is recognised that this is a large range. However, since conservative predictions are preferred, and a smaller clearance results in more conservative predictions, a hole clearance of 0.5% is used as recommended value.

Since the compressive characteristic distance, used to calculate the CPSED (Kweon’s definition Section 4.2), is dependent on the stress field around the hole and the stress field around the hole is dependent on the hole size, the hole size for determination of the CPSED is crucial for the prediction of notched failure. In his research, Kweon [3] uses a hole diameter of 6.35 [mm]. However, since the hole size for CPSED has such a significant effect on the predicted failure strength, it is decided to determine an optimal value by calibration with experimental data. For this purpose, using the aforementioned clearance value of 0.5%, predictions are made using several hole diameters ranging between 2 [mm] to 10 [mm] for experimental configurations from [27, 28]. [27] describes open (small and large) hole uniaxial compression and tension experiments on CFRP-epoxy laminates with a soft, hard and quasi-isotropic layup. [28] outlines both open hole and pinned-hole tensile tests on the same type of laminates. Together, both datasets contain 12 experiments which are considered representative for the other experimental data used in Section 6.2.3. Therefore, if conclusions from these limited number of configurations for the hole size for CPSED are drawn, the conclusions should be applicable to the other experimental data. Plotting the discrepancy in percent be-

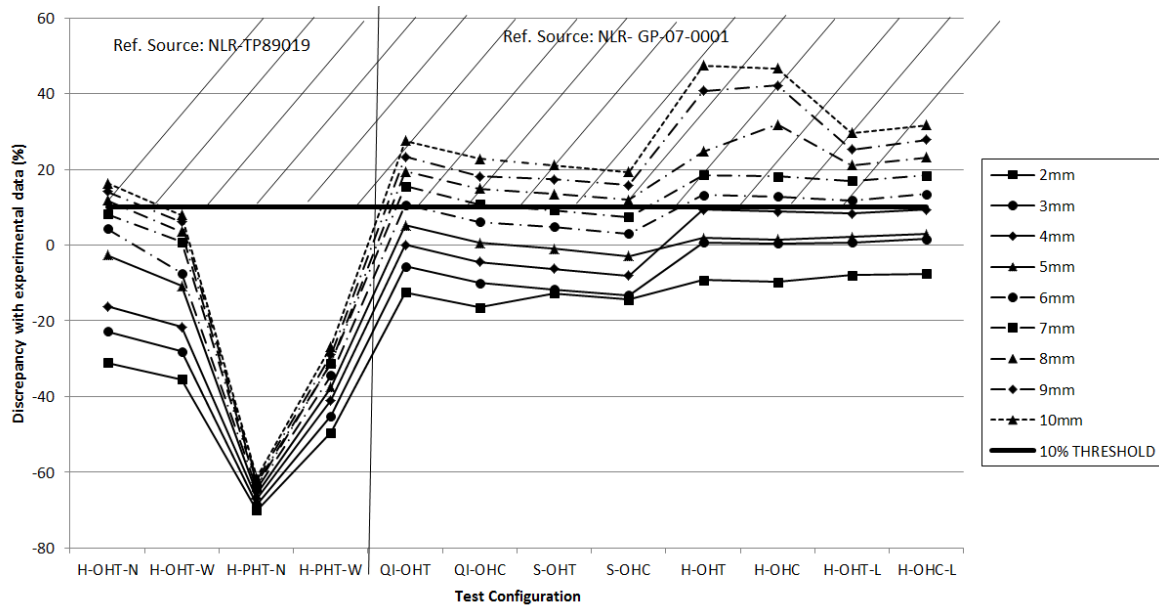


Figure 6.32: Discrepancy with experiments from [27] (right) and [28] (left) when the hole size for the determination of the CPSED is varied. OHT = Open Hole Tension, OHC = Open Hole Compression, PHT = Pinned Hole Tension, S = Soft, H = Hard, QI = Quasi-Isotropic, N = Narrow W/D, W = Wide W/D, L = Large hole

Table 6.3: Least square error for hole sizes below 6 [mm] based on Figure 6.32

Hole diameter for CPSED (mm)	Least square error
2	10694
3	8481
4	7352
5	5918

tween the predicted failure and measured failure for every hole size for CPSED against every configuration results in Figure 6.32. In the figure it can be seen that there exists a general trend in prediction vs hole size. Namely, the predictions from larger hole sizes lie above the predictions from lower hole sizes. This is expected since a higher hole size for CPSED results in a higher CPSED which in turn results in a higher failure load. Additionally, it is observed that the discrepancy for pin-loaded holes is highly conservative.

The recommended value for the hole size of the CPSED is now determined in the following manner. From discussions with supervisors at Fokker Aerostructures B.V., it is concluded that, for the new criterion to be immediately applicable in industry, the discrepancy between predicted and measured value should be lower than +10%. When this restriction is respected, the discrepancy should be as close to 0% as possible. The +10% threshold is drawn in Figure 6.32 from which it is concluded that the hole sizes above 5 [mm] are excluded for consideration. Next, the sum of the least square errors of the remaining hole sizes are calculated to assess which curve is closest to 0% discrepancy. The calculated values are shown in Table 6.3 from which it can be seen that the lowest value, thus the graph closest to 0%, occurs when a hole diameter for CPSED of 5 [mm] is used.

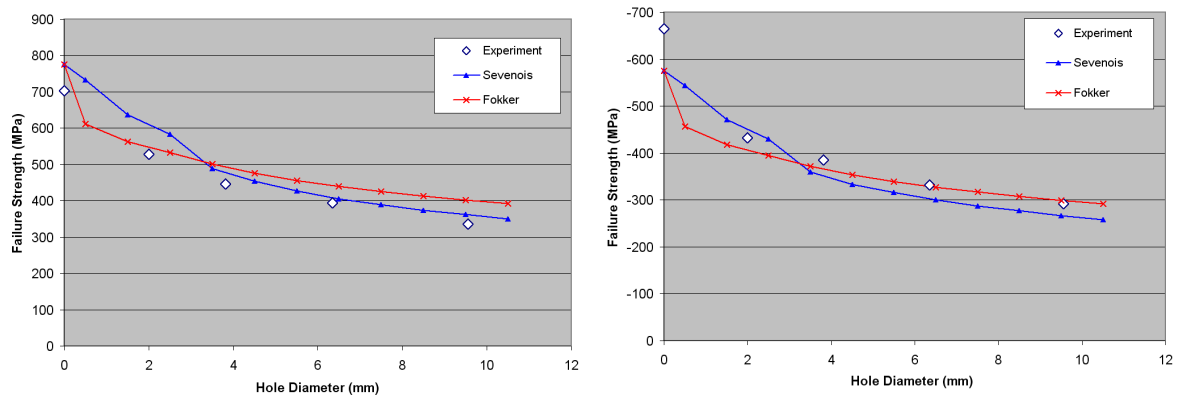


Figure 6.33: Uniaxial tensile (left) and compressive (right) failure for AS4/3501-6 [29], QI CFRP layup, fixed specimen size

Concluding, the recommended values for the remaining free parameters, pin-hole clearance and hole diameter for CPSED are 0.5% and 5 [mm] respectively. The value for the pin-hole clearance is determined based on a logical reasoning while the value for the hole diameter is determined by calibration with a representative selection of test data.

6.2.3 Notched Failure Criterion - Comparison to Experimental Data

With the determination of all “free” parameters, the performance of the notched failure criterion can be assessed. Experimental results from 9 sources [19, 27, 29–35] are obtained and compared to predicted failure loads from the analytic tool and the current criterion in use at Fokker Aerostructures B.V. In the first paragraphs, no distinction is made between configurations which comply and configurations which violate the tool directionality boundary (less than 1.13) determined in Section 6.1.2. This is done on purpose such that a quantitative discussion on results with and without this distinction is possible at a later stage. All predictions in this section are calculated using the “optimal” settings for the “free” parameters.

The obtained datasets are divided in four categories: uniaxial, biaxial, bearing and bearing-bypass tests. In the uniaxial category Wang [29] and Bos [27] performed tensile and compressive failure tests on laminates from UD AS4/3501-6 and TH5.698/601 respectively. Wang used a QI layup and varied the hole size while keeping a fixed specimen size. Bos tested a QI, soft and hard layup while keeping a fixed hole size. The results from both investigations are shown in Figure 6.33 and Figure 6.34 respectively. From the Figures, it is observed that there is a good, although sometimes unconservative, agreement between prediction and experiment in the tensile configurations for both the Fokker and Sevenois criterion. Additionally, it appears that, for hole sizes larger than 3 [mm], Sevenois’ criterion is more conservative than the Fokker criterion. For lower hole sizes the opposite is true. In the compression experiments, it is observed that the Fokker method has a better fit for Wang’s experiments while it overestimates three of the four (compressive) experimental failure loads by Bos. The Sevenois model is always conservative but in one datapoint from Wang.

Two other datasets for uniaxial compressive failure were obtained from Hodge [30] and Soutis [31]. Both authors investigated the effect of increasing the hole size on the compressive

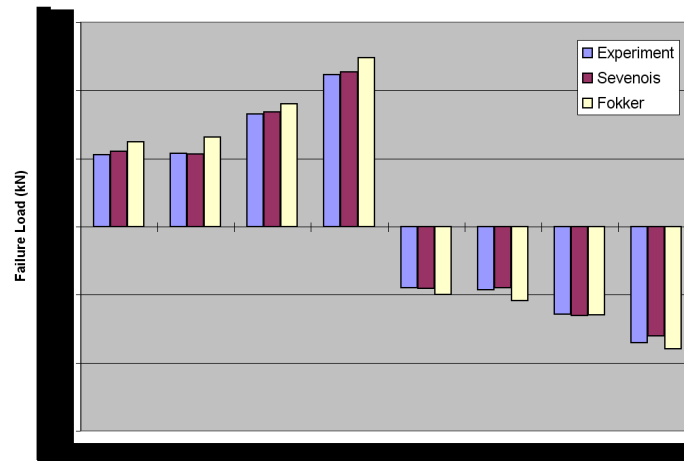


Figure 6.34: Uniaxial tensile and compressive failure for TH5.698/601 [27], Hard, Soft and QI layup, hole diameter: normal = 6.35 [mm], Large = 9.52 [mm]

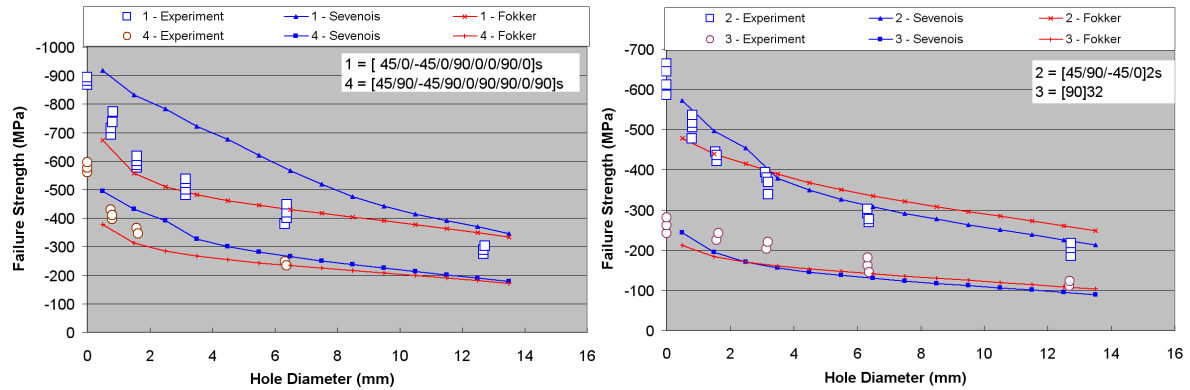


Figure 6.35: Uniaxial compressive failure for IM7/8552-1 [30] when changing hole size, fixed specimen size

failure strength. Hodge used IM7/8552-1 UD prepreg while Soutis used T800/924C prepreg and investigated multiple layups. The results are shown in Figure 6.35, Figure 6.36 and Figure 6.37 where it can be seen that, in contrast to the conclusions from the previous results, the discrepancies between prediction and measurement are much larger. This for layup nr. 1 in Figure 6.35, and nr. 1,3,4, 5 in Figure 6.36 and Figure 6.37. In 60% of the cases the Sevenois criterion predicts a lower failure load than the Fokker criterion. Both criteria do follow the trend (decreasing strength with increasing hole size) of the data .

Experimental data from biaxial load experiments is obtained from 3 sources. Daniel, [32,33] performed biaxial tension-tension experiments on QI and $[0_2/\pm 45]_s$ laminates from UD SP-286T300 CFRP. For all experiments Daniel tested several hole sizes for the same loading ratio. For the QI layup, the loading $\sigma_x - \sigma_y$ was 1/1 while for the $[0_2/\pm 45]_s$ laminate the loading ratio was 2/1. In contrast to other researchers, the hole sizes from Daniel were rather large, in to order of some [cm]'s rather than the more common [mm] size. The results, shown in Figure 6.38, indicate that their is only a minor difference between the new criterion and the Fokker criterion where the Fokker criterion in all but one case predicts a higher

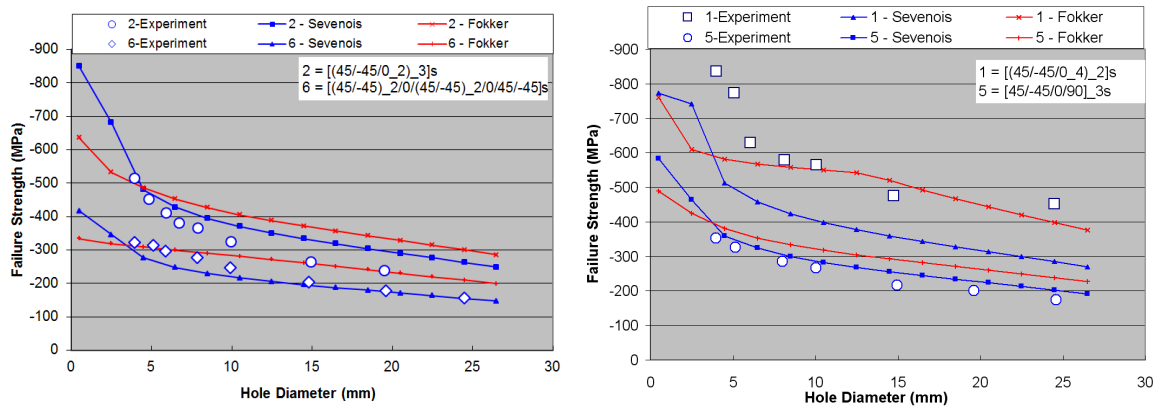


Figure 6.36: Uniaxial compressive failure for T800/924C [31] when changing hole size, fixed specimen size, part 1

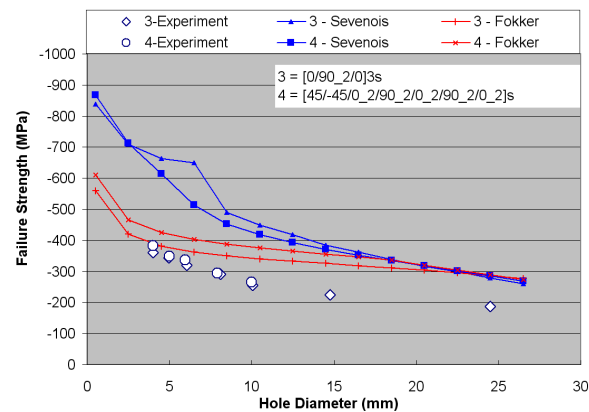


Figure 6.37: Uniaxial compressive failure for T800/924C [31] when changing hole size, fixed specimen size, part 2

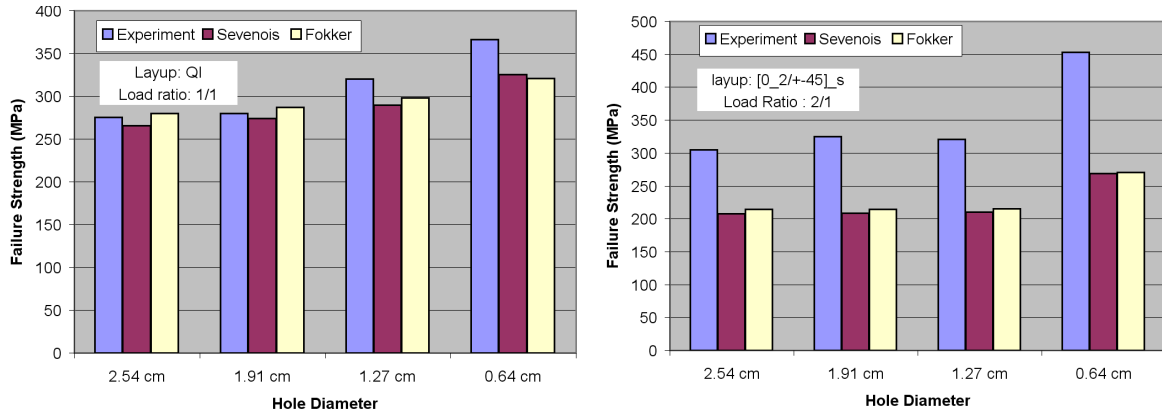


Figure 6.38: Biaxial failure strength and prediction [32,33] for SP-286T300

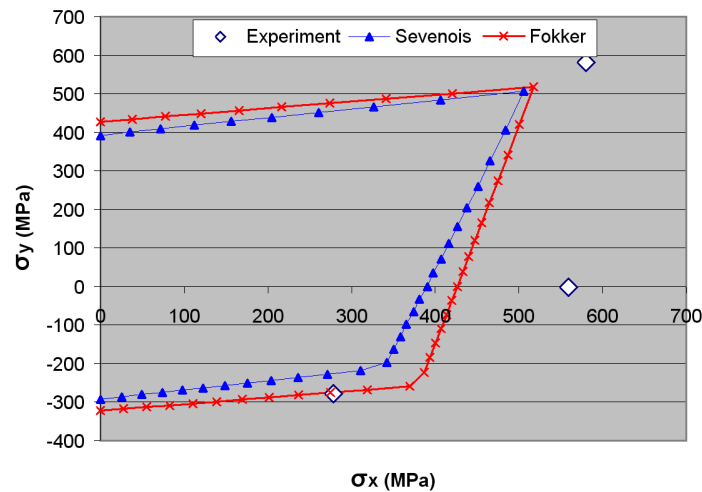


Figure 6.39: Biaxial failure envelope for QI laminate of IM7/8552 with 10 [mm] hole [34] and prediction

failure strength with regard to the Sevenois criterion. Furthermore, the discrepancies with the measurements are small with the QI-layup while they are rather high (but conservative) in case of the $[0_2/\pm 45]_s$ layup. Huang [34] used a QI layup of IM7/8552 to construct a biaxial failure envelope. This is shown in Figure 6.39 where it can be seen that, here too, both criteria produce conservative predictions where the Fokker criterion is closer to the experimental data.

Chang [35] performed an extensive experimental investigation on the pinned strength of T300/1034C laminates. Three basic specimen designs: single hole, two holes in parallel and two holes in series, were tested up to failure with 7 different layups (Figure 6.41). Additionally, the basic dimensions of the specimens were varied to investigate edge effects. The measured strengths and the predictions are shown in Figure 6.40 to Figure 6.42. In each figure, the specimen dimensions are indicated. For almost all layups and configurations both the Fokker and Sevenois criterion underestimate the strength of the joint. Furthermore, with the single hole specimens the magnitude of the discrepancy between measurement and pre-

diction seems to be dependent on the specimen size. Compare, for example Figure 6.40(a) with Figure 6.40(c) and (d) where it is observed that, overall, the discrepancy with (d) is much smaller with regard to the other two cases. With the two hole series this observation can not be made with confidence. It seems, however, that the predictions for the two hole specimens in series are closer to the measured failure strengths. Especially, when comparing Figure 6.40(a), Figure 6.41(b) and Figure 6.40(b), Figure 6.41(c).

Crews [19] performed bearing bypass experiments on QI graphite epoxy laminates in an attempt to generate the complete bearing bypass curve. Crews measured both initial failure and final failure of the specimens. The comparison to Sevenois and Fokker is shown in Figure 6.43 where it can be seen that both criteria underestimate the ultimate failure strength significantly. Instead, the predicted failure loads seems to coincide with the onset of failure with the Sevenois criterion being the most conservative. Additionally, it is noted that the curve does not coincide well in the compressive bearing bypass region. This is attributed to the contact angle algorithm which was not designed for this purpose.

Qualitatively, it seems that the performance of the new criterion is an improvement over the current Fokker criterion since it provides better predictions which are almost always conservative or close to the measured values for open hole configurations. Qualitative observations, however, are somewhat sensitive to subjectivity and in the following an attempt is made to quantify the predictions. Two graphs, one for unloaded and one for loaded configurations, are constructed where prediction is set out against measurement for all 151 datapoints. The boundaries for 60%, 40%, 20% and 0% discrepancy are indicated in the graphs which are shown in Figure 6.44 and Figure 6.45. In Figure 6.44 it immediately stands out that there is more compressive than tensile data. In the tensile case, all predicted values are within +20% and -40% of the measured failure load. In the compressive case, however, scatter is much larger. Here the Fokker criterion overestimates some experiments by over 40% while the Sevenois criterion produces predictions between +20% and -40% of the measured value. Most predictions, however are located in the boundary -20%, +20%. Looking at the graph for the loaded experiments, Figure 6.45, scatter is much larger. Most predictions are conservative concentrating in the -20% to -60% region. A great deal are, more Sevenois than Fokker, overestimations. This is quite worrying since, this way, it appears that one cannot determine confidence bounds for the loaded hole experiments. Up to now, the boundaries of the tool, determined in the previous sections, were not taking into account. Applying these boundaries and eliminating the measurements where $[0/90]_s$ laminates (early microbuckling occurred [31] which is not taken into account by the failure criterion) are used, resulted in the exclusion of 39% of the datapoints to a total amount of 92 (38 measurement points unloaded and 54 measurement points loaded holes together). Replotting the graphs results in Figure 6.46 and Figure 6.47.

As expected, one can see that now, with the inclusion of the tool boundaries, the results have significantly improved. For the Sevenois criterion in the unloaded configurations all predictions are within +20% and -40% of the measured value. The Fokker criterion has some overestimations in the +20%, +40% region. For unloaded holes, the Sevenois criterion performs thus better than the Fokker criterion. In the loaded case, Figure 6.47, the great deal of conservative predictions between -20% and -60% is still present. The overestimations by the Sevenois criterion, however, have reduced to lower than +20% while the Fokker criterion still has some predictions above +20% discrepancy. Remarkable is that there are 5 datapoints where the prediction is lower than 60% of the measured value. Also, for these datapoints, the

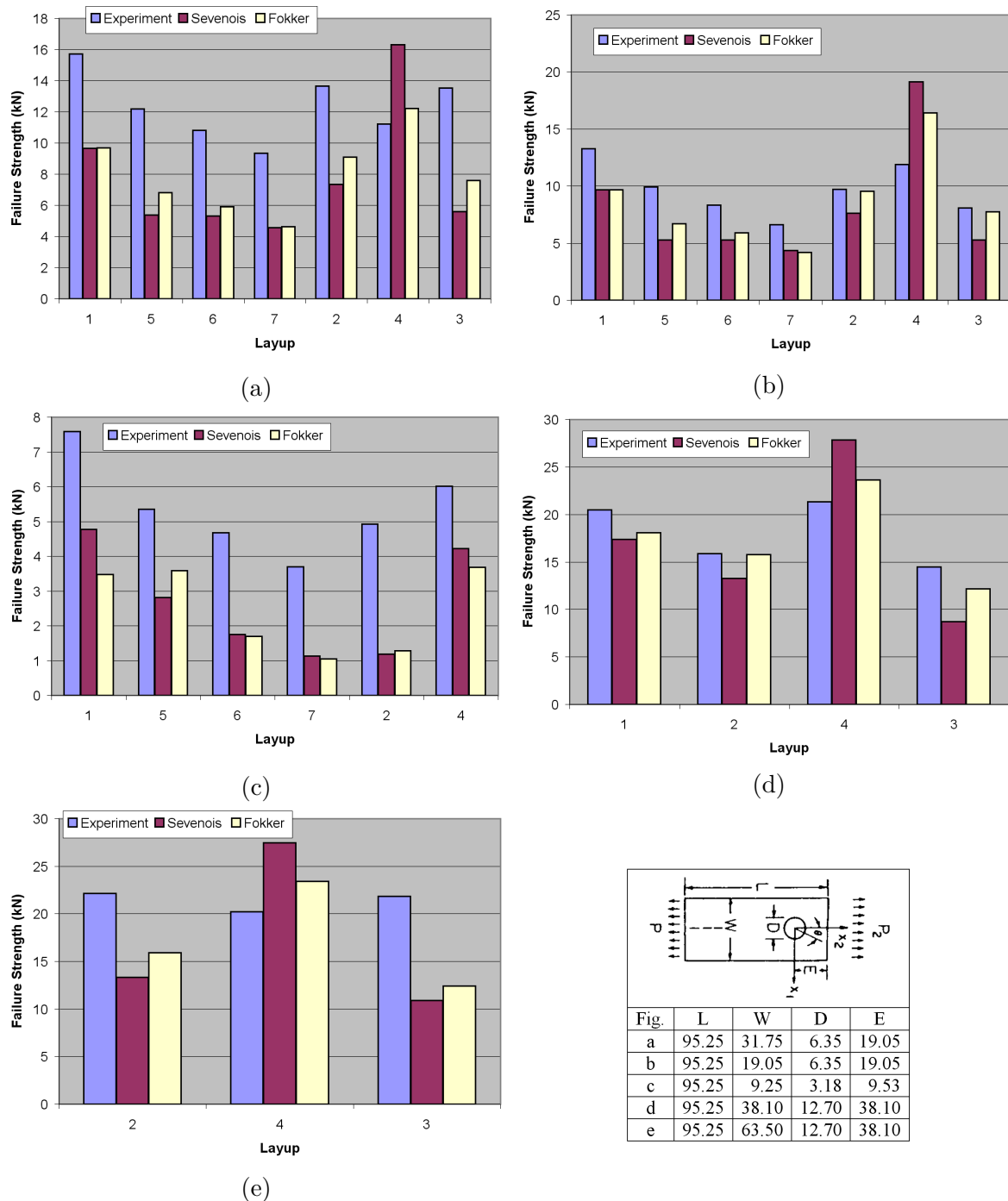


Figure 6.40: Failure strength of single hole specimens wrt predictions [35]

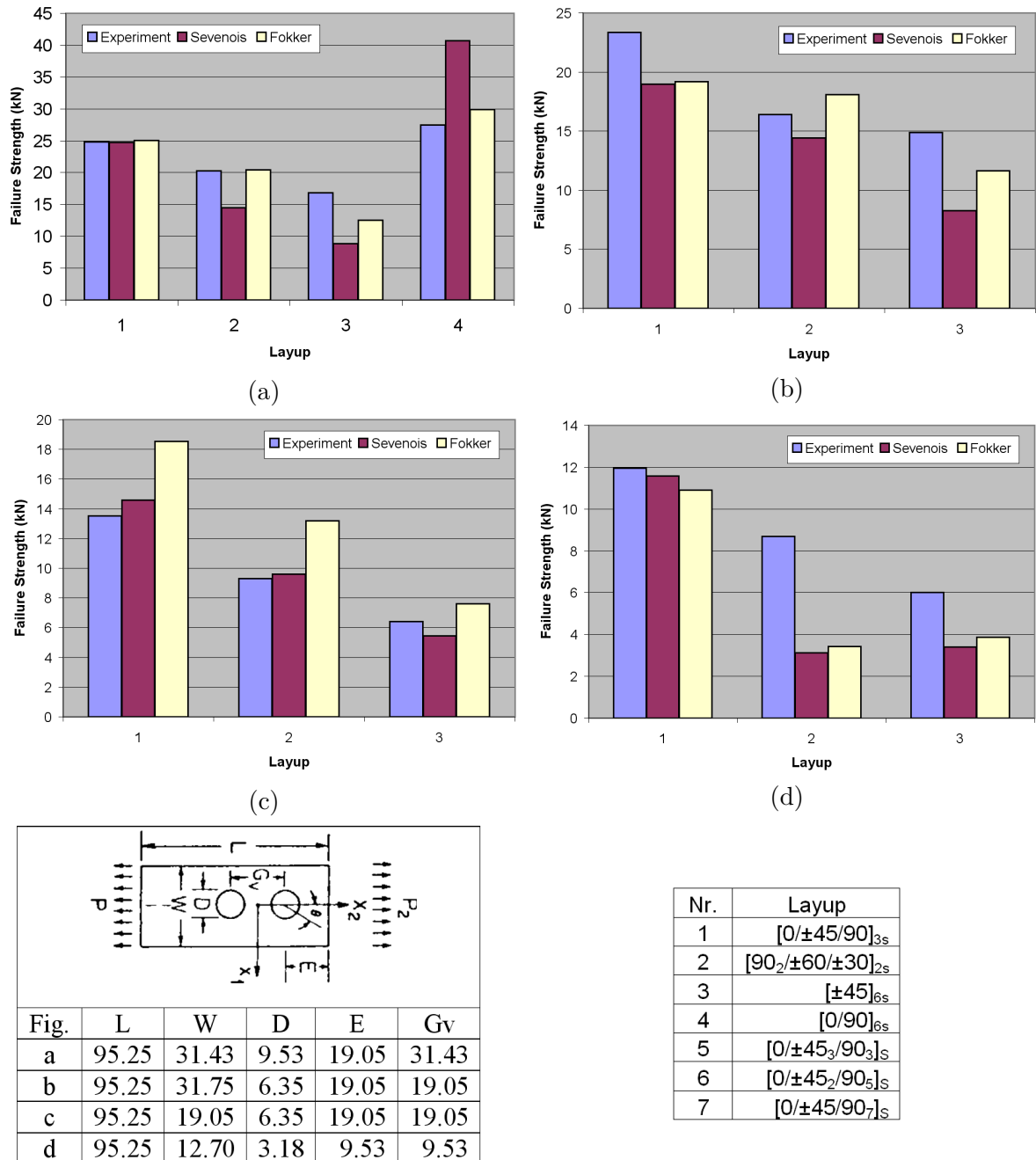


Figure 6.41: Failure strength of holes in series specimens wrt predictions [35]

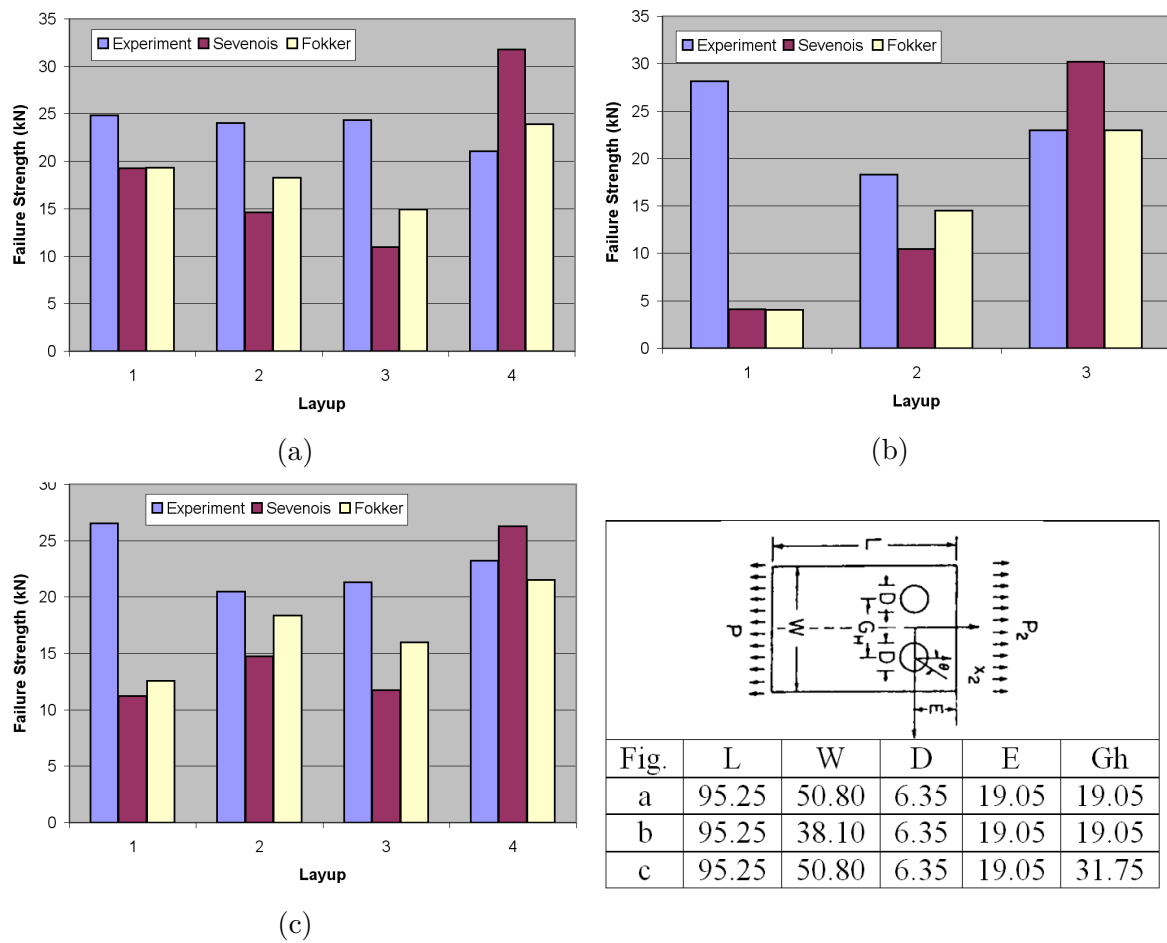


Figure 6.42: Failure strength of holes in parallel specimens wrt predictions [35]

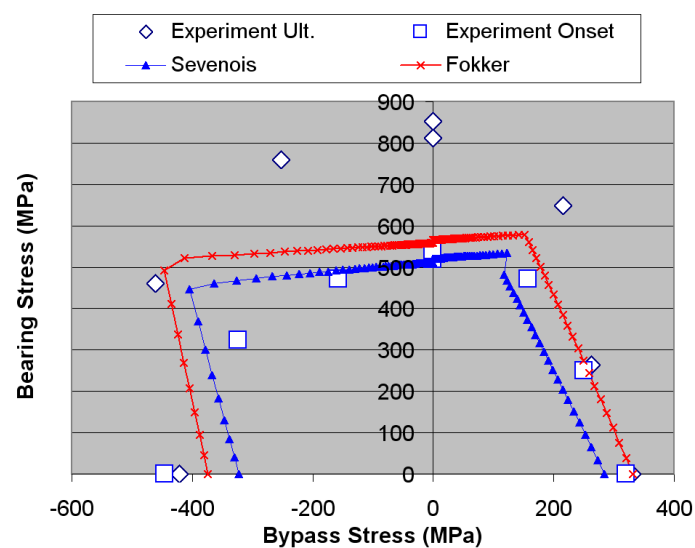


Figure 6.43: Bearing-bypass envelope for QI graphite epoxy laminate [19]

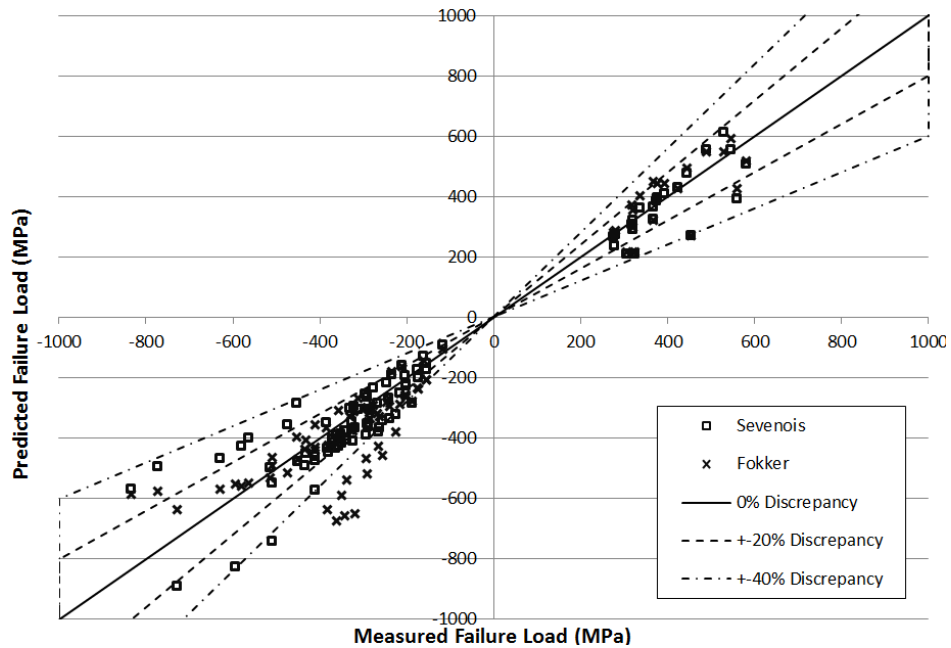


Figure 6.44: Prediction vs measurement for unloaded hole experiments, unlimited

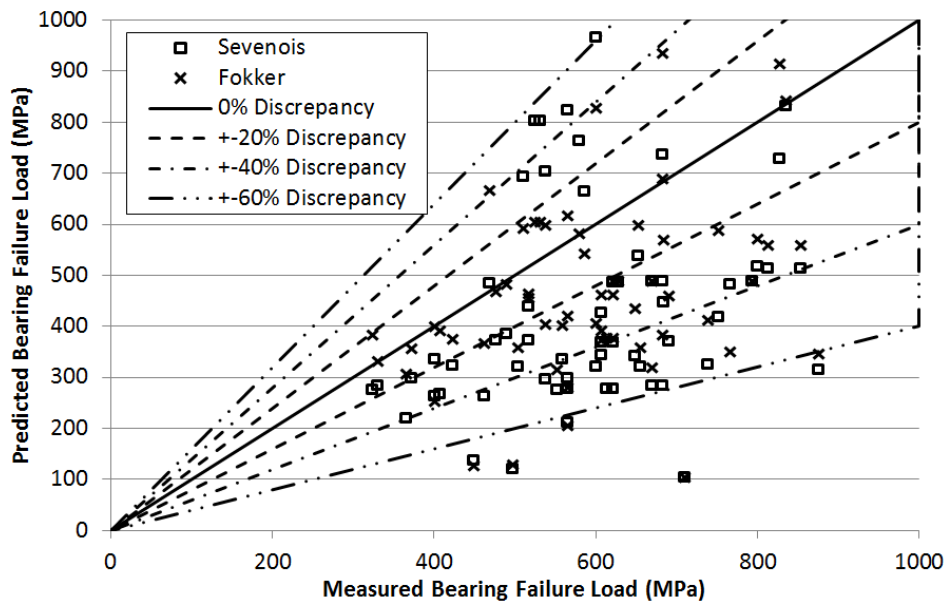


Figure 6.45: Prediction vs measurement for loaded hole experiments, unlimited

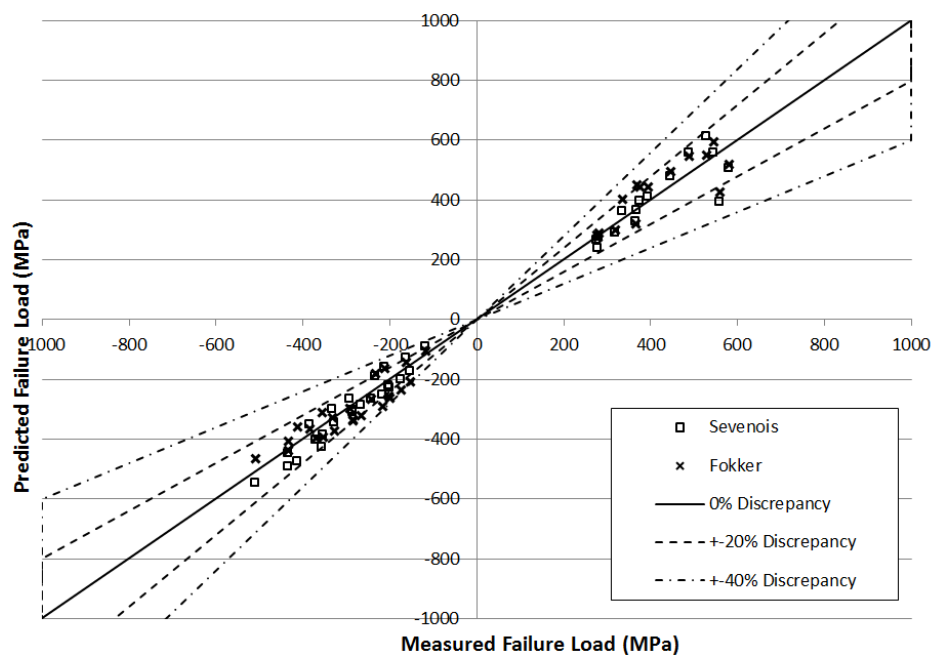


Figure 6.46: Prediction vs measurement for unloaded configurations, limited

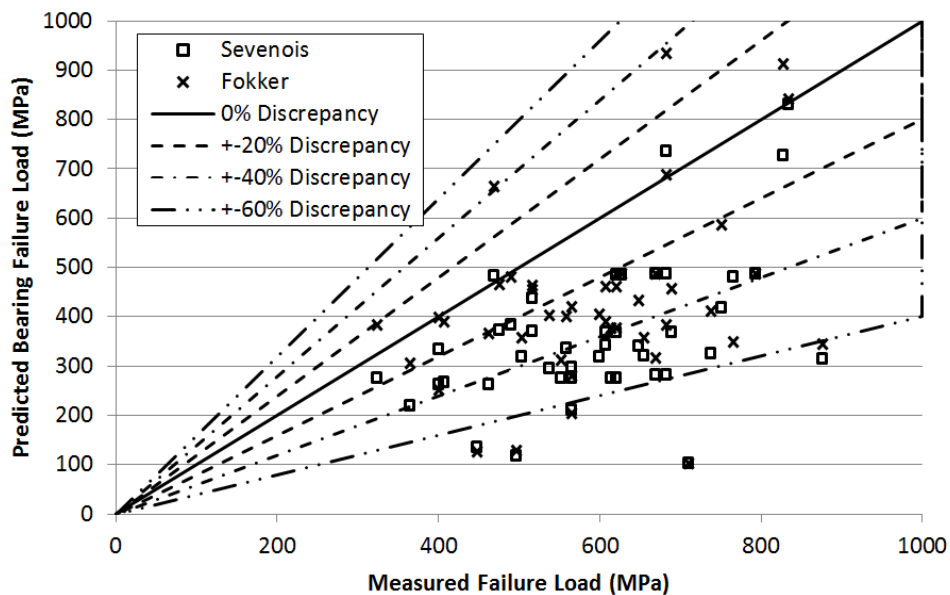


Figure 6.47: Prediction vs measurement for loaded configurations, limited

predicted failure value from the Fokker and Sevenois criterion is almost equal. Upon detailed inspection of these specific configurations, it was found out that, in these cases, the stress algorithm was unable to converge to a steady solution resulting in an unrealistic stress field which again resulted in an unrealistic failure load. They should thus be neglected.

One cannot say that the performance of the current criterion for notched holes at Fokker, which is based on a constant characteristic distance approach, is unusable. In most of the cases it predicts a value which is within $\pm 40\%$ of the measured value which is acceptable considering the rudimentary approach taken. However, in the discussion above it is shown that the new criterion, with an equally fast and simple set-up, provides a better estimation of the failure strength of notched laminated plates. Additionally, it is able to cope with multiaxial stress conditions which the Fokker criterion was never designed for and provides fast linear stress field analysis. For unloaded holes, all predictions are within $+20\%$ and -40% of the measured value. For loaded holes the predictions are within $+20\%$ and -60% .

Discussion, Conclusions and Recommendations

The determination of the stress field and evaluation of failure in orthotropic plates with holes subjected to arbitrary boundary conditions is one of the key challenges during the design of composite structures. Up to now, no relatively simple methodology for general configurations existed but has now been resolved.

The goal of this project was to construct an analytic tool for the determination of the stress field and prediction of failure of rectangular orthotropic plates with holes subjected to arbitrary boundary conditions. Initially, it was envisioned to validate the tool only for unloaded holes but during the construction of the new criterion it was recognized that also loaded holes could be analyzed. Hence, the criterion was also validated for this type of holes. Because the analytic tool will be used in a design environment by a general engineer, the tool had to be fast, simple to use and its functioning easy enough to understand. Additionally, the failure criterion had to be valid for multiaxial load scenarios.

First it was investigated which theories already existed for the analysis of stresses in orthotropic notched plates and the prediction of failure based on these stress fields. From this investigation it was concluded that simplicity had to go to the wall for a performant stress analysis and a complex stress analysis on the basis of Lekhnitskii [4] in conjunction with the theory from Xiong and Poon [2] was constructed. Their research was expanded to account for multiple (loaded) holes and shear loading on the hole and plate edges. The sign selection method by Koussios [194] was also expanded to account for all types of orthotropic laminates. For failure prediction no definite conclusion on which failure criterion would be best to use could be drawn. Considerations on the basis of the intended use and required speed of the tool led to the birth of the modified critical energy point-stress criterion for failure prediction. A novel criterion which has its roots in the PSC by Whitney and Nuismer [10] in conjunction with Kweon [3].

Both stress and failure prediction algorithms were verified thoroughly to ensure a correct functioning of the tool. Comparisons to analytic stress fields from other authors resulted

in a very good agreement. The effects of changing the amount of summations N and the integration tolerance TOL were investigated from which it followed that the recommended minimum values for these parameters are:

- $N \geq 7$
- $10^{-3} \geq TOL \geq 10^{-6} \vee 10^{-13} \geq TOL \geq 10^{-16}$

Validation of the stress field methodology with FEA revealed that, when the holes are very close to a plate edge, the solution becomes less accurate. Therefore the following restrictions with regard to the location of holes and plate edges are identified:

- $E/D \geq 2.5$
- $W/D \geq 4$

Additionally, validation of the method to determine the contact angle in pin-loaded holes restricted the tool usage for a laminate directionality lower than 1.13. Optimal values for the load displacement angle α and hole diameter for the computation of the CPSED were determined to be:

- $\alpha = \text{half the contact angle}$
- Hole diameter for computation of the CPSED = 5 [mm]

Validation of the failure prediction methodology was done by comparing the predictions from the tool to experimental data and the current failure prediction methods at Fokker Aerostructures B.V. A total of 151 experimental datapoints, mainly from single hole compression, tensile and bearing tests, were used of which 87 were for unloaded and 64 for loaded hole configurations with biaxial and bearing bypass loading configurations. Eventually, 59 of these experimental points were neglected due to the tool boundaries and preliminary ply buckling. 92 experimental datapoints remained from which it was concluded that, for unloaded holes, the prediction lies between +20% and -40% of the measured value with all but a few in the $\pm 20\%$ region. For loaded holes this is between +20% and -60%. The new criterion is an improvement over the current design methodology.

Strikingly, the unloaded hole predictions are better than the loaded hole predictions. This while it was expected that the loaded hole predictions would be better than the unloaded hole predictions because Kweon's failure criterion is based on a failure for loaded holes. During the course of validation, several causes for this phenomenon were put forward. It is known, for example, that the assumed stress distribution of the pin on the hole edge does not adequately represent the actual contact problem at other angles than 0° and the contact angle. This causes a high tangential stress at the location of the contact angle which sometimes causes the prediction of early failure. Another possible reason is the use of a fixed hole size to determine the CPSED. It is true that, using the actual hole size to determine the CPSED is beneficial for the prediction of loaded holes (it increases the failure load between 0% and 10%). Using a fixed hole size, however, is one of the cornerstones of the criterion and changing this would negatively affect the unloaded hole predictions. Because of the entanglement of

unnotched and notched failure it is impossible to find a cause related to the tool which does not affect the unloaded hole predictions. Since these predictions are acceptable, and in fact, quite good, the cause of the discrepancy is sought elsewhere. Namely, the test data itself. As already indicated in Section 6.2.3, Figure 6.43, it is possible that the notched failure criterion actually predicts the onset of failure instead of final failure. For unloaded holes this should not be of significant concern as onset is usually quite close to final failure. For loaded holes, however, final failure and onset can be far apart due to several strengthening and interlocking mechanisms in the joint. Unfortunately, no details on the failure mechanisms leading up to failure was found from the literature. It is thus quite hard to determine whether this statement is true. It is however, the most plausible cause.

Unfortunately, due to the directionality boundary condition, the design space where the tool can confidently be used does not cover all possible laminates. To allow usage in the complete design space, the directionality restriction due to the contact angle estimation procedure needs to be resolved. This ultimately means that the contact angle and pin-hole stress distribution need to be improved which can be done using Gerhardt's model [18]. This model was developed during the construction of this thesis but was, when finalizing this work, not yet ready for implementation. Other recommended improvements to the tool are:

- Include compression bearing-bypass loading in the pin-hole boundary condition
- Include additional effects in the unnotched failure method such as ply buckling and delamination
- Investigate other/better numerical integration routines for the determination of the stress field

When these challenges are resolved and validated, the tool can easily be used in the Fokker design environment.

Apart from these issues with the loaded predictions, it is emphasized that the majority of the predictions are moderately to highly conservative while the unloaded predictions are situated in the +20%, -40% region. Although it was mentioned in Section 6.2.2 that a maximum discrepancy of +10% is viable for industry, and the “free” parameters were scaled to obtain this result, the finally obtained +20% for the entire dataset is a remarkably close value. It proves that, with a select number of experimental measurements, the basic conclusions from a failure criterion can be made when one is careful with experimental data. The structural element: orthotropic rectangular plate with multiple (un)loaded holes subjected to arbitrary boundary conditions can be evaluated with confidence when keeping to the determined boundaries.

References

- [1] P.D. Soden, A.S. Kaddour, and M.J. Hinton. Recommendations for designers and researchers resulting from the world-wide failure exercise. *Composites Science and Technology*, 64(3-4):589–604, March 2004.
- [2] Y. Xiong. An analytical method for failure prediction of multi-fastener composite joints. *International Journal of Solids and Structures*, 33(29):4395–4409, December 1996.
- [3] J.-H. Kweon, H.-S. Ahn, and J.-H. Choi. A new method to determine the characteristic lengths of composite joints without testing. *Composite Structures*, 66(1-4):305–315, October 2004.
- [4] S. Lekhnitskii. *Anisotropic Plates*. Routledge, 1968.
- [5] A. Puck and H. Schürmann. Failure Analysis of FRP Laminates by Means of Physically based Phenomenological Models. *Composites Science and Technology*, 58(7):1045–1067, July 1998.
- [6] C.G. Dávila, P.P. Camanho, and C.A. Rose. Failure criteria for FRP laminates. *Journal of Composite Materials*, 39(4):323–345, 2005.
- [7] S.T. Pinho, C.G. Dávila, and P.P. Camanho. Failure models and criteria for FRP under in-plane or three-dimensional stress states including shear non-linearity. Technical Report February, NASA, 2005.
- [8] S.W. Tsai. *Theory of Composites Design*. Think Composites, Palo Alto, 1992.
- [9] M.E. Waddoups, J.R. Eisenmann, and B.E. Kaminski. Macroscopic Fracture Mechanics of Advanced Composite Materials. *Journal of Composite Materials*, 5(4):446–454, January 1971.
- [10] J.M. Whitney and R.J. Nuismer. Stress Fracture Criteria for Laminated Composites Containing Stress Concentrations. *Journal of Composite Materials*, 8(3):253–265, January 1974.

- [11] T. de Jong. *On the calculation of stresses in pin-loaded anisotropic plates*. PhD thesis, Delft University of Technology, 1987.
- [12] X.W. Xu, T.M. Yue, and H.C. Man. Stress analysis of finite composite laminate with multiple loaded holes. *International Journal of Solids and Structures*, 36(6):919–931, 1999.
- [13] N.A. Tomlinson. *Determination of Contact Stress Distribution in Pin Loaded Orthotropic Plates*. PhD thesis, Howard University, 2006.
- [14] Jr. Crews, J.H. and R.A. Naik. Bearing-Bypass Loading on Bolted Composite Joints. Technical Report NASA-TM89153, NASA, 1987.
- [15] VDI. VDI 2014, Development of Fibre-Reinforced Plastics components Analysis. Technical report, Düsseldorf, 2006.
- [16] C. Kassapoglou. *Design and Analysis of Composite Structures*. John Wiley & Sons, Ltd, Chichester, UK, September 2010.
- [17] B.H.A.H. Tijs. Th3.331 - determination of open hole strength of carbon-epoxy laminates. Technical report, Fokker Aerostructures B.V., 2012.
- [18] F. Gerhardt. Internship report fokker aerostructures. Report, Fokker Aerostructures BV, 2013.
- [19] J.H. Crews Jr and R.A. Naik. Combined bearing and bypass loading on a graphite/epoxy laminate. *Composite Structures*, 6(1-3):21 – 40, 1986. Special Issue Joining and Repair of Fibre-Reinforced Plastics.
- [20] O.C. Zienkiewicz and R.L. Taylor. *The Finite Element Method*. Buterworth-Heinemann, Oxford, fifth edition, 2000.
- [21] T. Belytschko, R. Gracie, and G. Ventura. A review of extended/generalized finite element methods for material modeling. *Modelling and Simulation in Materials Science and Engineering*, 17(4):043001, June 2009.
- [22] P.D. Soden, M.J. Hinton, and A.S. Kaddour. Biaxial test results for strength and deformation of a range of E-glass and carbon fibre reinforced composite laminates: failure exercise benchmark data. *Composites Science and Technology*, 62(12-13):1489–1514, September 2002.
- [23] X. Chen. Mechanism-based Failure Laws for Biaxially Compressed IM7/8551-7 Graphite-Epoxy Laminates. *Journal of Composite Materials*, 40(10):899–923, July 2005.
- [24] G.E. Colvin and S.R. Swanson. Mechanical Characterization of IM7/8551-7 Carbon/Epoxy Under Biaxial Stress. *Journal of Engineering Materials and Technology*, 112(1):61, 1990.
- [25] J.S. Welsh, A.C. Biskner, and E.E. Nelson. Experimental and Numerical Failure Predictions of Biaxially-Loaded Unidirectional Carbon Composite Laminates. In *17th International Conference on Composite Materials*, Edinburghm UK, 2009. ICCM.

-
- [26] H. Koerber, J. Xavier, and P.P. Camanho. High strain rate characterisation of uni-directional carbon-epoxy IM7-8552 in transverse compression and in-plane shear using digital image correlation. *Mechanics of Materials*, 42(11):1004–1019, November 2010.
 - [27] G. Bos. Test results notched strength test program, 2007. COMPANY CONFIDENTIAL.
 - [28] P. Lamaris, J.; Minderhoud. The static strength of mechanically fastened carbon-epoxy joints without bending. Technical Publication TP89019L, National Aerospace Laboratory NLR, 1989.
 - [29] J. Wang, P.J. Callus, and M.K. Bannister. Experimental and numerical investigation of the tension and compression strength of un-notched and notched quasi-isotropic laminates. *Composite Structures*, 64(3-4):297–306, June 2004.
 - [30] A.J. Hodge, A.T. Nettles, and J.R. Jackson. Comparison of Open-Hole Compression Strength and Compression After Impact Strength on Carbon Fiber / Epoxy Laminates for the Ares I Composite Interstage. Technical Report March, National Aeronautics and Space Administration, Alabama, 2011.
 - [31] C. Soutis, P. Curtis, and N. Fleck. Compressive Failure of Notched Carbon-Fiber Composites. In *Mathematical and Physical Sciences*, page 15. The Royal Society, 1993.
 - [32] I.M. Daniel. Behavior of graphite/epoxy plates with holes under biaxial loading. *Experimental Mechanics*, 20(1):1–8, January 1980.
 - [33] I.M. Daniel. Biaxial Testing of [0/+– 45]_S Graphite / Epoxy Plates with Holes. *Experimental Mechanics*, 22(5):188–195, 1982.
 - [34] Y. Huang, S.K. Ha, J. Koyanagi, J.D.D. Melo, H. Kumazawa, and I. Susuki. Effects of an Open Hole on the Biaxial Strengths of Composite Laminates. *Journal of Composite Materials*, 44(20):2429–2445, June 2010.
 - [35] Fu-Kuo Chang, Richard A. Scott, and George S. Springer. Failure of composite laminates containing pin loaded holes—method of solution. *Journal of Composite Materials*, 18(3):255–278, 1984.
 - [36] A. Puck, J. Kopp, and M. Knops. Guidelines for the Determination of the Parameters In Puck’s Action Plane Strength Criterion. *Composites Science and Technology*, 62(3):371–387, 2002.
 - [37] R.D.B. Sevenois. Review of stress analysis and failure criteria for orthotropic plates with holes. Report, Delft University of Technology.
 - [38] R.D. Cook, D.S. Malkus, and M.E. Plesha. *Concepts and Applications of Finite Element Analysis*. Number October. John Wiley & Sons Inc., Wisconsin, third edition, 1989.
 - [39] G.N. Savin. *Stress Concentration Around Holes*. Pergamon Press, London, 1961.
 - [40] T.C.T. Ting. *Anisotropic Elasticity: Theory and Applications*. Oxford University Press, Oxford, 1996.

- [41] C. Hwu. *Anisotropic Elastic Plates*. Springer US, Boston, MA, 2010.
- [42] S.C. Tan. Finite-Width Correction Factors for Anisotropic Plate Containing a Central Opening. *Journal of Composite Materials*, 22(11):1080–1097, November 1988.
- [43] J. Schijve. *Fatigue of Structures and Materials*. Springer Science + Business Media, B.V., Delft, second edition, 2009.
- [44] N.I. Muskhelishvili. *Some Basic Problems of the Mathematical Theory of Elasticity*. Springer, April 1953.
- [45] T. de Jong. Stresses around Rectangular Holes in Orthotropic Plates. *Journal of Composite Materials*, 15:311–328, 1981.
- [46] K. Rajaiah and N.K. Naik. Quasi-Rectangular Holes with Minimum Stress Concentration in Orthotropic Plates. *Journal of Reinforced Plastics and Composites*, 2(3):164–177, July 1983.
- [47] M.E. Grayley. Elastic Stress and Strain Distributions Around Circular Holes In Infinite Plates Of Orthotropic Material (Applicable to Fibre Reinforced Composites). Technical report, ESDU, 1985.
- [48] T.K. Tung. On Computation of Stresses Around Holes in Anisotropic Plates. *Journal of Composite Materials*, 21(2):100–104, February 1987.
- [49] C.C. Lin and C.-C. Ko. Stress and Strength Analysis of Finite Composite Laminates with Elliptical Holes. *Journal of Composite Materials*, 22(4):373–385, January 1988.
- [50] X. Xu, L. Sun, and X. Fan. Stress concentration of finite composite laminates with elliptical hole. *Computers & Structures*, 57(1):29–34, 1995.
- [51] T.D. Gerhardt. A Hybrid/Finite Element Approach for Stress Analysis of Notched Anisotropic Materials. *Journal of Applied Mechanics*, 51(4):804–810, December 1984.
- [52] X. Xu, L. Sun, and X. Fan. Stress concentration of finite composite laminates weakened by multiple elliptical holes. *International Journal of Solids and Structures*, 32(20):3001–3014, October 1995.
- [53] W. Hufenbach and L. Kroll. Stress analysis of notched anisotropic finite plates under mechanical and hygrothermal loads. *Archive of Applied Mechanics*, 69(June 1998), 1999.
- [54] W. Hufenbach, B. Gruber, R. Gottwald, M. Lepper, and B. Zhou. Analytical and Experimental Analysis of Stress Concentration in Notched Multilayered Composites with Finite Outer Boundaries. *Mechanics of Composite Materials*, 46(5):531–538, 2010.
- [55] J. Daoust and S.V. Hoa. An analytical solution for anisotropic plates containing triangular holes. *Composite Structures*, 19(2):107–130, 1991.
- [56] V.G. Ukadgaonker and D.K.N. Rao. Stress distribution around triangular holes in anisotropic plates. *Composite Structures*, 45(3):171–183, June 1999.

-
- [57] X.-L. Gao. A general solution of an infinite elastic plate with an elliptic hole under biaxial loading. *International Journal of Pressure Vessels and Piping*, 67(1):95–104, June 1996.
 - [58] H.A. Whitworth and H. Mahase. Stress concentration in graphite/epoxy laminates containing a circular hole. *Journal of Advanced Materials*, 31(4):45–51, 1999.
 - [59] V.G. Ukadgaonker and D.K.N. Rao. A general solution for stresses around holes in symmetric laminates under inplane loading. *Composite Structures*, 49(3):339–354, July 2000.
 - [60] V.G. Ukadgaonker and D.K.N. Rao. A general solution for moments around holes in symmetric laminates. *Composite Structures*, 49(1):41–54, 2000.
 - [61] V.G. Ukadgaonker and V. Kakhandki. Stress analysis for an orthotropic plate with an irregular shaped hole for different in-plane loading conditions—Part 1. *Composite Structures*, 70(3):255–274, September 2005.
 - [62] D.K.N. Rao, M.R. Babu, K.R.N. Reddy, and D. Sunil. Stress around square and rectangular cutouts in symmetric laminates. *Composite Structures*, 92(12):2845–2859, November 2010.
 - [63] D.S. Sharma. Stress Concentration around Circular/Elliptical/Triangular Cutouts in Infinite Composite Plate. *Lecture Notes in Engineering and Computer Science*, III:6–11, 2011.
 - [64] W. Becker. Complex method for the elliptical hole in an unsymmetric laminate. *Archive of Applied Mechanics*, 63(3):159–169, 1993.
 - [65] V.G. Ukadgaonker and D.K.N. Rao. A general solution for stress resultants and moments around holes in unsymmetric laminates. *Composite Structures*, 49(1):27–39, 2000.
 - [66] P. Chen and Z. Shen. Stress resultants and moments around holes in unsymmetrical composite laminates subjected to remote uniform loading. *Mechanics Research Communications*, 30(1):79–86, January 2003.
 - [67] Y. Xiong and C. Poon. Stresses around a biaxially loaded fastener hole in a laminate of finite geometry. *Journal of Thermoplastic Composite Materials*, 11(3):261–271, 1998.
 - [68] Y. Xiong. A Complex Variational Approach for Single Loaded/Unloaded Hole in Finite Laminated Plate Under General In-Plane Loads. *Science and Engineering of Composite Materials*, 8(5), January 1999.
 - [69] B. Grüber, W. Hufenbach, L. Kroll, M. Lepper, and B. Zhou. Stress concentration analysis of fibre-reinforced multilayered composites with pin-loaded holes. *Composites Science and Technology*, 67(7-8):1439–1450, 2007.
 - [70] P. Berbinau, C. Filiou, and C. Soutis. Stress and Failure Analysis of Composite Laminates with an Inclusion under Multiaxial Compression-Tension Loading. *Applied Composite Materials*, (8):307–326, 2001.

- [71] Xi. Zheng and X. Xu. Stress Analysis of Finite Composite Laminates with Elliptical Inclusion. *Computers & structures*, 70(3):0–4, 1999.
- [72] Z.Y. Lin and X.W. Xu. Stress concentration analysis of stiffened composite laminates with multiple elliptical holes or inclusions. *Jisuan Lixue Xuebao/Chinese Journal of Computational Mechanics*, 25(3):379–384+391, 2008.
- [73] J D Eshelby, W T Read, and W Shockley. Anisotropic elasticity with applications to dislocation theory. *Acta Metallurgica*, 1(3):251–259, May 1953.
- [74] A.N. Stroh. Dislocations and Cracks in Anisotropic Elasticity. *Philosophical Magazine*, 3(30):625–646, June 1958.
- [75] A.N. Stroh. Steady State Problems in Anisotropic Elasticity. *Journal of Mathematics and Physics*, 41(2):77–&, 1962.
- [76] T.C.T. Ting. Effects of change of reference coordinates on the stress analyses of anisotropic elastic materials. *International Journal of Solids and Structures*, 18(2):139–152, 1982.
- [77] T.C.T. Ting. The wedge subjected to tractions: a paradox re-examined. *Journal of Elasticity*, 14(3):235–247, 1984.
- [78] T.C.T. Ting. Elastic wedge subjected to antiplane shear tractions-a paradox explained. *Quarterly Journal of Mechanics and Applied Mathematics*, 38(2):245–255, 1985.
- [79] T.C.T. Ting and C. Hwu. Sextic formalism in anisotropic elasticity for almost non-semisimple matrix N . *International Journal of Solids and Structures*, 24(1):65–76, 1988.
- [80] T.C.T. Ting. Barnett-Lothe tensors and their associated tensors for monoclinic materials with the symmetry plane at $x_3=0$. *Journal of Elasticity*, 27(2):143–165, 1992.
- [81] T.C.T. Ting and W. Minzhong. Generalized stroh formalism for anisotropic elasticity for general boundary conditions. *Acta Mechanica Sinica*, 8(3):193–207, 1992.
- [82] T.C.T. Ting. Symmetric Representation of Stress and Strain in the Stroh Formalism and Physical Meaning of the Tensors L , S , $L(\theta)$ and $S(\theta)$. *Journal of Elasticity*, 50(1):91–96, 1998.
- [83] T.C.T. Ting. A modified Lekhnitskii formalism à la Stroh for anisotropic elasticity and classifications of the 6 by 6 matrix N . *Proceedings of the Royal Society A: Mathematical, Physical and Engineering Sciences*, 455(1981):69–89, 1999.
- [84] T.C.T. Ting. Recent developments in anisotropic elasticity. *International Journal of Solids and Structures*, 37(1-2):401–409, 2000.
- [85] T.C.T. Ting. Transverse waves in anisotropic elastic materials. *Wave Motion*, 44(2):107–119, 2006.
- [86] T.C.T. Ting. Existence of one-component Rayleigh waves, Stoneley waves, love waves, slip waves and one-component waves in a plate or layered plate. *Journal of Mechanics of Materials and Structures*, 4(4):631–647, 2009.

-
- [87] T.C.T. Ting. Surface waves in an exponentially graded, general anisotropic elastic material under the influence of gravity. *Wave Motion*, 48(4):335–344, 2011.
 - [88] C. Hwu and T.C.T. Ting. Two-dimensional problems of the anisotropic elastic solid with an elliptic inclusion. *Quarterly Journal of Mechanics and Applied Mathematics*, 42(4):553–572, 1989.
 - [89] C. Hwu. Anisotropic plates with various openings under uniform loading or pure bending. *Journal of Applied Mechanics, Transactions ASME*, 57(3):700–706, 1990.
 - [90] C. Hwu. Thermal stresses in an anisotropic plate disturbed by an insulated elliptic hole or crack. In *American Society of Mechanical Engineers (Paper)*, 1990.
 - [91] C. Hwu and W.-Y. Wang. Various rigid inclusions in anisotropic media. *Journal of the Chinese Society of Mechanical Engineers, Transactions of the Chinese Institute of Engineers, Series C/Chung-Kuo Chi Hsueh Kung Ch'eng Hsuebo Pao*, 13(1):10–16, 1992.
 - [92] C. Hwu and W.J. Yen. On the anisotropic elastic inclusions in plane elastostatics. *Journal of Applied Mechanics, Transactions ASME*, 60(3):626–632, 1993.
 - [93] C. Hwu and C.Y. Liao. A special boundary element for the problems of multi-holes, cracks and inclusions. *Computers and Structures*, 51(1):23–31, 1994.
 - [94] C. Hwu. Stroh-like formalism for the coupled stretching-bending analysis of composite laminates. *International Journal of Solids and Structures*, 40(13-14):3681–3705, 2003.
 - [95] C. Hwu. Stroh-like complex variable formalism for the bending theory of anisotropic plates. *Journal of Applied Mechanics, Transactions ASME*, 70(5):696–707, 2003.
 - [96] C. Hwu. Stroh formalism and its extensions to coupled inplane-bending problems. *Journal of Mechanics*, 19(1):41–53, 2003.
 - [97] C. Hwu. Boundary element formulation for the coupled stretching-bending analysis of thin laminated plates. *Engineering Analysis with Boundary Elements*, 36(6):1027–1039, 2012.
 - [98] H. Gao. Stress analysis of holes in anisotropic elastic solids: Conformal mapping and boundary perturbation. *Quarterly Journal of Mechanics and Applied Mathematics*, 45(2):149–168, 1992.
 - [99] G. Caviglia and A. Morro. Wave propagation in multilayered anisotropic solids. *International Journal of Engineering Science*, 38(8):847–863, 2000.
 - [100] L. Wang. Space of degeneracy in the Stroh eigensystem and surface waves in transversely isotropic elastic media. *Wave Motion*, 40(2):173–190, 2004.
 - [101] X.-F. Wu and Y.A. Dzenis. Antiplane surface acoustic waves propagating in elastic half-space coated with an anisotropic laminate. *Composites Science and Technology*, 65(11-12):1761–1768, 2005.
 - [102] K. Tanuma and C.-S. Man. Perturbation of Rayleigh waves in anisotropic media. *Journal of Physics: Conference Series*, 73(1), 2007.

- [103] M.Y. Chung and T.C.T. Ting. Piezoelectric solid with an elliptic inclusion or hole. *International Journal of Solids and Structures*, 33(23):3343–3361, 1996.
- [104] J.Y. Liou and J.C. Sung. On the generalized Barnett-Lothe tensors for monoclinic piezoelectric materials. *International Journal of Solids and Structures*, 44(16):5208–5221, 2007.
- [105] T. Ikeda, H. Hirai, M. Abe, M. Chiba, and N. Miyazaki. Stress intensity factor analysis of an interfacial corner between piezoelectric bimetals in a two dimensional structure using the H-integral method. In *ASME 2011 Pacific Rim Technical Conference and Exhibition on Packaging and Integration of Electronic and Photonic Systems, InterPACK 2011*, volume 1, pages 463–471, 2011.
- [106] H.J. Konish and J.M. Whitney. Approximate Stresses in an Orthotropic Plate Containing a Circular Hole. *Journal of Composite Materials*, 9(2):157–166, January 1975.
- [107] W.D. Pilkey and D.F. Pilkey. *Peterson's Stress Concentration Factors*. John Wiley & Sons Inc., Hoboken, third edition, 2008.
- [108] S.C. Tan. *Stress Concentrations in Laminated Composite*. Technomic, 1994.
- [109] S.C. Tan and R.Y. Kim. Strain and stress concentrations in composite laminates containing a hole. *Experimental Mechanics*, 30(4):345–351, 1990.
- [110] C. Zhang, S.V. Hoa, and R. Ganesan. Approximate Solutions for Stresses around Pin-Loaded Holes in Symmetric Composite Laminates. *Journal of Reinforced Plastics and Composites*, 17(9):800–818, June 1998.
- [111] C. Soutis and C. Filiou. Stress Distributions around Holes in Composite Laminates Subjected to Biaxial Loading. *Applied Composite Materials*, 5(365-378):365–378, 1998.
- [112] A. Russo and B. Zuccarello. An accurate method to predict the stress concentration in composite laminates with a circular hole under tensile loading. *Mechanics of Composite Materials*, 43(4):359–376, 2007.
- [113] L.-C. Shiau and G.C. Lee. Stress concentration around holes in composite laminates with variable fiber spacing. *Composite Structures*, 24(2):107–115, January 1993.
- [114] M. Ozbay and D. Ozer. The Analysis of Elasto-plastic Stresses in the Composite Laminate with a Circular Hole Subjected to In-plane Loads by Means of Finite Element Method. *Journal of Reinforced Plastics and Composites*, 24(6):621–631, April 2005.
- [115] Y. Abdelaziz and A. Hamouine. A survey of the extended finite element. *Computers & Structures*, 86(11-12):1141–1151, June 2008.
- [116] A. Yazid, N. Abdelkader, and H. Abdelmadjid. A state-of-the-art review of the X-FEM for computational fracture mechanics. *Applied Mathematical Modelling*, 33(12):4269–4282, December 2009.
- [117] MSC Software. *MSC Laminate Modeler User's Guide*, 2013.
- [118] H. Lo, E. Wu, and D.Y. Konishi. Failure Strength of Notched Composite Laminates. *Journal of Composite Materials*, 17(5), 1983.

-
- [119] T. Flatscher, C. Schuecker, and H.E. Pettermann. Prediction of plastic strain accumulation in continuous fiber reinforced laminates by a constitutive ply model. *International Journal of Fracture*, 158(2):145–156, May 2009.
 - [120] S.W. Tsai and E.M. Wu. A General Theory of Strength for Anisotropic Materials. *Journal of Composite Materials*, 5(1):58–80, January 1971.
 - [121] S.E. Yamada and C.T. Sun. Analysis of Laminate Strength and Its Distribution. *Journal of Composite Materials*, 12(3):275–284, January 1978.
 - [122] A. Rotem. Prediction of Laminate Failure with the Rotem Failure Criterion. *Composites Science and Technology*, 58(7):1083–1094, July 1998.
 - [123] I.M. Daniel and O. Ishai. *Engineering mechanics of composite materials*. Oxford University Press, New York, second edition, 2006.
 - [124] H.A. Whitworth and S.W. Yin. A failure criterion for laminated fiber-reinforced composites. *Composites Engineering*, 1(2):61–67, 1991.
 - [125] L.J. Hart-Smith. Predictions of the original and truncated maximum-strain failure models for certain fibrous composite laminates. *Composites Science and Technology*, 58(7):1151–1178, July 1998.
 - [126] L.J. Hart-Smith. Predictions of a generalized maximum-shear-stress failure criterion for certain fibrous composite laminates. *Composites Science and Technology*, 58(7):1179–1208, July 1998.
 - [127] Failure criteria for composite laminates. *Composites Science and Technology*, 45(3):283–284, 1992.
 - [128] M.J. Hinton and P.D. Soden. Predicting failure in composite laminates: the background to the exercise. *Composites Science and Technology*, 58(7):1001–1010, July 1998.
 - [129] M.J. Hinton, A.S. Kaddour, and P.D. Soden. Evaluation of failure prediction in composite laminates: background to part B of the exercise. *Composites Science and Technology*, 62(12-13):1481–1488, September 2002.
 - [130] P.D. Soden, M.J. Hinton, and A.S. Kaddour. Lamina properties, lay-up configurations and loading conditions for a range of fibre-reinforced composite laminates. *Composites Science and Technology*, 58(7):1011–1022, July 1998.
 - [131] A.S. Kaddour, M.J. Hinton, and P.D. Soden. A comparison of the predictive capabilities of current failure theories for composite laminates: additional contributions. *Composites Science and Technology*, 64(3-4):449–476, March 2004.
 - [132] P.A. Zinoviev, S.V. Grigoriev, O.V. Lebedeva, and L.P. Tairova. The strength of multilayered composites under a plane-stress state. *Composites Science and Technology*, 58(7):1209–1223, July 1998.
 - [133] P.A. Zinoviev, O.V. Lebedeva, and L.P. Tairova. A coupled analysis of experimental and theoretical results on the deformation and failure of composite laminates under a state of plane stress. *Composites Science and Technology*, 62(12-13):1711–1723, September 2002.

- [134] K.-D. Liu and S.W. Tsai. A Progressive Quadratic Failure Criterion for a Laminate. *Composites Science and Technology*, 58(7):1023–1032, July 1998.
- [135] A. Kuraishi, S.W. Tsai, and Kevin K.S. Liu. A progressive quadratic failure criterion, part B. *Composites Science and Technology*, 62(12-13):1683–1695, September 2002.
- [136] T.A. Bogetti, C.P.R. Hoppel, V.M. Harik, J.F. Newill, and B.P. Burns. Predicting the nonlinear response and progressive failure of composite laminates. *Composites Science and Technology*, 64(3-4):329–342, March 2004.
- [137] T.A. Bogetti, C.P.R. Hoppel, V.M. Harik, J.F. Newill, and B.P. Burns. Predicting the nonlinear response and failure of composite laminates: correlation with experimental results. *Composites Science and Technology*, 64(3-4):477–485, March 2004.
- [138] A. Puck and H. Schürmann. Failure analysis of FRP laminates by means of physically based phenomenological models. *Composites Science and Technology*, 62(12-13):1633–1662, September 2002.
- [139] R.G. Cuntze and A. Freund. The predictive capability of failure mode concept-based strength criteria for multidirectional laminates. *Composites Science and Technology*, 64(3-4):343–377, March 2004.
- [140] R.G. Cuntze. The predictive capability of failure mode concept-based strength criteria for multi-directional laminates part B. *Composites Science and Technology*, 64(3-4):487–516, March 2004.
- [141] C. Bisagni and R. Vescovini. Assessment of the Damage Tolerance of Postbuckled Hat-Stiffened Panels using Single-Stringer Specimens. Technical report, National Aeronautical and Space Agency, Hampton, Virginia, 2010.
- [142] P. Maimí, P.P. Camanho, J.A. Mayugo, and C.G. Dávila. A Thermodynamically Consistent Damage Model for Advanced Composites. Technical Report March, National Aeronautics And Space Administration, 2006.
- [143] G.M. Vyas and S.T. Pinho. Computational implementation of a novel constitutive model for multidirectional composites. *Computational Materials Science*, 51(1):217–224, January 2012.
- [144] V. Las, R. Zemčík, T. Kroupa, and R. Kottner. Failure prediction of composite materials. *Bulletin of Applied Mechanics*, 4(14):81–87, 2008.
- [145] R. Satheesh, G.N. Naik, and R. Ganguli. Conservative Failure Criteria for Optimal Design of Composite Structures Including Effect of Shear Loading. *Mechanics of Advanced Materials and Structures*, 19(8):625–640, December 2012.
- [146] M.J. Hinton and A.S. Kaddour. The background to the Second World-Wide Failure Exercise. *Journal of Composite Materials*, 46(19-20):2283–2294, June 2012.
- [147] A.S. Kaddour, M.J. Hinton, S. Li, and P. Smith. Damage theories for fibre-reinforced polymer composites: the third world-wide failure exercise (WWFE-III). In *Proceedings of the 16th International Conference on Composite Materials*, Kyoto, 2007. QinetiQ Limited.

-
- [148] M.J. Hinton. Failure Criteria in Fibre Reinforced Polymer Composites : Can any of the Predictive Theories be Trusted ? In *NAFEMS World Congress*, number May, Boston, 2011. QinetiQ Limited.
- [149] AS Kaddour and MJ Hinton. Maturity of 3d failure criteria for fibre-reinforced composites: Comparison between theories and experiments: Part b of wwfe-ii. *Journal of Composite Materials*, 47(6-7):925–966, 2013.
- [150] T.A. Bogetti, J. Staniszewski, B.P. Burns, C.P. Hoppel, J.W. Gillespie, and J. Tierney. Predicting the nonlinear response and progressive failure of composite laminates under tri-axial loading. *Journal of Composite Materials*, 46(19-20):2443–2459, June 2012.
- [151] C.C. Chamis and L. Minnetyan. Multiscale Multifunctional Progressive Fracture of Composite Structures. Technical Report September, National Aeronautics and Space Administration, Ohio, 2012.
- [152] M.H. Deuschle and B.-H. Kroplin. Finite element implementation of Puck’s failure theory for fibre-reinforced composites under three-dimensional stress. *Journal of Composite Materials*, 46(19-20):2485–2513, October 2012.
- [153] A.S. Kaddour and M.J. Hinton. *Benchmarking of triaxial failure criteria for composite laminates: Comparison between models of 'Part (A)' of 'WWFE-II'*, volume 46. June 2012.
- [154] ST Pinho, GM Vyas, and P Robinson. Material and structural response of polymer-matrix fibre-reinforced composites: Part b. *Journal of Composite Materials*, 47(6-7):679–696, 2013.
- [155] N Carrere, F Laurin, and J-F Maire. Micromechanical-based hybrid mesoscopic three-dimensional approach for non-linear progressive failure analysis of composite structures-part b: Comparison with experimental data. *Journal of Composite Materials*, 47(6-7):743–762, 2013.
- [156] H Matthias Deuschle and Alfred Puck. Application of the puck failure theory for fibre-reinforced composites under three-dimensional stress: Comparison with experimental results. *Journal of Composite Materials*, 47(6-7):827–846, 2013.
- [157] N.K. Naik, S.I. Tiwari, and R.S. Kumar. An analytical model for compressive strength of plain weave fabric composites. *Composites Science and Technology*, 63(5):609–625, April 2003.
- [158] M. Nasr, M. N. Abouelwafa, a. Gomaa, a. Hamdy, and E. Morsi. A New Failure Criterion for Woven-Roving Fibrous Composites Subjected to Tension-Compression Local Plane Stresses With Different Stress Ratios. *Journal of Engineering Materials and Technology*, 127(1):130, 2005.
- [159] C. Hochard, J. Payan, and C. Bordreuil. A progressive first ply failure model for woven ply CFRP laminates under static and fatigue loads. *International Journal of Fatigue*, 28(10):1270–1276, October 2006.
- [160] J. Backlund. Fracture analysis of notched composites. *Computers & Structures*, 13(1-3):145–154, June 1981.

- [161] C. Soutis, N.A. Fleck, and P.A. Smith. Failure prediction technique for compression loaded carbon fibre-epoxy laminate with open holes. *Journal of Composite Materials*, 25(11):1476, 1991.
- [162] R.J. Nuismer and J.D. Labor. Applications of the Average Stress Failure Criterion: Part II – Compression. *Journal of Composite Materials*, 13(1):49–60, January 1979.
- [163] R.J. Nuismer and J.D. Labor. Applications of the Average Stress Failure Criterion: Part I – Tension. *Journal of Composite Materials*, 12(3):238–249, January 1978.
- [164] R.B. Pipes, R.C. Wetherhold, and J.W. Gillespie. Notched Strength of Composite Materials. *Journal of Composite Materials*, 13(2):148–160, April 1979.
- [165] S.P. Garbo. Design and Analysis of Composite Structures with stress concentrations, 1982.
- [166] N.K. Naik and P. Shembekar. Notched strength of fabric laminates I: Prediction. *Composites Science and Technology*, 44(1):1–12, 1992.
- [167] P. Shembekar and N. Naik. Notched strength of fabric laminates. II: Effect of stacking sequence. *Composites Science and Technology*, 44(1):13–20, 1992.
- [168] P.G. Potti, N.B. Rao, and V. Srivastava. Notched strength of carbon fibre/epoxy composite laminates with a circular hole. *Forschung im Ingenieurwesen*, 65(7):295–300, 1999.
- [169] X.W. Xu, H.C. Man, and T.M. Yue. Strength prediction of composite laminates with multiple elliptical holes. *International Journal of Solids and Structures*, 37(21):2887–2900, May 2000.
- [170] B.G. Green, M.R. Wisnom, and S.R. Hallett. An experimental investigation into the tensile strength scaling of notched composites. *Composites Part A: Applied Science and Manufacturing*, 38(3):867–878, March 2007.
- [171] C.-L. Hwan, K.-H. Tsai, W.-L. Chen, C.-H. Chiu, and C. M. Wu. Strength prediction of braided composite plates with a center hole. *Journal of Composite Materials*, 45(19):1991–2002, March 2011.
- [172] S.-Y. Kim, J.-M. Koo, D. Kim, and C.-S. Seok. Prediction of the static fracture strength of hole notched plain weave CFRP composites. *Composites Science and Technology*, 71(14):1671–1676, September 2011.
- [173] L.A. Carlsson, C.G. Aronsson, and J. Backlund. Notch Sensitivity of Thermoset and Thermoplastic Laminates Loaded in Tension. *Journal of Materials Science*, 24(5):1670–1682, 1989.
- [174] C.G. Aronsson. Strength of carbon/epoxy laminates with countersunk hole. *Composite Structures*, 24(4):283–289, January 1993.
- [175] K. Hollmann. Failure Analysis of Bolted Composite Joints Exhibiting In-Plane Failure Modes. *Journal of Composite Materials*, 30(3):358–383, February 1996.

-
- [176] I. Eriksson and C.-G. Aronsson. Strength of Tensile Loaded Graphite/Epoxy Laminates Containing Cracks, Open and Filled Holes. *Journal of Composite Materials*, 24(5):456–482, May 1990.
- [177] C.J. Liu, A.H.J. Nijhof, L.J. Ernst, and R0 Marissen. A new ultimate strength model of notched composite laminates -Including the effects of matrix failure. *Journal of Composite Materials*, 44(11):1335–1349, 2010.
- [178] K.-Y. Chang, S. Liu, and F.-K. Chang. Damage tolerance of laminated composites containing an open hole and subjected to tensile loadings. *Journal of Composite Materials*, 25(3):274–301, 1991.
- [179] P.D. Shah, J.D.D. Melo, C.A. Cimini, and M. Ridha. Evaluation of Notched Strength of Composite Laminates for Structural Design. *Journal of Composite Materials*, 44(20):2381–2392, May 2010.
- [180] N.F.Jr. Knight. User-Defined Material Model for Progressive Failure Analysis. Technical Report December, Virginia, 2006.
- [181] A. Satyanarayana and A. Przekop. Predicting Failure Progression and Failure Loads in Composite Open-Hole Tension Coupons. Technical Report May, ATK Space Sysems Inc., Virginia, 2010.
- [182] T. Flatscher and H.E. Pettermann. A constitutive model for fiber-reinforced polymer plies accounting for plasticity and brittle damage including softening - Implementation for implicit FEM. *Composite Structures*, 93(9):2241–2249, August 2011.
- [183] T. Flatscher, M. Wolfahrt, G. Pinter, and H.E. Pettermann. Simulations and experiments of open hole tension tests - Assessment of intra-ply plasticity, damage, and localization. *Composites Science and Technology*, 72(10):1090–1095, June 2012.
- [184] E. Abisset, F. Daghia, and P. Ladevèze. On the validation of a damage mesomodel for laminated composites by means of open-hole tensile tests on quasi-isotropic laminates. *Composites Part A: Applied Science and Manufacturing*, 42(10):1515–1524, October 2011.
- [185] A. Farrokhhabadi, H. Hosseini-Toudeshky, and B. Mohammadi. Development of a Damage Analysis Method in Laminated Composites Using Finite Fracture Toughness of Single Lamina. *Mechanics of Advanced Materials and Structures*, 20(3):177–188, March 2013.
- [186] A.R. Curtis and P. Grant. The Strength of Carbon-Fiber Composite Plates with Loaded and Unloaded Holes. *Composite Structures*, 2(3):201–221, 1984.
- [187] S. Toll and C.G. Aronsson. Notched Strength of Long-Fiber and Short-Fiber Reinforced Polyamide. *Composites Science and Technology*, 45(1):43–54, 1992.
- [188] A.S. Rao, Y. Krishna, and B.N. Rao. Comparison of fracture models to assess the notched strength of composite/solid propellant tensile specimens. *Materials Science and Engineering: A*, 385(1-2):429–439, November 2004.

- [189] V.K. Kannan, V. Murali, A. Rajadurai, and B.N. Rao. Tension and Compression Strength Evaluation of Composite Plates with Circular Holes. *Journal of Reinforced Plastics and Composites*, 29(10):1500–1514, 2010.
- [190] V.K. Kannan, V. Murali, A. Rajadurai, and B.N. Rao. Finite element analysis and notched tensile strength evaluation of center-hole 2D carbon/carbon laminates. *Advanced Composite Materials*, 20(3):289–300, 2011.
- [191] J. Su, H. Gou, Y. Li, G. Wu, and G. Chen. Strength prediction of tensile loaded graphite fiber-reinforced aluminum composites containing circular holes. *Journal of Reinforced Plastics and Composites*, 30(7):601–607, June 2011.
- [192] C.H. Wang, A.J. Gunnion, A.C. Orifici, and A. Rider. Residual strength of composite laminates containing scarfed and straight-sided holes. *Composites Part A: Applied Science and Manufacturing*, 42(12):1951–1961, December 2011.
- [193] W. Fan and J.-G. Wu. Stress concentration of a laminate weakened by multiple holes. *Composite structures*, 10:303–319, 1988.
- [194] S. Koussios. Continuity of the solutions obtained by Lekhnitskii’s theory for anisotropic plates: Sign selection strategies. In *American Society for Composites - 23rd Technical Conference of the American Society for Composites 2008*, volume 1, pages 289–307, 2008.
- [195] A. Puck. Festigkeitsanalyse von Faser-Matrix-Laminaten - Modelle für die Praxis. *Carl Hanser Verlag*, 1996.
- [196] M. Flemming and S. Roth. Faserverbundbaueisen, Eigenschaften, mechanische, konstruktive, thermische, elektrische, ökologisch, wirtschaftliche Aspekte. *Springer*, 2003.
- [197] H. Schürmann. Konstruieren mit Faser-Kunststoffen Verbunden. *Springer*, 2005.
- [198] M. Knops. The Puck Theory of Failure in fiber Polymer Laminates: Fundamentals, Verification and Application. *Springer*, 2007.
- [199] Stork AESP B.V. *FEM Modeling Handbook*, 2010.
- [200] M. Bakker. Analytic stress field and failure prediction of mechanically fastened composite joints. Master’s thesis, Delft University of Technology, Faculty of Aerospace Engineering, Aerospace Structures and Materials, 2012.
- [201] G. Bos. Test results undisturbed laminates test program. COMPANY CONFIDENTIAL.
- [202] A. Abdoella. Handboek omrekengegevens. Technical report, Fokker-VFW B.V., 1994.

Appendix A

Derivation of the Sign Selection Algorithm

In this Chapter the derivation of the sign selection algorithm is given. For this algorithm the algorithm provided by Koussios [194] was taken as a basis. This algorithm is given by:

IF $\alpha = 0$

$s = \text{sign}(y - y_m)$ IF $x = 0$

$s = \text{sign}(x - x_m)$ OTHERWISE

IF $\alpha > 0$

IF $(y - y_m \leq 0 \wedge R < 0 \wedge M < 0) \vee (S > 0 \wedge R > 0) \vee (S > 0 \wedge M \geq 0)$

$s = +1$

OTHERWISE $s = -1$

IF $\alpha < 0$

IF $(y - y_m \leq 0 \wedge R < 0 \wedge M \geq 0) \vee (S > 0 \wedge R > 0) \vee (S > 0 \wedge M < 0)$

$s = -1$

OTHERWISE $s = +1$

and is based on the fact that the sign s before the square root of Eq. (A.1) should change when the sign of the imaginary part inside the square root changes sign.

$$\xi(x, y)_{mj} = \frac{z_j(x, y) + s\sqrt{z_j(x, y)^2 - 4R_{mj}^2 t_{mj}}}{2R_{mj}} \quad (\text{A.1})$$

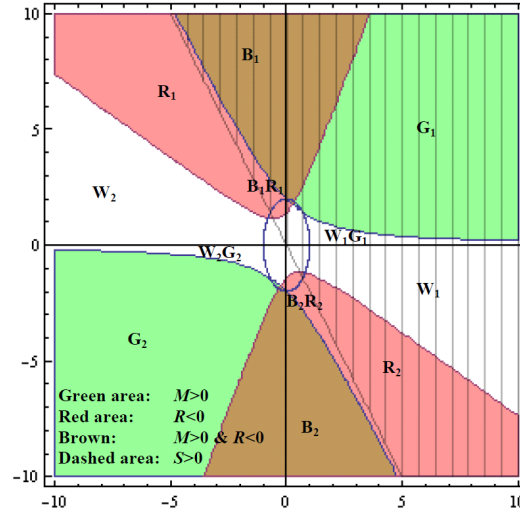


Figure A.1: Basis of the algorithm by Koussios [194]

R and M are the real respectively imaginary part of the equation inside the square root. S is the asymptote of the region bounded by $M = 0$. They can be represented in equation form using:

$$R = ((x - x_m)^2 - a^2) + ((y - y_m)^2 - H^2)(\alpha^2 - \beta^2)(\alpha^2 - \beta^2) + 2\alpha(x - x_m)(y - y_m) \quad (\text{A.2a})$$

$$M = 2\beta \left(\alpha \left((y - y_m)^2 - b^2 \right) + (x - x_m)(y - y_m) \right) \quad (\text{A.2b})$$

$$S = (y - y_m) + \frac{x - x_m}{\alpha} \quad (\text{A.2c})$$

where a and b are the ellipse semi major and minor axes. α is the real and β the imaginary part of the material eigenvalue μ . A sign plot of these three functions which is shown in Figure A.1 is used. For each region in this plot it was identified which parameters should result in a positive or negative sign and on this basis the algorithm was constructed. The plot, however, is not valid for every combination of α and β . More specifically, the region $R < 0$ does not always consist of two parts but sometimes also forms one region. This happens when $\beta < |\alpha|$. As shown in Figure A.2 this induces additional regions which are not captured by the algorithm. Also when $\beta \cong 2|\alpha|$ additional regions are invoked as shown in Figure A.3. To incorporate these regions in the sign selection algorithm an additional distinction is made for the case when $\beta < |\alpha|$ and the original requirements for "+" or "-" sign adapted. This results in the algorithm below:

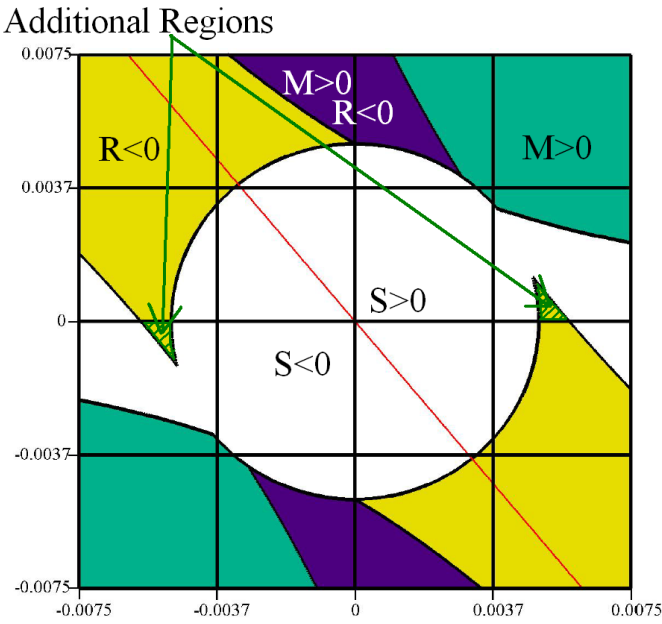


Figure A.2: Sign regions for $\beta < |\alpha|$

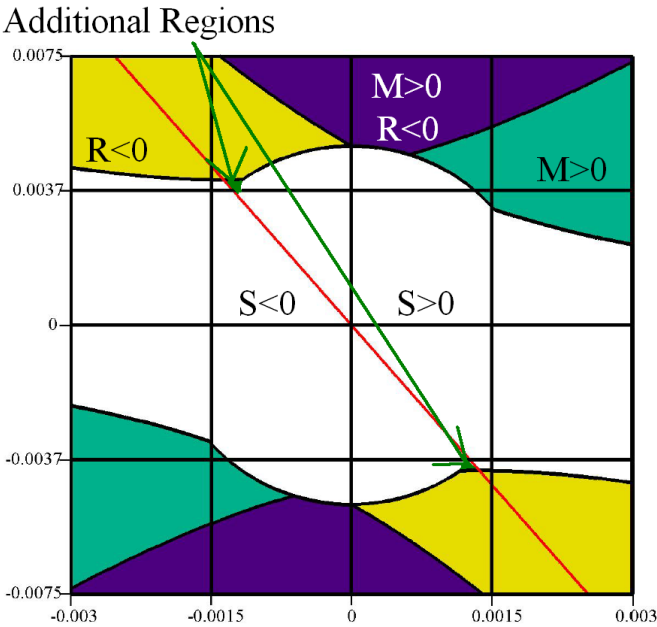


Figure A.3: Sign regions for $\beta \approx 2|\alpha|$

IF $\alpha = 0$

$s(x, y, j, m) = \text{sign}(y - y_m)$ IF $x = 0$

$s(x, y, j, m) = \text{sign}(x - x_m)$ OTHERWISE

IF $\beta > |\alpha|$

IF $\alpha > 0$

IF $(y - y_m \leq 0 \wedge R < 0 \wedge M < 0 \wedge -x_m \geq 0) \vee$

$(S > 0 \wedge R > 0 \wedge x - x_m \geq 0) \vee$

$(S > 0 \wedge M \geq 0) \vee$

$(S > 0 \wedge R < 0 \wedge x - x_m \geq 0) \vee$

$(S < 0 \wedge R > 0 \wedge x - x_m \geq 0)$

$s = +1$

OTHERWISE $s = -1$

IF $\alpha < 0$

IF $(y - y_m \leq 0 \wedge R < 0 \wedge M \geq 0 \wedge x - x_m \leq 0) \vee$

$(S > 0 \wedge R > 0 \wedge x - x_m \leq 0) \vee$

$(S > 0 \wedge M < 0) \vee (S > 0 \wedge R < 0 \wedge x - x_m \leq 0) \vee$

$(S < 0 \wedge R > 0 \wedge x - x_m \leq 0)$

$s(x, y, j, m) = -1$

OTHERWISE $s(x, y, j, n) = +1$

OTHERWISE

IF $\alpha > 0$

IF $(y - y_m \leq 0 \wedge R < 0 \wedge M < 0 \wedge x - x_m \geq 0) \vee$

$(S > 0 \wedge R > 0 \wedge x - x_m \geq 0) \vee$

$(S > 0 \wedge M \geq 0) \vee$

$(S > 0 \wedge R < 0 \wedge x - x_m \geq 0)$

$s(x, y, j, m) = +1$

OTHERWISE $s(x, y, j, m) = -1$

IF $\alpha < 0$

IF $(y - y_m \leq 0 \wedge R < 0 \wedge M \geq 0 \wedge x - x_m \leq 0) \vee$

$(S > 0 \wedge R > 0 \wedge x - x_m \leq 0) \vee (S > 0 \wedge M < 0) \vee$

$(S > 0 \wedge R < 0 \wedge x - x_m \leq 0)$

$s = -1$

OTHERWISE $s = +1$

The algorithm above is tested for multiple layups and hole shapes as shown in Figure A.4 to Figure A.19 from which it is concluded that the algorithm now does choose the correct sign for all possible cases (the red line is the line where the sign changes from + to -).

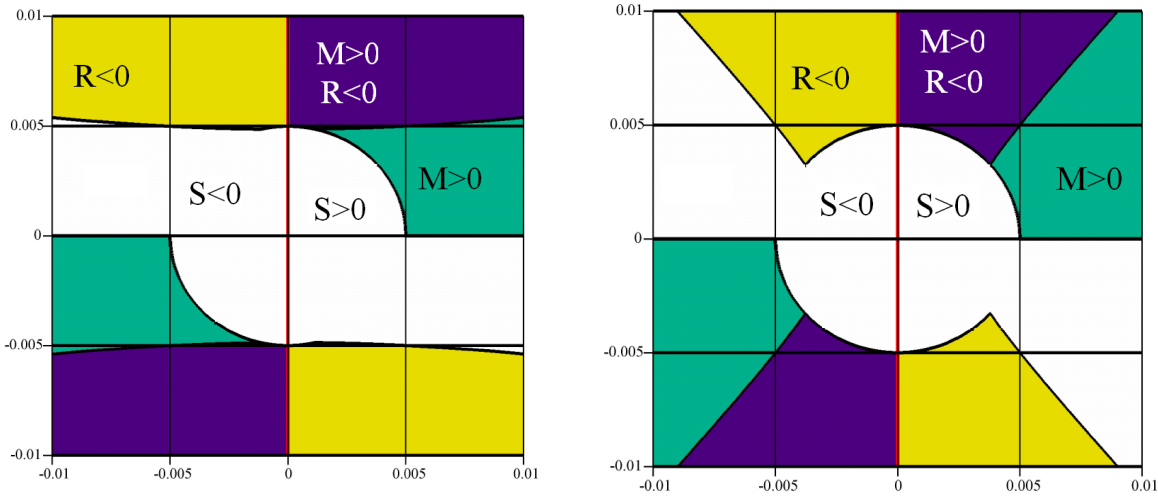


Figure A.4: Layup: $[0]_s$

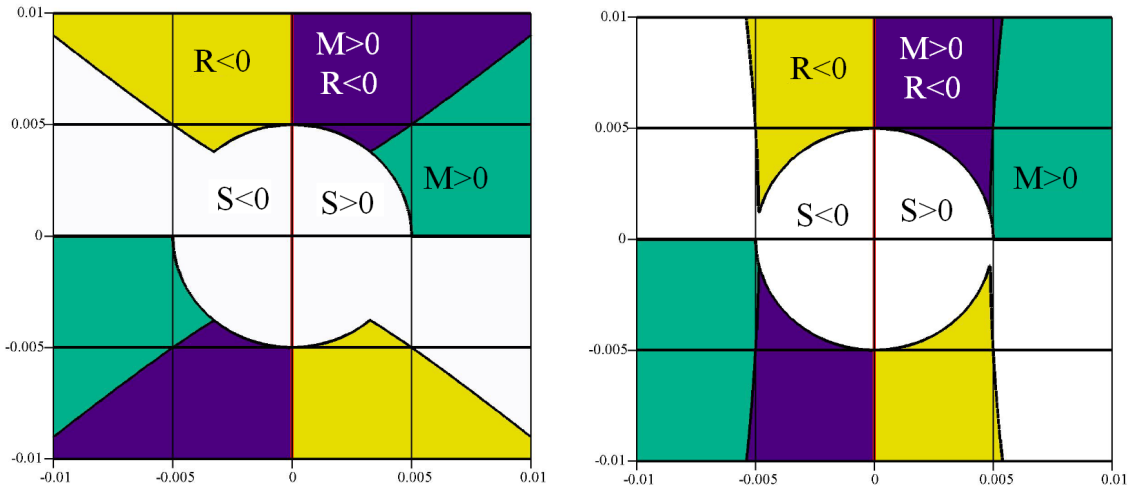
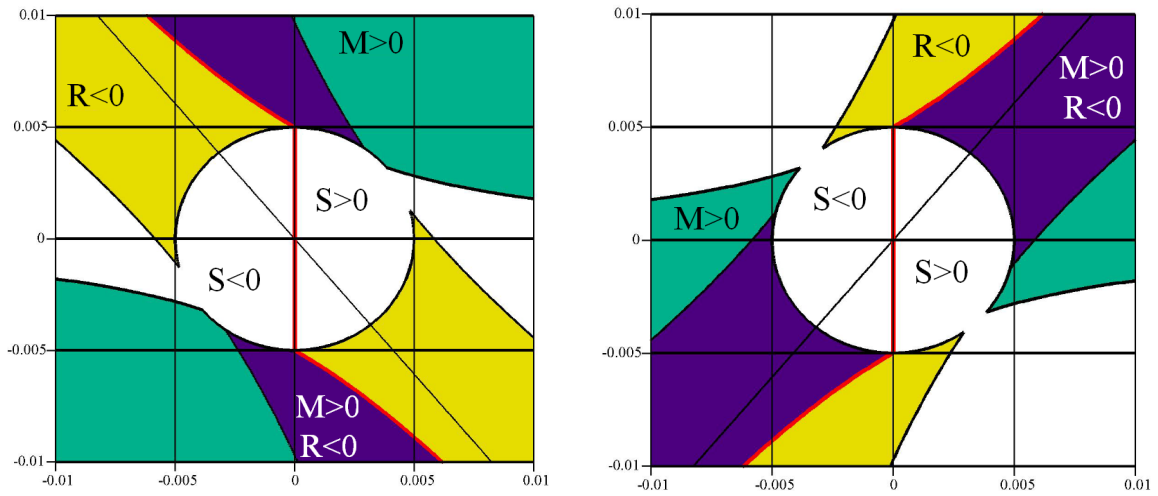
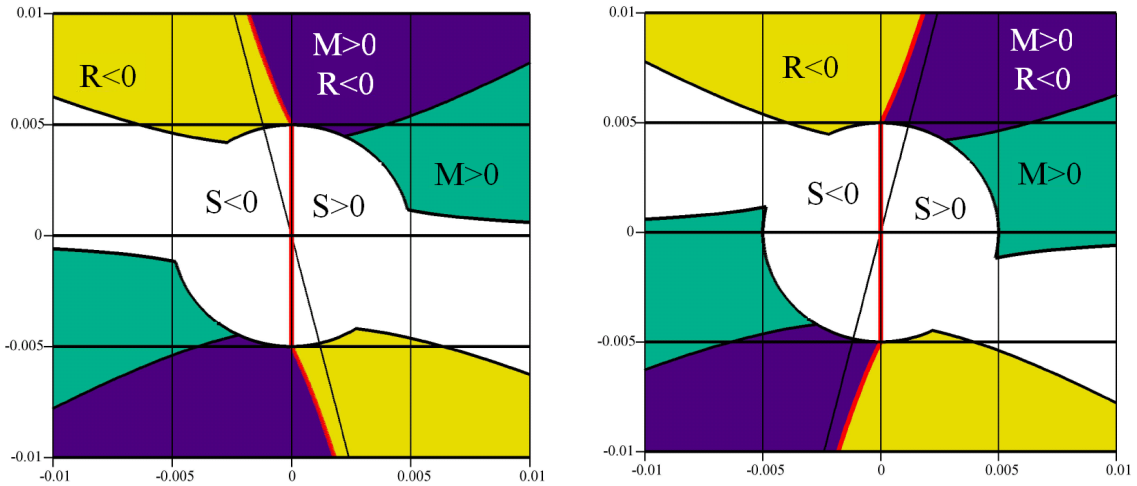
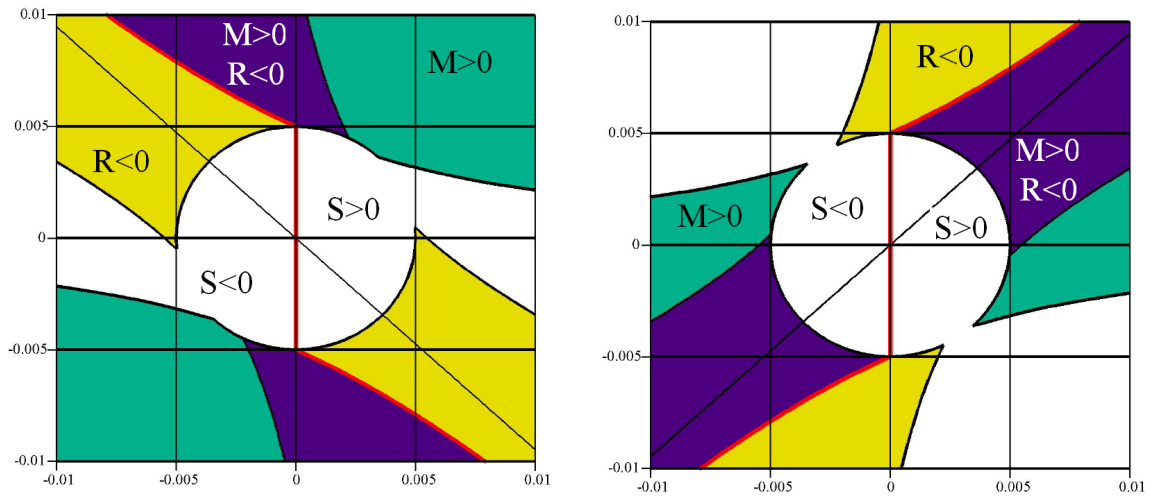
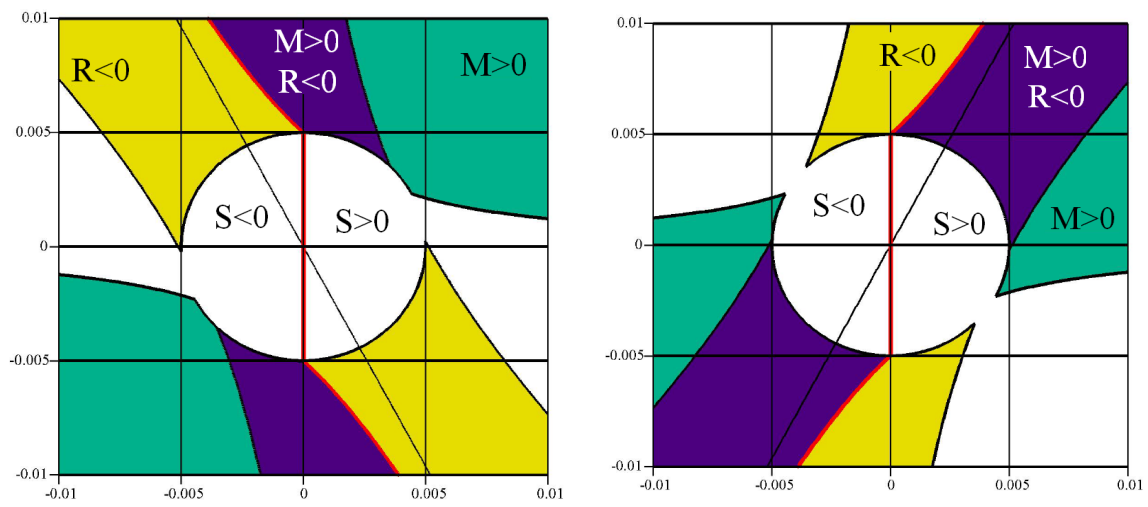
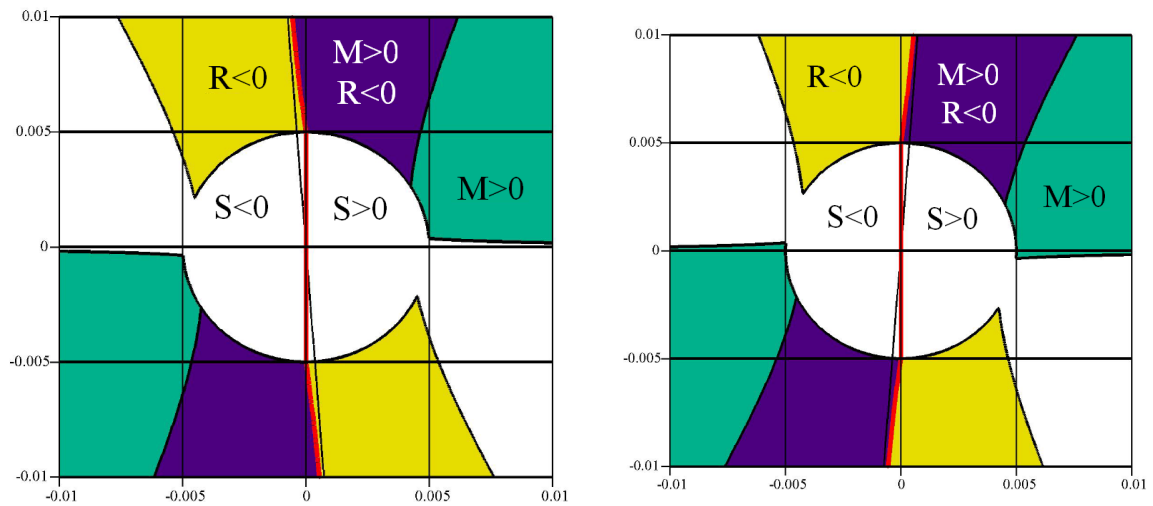
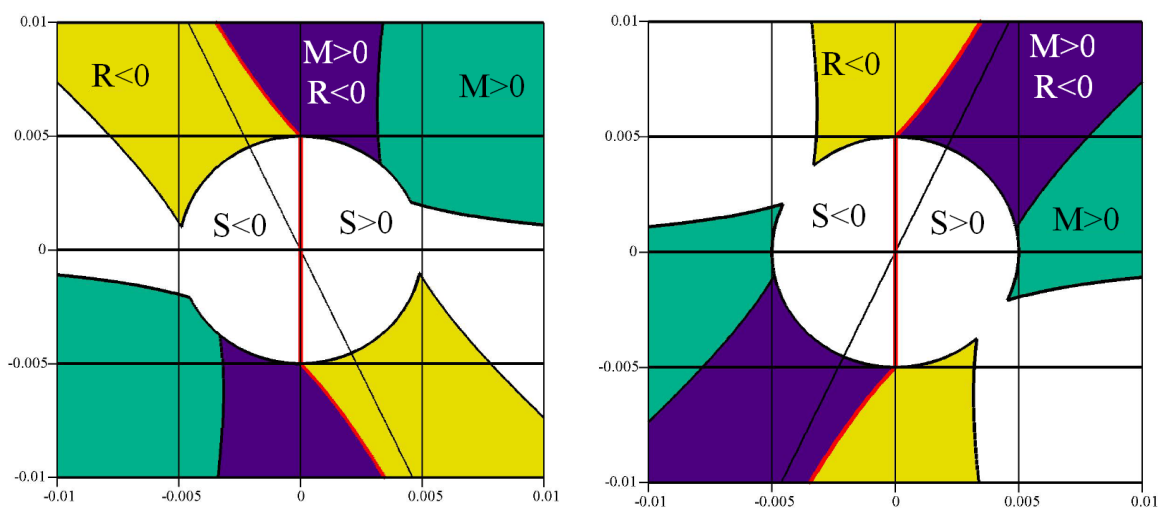


Figure A.5: Layup: $[90]_s$

Figure A.6: Layout: $[\pm 45]_s$ Figure A.7: Layout: $[\pm 15]_s$ Figure A.8: Layout: $[\pm 30]_s$

Figure A.9: Layup: $[\pm 60]_s$ Figure A.10: Layup: $[\pm 75]_s$ Figure A.11: Layup: $0\%0^\circ, 50\% \pm 45^\circ, 50\%90^\circ$

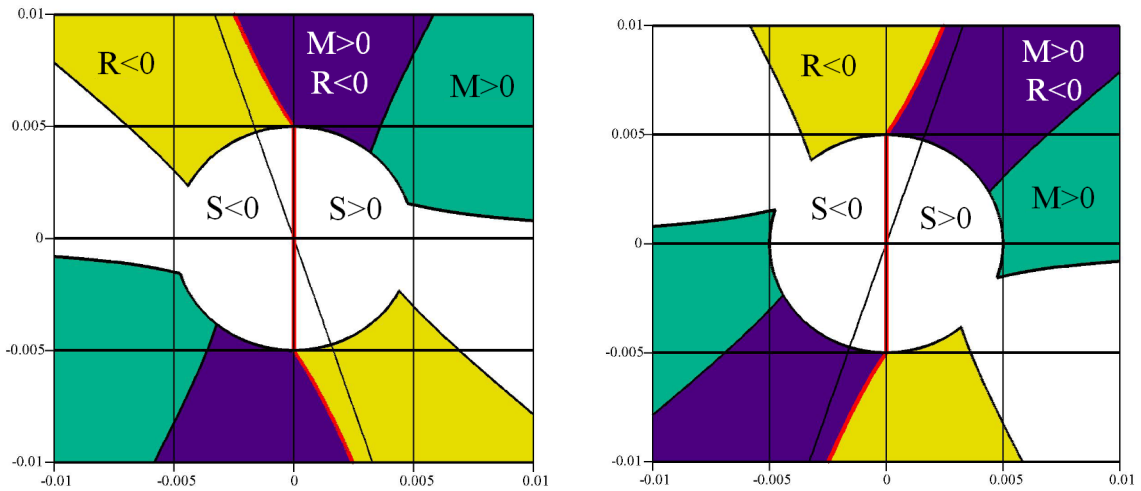


Figure A.12: Layup: 20%0°, 40%±45°, 40%90°

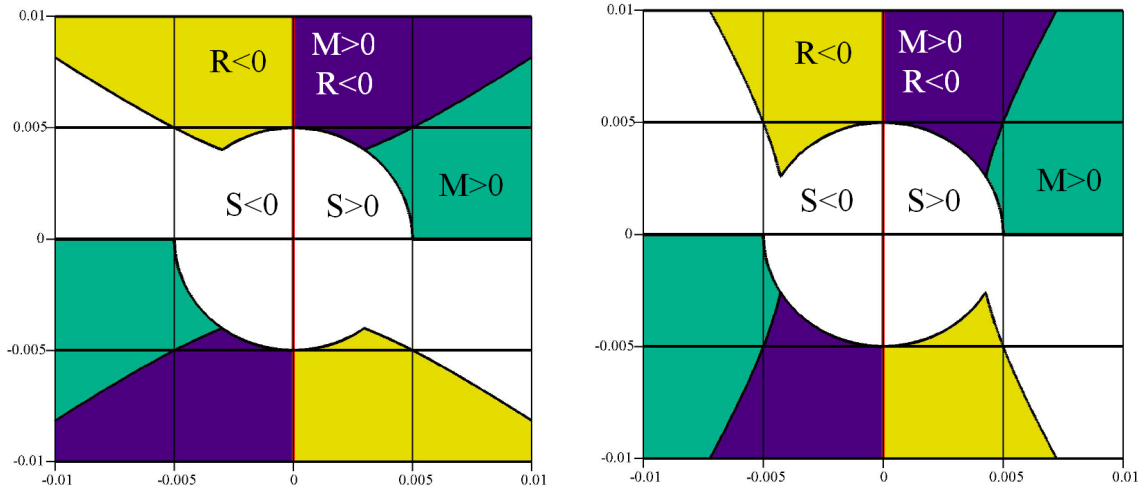


Figure A.13: Layup: 25%0°, 25%±45°, 50%90°

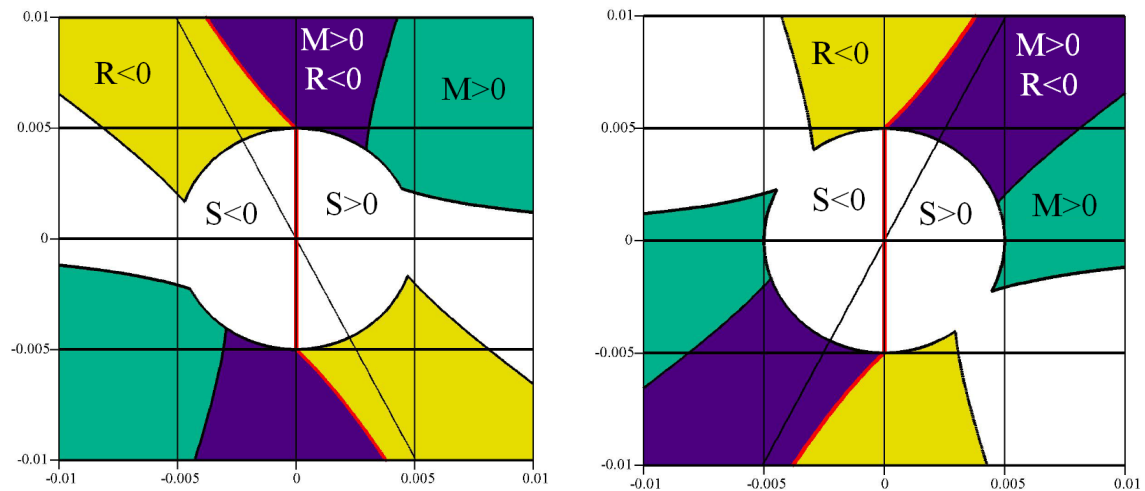


Figure A.14: Layup: 25%0°, 50%±45°, 25%90°

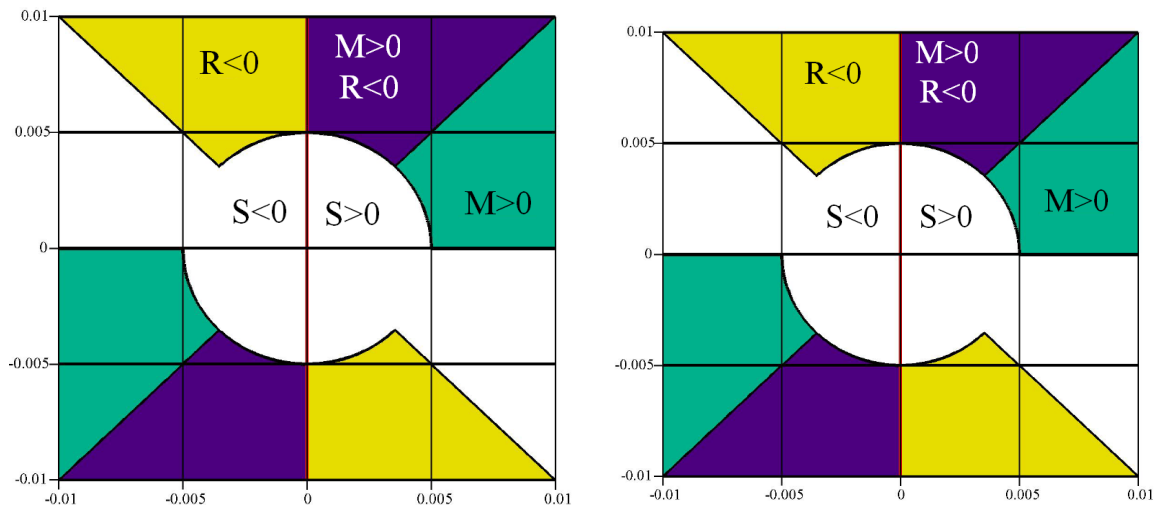


Figure A.15: Layup: 33%0°, 33%±45°, 33%90°

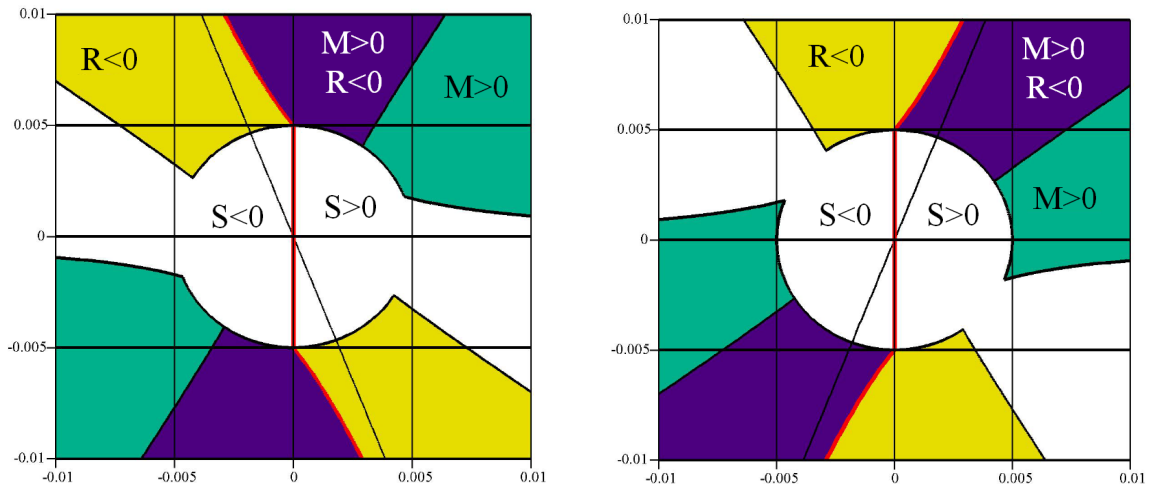


Figure A.16: Layup: 40%0°, 40%±45°, 20%90°

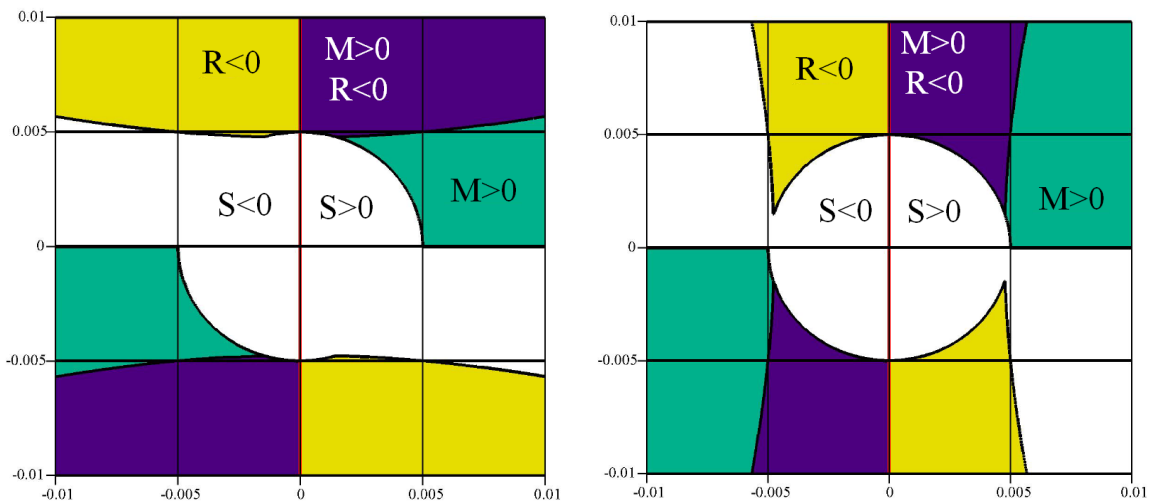


Figure A.17: Layup: 50%0°, 0%±45°, 50%90°

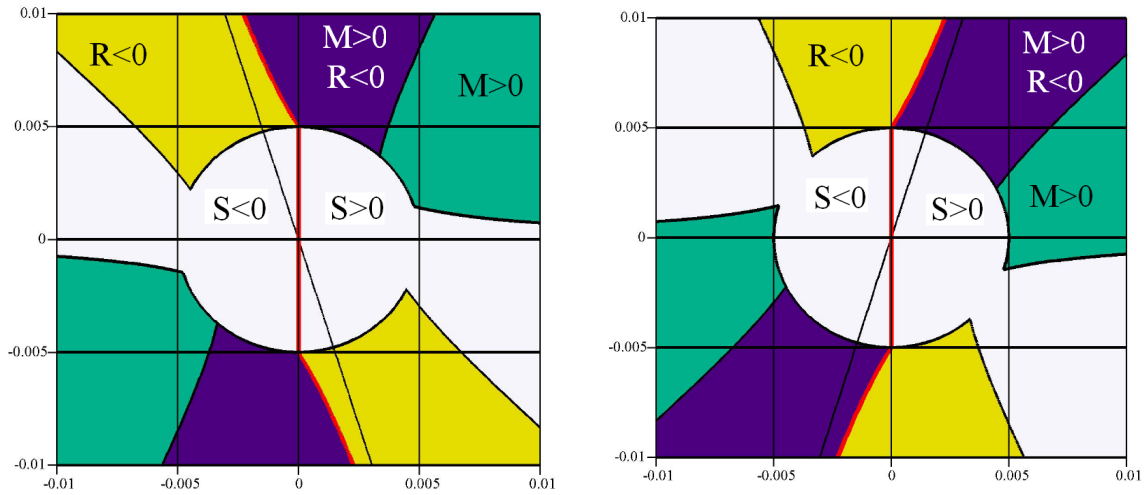


Figure A.18: Layup: 50%0°, 25% $\pm 45^\circ$, 25%90°

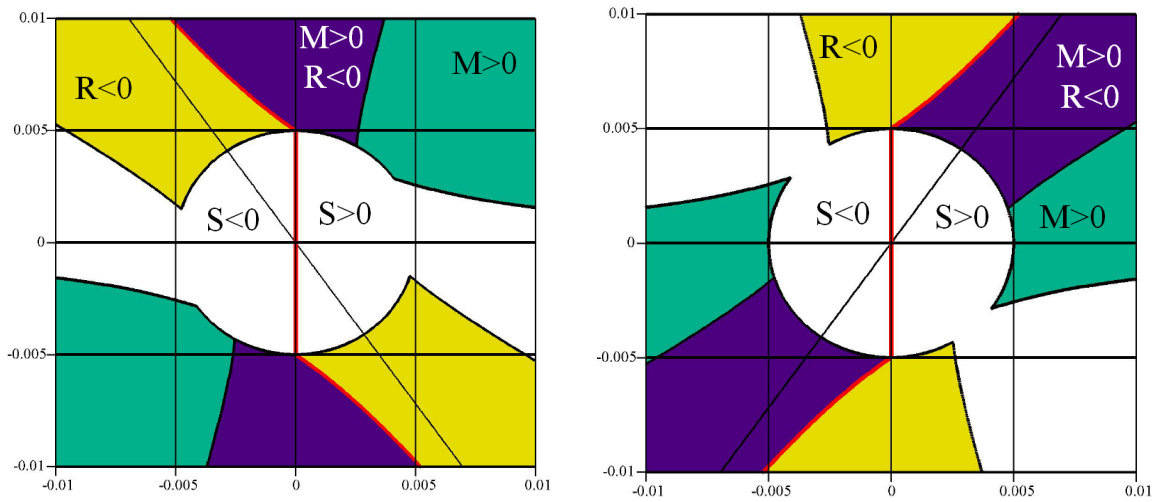


Figure A.19: Layup: 50%0°, 50% $\pm 45^\circ$, 0%90°

Appendix B

Discussion on Kweon's Tensile Characteristic Length

In this chapter a discussion is provided on the definition of the tensile characteristic length for the PSC by Kweon [3]. This definition is: "The distance from the side edge of the fastener hole to a point where the tensile stress by the failure load of the notched laminate is the same as the tensile strength of the notched laminate" and it implies that when the mean stress in the cross-section equals the unnotched strength, the plate is considered failed.

Following the derivation by Kweon [3], to determine the tensile characteristic length according to his definition, one applies an arbitrary far-field load σ_∞ as shown in Figure B.1. Next, the mean stress in the cross section is calculated with:

$$\sigma_m = \sigma_\infty \left(1 - \frac{2a}{w}\right) \quad (\text{B.1})$$

Subsequently, from the analysis of the stress field, the distance from the edge to the point where the stress equals σ_m is determined and taken as the characteristic distance. Now,

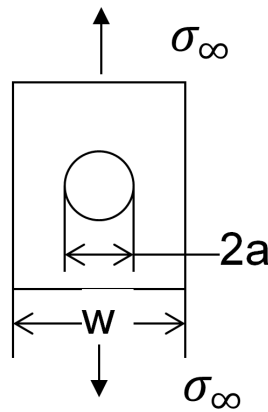


Figure B.1: Specimen with center hole and uniaxial tensile load

when the stress at this characteristic distance equals the unnotched strength, the specimen is considered failed. However, since the stress at this point equals the mean stress in the specimen due to the far-field load, this is the same as evaluating the mean stress due to the cross-section against the unnotched strength. Any composite strength engineer, when presented with this conclusion, will judge that this approach is incorrect. Hence Kweon's definition of the tensile characteristic length is incorrect.

Appendix C

Flow Charts of Individual Code Segments

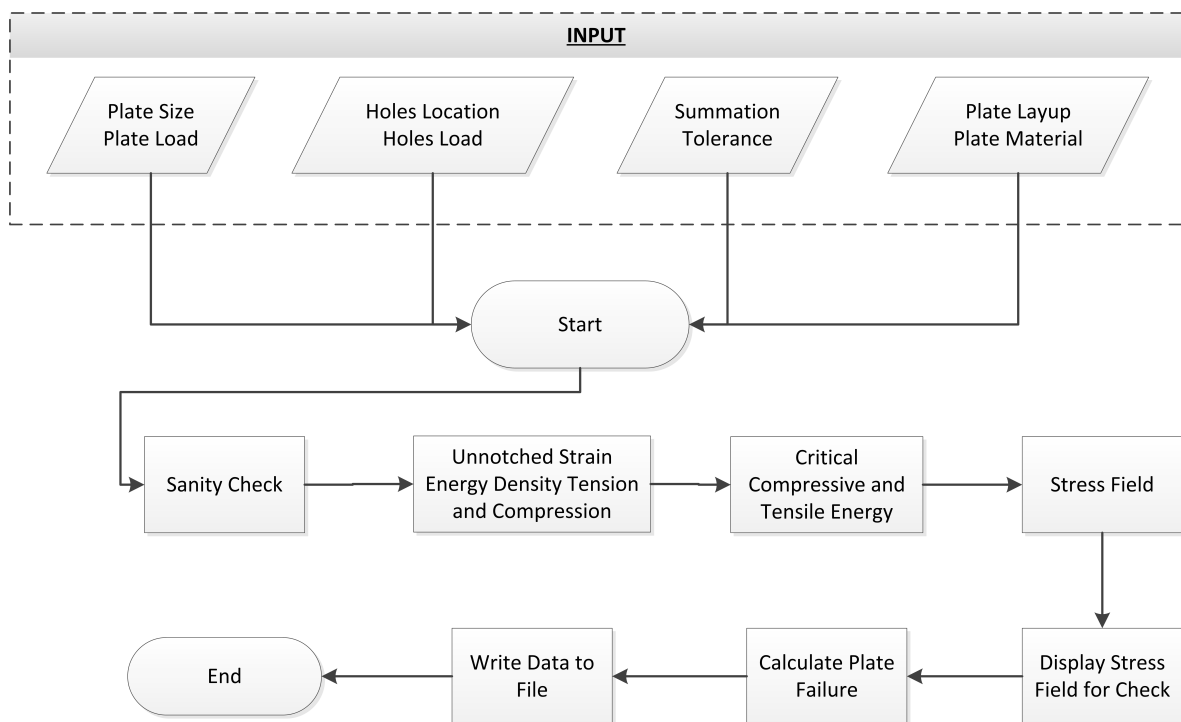


Figure C.1: Main program assembly algorithm

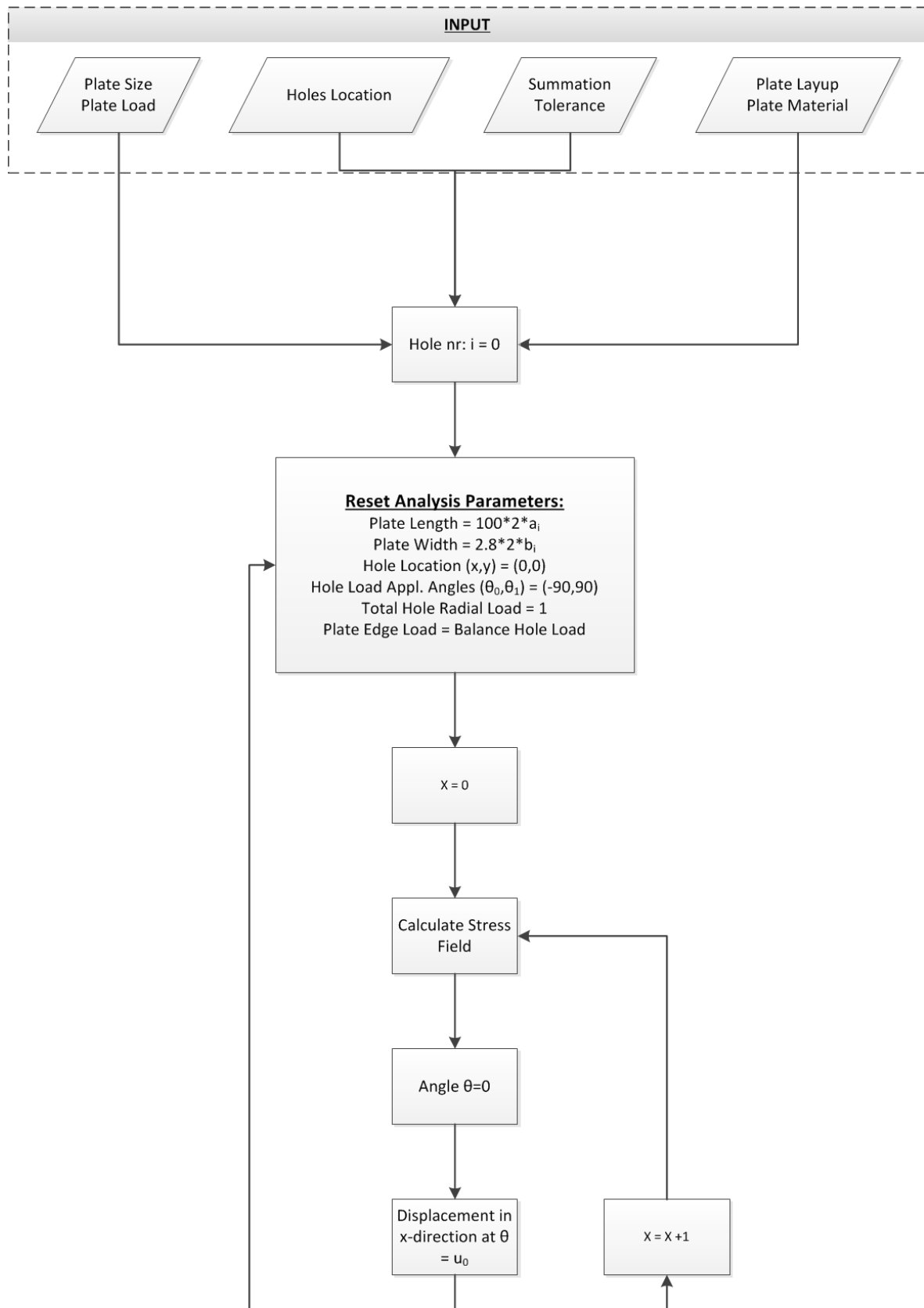
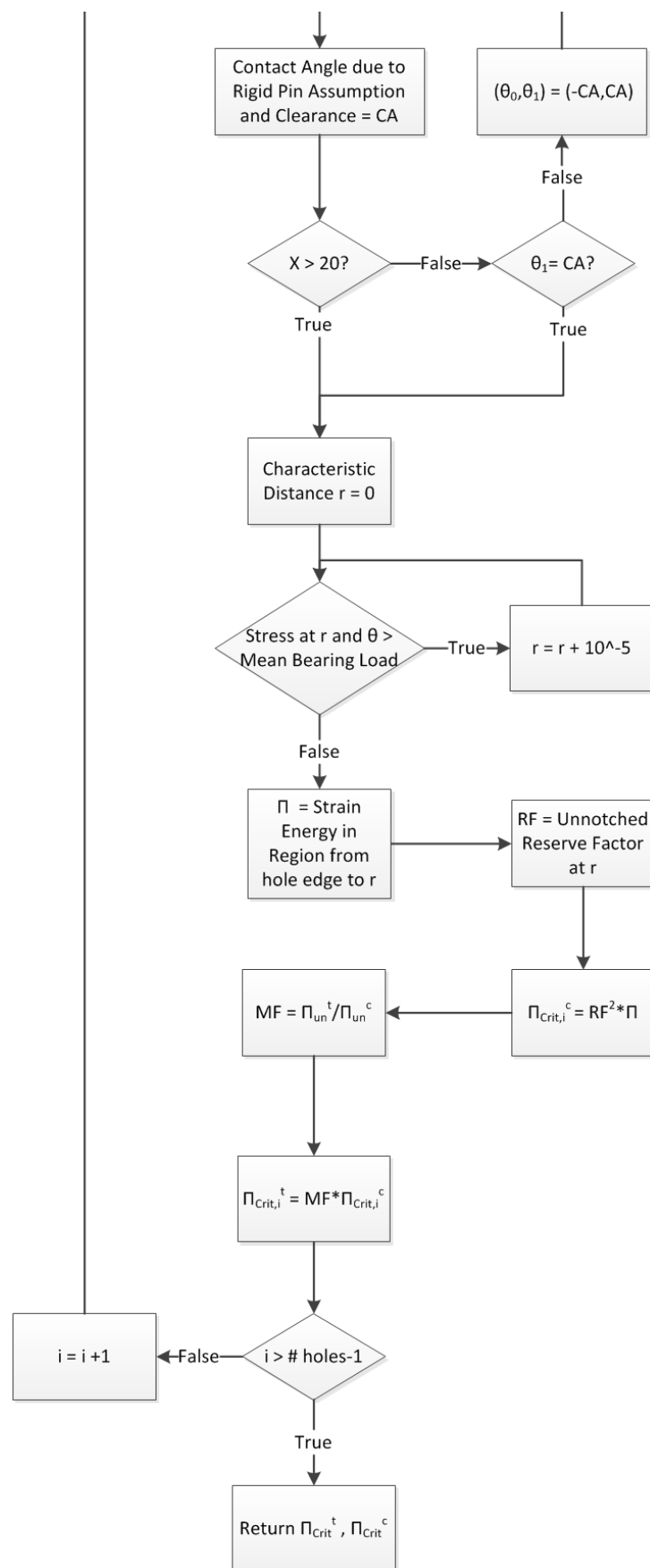
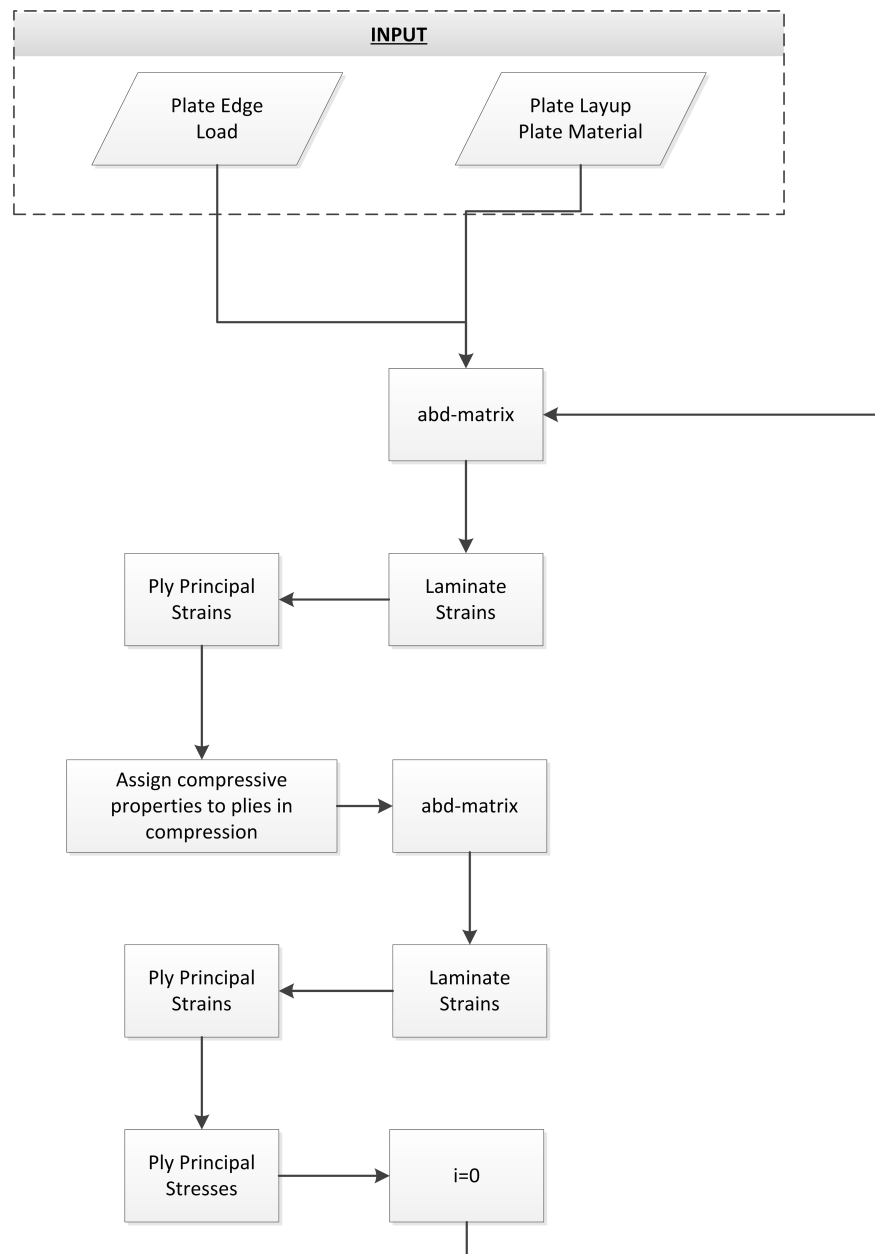


Figure C.2: Critical Energies algorithm, part1



**Figure C.4:** Unnotched failure algorithm, part 1

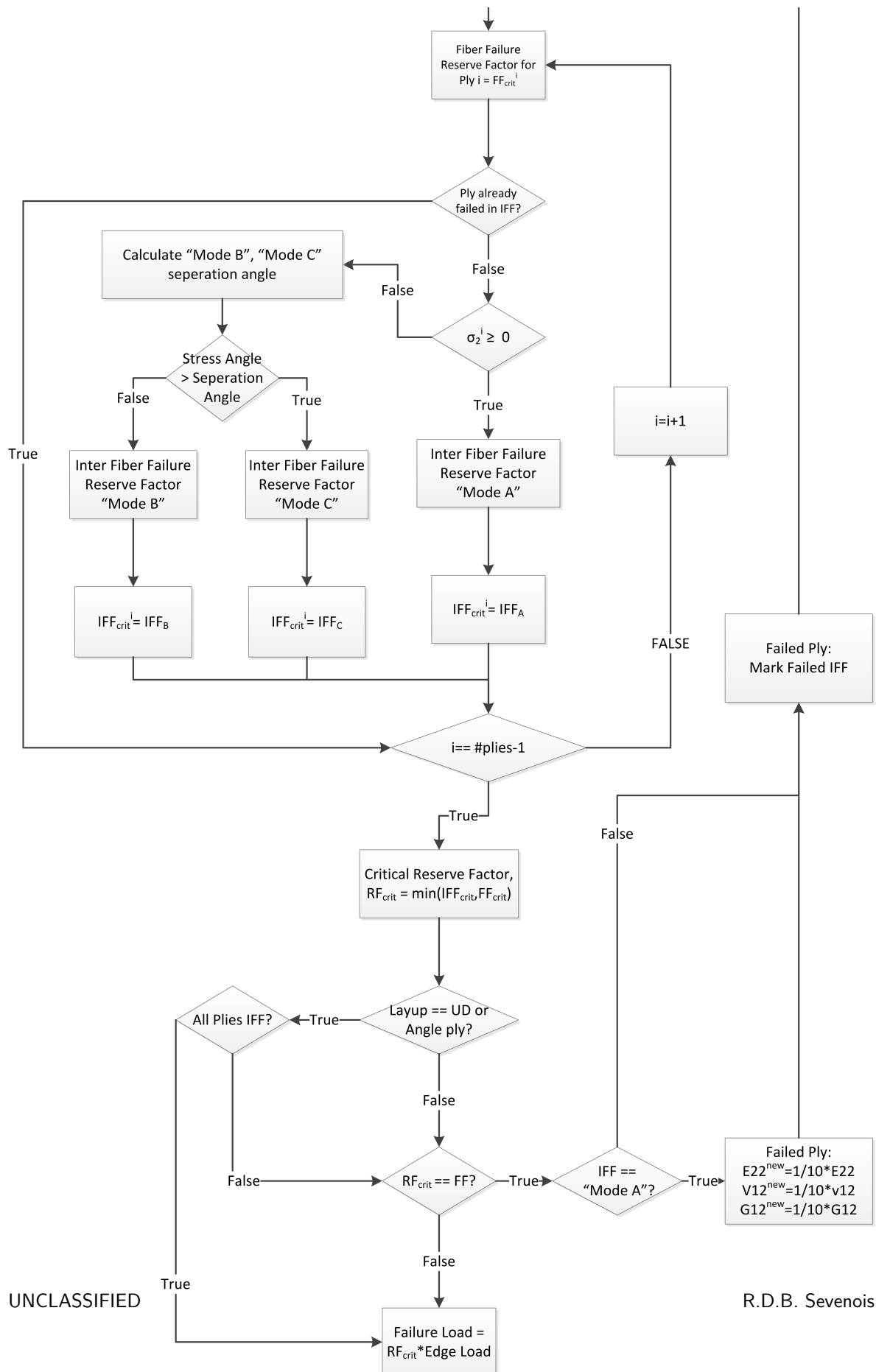


Figure C.5: Unnotched failure algorithm, part 2

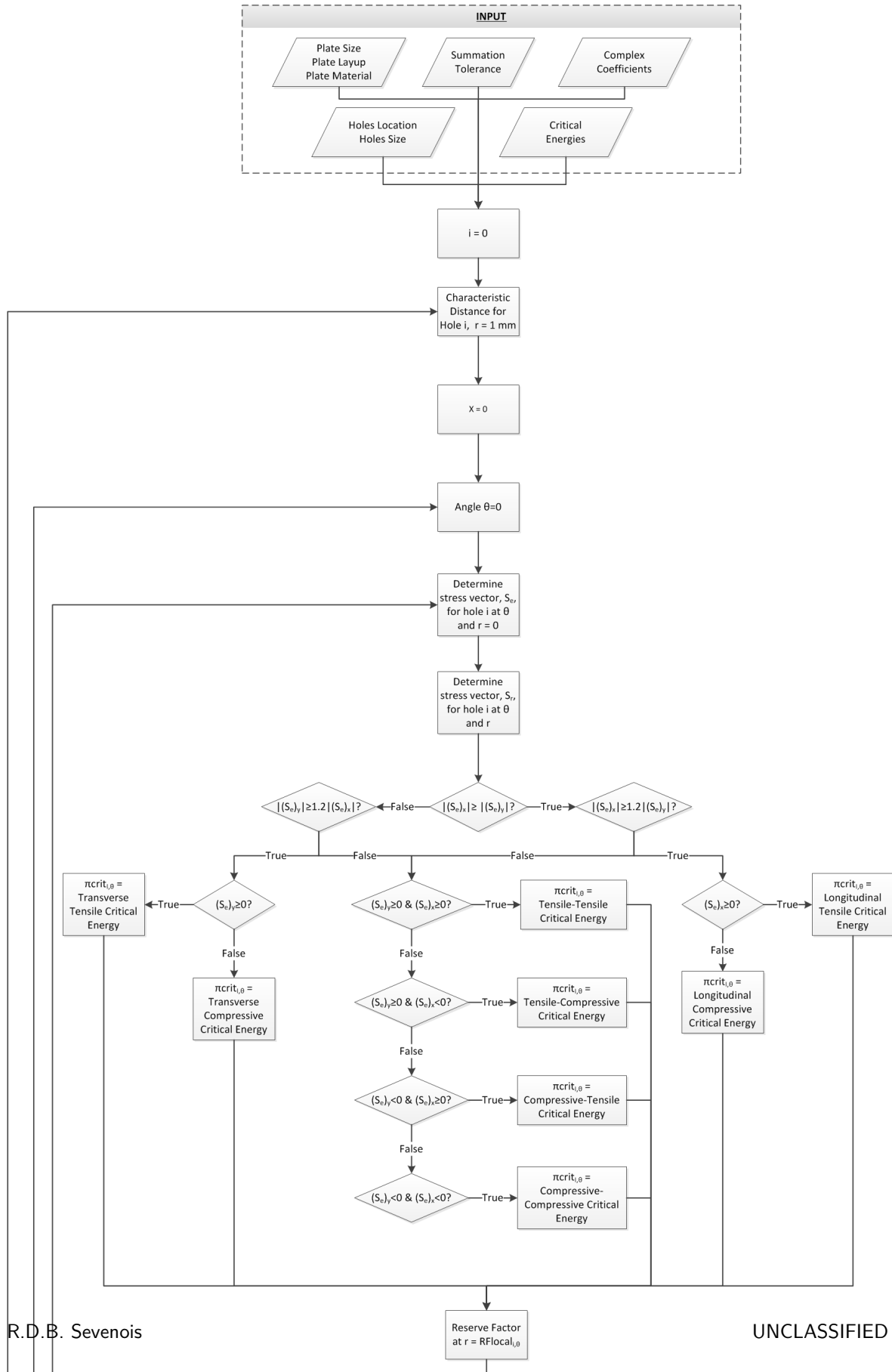


Figure C.6: Notched failure algorithm, part 1

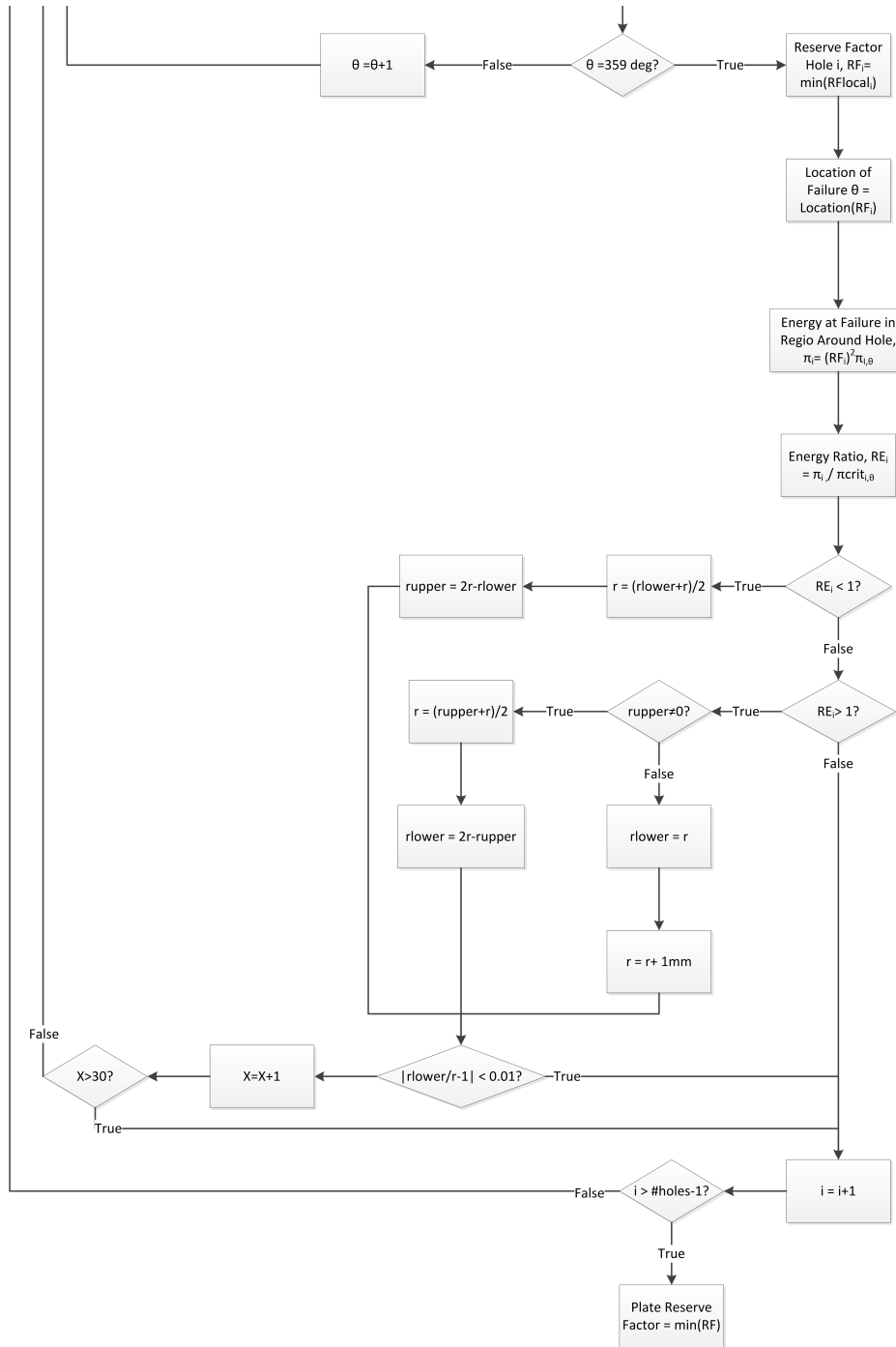


Figure C.7: Notched failure algorithm, part 2

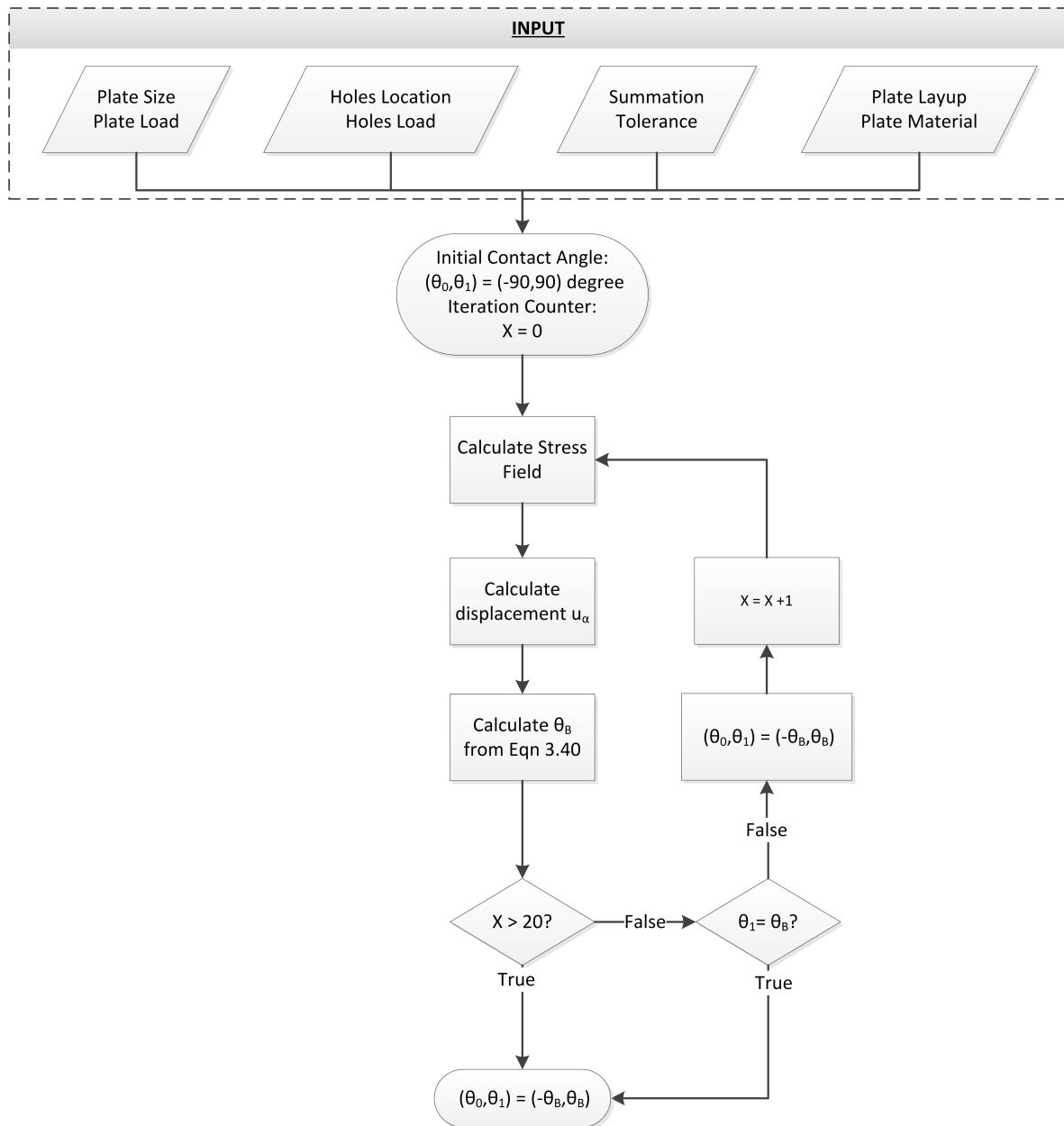


Figure C.8: Contact angle determination algorithm

Appendix D

Results from Verification

In this chapter the results from the verification process of the stress field algorithm and failure prediction algorithm is presented. For every verification step the input to the (sub)part of the algorithm is provided and the output is given. Also the expected output by hand calculation is provided for comparison.

abd-matrix

Table D.1: Material properties used for verification. Stiffnesses (GPa), strengths (MPa)

Nr.	E_{11}	E_{22}	G_{12}	$\nu_{12}(-)$	X^t	X^c	Y^t	Y^c	S	$t_{ply}(\text{mm})$
0	151.0	10.6	6.6	0.31	1401	1132	54	211	72	0.13
1	148.0	8.6	5.9	0.27	2760	1620	75	185	85	0.13
2	142.0	10.3	7.2	0.27	2280	1440	57	228	71	0.13

Table D.2: Verification input abd-matrix

Input	1	2
Layup	[90/0/0/90/0/0/90/0/0/90/0/0/90/0/0/90]	[90/45/-45/90/0/0/90/-45/45/90]
Material	All Material 2	[0/2/2/2/2/2/2/2/2/0]

Result tool input 1:

$$\text{abd} = \begin{bmatrix} 5.0895 * 10^{-9} & -2.3714 * 10^{-10} & 0 & 0 & 0 & 0 \\ -2.3714 * 10^{-10} & 7.8971 * 10^{-9} & 0 & 0 & 0 & 0 \\ 0 & 0 & 6.5722 * 10^{-8} & 0 & 0 & 0 \\ 0 & 0 & 0 & 1.5628 * 10^{-2} & -6.0988 * 10^{-4} & 0 \\ 0 & 0 & 0 & -6.0988 * 10^{-4} & 1.7772 * 10^{-2} & 0 \\ 0 & 0 & 0 & 0 & 0 & 1.7659 * 10^{-1} \end{bmatrix} \text{N, m}$$

(D.1)

Result KolibriV2©input 1:

$$abd = \begin{bmatrix} 5.0888 * 10^{-9} & -2.3710 * 10^{-10} & 0 & 0 & 0 & 0 \\ -2.3710 * 10^{-10} & 7.8959 * 10^{-9} & 0 & 0 & 0 & 0 \\ 0 & 0 & 6.5712 * 10^{-8} & 0 & 0 & 0 \\ 0 & 0 & 0 & 1.5621 * 10^{-2} & -6.0960 * 10^{-4} & 0 \\ 0 & 0 & 0 & -6.0960 * 10^{-4} & 1.7764 * 10^{-2} & 0 \\ 0 & 0 & 0 & 0 & 0 & 1.7651 * 10^{-1} \end{bmatrix} \text{N, m} \quad (\text{D.2})$$

Result tool with input 2:

$$abd = \begin{bmatrix} 1.5538 * 10^{-8} & -2.8921 * 10^{-9} & 0 & 0 & 0 & 0 \\ -2.8921 * 10^{-9} & 1.0086 * 10^{-8} & 0 & 0 & 0 & 0 \\ 0 & 0 & 3.9993 * 10^{-8} & 0 & 0 & 0 \\ 0 & 0 & 0 & 2.1333 * 10^{-1} & -3.2164 * 10^{-2} & 4.2873 * 10^{-2} \\ 0 & 0 & 0 & -3.2164 * 10^{-2} & 5.6564 * 10^{-2} & 5.7742 * 10^{-3} \\ 0 & 0 & 0 & 4.2873 * 10^{-2} & 5.7742 * 10^{-3} & 2.7008 * 10^{-1} \end{bmatrix} \text{N, m} \quad (\text{D.3})$$

Result KolibriV2©with input 2:

$$abd = \begin{bmatrix} 1.5536 * 10^{-8} & -2.8919 * 10^{-9} & 0 & 0 & 0 & 0 \\ -2.8919 * 10^{-9} & 1.0085 * 10^{-8} & 0 & 0 & 0 & 0 \\ 0 & 0 & 3.9988 * 10^{-8} & 0 & 0 & 0 \\ 0 & 0 & 0 & 2.1325 * 10^{-1} & -3.2155 * 10^{-2} & 4.2856 * 10^{-2} \\ 0 & 0 & 0 & -3.2155 * 10^{-2} & 5.6547 * 10^{-2} & 5.7725 * 10^{-3} \\ 0 & 0 & 0 & 4.2856 * 10^{-2} & 5.7725 * 10^{-3} & 2.6997 * 10^{-1} \end{bmatrix} \text{N, m} \quad (\text{D.4})$$

material eigenvalues

Input 1:

$$abd = \begin{bmatrix} 1.5538 * 10^{-8} & -2.8921 * 10^{-9} & 0 & 0 & 0 & 0 \\ -2.8921 * 10^{-9} & 1.0086 * 10^{-8} & 0 & 0 & 0 & 0 \\ 0 & 0 & 3.9993 * 10^{-8} & 0 & 0 & 0 \\ 0 & 0 & 0 & 2.1333 * 10^{-1} & -3.2164 * 10^{-2} & 4.2873 * 10^{-2} \\ 0 & 0 & 0 & -3.2164 * 10^{-2} & 5.6564 * 10^{-2} & 5.7742 * 10^{-3} \\ 0 & 0 & 0 & 4.2873 * 10^{-2} & 5.7742 * 10^{-3} & 2.7008 * 10^{-1} \end{bmatrix} \text{N, m} \quad (\text{D.5})$$

Input 2:

$$abd = \begin{bmatrix} 1.5538 * 10^{-8} & -2.8921 * 10^{-9} & 0 & 0 & 0 & 0 \\ -2.8921 * 10^{-9} & 1.5538 * 10^{-8} & 0 & 0 & 0 & 0 \\ 0 & 0 & 3.9993 * 10^{-8} & 0 & 0 & 0 \\ 0 & 0 & 0 & 2.1333 * 10^{-1} & -3.2164 * 10^{-2} & 4.2873 * 10^{-2} \\ 0 & 0 & 0 & -3.2164 * 10^{-2} & 5.6564 * 10^{-2} & 5.7742 * 10^{-3} \\ 0 & 0 & 0 & 4.2873 * 10^{-2} & 5.7742 * 10^{-3} & 2.7008 * 10^{-1} \end{bmatrix} \text{N, m} \quad (\text{D.6})$$

Result from Input 1:

Table D.3: Hand calculation and tool result material eigenvalues from input 1

	Hand	Tool	Difference (%)
μ_1	$0 + 1.361i$	$0 + 1.361i$	0
μ_2	$0 + 0.5921i$	$0 + 0.592i$	0

Result from Input 2:

Table D.4: Hand calculation and tool result material eigenvalues from input 2

	Hand	Tool	Difference (%)
μ_1	$0 + 1.04i$	$0 + 1.04i$	0
μ_2	$0 + 0.98i$	$0 + 0.98i$	0

Complex parameters p_j and q_j

Input:

$$a = \begin{bmatrix} 1.1274 * 10^{-8} & -6.9481 * 10^{-9} & 0 \\ -6.9481 * 10^{-9} & 3.7359 * 10^{-8} & 0 \\ 0 & 0 & 4.294 * 10^{-8} \end{bmatrix} \text{N, m} \quad (\text{D.7a})$$

$$\mu = \begin{pmatrix} 0.5158 + 1.2467i \\ -0.5158 + 1.2467i \end{pmatrix} \quad (\text{D.7b})$$

Result:

Table D.5: Results from hand calculation and tool for p_j and q_j

	Hand	Tool	Difference (%)
p_1	$-2.147 * 10^{-8} + 1.45 * 10^{-8}i$	$-2.147 * 10^{-8} + 1.45 * 10^{-8}i$	0
p_2	$-2.147 * 10^{-8} - 1.45 * 10^{-8}i$	$-2.147 * 10^{-8} - 1.45 * 10^{-8}i$	0
q_1	$7.002 * 10^{-9} - 3.43 * 10^{-8}i$	$7.002 * 10^{-9} - 3.43 * 10^{-8}i$	0
q_2	$-7.002 * 10^{-9} - 3.43 * 10^{-8}i$	$-7.002 * 10^{-9} - 3.43 * 10^{-8}i$	0

Complex parameters R_j, t_j

Input:

Table D.6: Input for verification of R_j and t_j

Hole	x(m)	y(m)	a(m)	b(m)
0	-0.03	0.00	$5 * 10^{-3}$	$5 * 10^{-3}$
1	0.03	0.01	$2 * 10^{-3}$	$3 * 10^{-3}$

$$\mu = \begin{pmatrix} 0.5158 + 1.2467i \\ -0.5158 + 1.2467i \end{pmatrix} \quad (\text{D.8})$$

Results:

Table D.7: Results from hand calculation and tool for R_{mj} and t_{mj}

	Hand	Tool	Difference (%)
R_{01}	$5.62 * 10^{-3} - 1.29 * 10^{-3}i$	$5.62 * 10^{-3} - 1.29 * 10^{-3}i$	0
R_{02}	$5.62 * 10^{-3} + 1.29 * 10^{-3}i$	$5.62 * 10^{-3} + 1.29 * 10^{-3}i$	0
t_{01}	$-0.154 + 0.194i$	$-0.154 + 0.194i$	0
t_{02}	$-0.154 - 0.194i$	$-0.154 - 0.194i$	0
R_{11}	$2.87 * 10^{-3} - 7.738 * 10^{-4}i$	$2.87 * 10^{-3} - 7.738 * 10^{-4}i$	0
R_{12}	$2.87 * 10^{-3} + 7.738 * 10^{-4}i$	$2.87 * 10^{-3} + 7.738 * 10^{-4}i$	0
t_{11}	$-0.35 + 0.175i$	$-0.35 + 0.175i$	0
t_{12}	$-0.35 - 0.175i$	$-0.35 - 0.175i$	0

Sign Selection Algorithm

See Appendix [A](#)

Verification of z_j^k, ξ_j^k and their derivatives

Verification of z_j and ξ_j , input:

Table D.8: Input values for verification of z_j and ξ_j

x(m)	y(m)	μ_j	R_{mj}	t_{mj}	z_{mj}	Sign
0.5	0.02	$1.23 - 2.54i$	$2.56 - 0.25i$	$2.35 + 5i$	$0.2 + 0.3i$	+1

Output:

Table D.9: Results from tool and hand calculation for z_j and ξ_j

	Hand	Tool
z_j	$0.5246 - 0.0508i$	$0.5246 - 0.0508i$
ξ_j	$2.0499 - 1.3213i$	$2.0549 - 1.3231i$

Verification of coefficient matrix ξ_j , input:

Table D.10: Input for verification of ξ matrix

Hole	x(m)	y(m)	a(m)	b(m)
0	-0.03	0.00	$5 * 10^{-3}$	$5 * 10^{-3}$
1	0.03	0.01	$2 * 10^{-3}$	$3 * 10^{-3}$
n	2	x(m)	-0.02	
z	$-0.02 + 1.247-4i$	y(m)	0.0001	
ξ_1	$1.7627 + 0.2901i$	ξ_2	$-16.8311 - 8.8180i$	

Result:

Table D.11: Results from verification of ξ matrix

	Hand	Tool
1	1	1
z	$-0.0199 + 1.2467 * 10^{-4}i$	$-0.0199 + 1.2467 * 10^{-4}i$
z^2	$3.9792 * 10^{-4} - 4.9739 * 10^{-6}i$	$3.9792 * 10^{-4} - 4.9739 * 10^{-6}i$
$\ln(\xi_1)$	$0.5802 + 0.1631i$	$0.5802 + 0.1631i$
ξ_1^{-1}	$0.5524 - 0.0909i$	$0.5523 - 0.0909i$
ξ_1^{-2}	$0.2968 - 0.1004i$	$0.2968 - 0.1004i$
$\ln(\xi_2)$	$2.9445 - 2.6590i$	$2.9445 - 2.659i$
ξ_2^{-1}	$-0.0466 + 0.0244i$	$-0.0466 + 0.0244i$
ξ_2^{-2}	$0.0016 - 0.0023i$	$1.5767 * 10^{-3} - 2.2772 * 10^{-3}i$
i	i	i
1	$-1.2467 * 10^{-4} - 0.0199i$	$-1.2467 * 10^{-4} - 0.0199i$
iz	$4.9739 * 10^{-6} + 3.9792 * 10^{-4}i$	$4.9739 * 10^{-6} + 3.9792 * 10^{-4}i$
iz^2	$4.9739 * 10^{-6} + 3.9792 * 10^{-4}i$	$4.9739 * 10^{-6} + 3.9792 * 10^{-4}i$
$i \ln(\xi_1)$	$-0.1631 + 0.5802i$	$-0.1631 + 0.5802i$
$i \xi_1^{-1}$	$0.0909 + 0.5524i$	$0.0909 + 0.5524i$
$i \xi_1^{-2}$	$0.1004 + 0.2968i$	$0.1004 + 0.2968i$
$i \ln(\xi_2)$	$2.6590 + 2.9445i$	$2.659 + 2.9445i$
$i \xi_2^{-1}$	$-0.0244 + 0.0466i$	$-0.0244 - 0.0466i$
$i \xi_2^{-2}$	$0.0023 + 0.0016i$	$2.2772 * 10^{-3} + 1.5767 * 10^{-3}i$

A similar calculation as performed for the coefficientmatrix of the derivative of z_j and ξ_j . The same input was used (Table D.10). The result is:

Table D.12: Results from verification of derivate ξ matrix

	Hand	Tool
0	0	0
$\frac{dz}{dz}$	1	1
$\frac{dz^2}{dz}$	$-0.0399 + 2.493 * 10^{-4}i$	$-0.0399 + 2.4934 * 10^{-4}i$
$\frac{d \ln(\xi_1)}{dz}$	$93.5623 + 12.5865i$	$93.5604 + 12.5838i$
$\frac{d\xi_1^{-1}}{dz}$	$-52.8234 + 1.5531i$	$-52.8205 + 1.5548i$
$\frac{d\xi_1^{-2}}{dz}$	$-58.0717 + 11.3194i$	$-58.0664 + 11.321i$
$\frac{d \ln(\xi_2)}{dz}$	$-17.2829 + 3.8318i$	$17.2828 + 3.8318i$
$\frac{d\xi_2^{-1}}{dz}$	$-0.7121 + 0.6007i$	$-0.7121 + 0.6007i$
$\frac{d\xi_2^{-2}}{dz}$	$0.0370 - 0.0908i$	$0.0370 - 0.0908i$
0	0	0
$\frac{diz}{dz}$	i	i
$\frac{diz^2}{dz}$	$-2.4934 * 10^{-4} - 0.0399i$	$-2.4934 * 10^{-4} - 0.0399i$
$\frac{di \ln(\xi_1)}{dz}$	$-12.5838 + 93.5604i$	$-12.5838 + 93.5604i$
$\frac{di\xi_1^{-1}}{dz}$	$-1.553 - 52.8234i$	$-1.5548 - 52.8205i$
$\frac{di\xi_1^{-2}}{dz}$	$-11.3194 + 58.0717i$	$-11.321 - 58.0664i$
$\frac{di \ln(\xi_2)}{dz}$	$-3.8318 - 17.2829i$	$-3.8318 - 17.2828i$
$\frac{di\xi_2^{-1}}{dz}$	$-0.6007 - 0.7121i$	$-0.6007 - 0.7121i$
$\frac{di\xi_2^{-2}}{dz}$	$0.0908 + 0.0370i$	$0.0908 + 0.037i$

Stress System Test

Input:

Material used: material 2
 Layups used:
 33/33/33
 100/0/0
 0/100/0
 0/0/100
 50/50/0
 0/50/50
 50/0/50
 50/25/25
 25/50/25
 25/25/50

Hole	x(m)	y(m)	a(m)	b(m)
0	0.00	0.00	$5 * 10^{-3}$	$2 * 10^{-3}$
Width	Length	n	TOL	
1.00	1.00	6	10^{-12}	

Uniform uniaxial tension at the plate edge

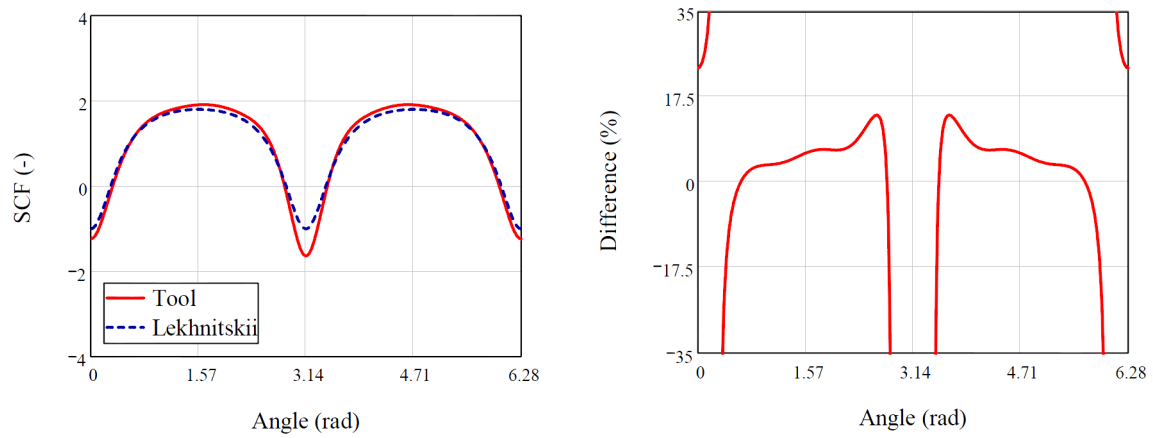


Figure D.1: Stress concentration factor at hole edge and difference between tool and Lekhnitskii. 33% $\pm 0^\circ$, 33% $\pm 45^\circ$, 33% $\pm 90^\circ$ uniaxial tension at 0° , $a = 5$ [mm], $b = 2$ [mm]

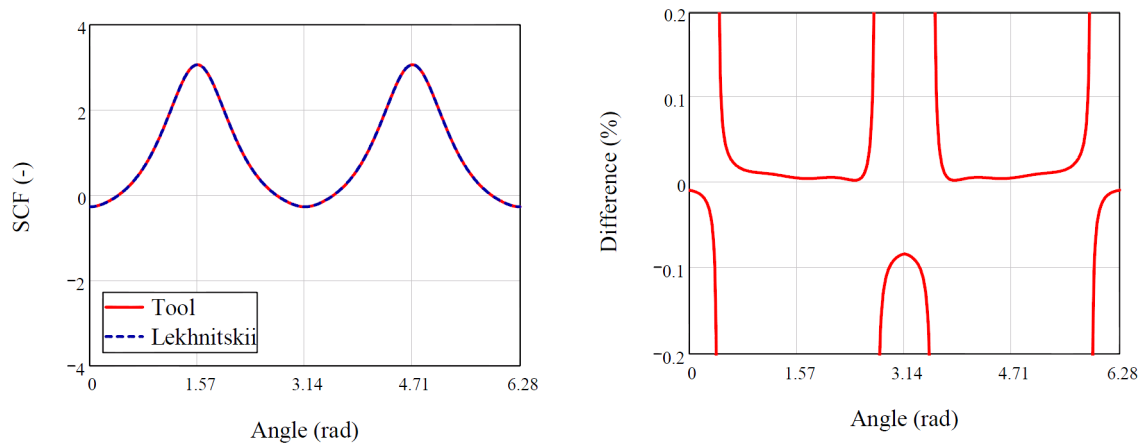


Figure D.2: Stress concentration factor at hole edge and difference between tool and Lekhnitskii. 100% UD, uniaxial tension at 0° , $a = 5$ [mm], $b = 2$ [mm]

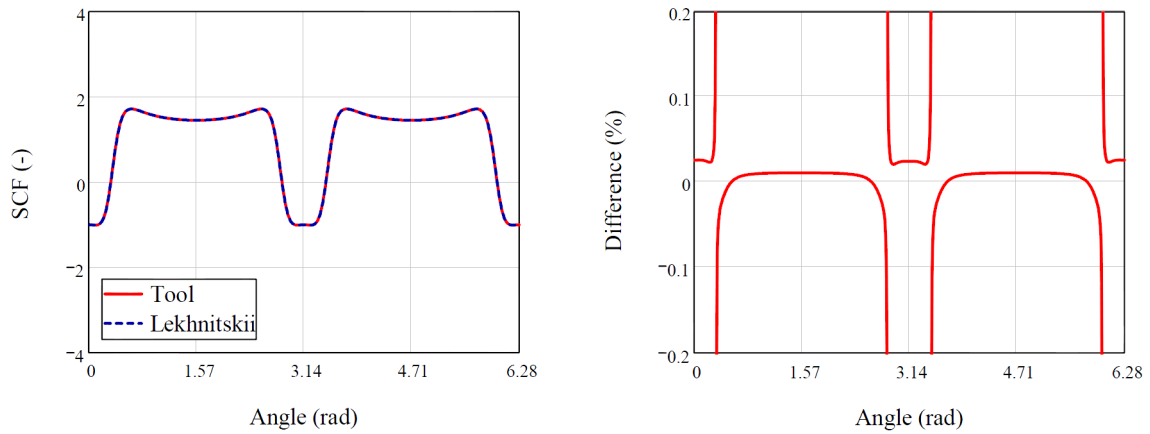


Figure D.3: Stress concentration factor at hole edge and difference between tool and Lekhnitskii. 100% $\pm 45^\circ$, uniaxial tension at 0° , $a = 5$ [mm], $b = 2$ [mm]

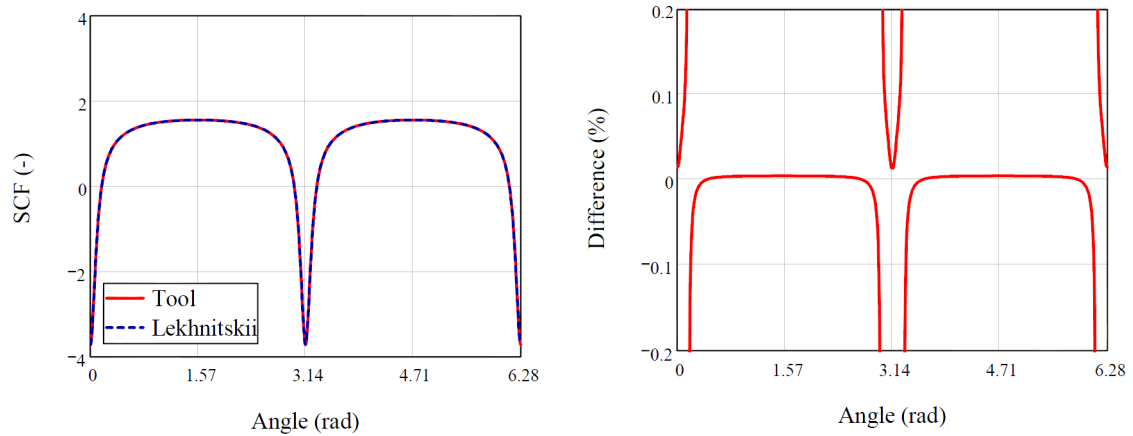


Figure D.4: Stress concentration factor at hole edge and difference between tool and Lekhnitskii. 100% 90° , uniaxial tension at 0° , $a = 5$ [mm], $b = 2$ [mm]

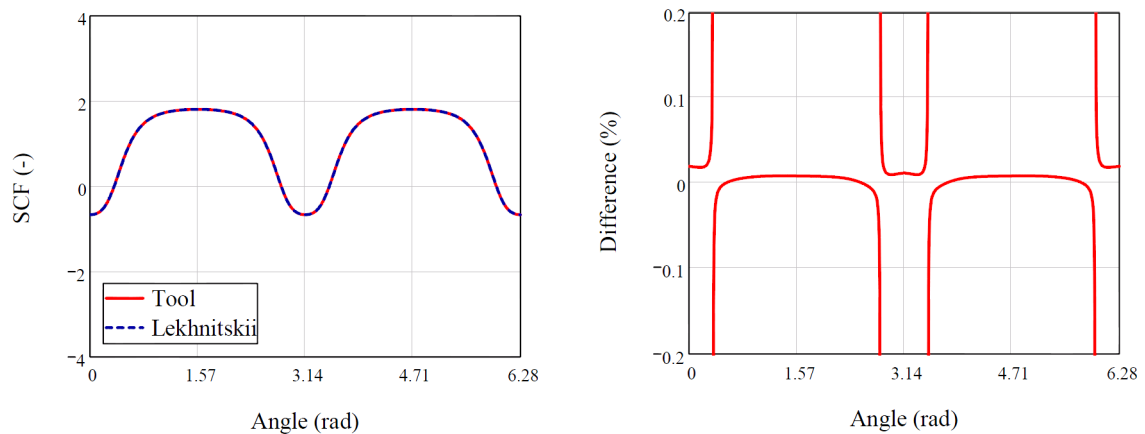


Figure D.5: Stress concentration factor at hole edge and difference between tool and Lekhnitskii. 50% 0° , 50% $\pm 45^\circ$ uniaxial tension at 0° , $a = 5$ [mm], $b = 2$ [mm]

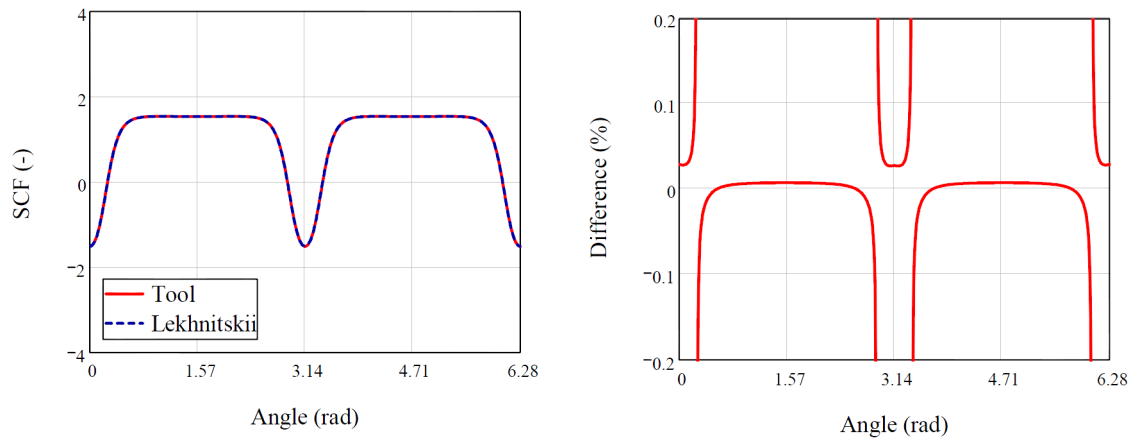


Figure D.6: Stress concentration factor at hole edge and difference between tool and Lekhnitskii.
50% 90°, 50% $\pm 45^\circ$ uniaxial tension at 0° , $a = 5$ [mm], $b = 2$ [mm]

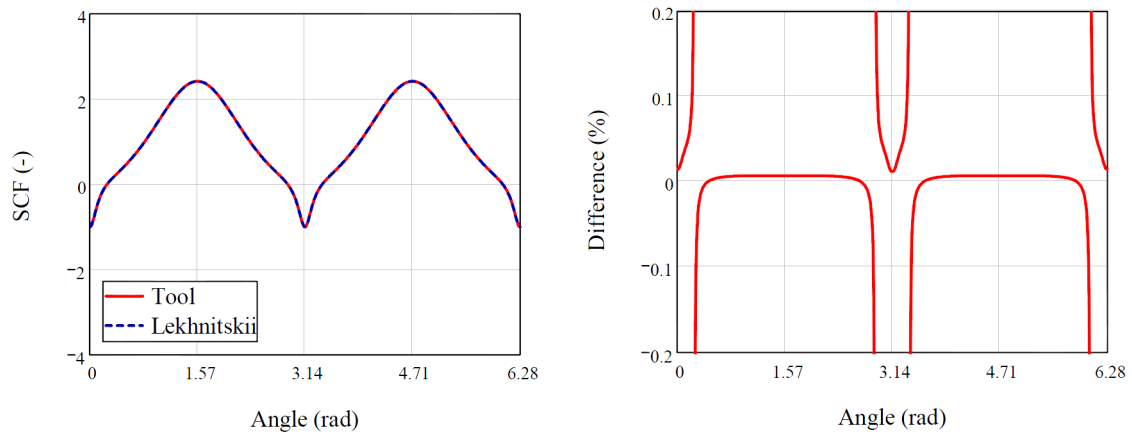


Figure D.7: Stress concentration factor at hole edge and difference between tool and Lekhnitskii.
50% 0° , 50% 90° uniaxial tension at 0° , $a = 5$ [mm], $b = 2$ [mm]

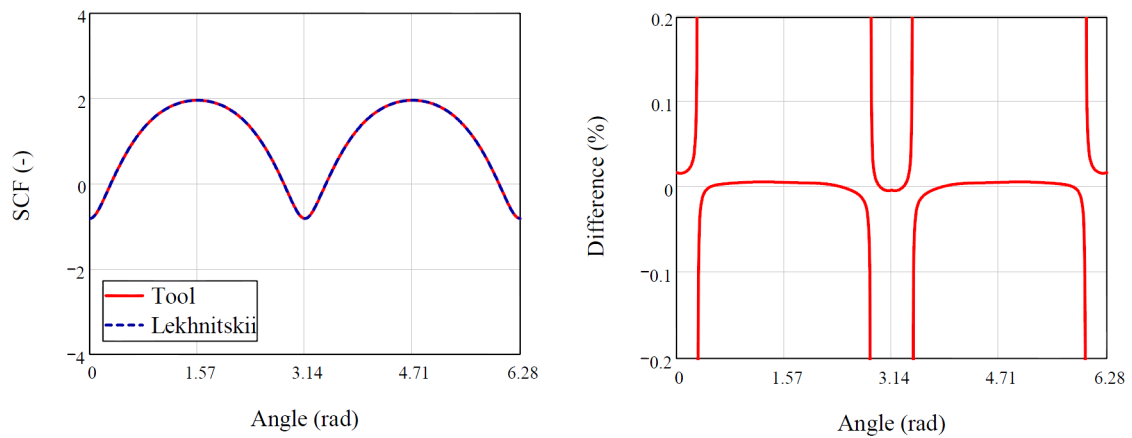


Figure D.8: Stress concentration factor at hole edge and difference between tool and Lekhnitskii.
50% $\pm 0^\circ$, 25% $\pm 45^\circ$, 25% $\pm 90^\circ$ uniaxial tension at 0° , $a = 5$ [mm], $b = 2$ [mm]

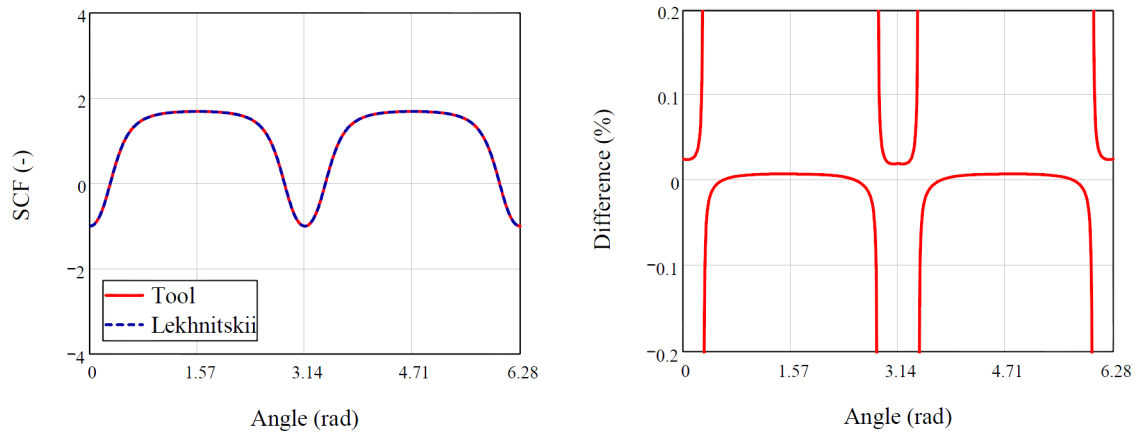


Figure D.9: Stress concentration factor at hole edge and difference between tool and Lekhnitskii. 25% $\pm 0^\circ$, 50% $\pm 45^\circ$, 25% $\pm 90^\circ$ uniaxial tension at 0° , $a = 5$ [mm], $b = 2$ [mm]

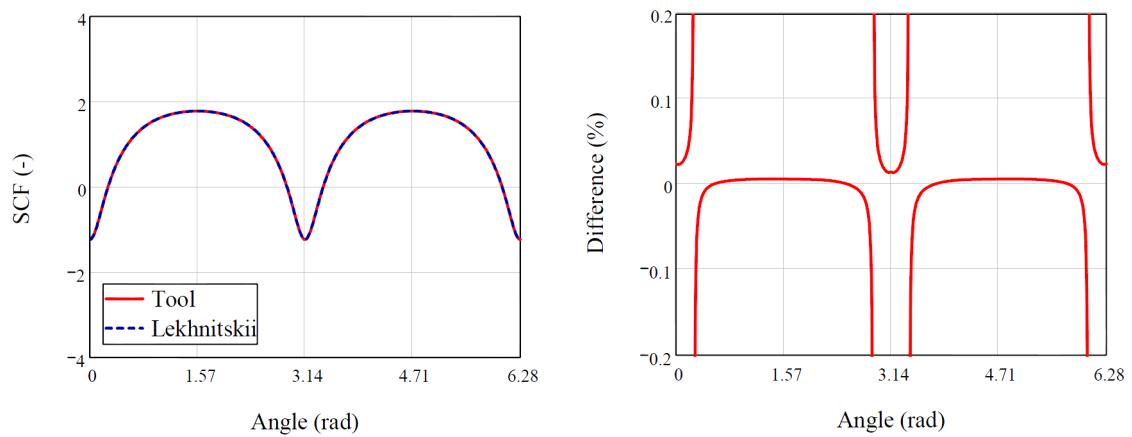


Figure D.10: Stress concentration factor at hole edge and difference between tool and Lekhnitskii. 25% $\pm 0^\circ$, 25% $\pm 45^\circ$, 50% $\pm 90^\circ$ uniaxial tension at 0° , $a = 5$ [mm], $b = 2$ [mm]

System test, uniform pressure at the hole edge

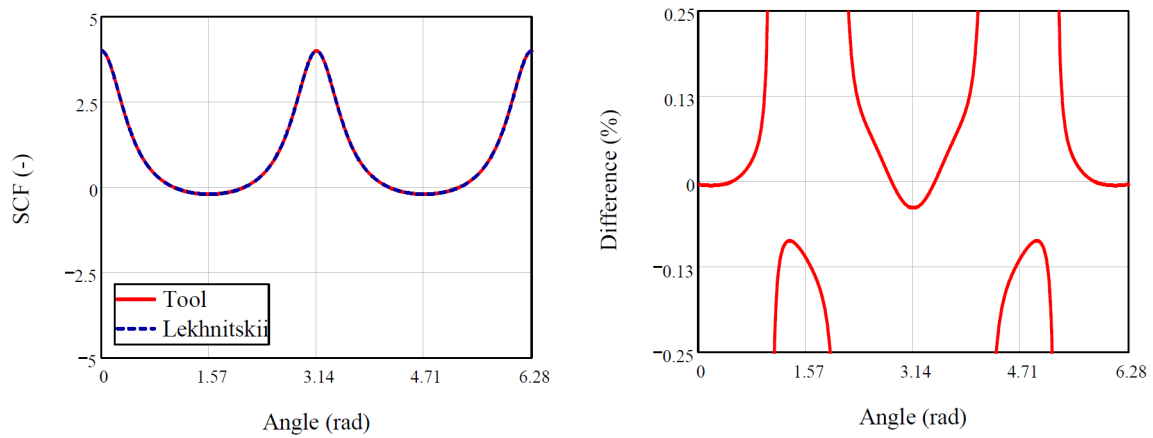


Figure D.11: Stress concentration factor at hole edge and difference between tool and Lekhnitskii. 33% $\pm 0^\circ$, 33% $\pm 45^\circ$, 33% $\pm 90^\circ$ uniform pressure at hole edge, $a = 5$ [mm], $b = 2$ [mm]

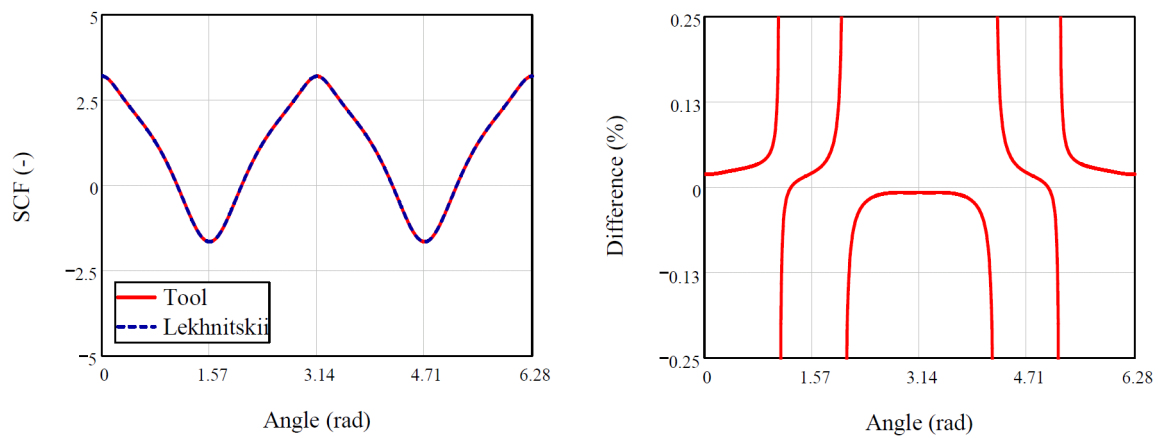


Figure D.12: Stress concentration factor at hole edge and difference between tool and Lekhnitskii. 100% UD uniform pressure at hole edge, $a = 5$ [mm], $b = 2$ [mm]

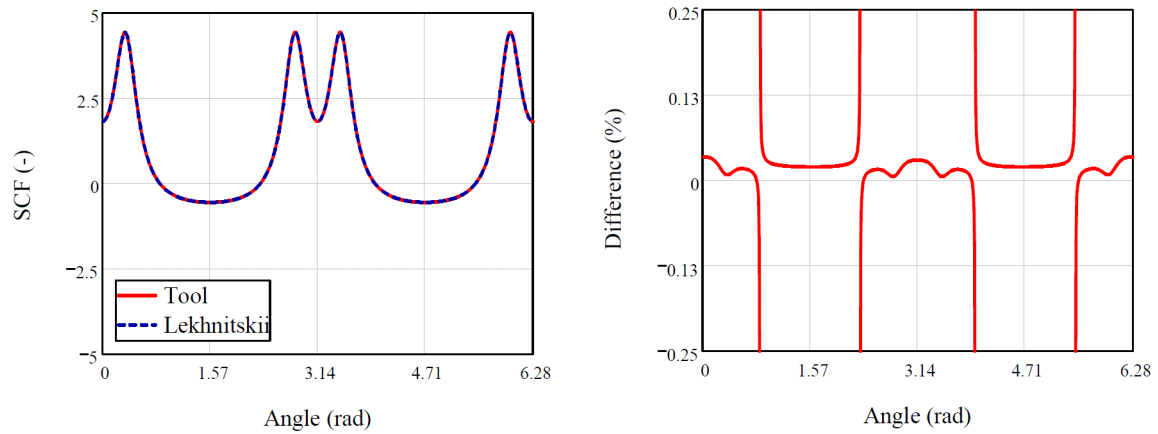


Figure D.13: Stress concentration factor at hole edge and difference between tool and Lekhnitskii. 100% $\pm 45^\circ$ uniform pressure at hole edge, $a = 5$ mm, $b = 2$ [mm]

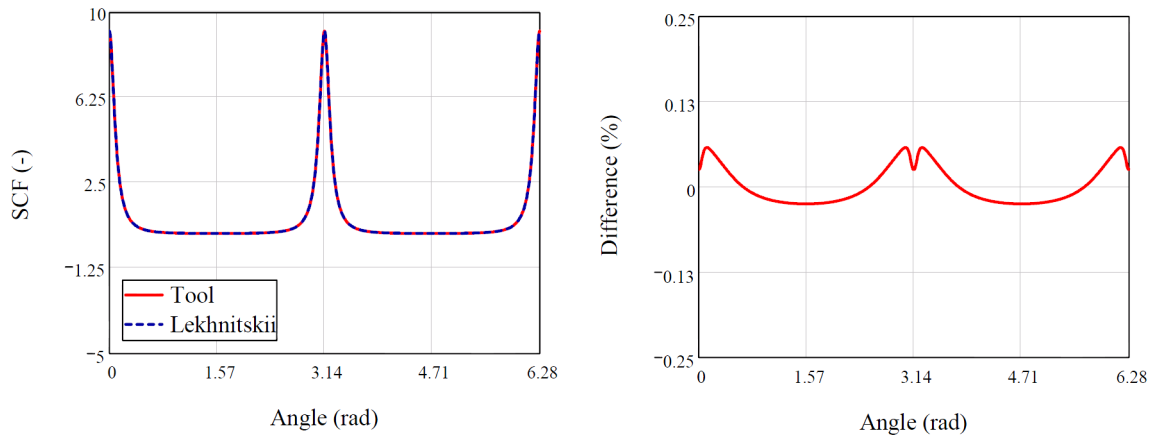


Figure D.14: Stress concentration factor at hole edge and difference between tool and Lekhnitskii. 100% $\pm 90^\circ$ uniform pressure at hole edge, $a = 5$ [mm], $b = 2$ [mm]

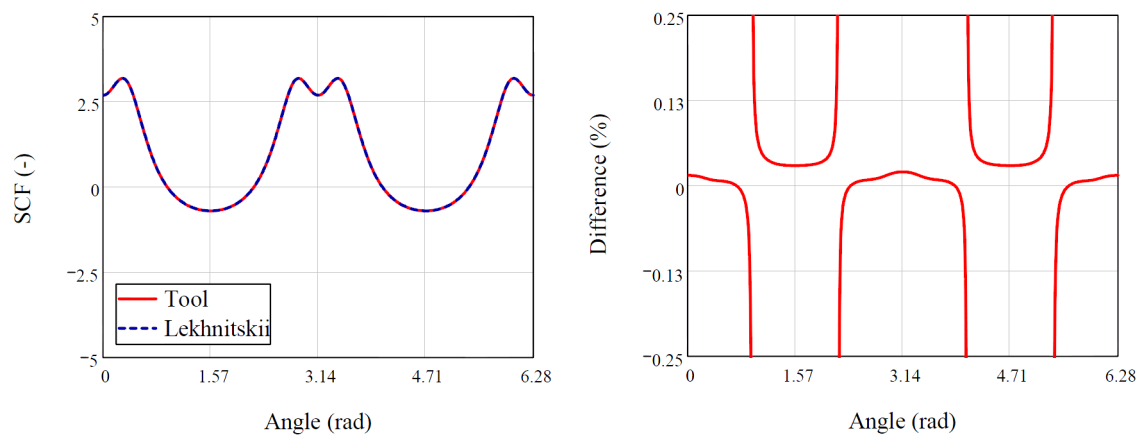


Figure D.15: Stress concentration factor at hole edge and difference between tool and Lekhnitskii. 50% 0° , 50% $\pm 45^\circ$ uniform pressure at hole edge, $a = 5$ [mm], $b = 2$ [mm]

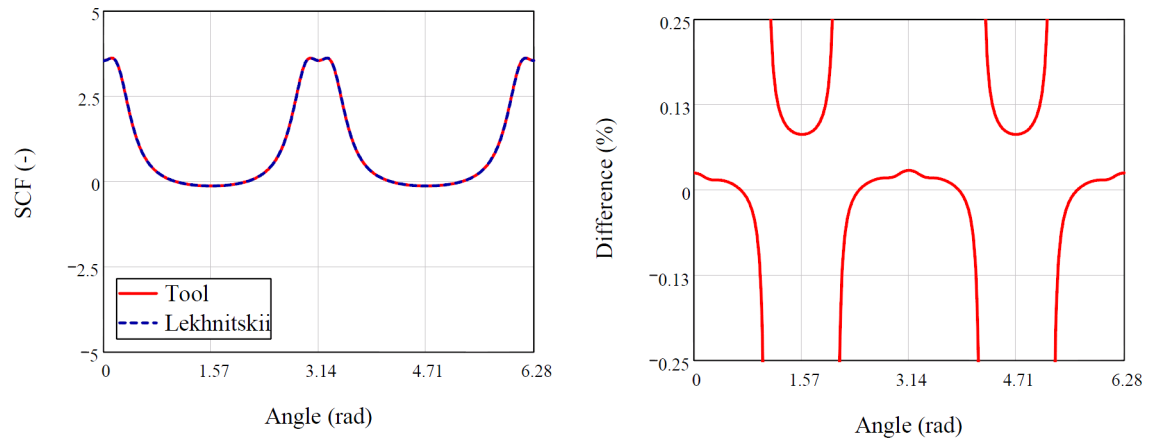


Figure D.16: Stress concentration factor at hole edge and difference between tool and Lekhnitskii. 50% 90°, 50% $\pm 45^\circ$ uniform pressure at hole edge, $a = 5$ [mm], $b = 2$ [mm]

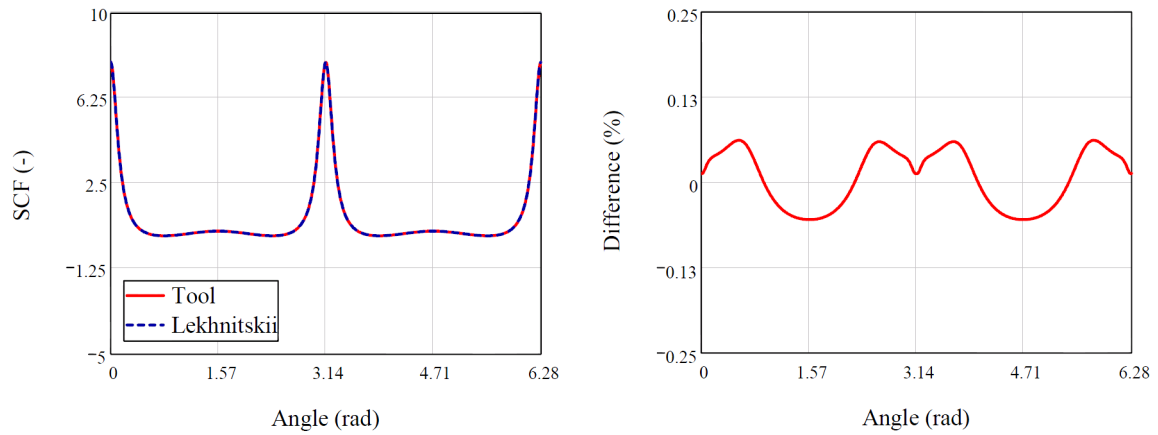


Figure D.17: Stress concentration factor at hole edge and difference between tool and Lekhnitskii. 50% 0°, 50% $\pm 90^\circ$ uniform pressure at hole edge, $a = 5$ [mm], $b = 2$ [mm]

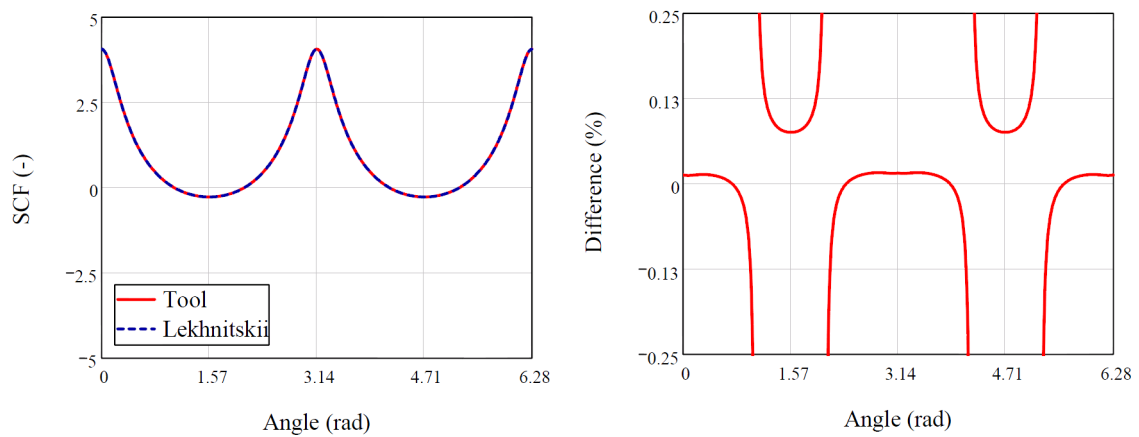


Figure D.18: Stress concentration factor at hole edge and difference between tool and Lekhnitskii. 50% 0°, 25% $\pm 45^\circ$, 25% $\pm 90^\circ$ uniform pressure at hole edge, $a = 5$ [mm], $b = 2$ [mm]

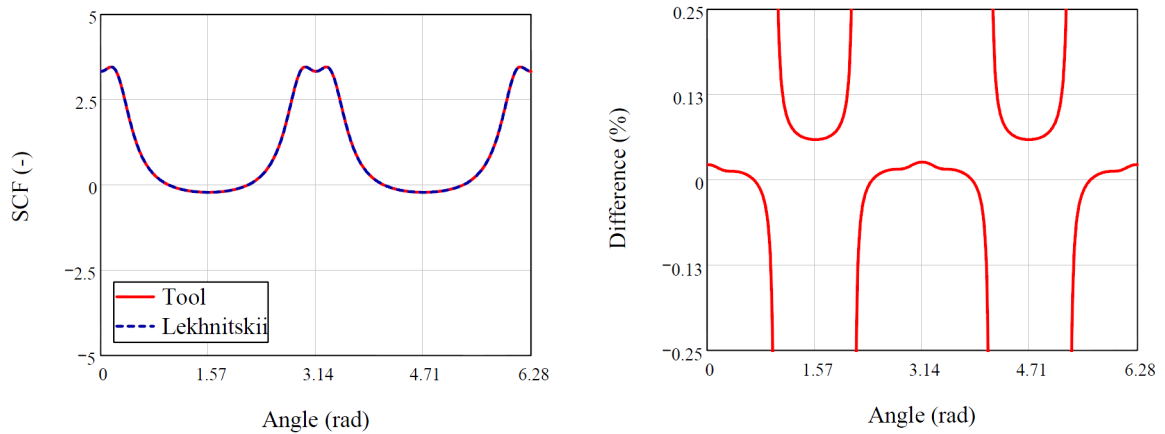


Figure D.19: Stress concentration factor at hole edge and difference between tool and Lekhnitskii. 25% 0° , 50% $\pm 45^\circ$, 25% $\pm 90^\circ$ uniform pressure at hole edge, $a = 5$ [mm], $b = 2$ [mm]

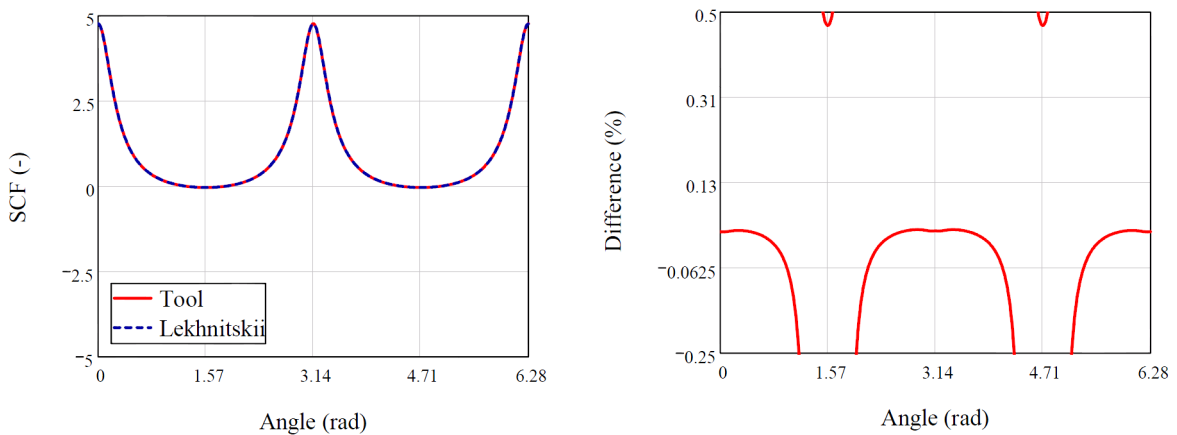


Figure D.20: Stress concentration factor at hole edge and difference between tool and Lekhnitskii. 25% 0° , 25% $\pm 45^\circ$, 50% $\pm 90^\circ$ uniform pressure at hole edge, $a = 5$ [mm], $b = 2$ [mm]

Unnotched Failure Algorithm

Table D.13: Verification of ply strain calculation

	Laminate Strain	0 deg		90 deg	
		Tool	Hand	Tool	Hand
ε_x	5.562e-009	5.562e-009	5.562e-009	-1.96e-009	-1.96e-009
ε_y	-1.96e-009	-1.96e-009	-1.96e-009	5.562e-009	5.562e-009
γ_{xy}	7.307e-025	7.307e-025	7.307e-025	-1.652e-024	-1.652e-24
	Laminate Strain	45 deg			
		Tool	Hand		
ε_x	5.562e-009	1.801e-009	1.801e-009		
ε_y	-1.96e-009	1.801e-009	1.801e-009		
γ_{xy}	7.307e-025	-7.522e-009	-7.522e-009		

Table D.14: Laminate properties used for unnotched failure verification

Type	E_{11}	E_{22}	G_{12}	$\nu_{12}(-)$	X^t	X^c	Y^t	Y^c	S	$t_{ply}(\text{mm})$
Tens.	142.0	8.1	4.5	0.3	2335	1635	80	215	120	0.184
Comp.	125.0	8.5	4.5	0.3	2335	1635	80	215	120	0.184

Table D.15: Laminate properties selected for unnotched failure verification. Stiffnesses (GPa), Strengths (MPa)

Ply	E_{11}	E_{22}	G_{12}	$\nu_{12}(-)$	X^t	X^c	Y^t	Y^c	S	$t_{ply}(\text{mm})$
0°	142.0	8.5	4.5	0.3	2335	1635	80	215	120	0.184
45°	142.0	8.1	4.5	0.3	2335	1635	80	215	120	0.184
90°	125.0	8.1	4.5	0.3	2335	1635	80	215	120	0.184

Table D.16: Verification of the ply stress calculation. Stiffnesses (GPa), Strengths (MPa)

Direction	Strain (-)	Stress (Pa)	
		Tool	Hand
longitudinal	4.25E-09	603.2	6.03E+02
transverse	-1.42E-09	-1.24	-1.24E+00
shear	1.02E-25	4.60E-16	4.60E-16

Table D.17: Verification of FF and IFF exposure

Ply	RFF (-)		FF (-)	
	Tool	Hand	Tool	Hand
0°	2.02e6	2.02e6	9.60e7	9.616e7
45°	6.11e6	6.11e6	2.106e6	2.106e6
90°	4.57e6	4.57e6	1.5e6	1.5e6

Table D.18: Changing of material properties upon IFF failure

Failure mode	Initial properties	Mode A	Mode B	Mode C
E_{11} (Pa)	140.0e9	140.0e9	140.0e9	140.0e9
E_{22} (Pa)	8.0e8	8.0e7	8.0e8	8.0e8
G_{12} (Pa)	5.0e8	5.0e7	5.0e8	5.0e8
ν_{12} (-)	0.03	0.02	0.03	0.03
t_{ply} (m)	1.29e-4	1.29e-4	1.29e-4	1.29e-4

Table D.19: System test results unnotched failure criterion

Layup	Load Vector	Tool (MPa)	Hand (MPa)
42% 0°, 42% ±45°, 16% 90°	(1,0,0)	816	826
42% 0°, 42% ±45°, 16% 90°	(-1,0,0)	-629	-629
100% 0°	(1,0,0)	1575	1575
100% 0°	(0,1,0)	60	60
100% 0°	(0,0,1)	113	113
50% 0°, 50% 90°	(1,0,0)	792	787.5
50% 0°, 50% 90°	(0,1,0)	792	787.5

Contact Angle Calculation

Table D.20: Verification of contact angle calculation.

	Tool	Hand
Clearance (%)	1.0	1.0
u_{α} (m)	2.457e-5	2.457e-5
r_h (m)	3.175e-3	3.175e-3
r_p (m)	3.143e-3	3.143e-3
Contact Angle (°)	55.265	55.265

Critical Potential Strain Energy Density Calculation and Selection

Table D.21: Verification of CPSED

	Scalefactor(-)		CPSED (Pa/m^2)	
	Tool	Hand	Tool	Hand
Long. Compr.	1.00	1.00	26.7156	26.7156
Long. Tens.	1.542	1.542	41.1914	41.1914
Biax Tens.	0.678	0.678	18.122	18.122
Biax Compr.	0.633	0.633	16.9168	16.9168
Biax Tens.-Comp.	0.518	0.518	13.8367	13.8367
Biax Compr.-Tens.	0.518	0.518	13.8367	13.8367
Trans. Compr.	0.411	0.411	10.9873	10.9873
Trans. Tens.	0.432	0.432	11.5395	11.5395

Table D.22: Verification of the calculation of the critical energy ratio

Input			
d (m)	Load Reserve Factor at r	Energy from edge to d (Pa/m^2)	(Pa/m^2)
0.001	293363	9.53e-12	214.10
Output			
Energy at failure (Pa/m^2)		CPSED ratio (-)	
Tool	Hand	Tool	Hand
82.04	82.04	2.61	2.61

In Figure D.21 the selection of the CPSED around a hole subjected to uniaxial tension is given. As explained in the thesis, the CPSED at a certain hole angle is chosen depending on the loading condition at that location. In the Figure it is shown that this is done correctly because of the transverse compression region around 0° and 180° and the longitudinal tensile region at 90° and 270° .

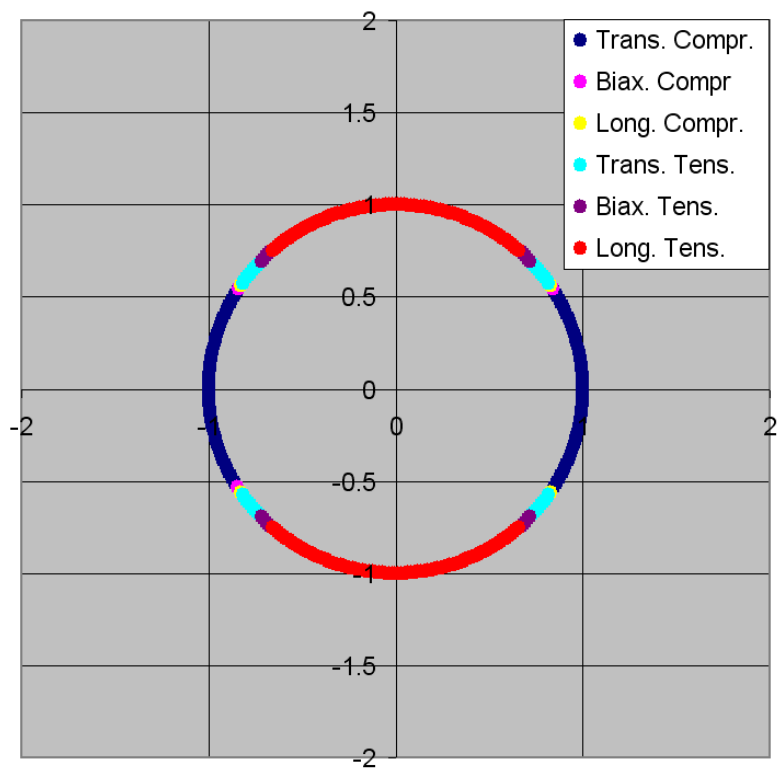


Figure D.21: Selection of the CPSED on a unit circle subjected to uniaxial tension in the horizontal direction

Notched Failure Algorithm

The behaviour of the notched failure algorithm is verified by looking at the change in characteristic distance, reserve factor and critical energy ratio over the amount of iteration steps. As one can see, they all converge to a steady value.

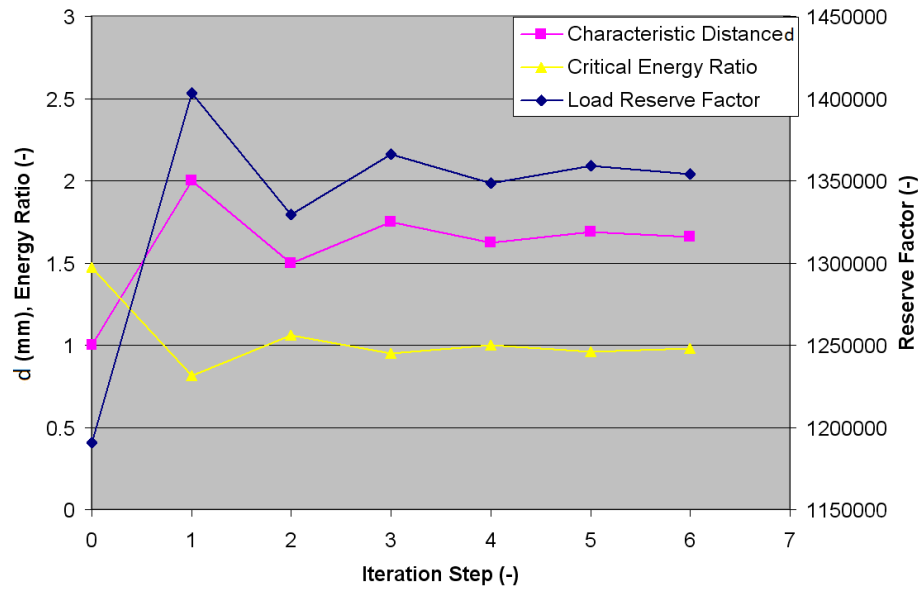


Figure D.22: Change of load reserve factor, r and critical energy ratio throughout the iteration process

Assembly Verification

Table D.23: Verification result of assembly tests

Case	Angle of failure (deg)		Failure Load (MPa)	
	Tool	Hand	Tool	Hand
1	270	$90^\circ \vee 270^\circ$	610	$372 \leq X \leq 1115$
2	0	$0^\circ \vee 180^\circ$	611	$372 \leq X \leq 1115$
3	358	0°	834	$0 \leq X \leq 905$

Appendix E

Contact Angle Comparisons FEA

In this Chapter, the results of the comparison of the contact angle algorithm to FEA are shown here. The figures show the result when the hole contact angle α is varied in the analytic tool and the result from FEA analysis. The title of each figure give the clearance used. In the figure legends, “S” denotes, Sevenois, “FEA” denotes Finite Element Analysis. The layup and corresponding directionality is also given according to the coding system below.

Coding: Model - Directionality - α factor; S = Sevenois; α = (α factor)*Contact Angle

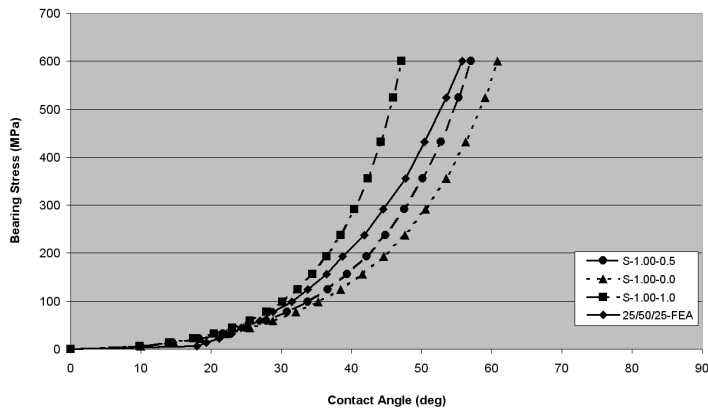


Figure E.1: Clearance = 2.0%

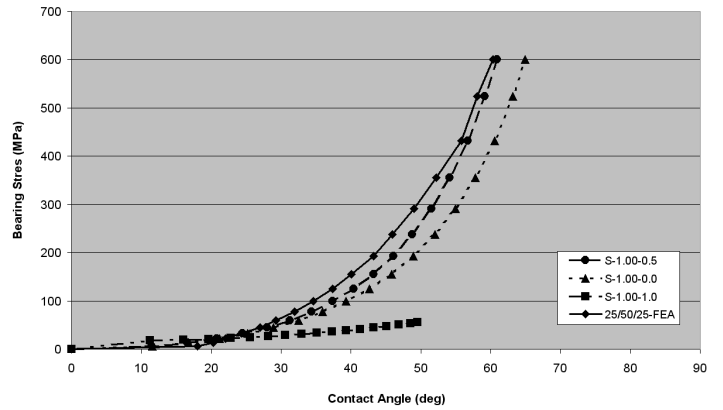


Figure E.4: Clearance = 1.5%

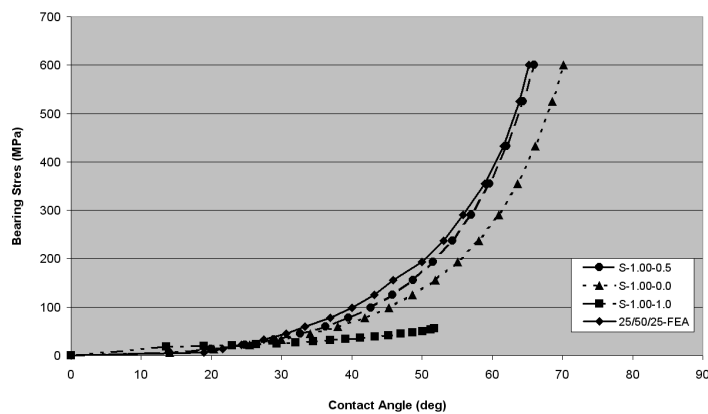


Figure E.2: Clearance = 1.0%

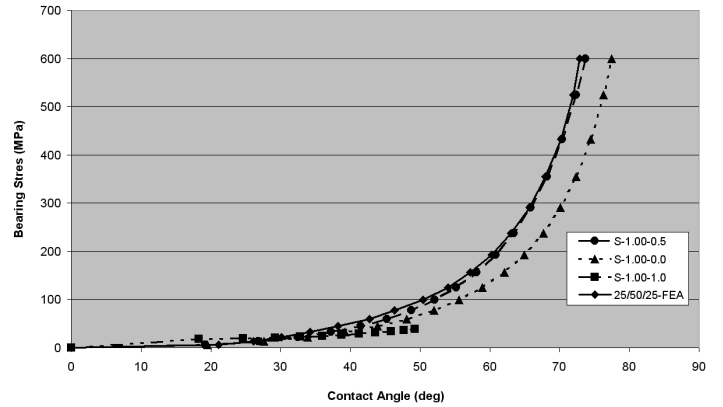


Figure E.5: Clearance = 0.5%

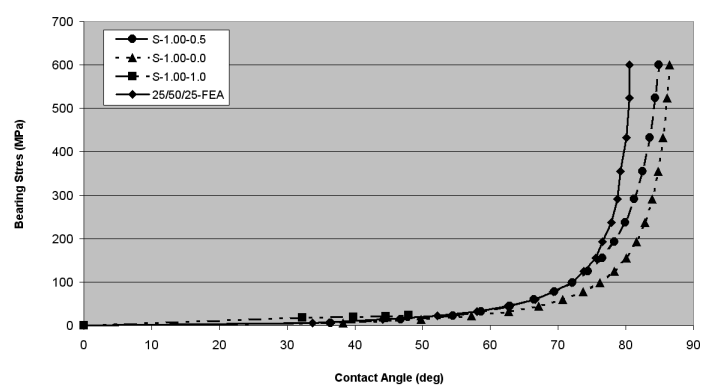


Figure E.3: Clearance = 0.1%

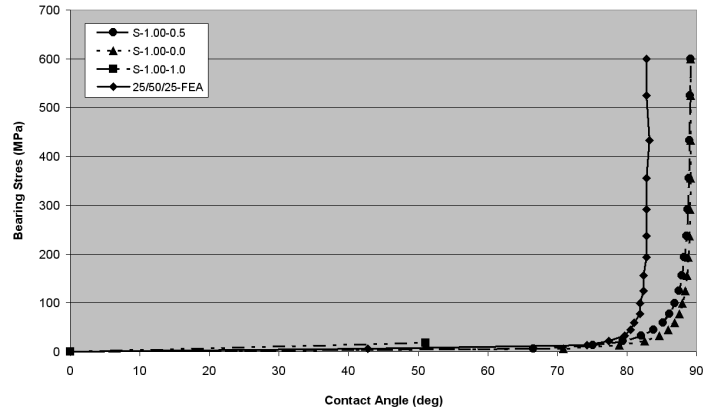


Figure E.6: Clearance = 0.01%

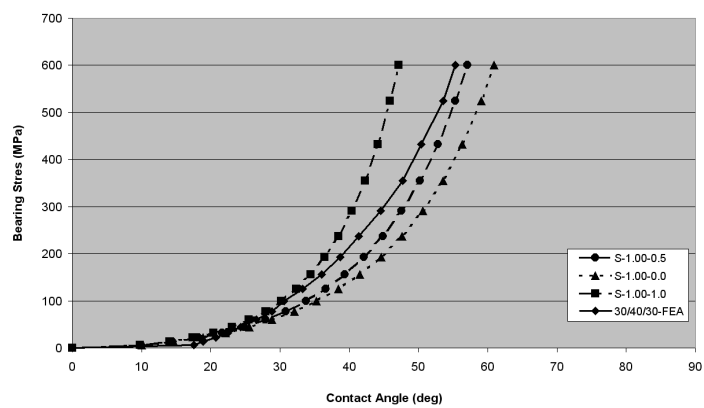


Figure E.7: Clearance = 2.0%

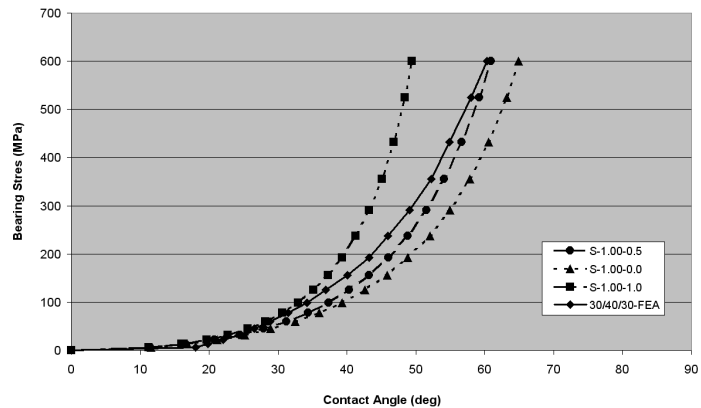


Figure E.10: Clearance = 1.5%

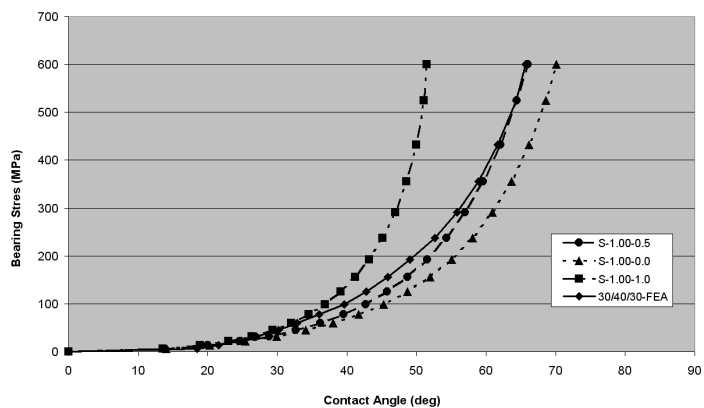


Figure E.8: Clearance = 1.0%

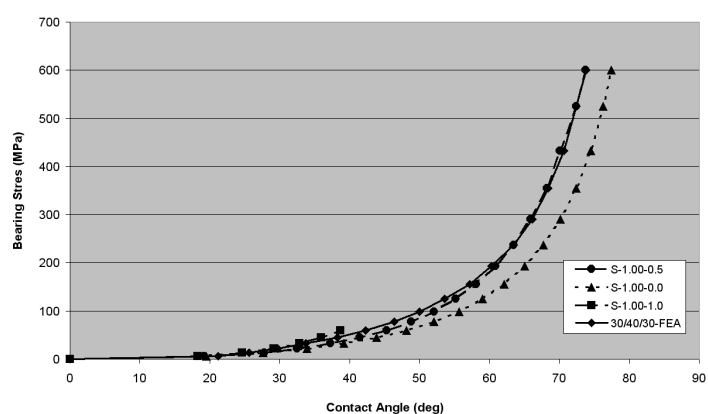


Figure E.11: Clearance = 0.5%

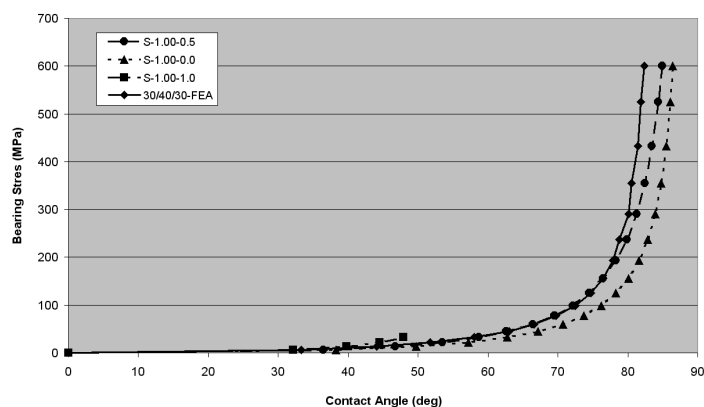


Figure E.9: Clearance = 0.1%

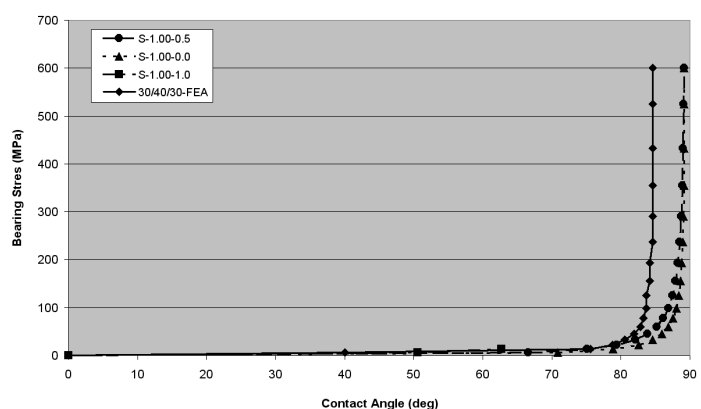


Figure E.12: Clearance = 0.01%

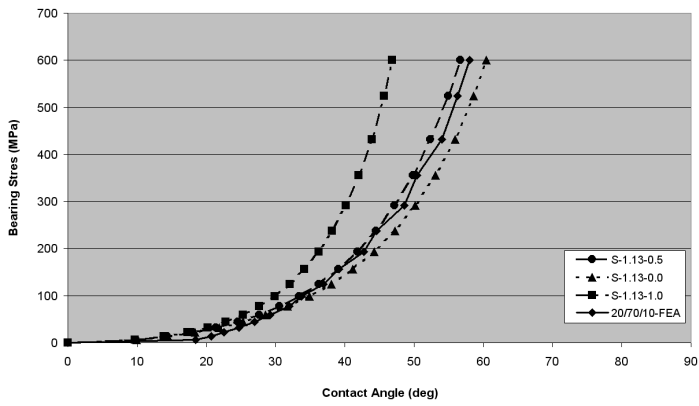


Figure E.13: Clearance = 2.0%

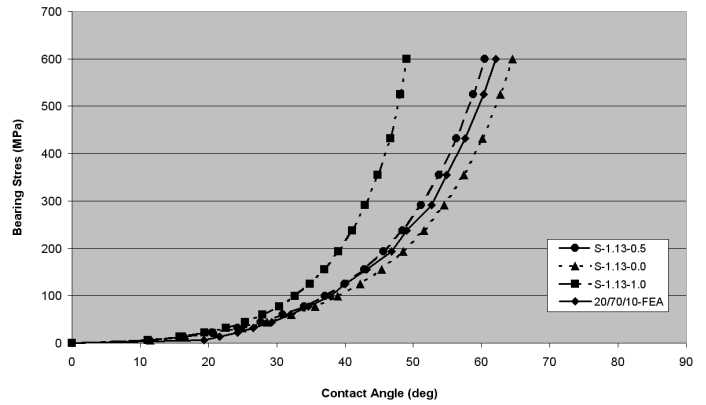


Figure E.16: Clearance = 1.5%

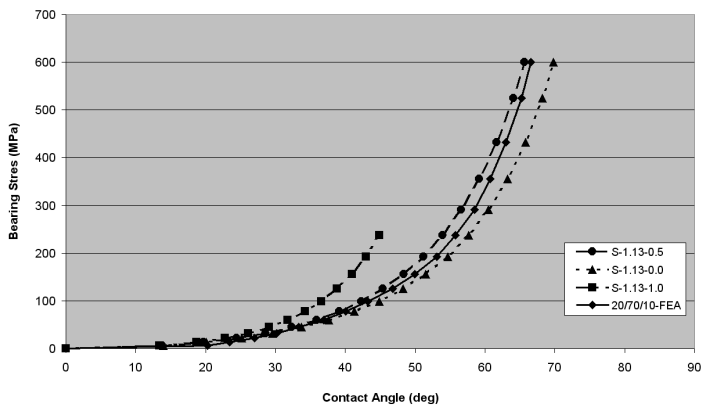


Figure E.14: Clearance = 1.0%

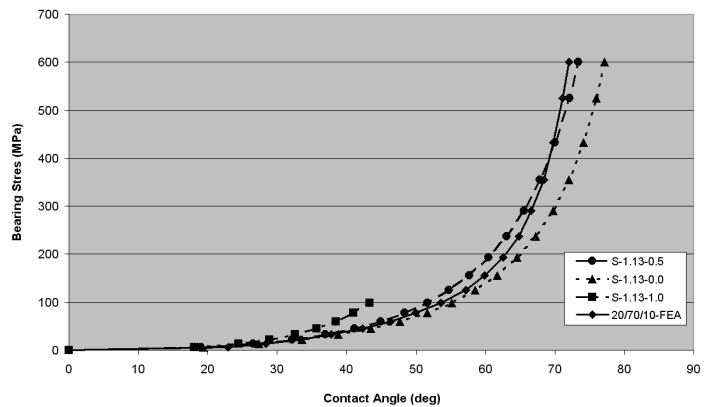


Figure E.17: Clearance = 0.5%

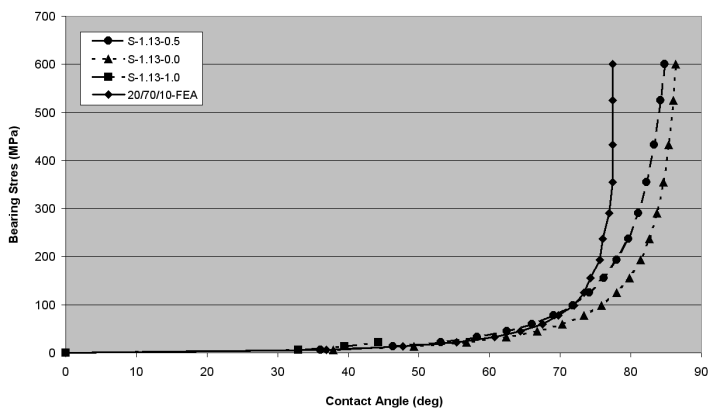


Figure E.15: Clearance = 0.1%

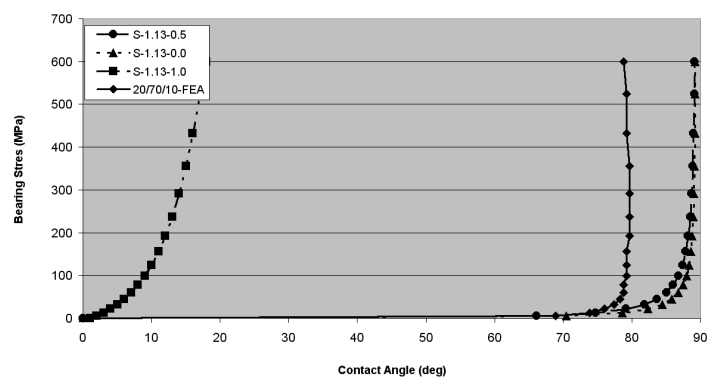


Figure E.18: Clearance = 0.01%

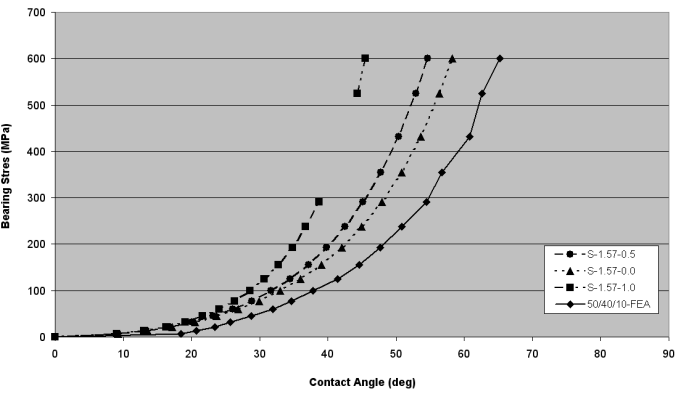


Figure E.19: Clearance = 2.0%

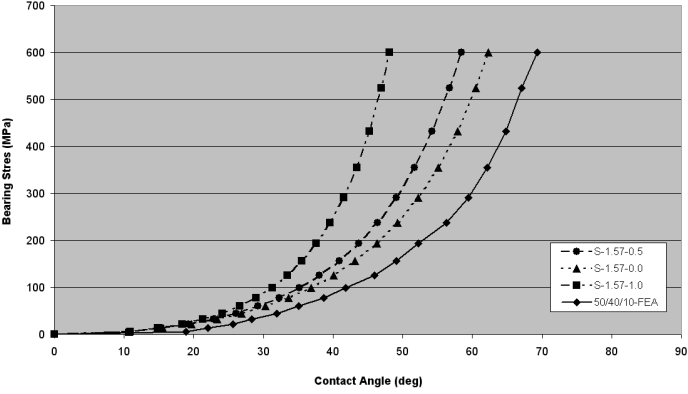


Figure E.22: Clearance = 1.5%

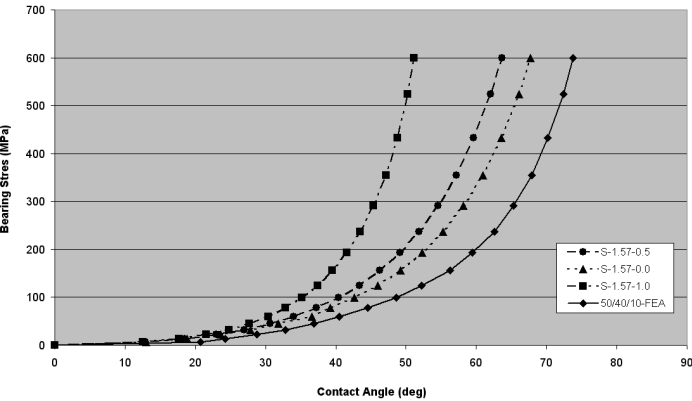


Figure E.20: Clearance = 1.0%

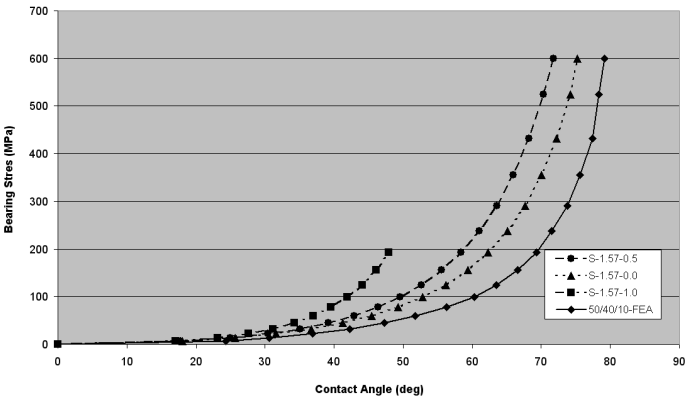


Figure E.23: Clearance = 0.5%

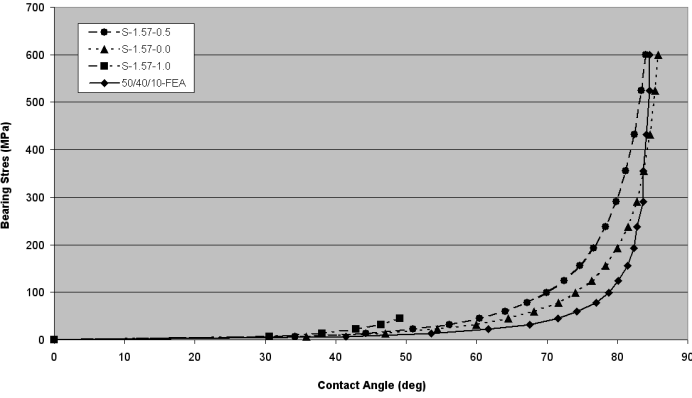


Figure E.21: Clearance = 0.1%

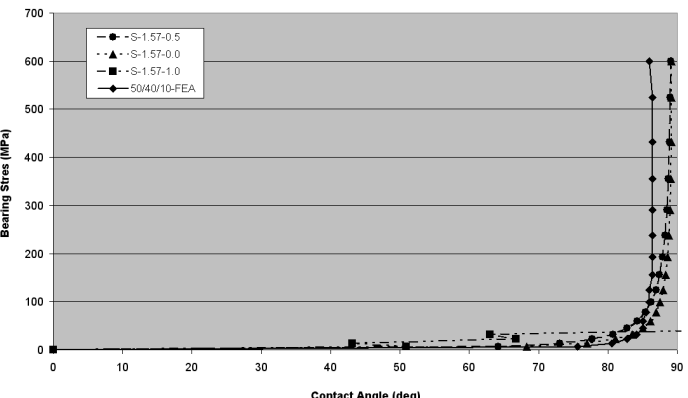


Figure E.24: Clearance = 0.01%

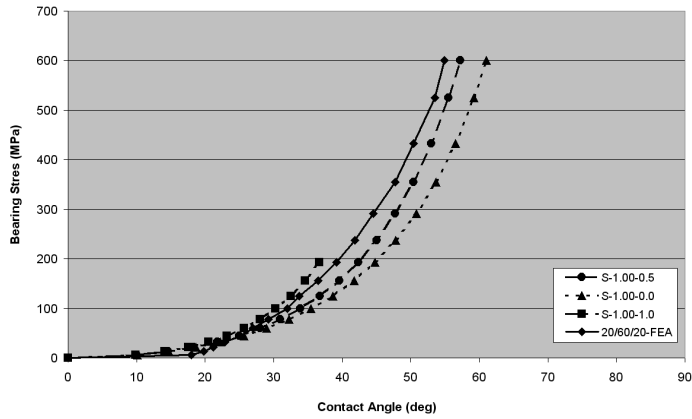


Figure E.25: Clearance = 2.0%

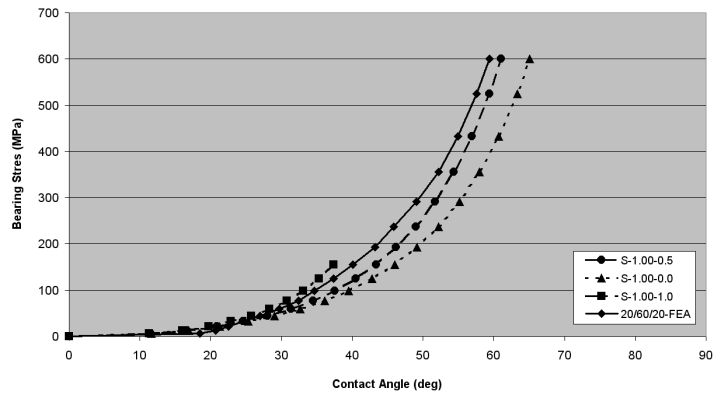


Figure E.28: Clearance = 1.5%

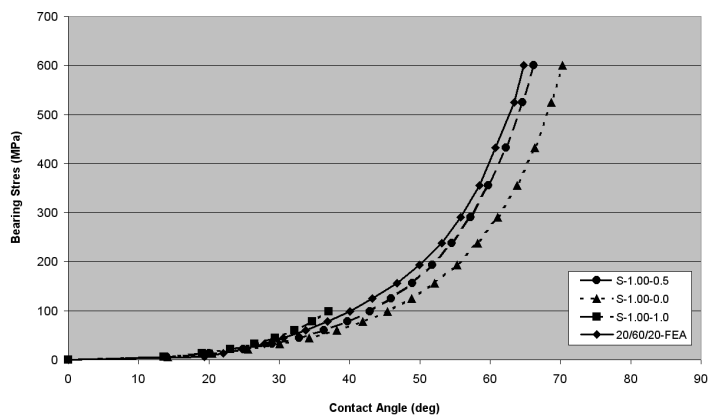


Figure E.26: Clearance = 1.0%

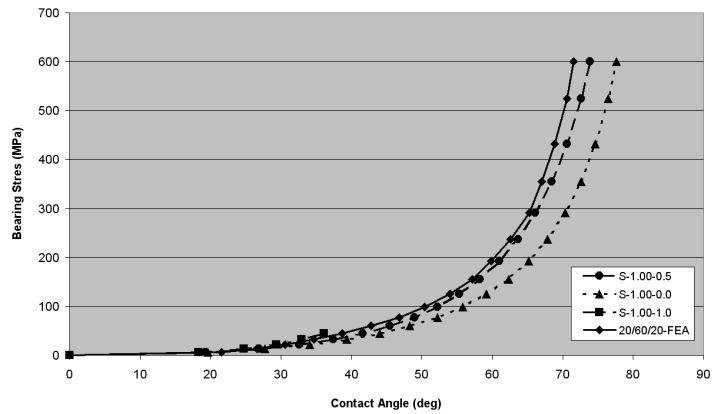


Figure E.29: Clearance = 0.5%

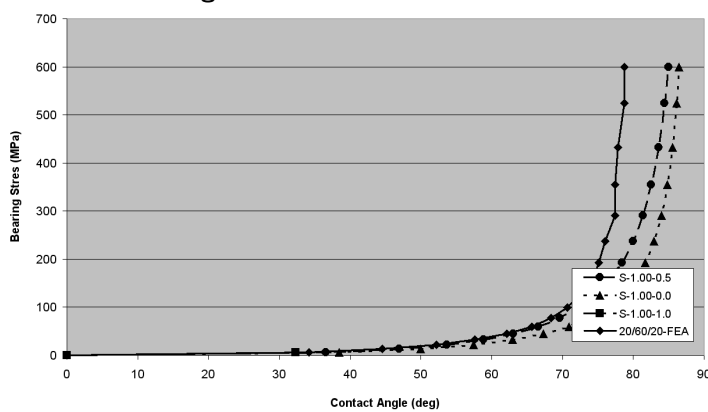


Figure E.27: Clearance = 0.1%

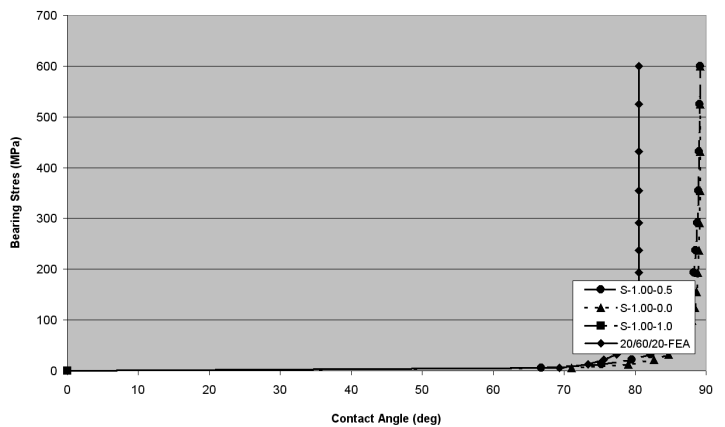


Figure E.30: Clearance = 0.01%

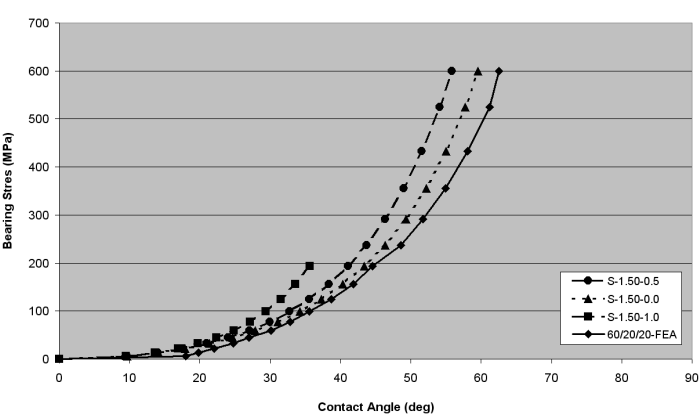


Figure E.31: Clearance = 2.0%

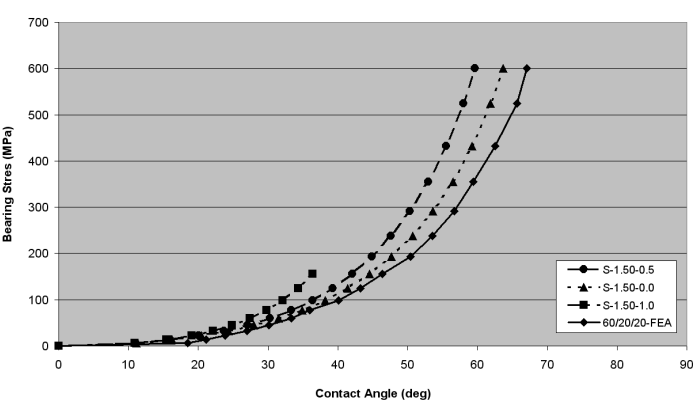


Figure E.34: Clearance = 1.5%

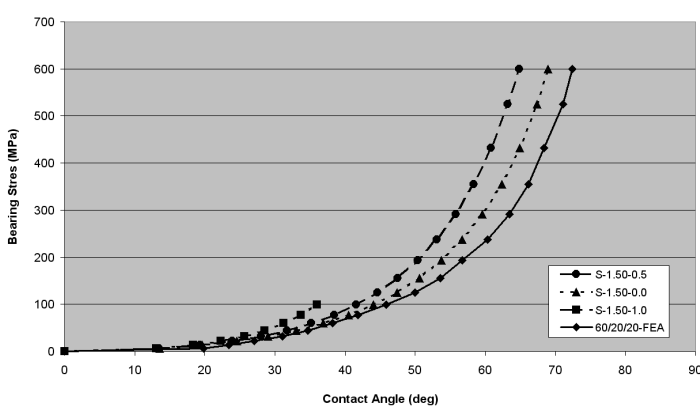


Figure E.32: Clearance = 1.0%

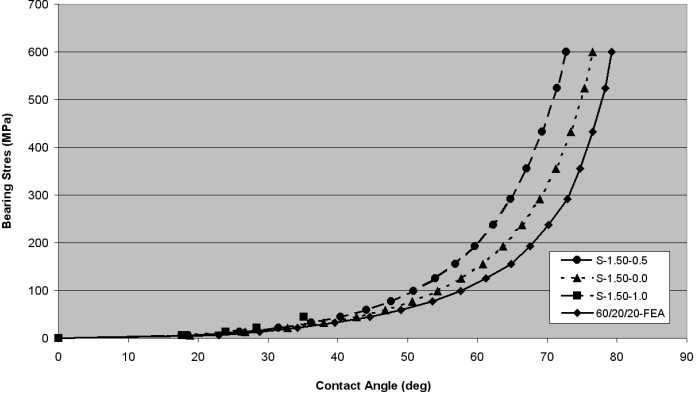


Figure E.35: Clearance = 0.5%

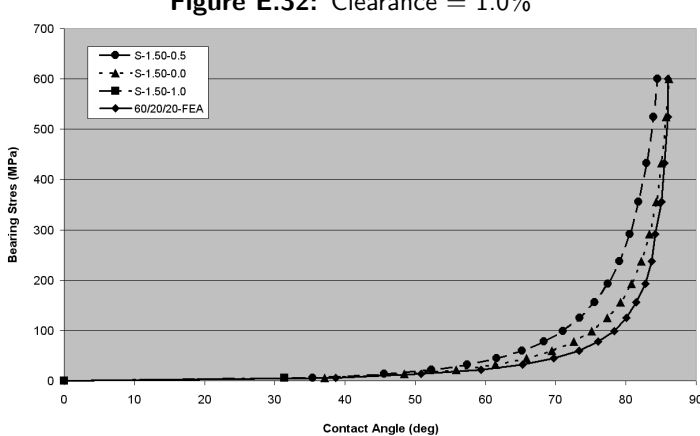


Figure E.33: Clearance = 0.1%

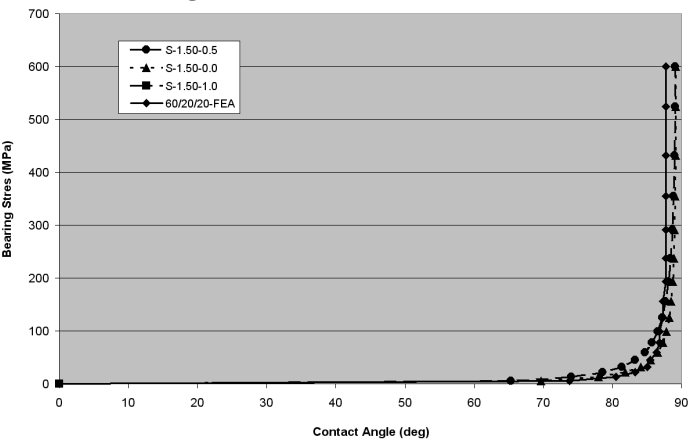


Figure E.36: Clearance = 0.01%

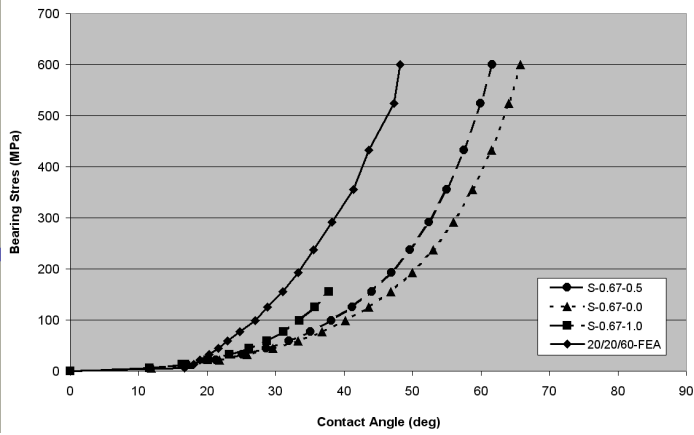


Figure E.37: Clearance = 2.0%

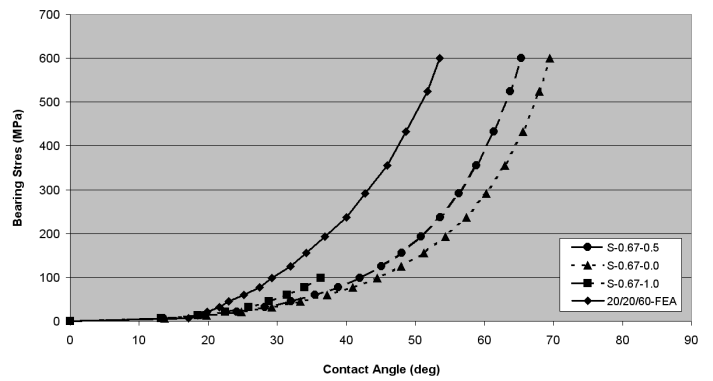


Figure E.40: Clearance = 1.5%

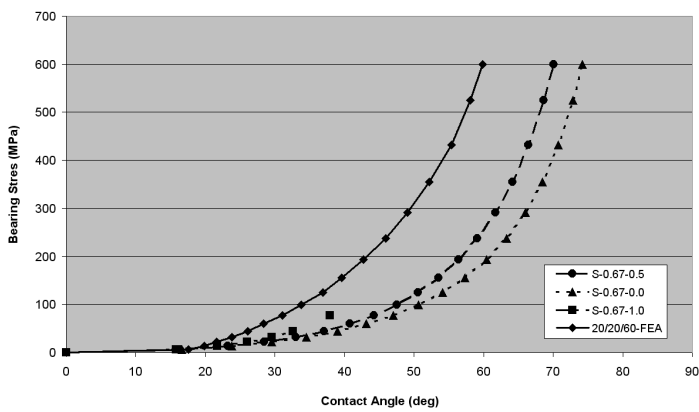


Figure E.38: Clearance = 1.0%

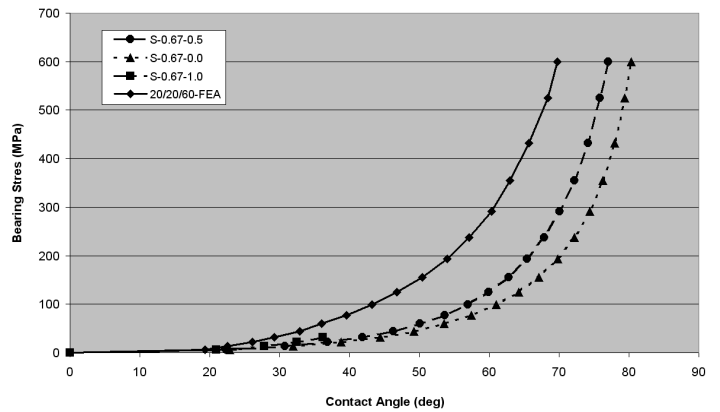


Figure E.41: Clearance = 0.5%

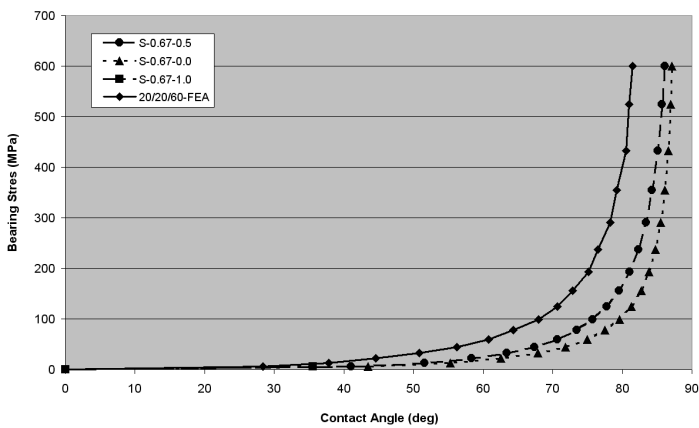


Figure E.39: Clearance = 0.1%

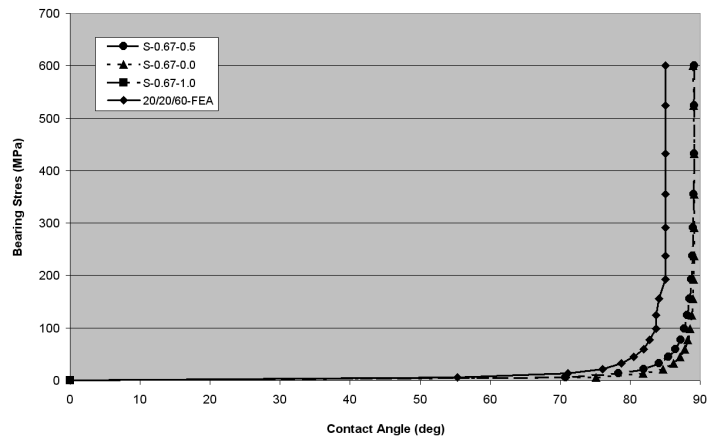


Figure E.42: Clearance = 0.01%

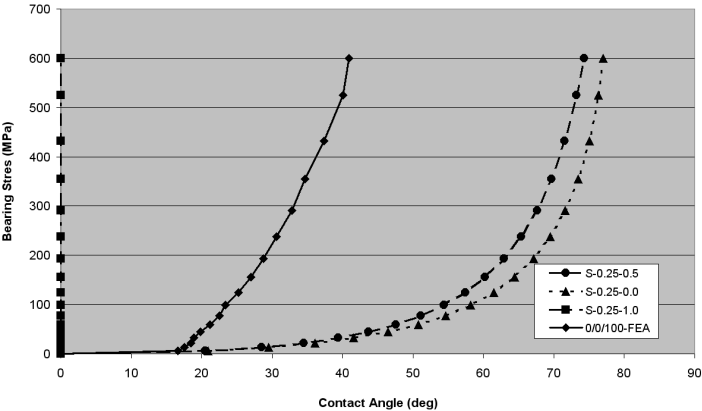


Figure E.43: Clearance = 2.0%

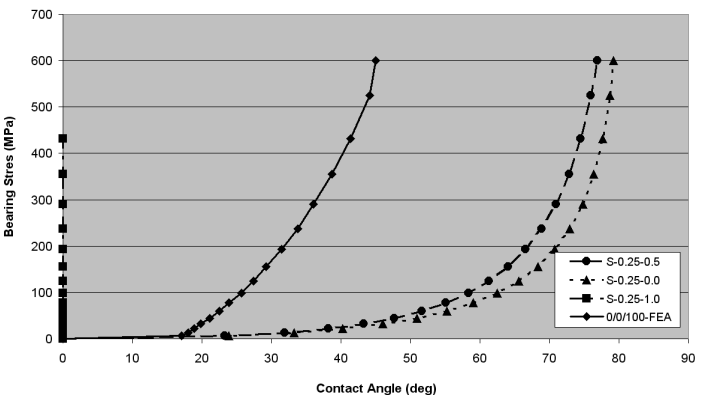


Figure E.46: Clearance = 1.5%

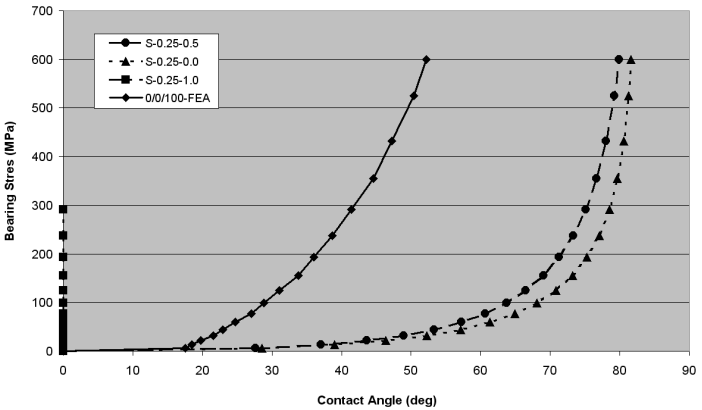


Figure E.44: Clearance = 1.0%

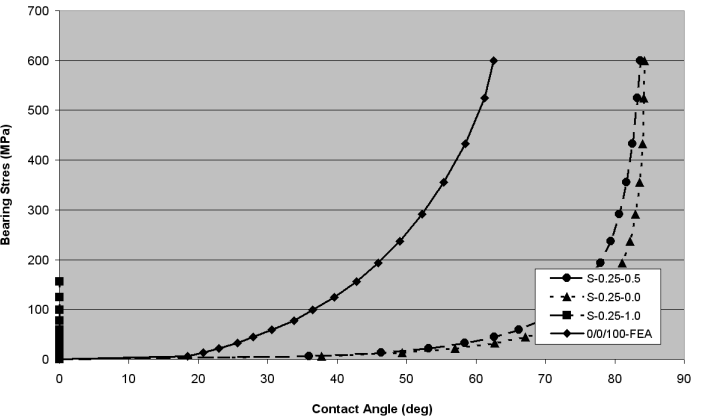


Figure E.47: Clearance = 0.5%

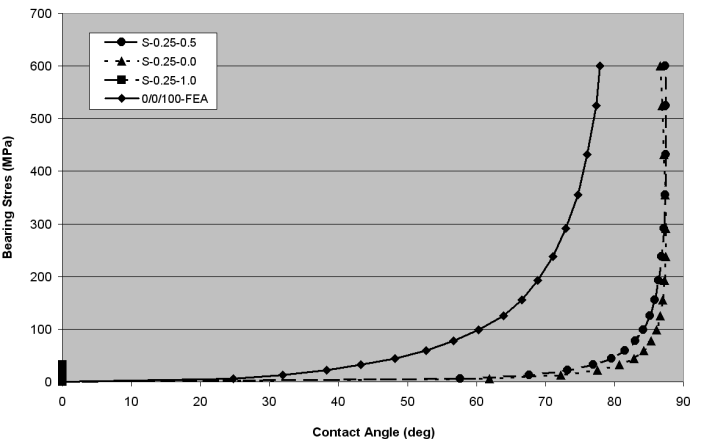


Figure E.45: Clearance = 0.1%

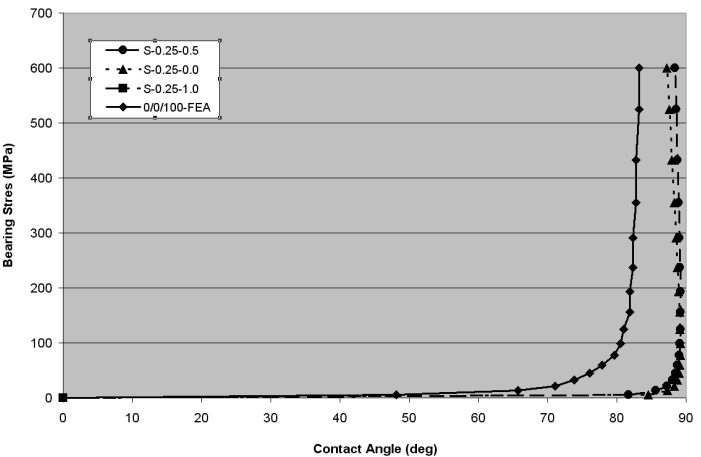


Figure E.48: Clearance = 0.01%

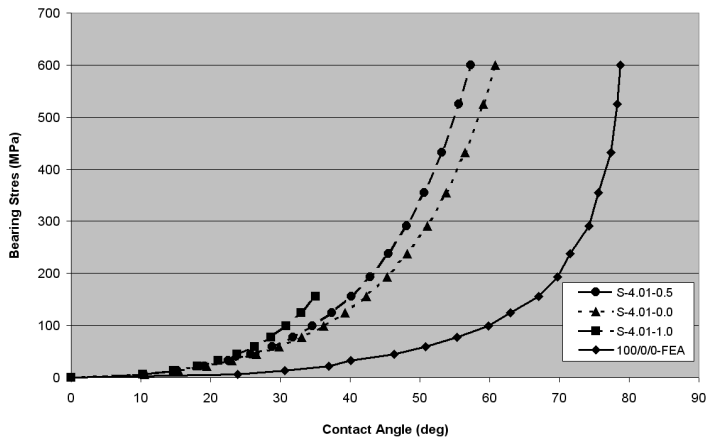


Figure E.49: Clearance = 2.0%

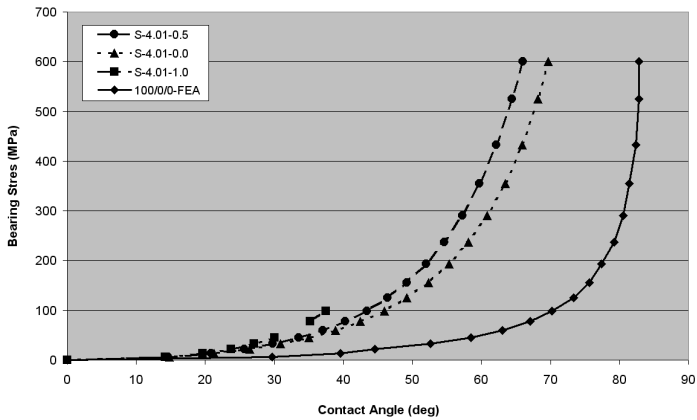


Figure E.50: Clearance = 1.0%

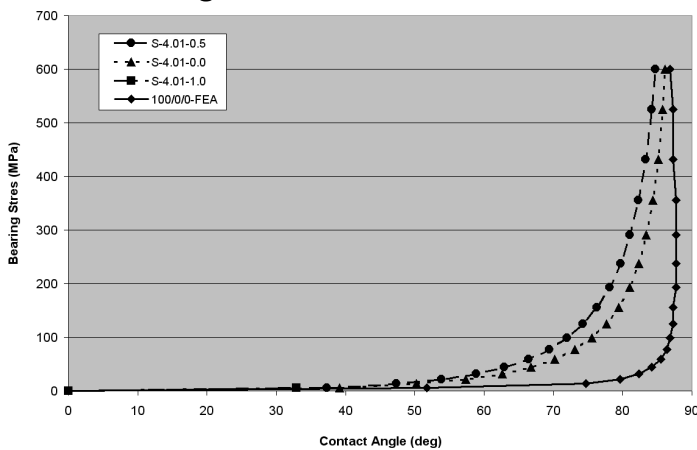


Figure E.51: Clearance = 0.1%

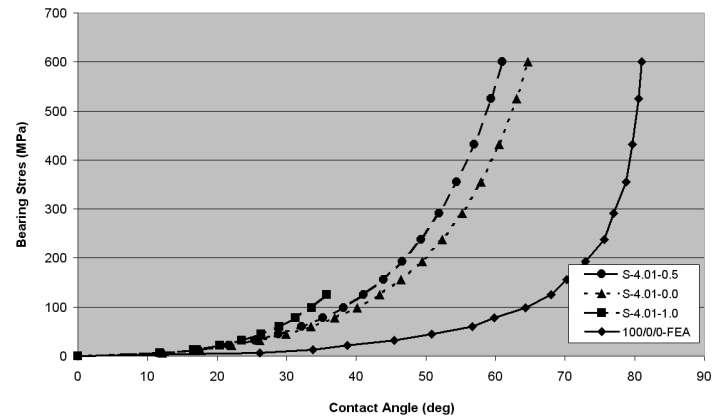


Figure E.52: Clearance = 1.5%

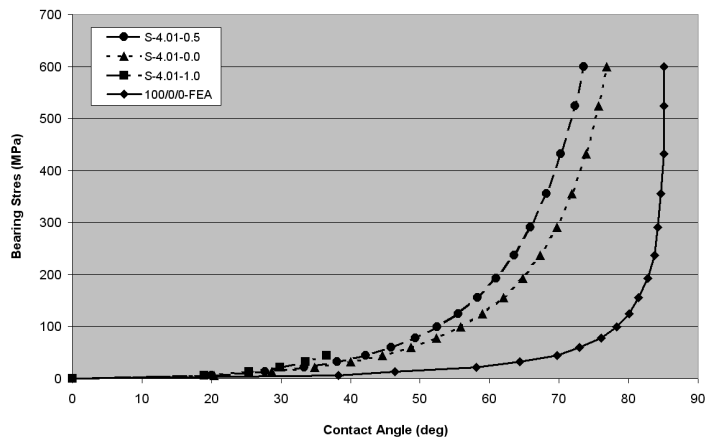


Figure E.53: Clearance = 0.5%

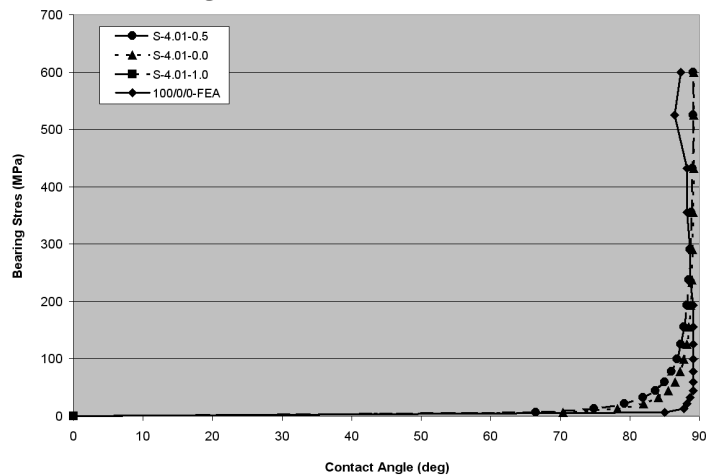


Figure E.54: Clearance = 0.01%

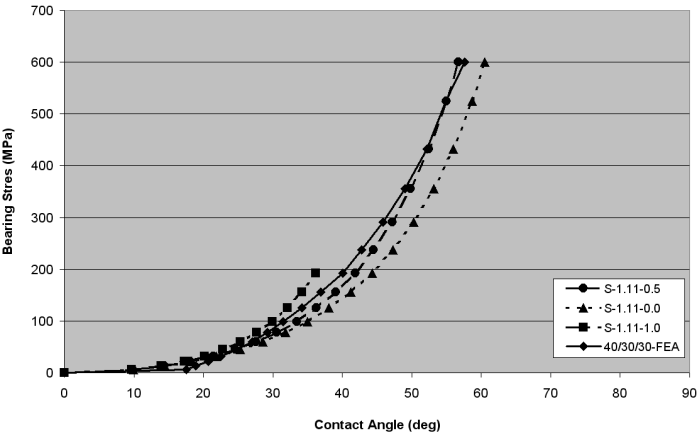


Figure E.55: Clearance = 2.0%

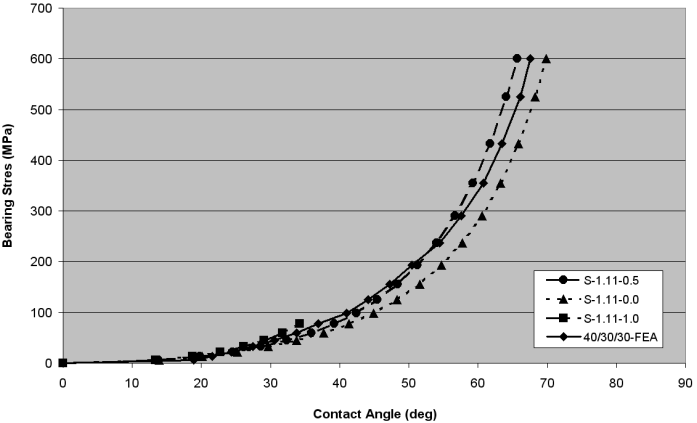


Figure E.56: Clearance = 1.0%

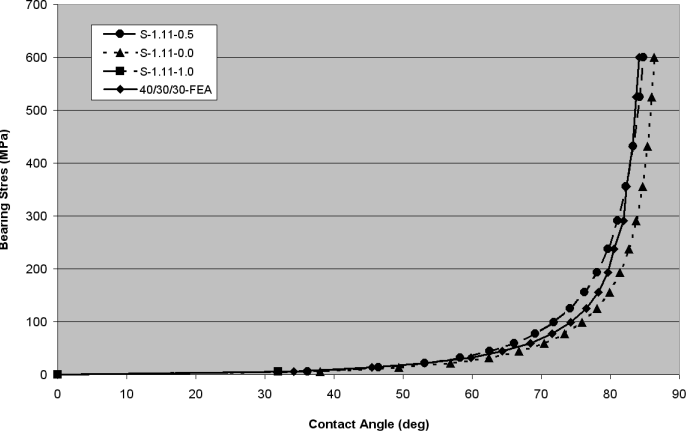


Figure E.57: Clearance = 0.1%

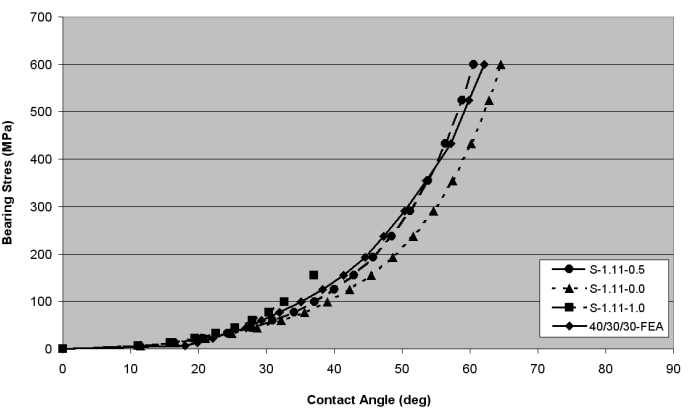


Figure E.58: Clearance = 1.5%

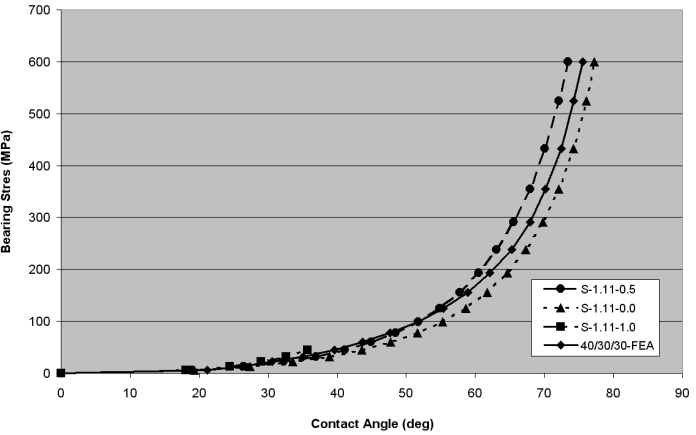


Figure E.59: Clearance = 0.5%

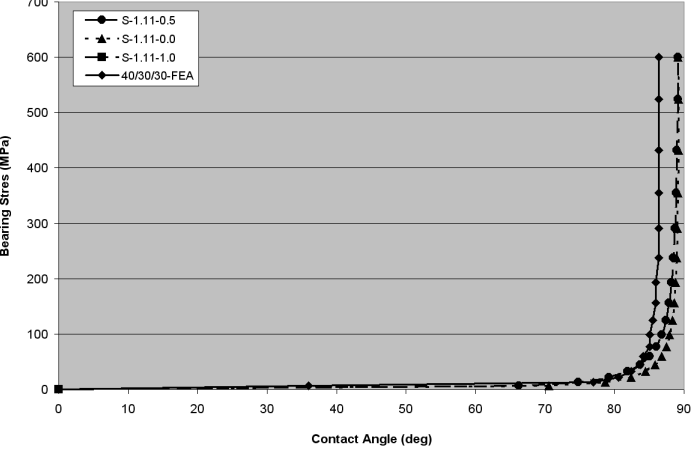


Figure E.60: Clearance = 0.01%

Appendix F

Results from Stress Validation

In this chapter, the results from the validation of the stress field theory by comparing them to FEA are presented.

The effect of varying E/D for an unloaded hole

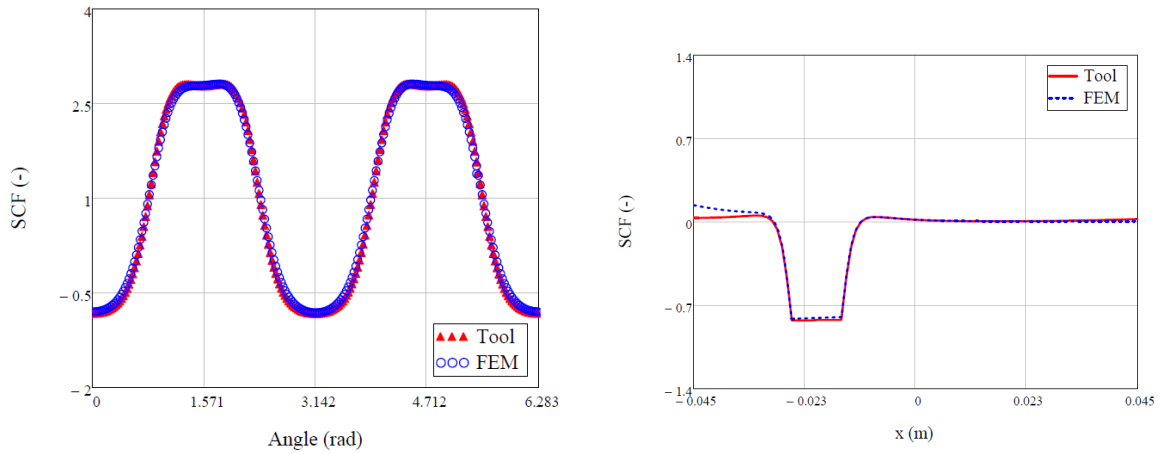


Figure F.1: SCF of σ_θ at the hole edge (left) and SCF of σ_y at $y = 0$ (right) when $E/D = 2.5$

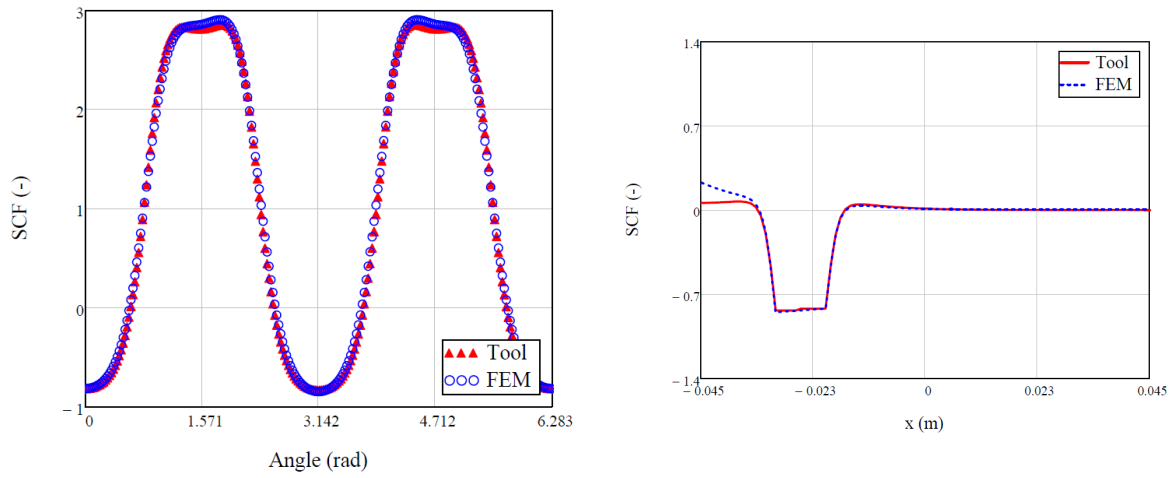


Figure F.2: SCF of σ_θ at the hole edge (left) and SCF of σ_y at $y = 0$ (right) when $E/D = 2.0$

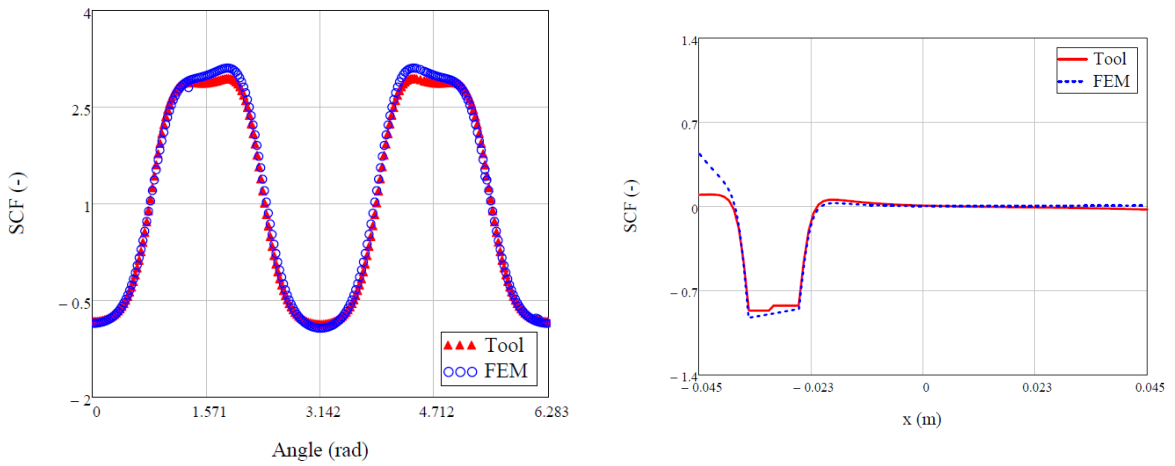


Figure F.3: SCF of σ_θ at the hole edge (left) and SCF of σ_y at $y = 0$ (right) when $E/D = 1.5$

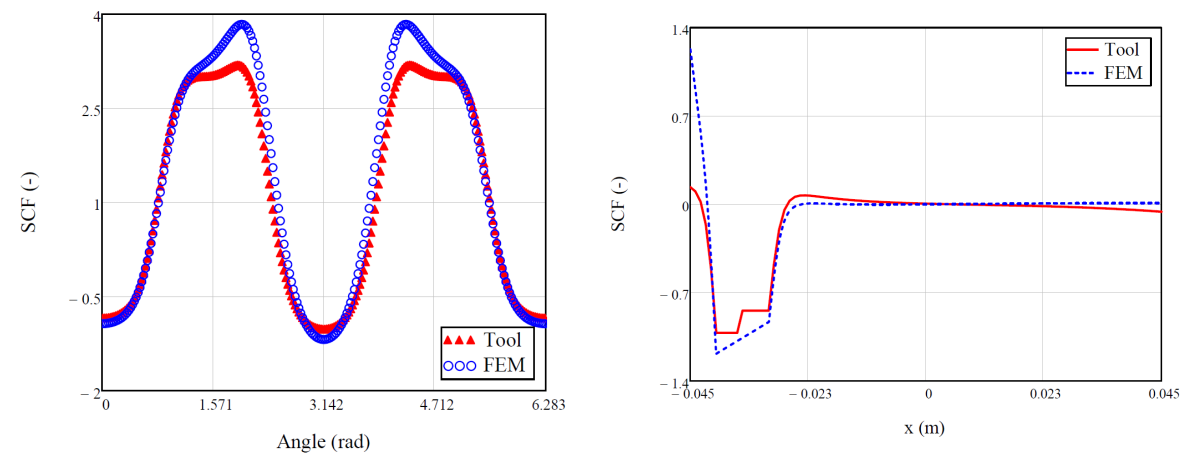


Figure F.4: SCF of σ_θ at the hole edge (left) and SCF of σ_y at $y = 0$ (right) when $E/D = 1$

The effect of varying W/D for an unloaded hole

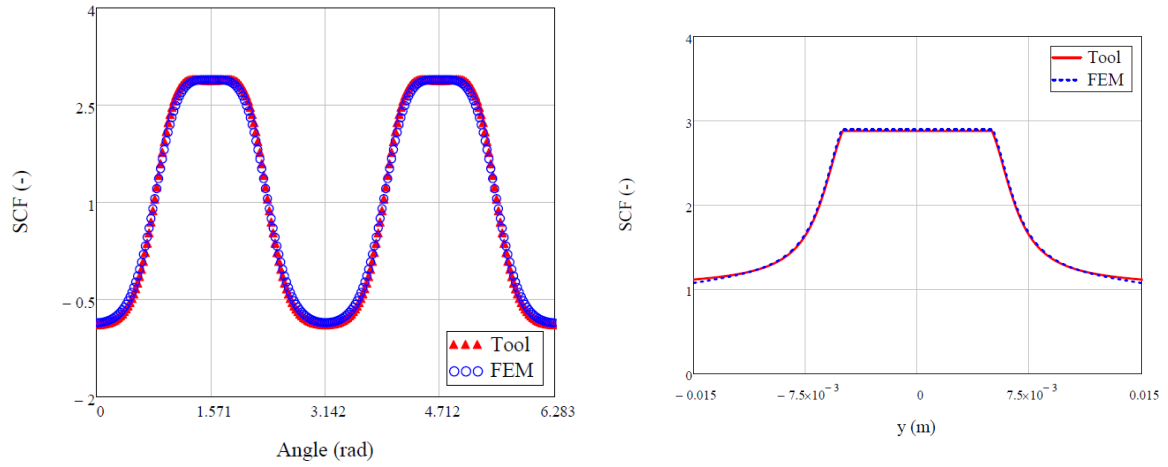


Figure F.5: SCF of σ_θ at the hole edge (left) and SCF of σ_x at $x = 0$ (right) when $W/D = 4$

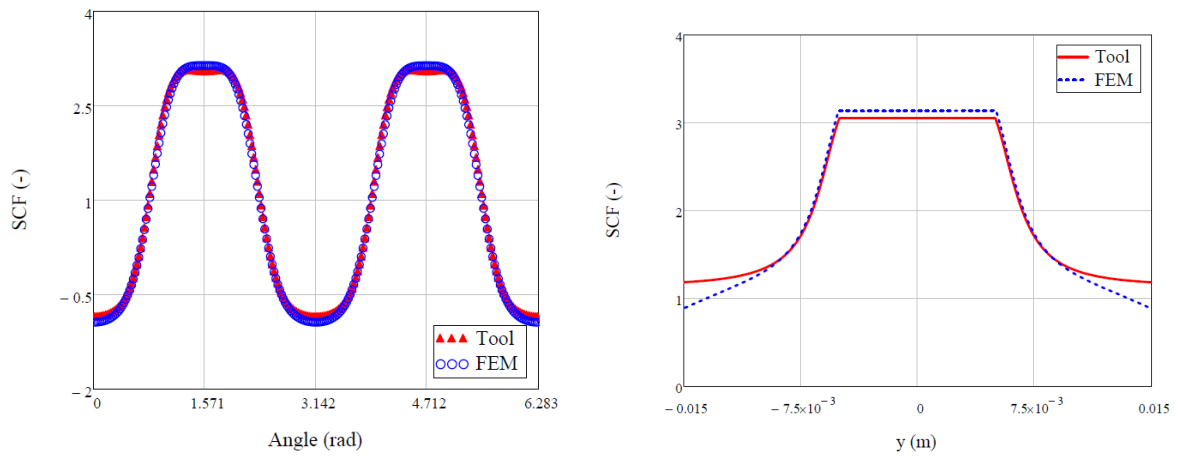


Figure F.6: SCF of σ_θ at the hole edge (left) and SCF of σ_x at $x = 0$ (right) when $W/D = 3$

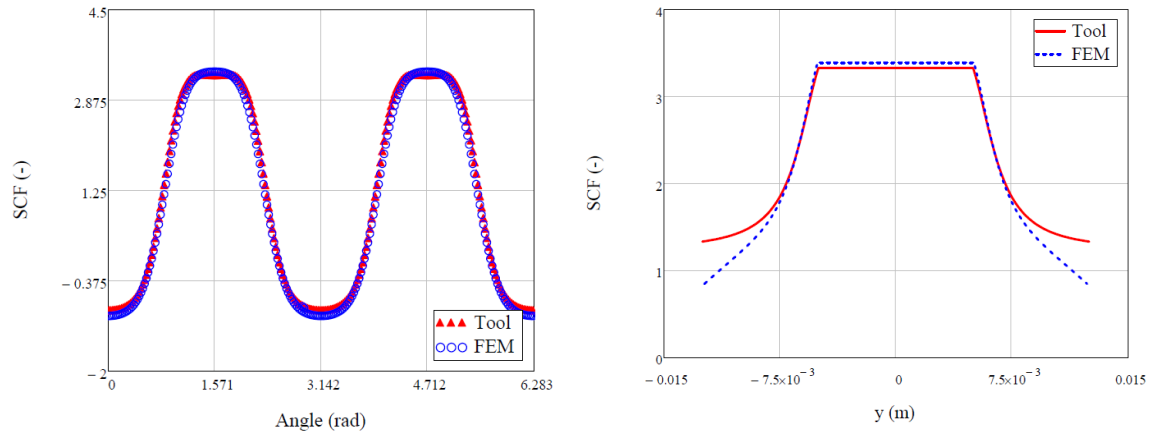


Figure F.7: SCF of σ_θ at the hole edge (left) and SCF of σ_x at $x = 0$ (right) when $W/D = 2.5$

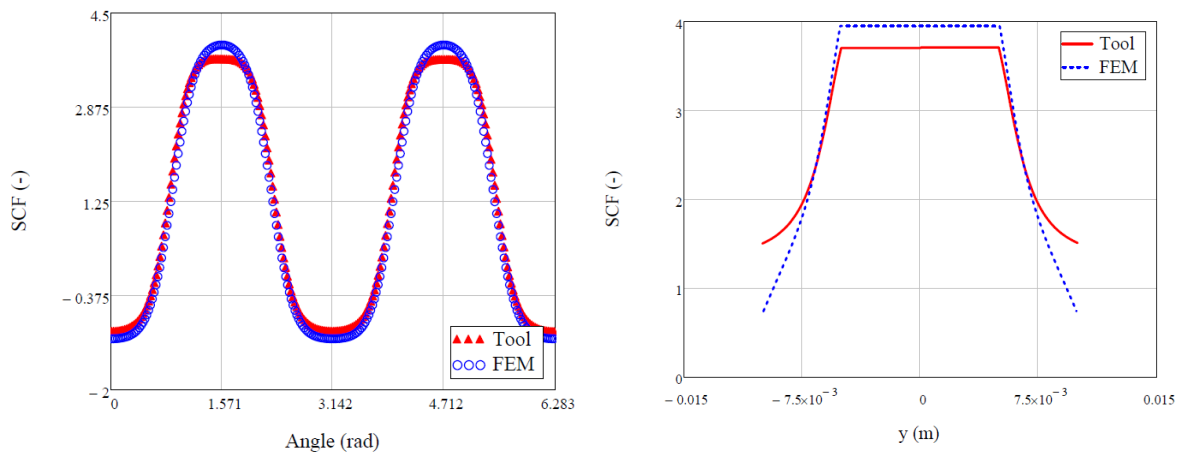


Figure F.8: SCF of σ_θ at the hole edge (left) and SCF of σ_x at $x = 0$ (right) when $W/D = 2$

The effect of varying E/D for a loaded hole

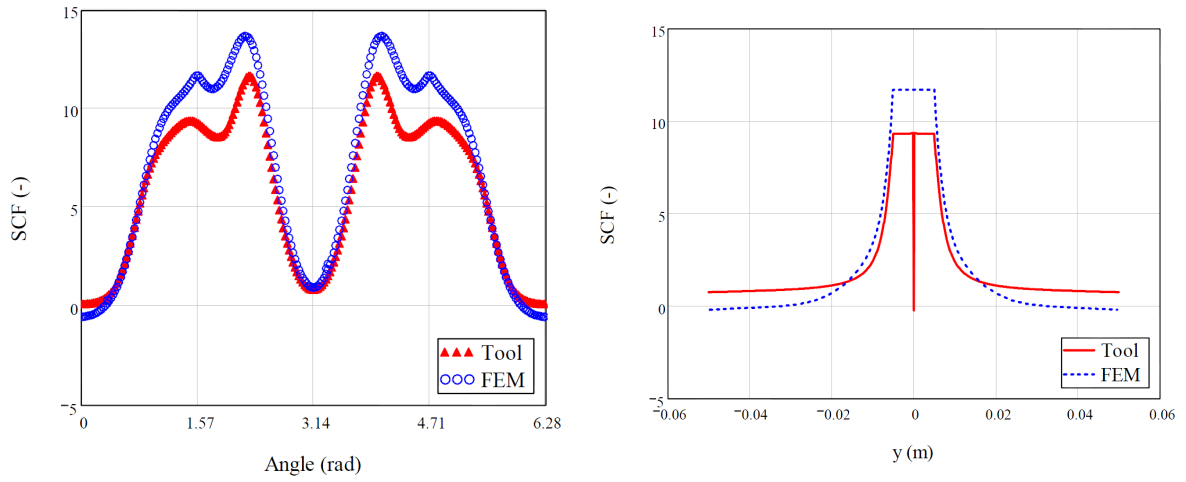


Figure F.9: SCF of σ_θ at the hole edge (left) and SCF of σ_x at $x = x_{hole}$ (right) when $E/D = 2.5$

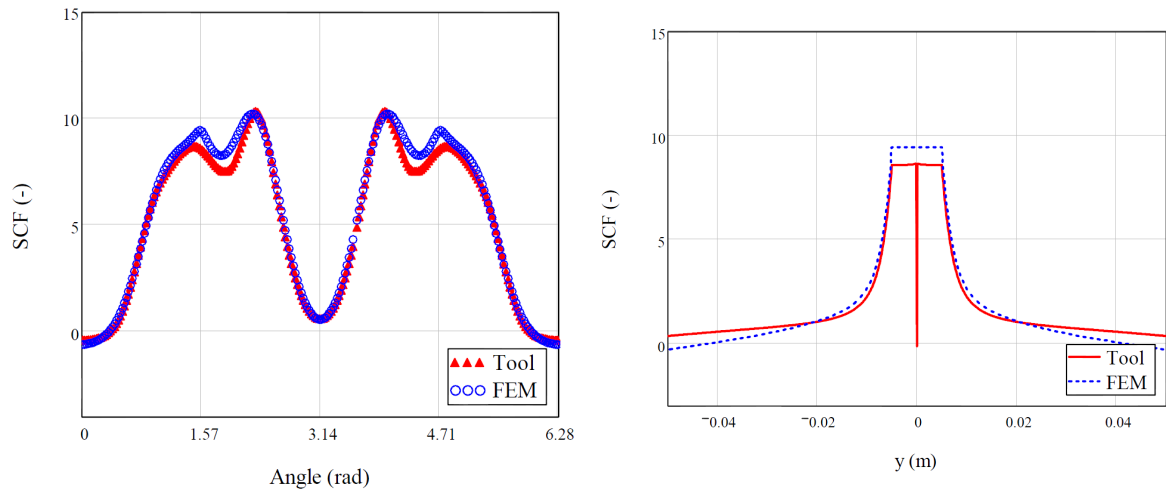


Figure F.10: SCF of σ_θ at the hole edge (left) and SCF of σ_x at $x = x_{hole}$ (right) when $E/D = 1.5$

The effects of having multiple loaded/unloaded holes

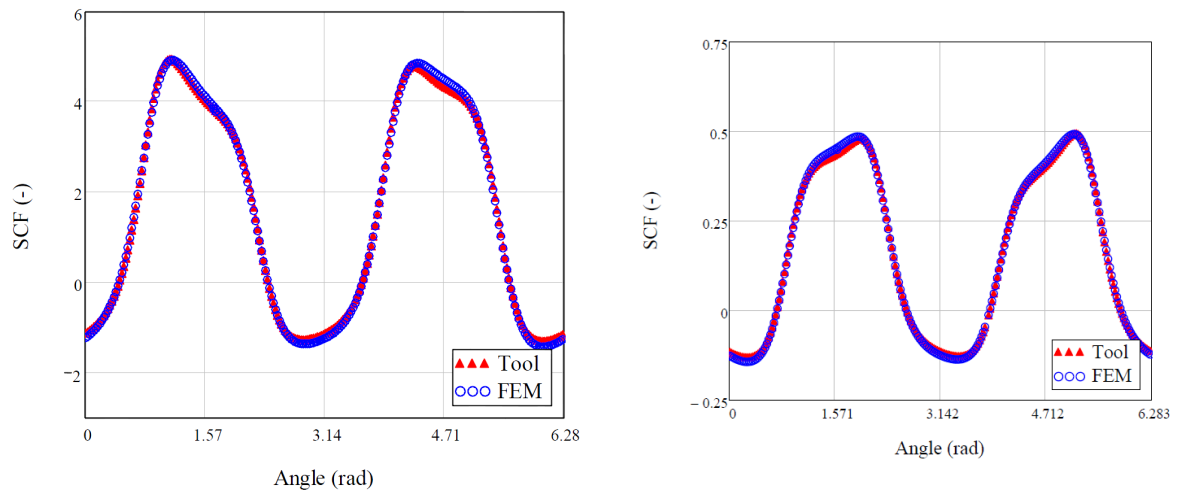


Figure F.11: multihole 1 and 2 unloaded

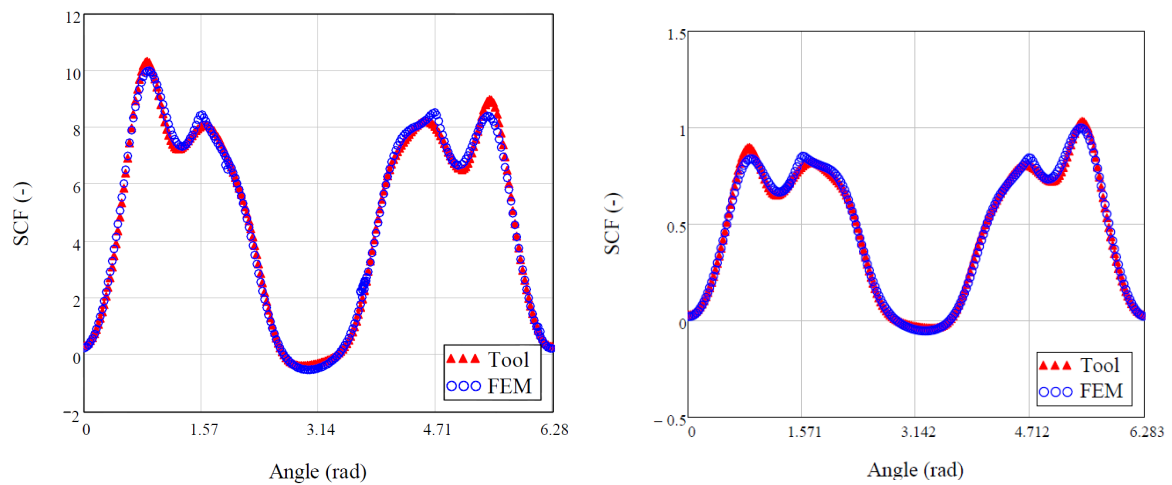


Figure F.12: multihole 3 and 4 loaded